1992

Numerical modeling of probe velocity effects for electromagnetic NDE

Young-Kil Shin
Iowa State University

Order Number 9311534

Numerical modeling of probe velocity effects for electromagnetic NDE

Shin, Young-Kil, Ph.D.

Iowa State University, 1992

U·M·I
300 N. Zeeb Rd.
Ann Arbor, MI 48106

Numerical modeling of probe velocity effects for electromagnetic NDE

by

Young-Kil Shin

A Dissertation Submitted to the

Graduate Faculty in Partial Fulfillment of the

Requirements for the Degree of

DOCTOR OF PHILOSOPHY

Department: Electrical Engineering and Computer Engineering
Major: Electrical Engineering (Electromagnetics)

Approved:

Signature was redacted for privacy.

In Charge of Major Work

Signature was redacted for privacy.

For the Major Department

Signature was redacted for privacy.

For the Graduate College

Iowa State University
Ames, Iowa

1992

TABLE OF CONTENTS

LIST OF TABLES

LIST OF FIGURES

LIST OF SYMBOLS

Symbol	Description	Unit
$\bar{A}$	Magnetic vector potential	Weber/m
A_θ	θ component of magnetic vector potential	Weber/m
A	θ or z component of magnetic vector potential	Weber/m
A_c	Centroidal value of A	Weber/m
AC	Alternating current	Ampere
$\bar{B}$	Magnetic flux density	Tesla (= 10^4 Gauss)
B_r , B_z	r and z component of $\bar{B}$	Tesla
$\dot{\bar{B}}$	Time derivative of magnetic flux density	
C	Grid Courant number ($V\Delta t / \Delta h$)	
c	Speed of light ($1/\sqrt{\mu_o \varepsilon_o}$)	m/sec
$\bar{D}$	Electric flux density	Coulomb/m^2
D / Dt	Convective derivative	
DC	Direct current	Ampere
$d\bar{l}$	Element of length	m
$d\bar{s}$	Element of surface area	m^2
dv	Element of volume	m^3
$\bar{E}$	Electric field intensity	Volt/m
$\bar{E}_e$	emf producing field associated with $\bar{J}_e$	Volt/m
emf	Electromotive force	Volt
F	Energy functional	Joule
f	Frequency	Hertz
$\bar{F}$	Force	newton

$\bar{H}$	Magnetic field intensity vector	Ampere/m
h, or Δh	Element length in the direction of probe movement	m
I_s	Current in the coil	Ampere
$\bar{J}$	Current density vector	Ampere/m^2
$\bar{J}_s$	Source current density	Ampere/m^2
J_s	θ or z component of source current density	Ampere/m^2
J_i	Induced current density	Ampere/m^2
$\bar{J}_e$	Eddy current density	Ampere/m^2
j	Complex operator ($\sqrt{-1}$)	
[J]	Jacobian matrix	
|J|	Determinant of Jacobian matrix	
L	Coil inductance	Henry
l	Charateristic length	m
N_i	Shape function at node i	
N_t	Number of turns in a coil	
n_x , n_y	x and y component of unit normal vector	
P	Total energy dissipated in the finite element region	Joule
q	Electric charge	Coulomb
$R(\cdot)$	Residual	
R	Coil resistance	ohm
r	Radius in the cylindrical coordinate system	m
r_c	Centroidal distance of an element	m
R_m	Magnetic Reynolds number ($\mu\sigma Vl$) or cell magnetic Reynolds number ($\mu\sigma Vh$)	

T	Period	sec
t^n	Old time level	sec
t^{n+1}	New (present) time level	sec
Δt or δt	Time step size	sec
u, v	local coordinates	
u_{nl}	Gauss points	
V	Probe velocity	m/sec
V_x , V_y , V_z	x, y, z component of probe velocity	m/sec
ΔV	Velocity step size	m/sec
W	Total stored energy in the finite element region	Joule
W_i or W^T	Weighting function	
W_{nl}	Weights used in Gaussian quadrature	
Z	Coil impedance	Ohm
z	Coordinate in the cartesian (x,y,z) or cylindrical (r,θ,z) coordinate system	
ω	Angular frequency ($2\pi f$)	Radian/sec
μ	Magnetic permeability ($\mu_o\mu_r$)	Henry/m
μ_o	Permeability of free space	Henry/m
μ_r	Relative permeability	
ν	Reluctivity ($1/\mu$)	m/Henry
ν^*	Artificial reluctivity	m/Henry
ε_o	Permittivity of free space	Farad/m
σ	Electrical conductivity	mho/m
α	Degree of upwinding	
δ	Skin depth ($1/\sqrt{\pi f\mu\sigma}$) or variation	m
$\vartheta(\cdot)$	Time truncation error	

ξ	Amplification factor in stability analysis or moving coordinate	
λ	Wave length	m
Φ	Electric scalar potential	Volt
θ	Time weighting factor or angular coordinate	
$\times$	Cross product	
$\cdot$	Dot product	
∇	Differential operator	
$\nabla\times$	Curl operator	
$\nabla\cdot$	Divergence operator	
$[\ ]^{-1}$	Inverse of a matrix	
$[\ ]^{T}$	Transpose of a matrix	

* Note : Primed variables denote the quantities measured in the moving coordinate system. Symbols not mentioned above are explained in the text.

ACKNOWLEDGMENTS

I would like to express my deep gratitude to my advisor, Dr. William Lord, for his invaluable guidance, support and encouragement throughout the graduate program. He is a respectable person for me not only as a professor but also as a senior of life.

I would like to extend my thanks to Dr. Satish Udpa and Dr. Lalita Udpa for sharing their rich knowledge and helpful discussions. I am also indebted to my former advisor, Dr. S. R. H. Hoole at Harvey Mudd college, for opening the world of numerical analysis to me, and to Professor David L. Atherton at Queen's University for his suggestion on the transient analysis.

I would also like to appreciate Dr. Vijay Vittal, Dr. Steve F. Russell and Dr. Frank Rizzo for willfully taking the time to serve on my graduate committee.

I would particularly like to express my thanks to my parents and family for their encouragement and support. Thanks are also due to my wife, Nam-Soon, whose support and patience made my graduate study very comfortable. During the period of writing this dissertation, I was happy to see my son, Seung-Jae, speak unexpected sentences and my daughter, Gina, begin to stand up. I thank them for waking up frequently at midnight to let me have a break.

Grateful acknowledgments are made to the American Gas Association for their support, and to Mr. and Mrs. Palmer for creating the Palmer Professorship, through which I was supported.

CHAPTER I
INTRODUCTION

A. NDE - General Considerations

Ever since people realized that they and their products may fail, they have recognized a need to inspect their products in order to prevent failures. These failures are related not only to economic losses but also to human lives and environmental issues.

There are two large groups of testing methods; one is destructive and the other is nondestructive. Destructive testing falls into two basic categories. The first is limit testing to the equipment's failure point, to ascertain safety margins and the most extreme conditions under which the equipment will perform its basic functions. The other is environmental testing under real life conditions, to see how reliably the equipment can withstand the rough handling of transportation, installation, and operation [1]. While the results of the destructive tests often end up in the dumpster, the requirement of nondestructive testing (NDT) is to inspect and evaluate materials or products without adversely affecting their serviceability [2]. In this respect, the practical benefits of nondestructive inspection are obvious, as long as the results are reliable and the inspection is cost-effective. Also, compared to conventional destructive testing on only a selected sample of the product, NDT techniques can be used on every sample to find random defects and discontinuities.

NDT serves not only to ensure quality in manufacturing processes but also to monitor the reliability and safety of the product after continued use, throughout its operational life. Because of this extended application and the expanded role of making accept/reject decisions, a newer term, 'non-destructive evaluation (NDE)' is coming into use [3]. Sometimes the two terms are used equally and interchangeably, while on other occasions they are not. NDT implies the testing procedure itself, whereas NDE involves the subsequent description of any detected flaws. From this, a decision is made on the serviceability of the tested item based on predefined standards or background knowledge. This decision is made by the designer so that it is very important for him/her to have such knowledge. A properly conducted design, as an another example, should ensure that an object is made in such a way so as to facilitate the use of the selected methods of testing. With the development of data analysis by computer together with pattern recognition and neural network methods, it is possible to analyze NDT data directly, in terms of component acceptability, so that the equipment can be programmed to produce a decision. These methods should therefore be described as NDE rather than NDT. In this dissertation, however, the term NDE is adopted because it generally represents the broadest definition of both testing and evaluation.

An important aid for monitoring and decision making is the use of computer modeling techniques to predict relationships between defect size and the signal indicated by an appropriate detector. These techniques are also of great value in the design of NDT instrumentation and the choice of its optimum operating conditions [4].

NDE has gained in importance as a result of the rapid technological progress made during the past half-century in areas such as aerospace and nuclear energy, in which there are high risks, and strict precautions are required to avoid catastrophic failure. It also forms a vital part of programs in various industries such as oil and gas, transportation and ordnance. In order to meet the requirements of the diverse range of applications, a variety of basic physical principles have been used for NDE. In general, all methods of NDE rely on some form of energy as a probing source to interact with the specimen under test and produce an output response signal which is then analyzed and interpreted in terms of specimen properties [5]. A general NDE procedure can be summarized in five essential steps as shown in Figure 1.1.

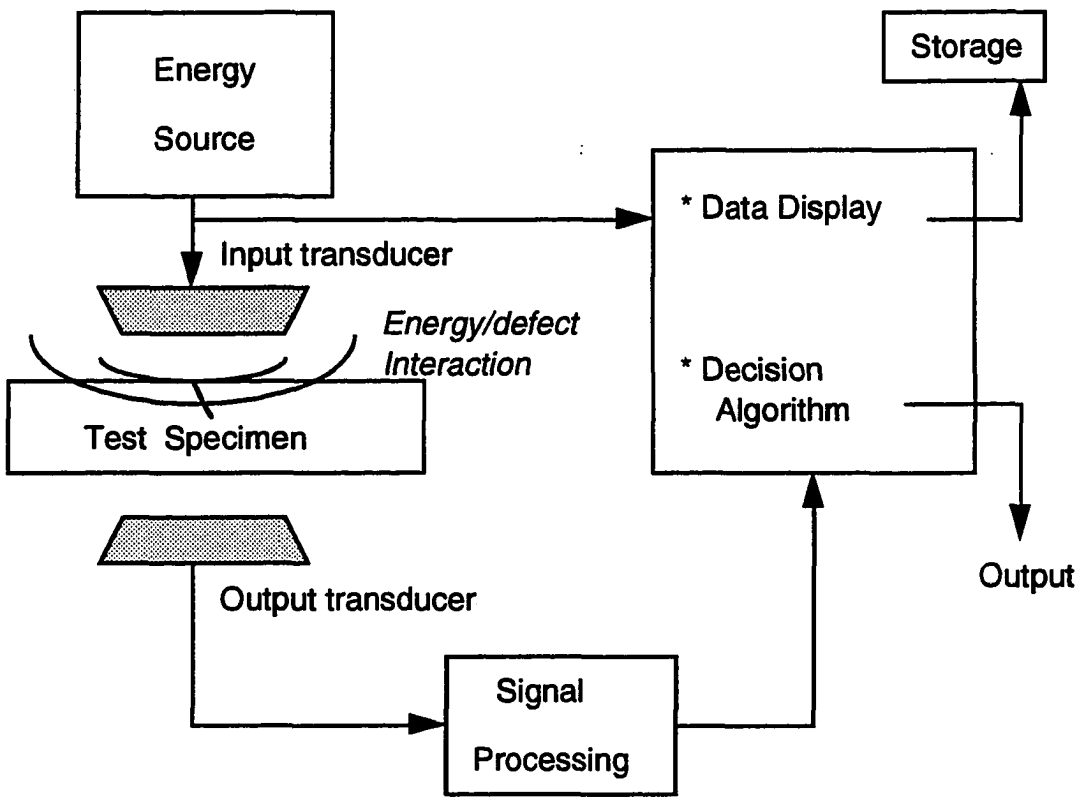

Figure 1.1. The generic NDE system (after Lord [5])

In practical situations, the interpretation of the output signal is the most important problem as the signal carries information about the defect. The size, shape and location of the defect, material inhomogeneities and property variations will affect the signal. This problem of deducing the defect information from the signal, commonly referred to as the 'inverse problem', is central in NDE and it can only be solved satisfactorily if appropriate theoretical models are developed, which are capable of generating defect signals given a certain defect size, shape and location (i.e. forward problem). This forward problem is therefore equally important in that it provides valuable training data for the inverse problem. Defect modeling studies are consequently very important since it is extremely difficult to replicate realistic defect shapes in a laboratory environment and it is seldom possible to describe energy/defect interaction in a closed form due to the presence of defects [6]. In addition, these models provide valuable insight into the nature of the physics involved in the interaction.

In general, the various NDE techniques can be placed into two categories: passive and active [7]. The passive techniques are those that monitor the item in question during a typical load environment and attempt to determine the presence of a defect through some reaction of the specimen. Acoustic emission, noise analysis, leak testing, visual inspection, and some residual magnetic flux leakage methods fall into this category. The active techniques, on the other hand, are those where something is introduced into or onto the specimen and a response is expected if a defect is present. Electromagnetic methods, ultrasonic methods and radiographic methods fall into this category. This dissertation, however, confines its attention to

electromagnetic methods in general and concentrates on the active magnetic flux leakage method in particular.

The choice of the method of testing depends on factors such as the type of material and its dimensions, the environment, the positions of interest within the structure or component under examination, e.g. whether internal or surface defects are sought, and the suitability for data acquisition and processing. For example, the magnetic method has been known to be more useful than the ultrasonic methods in the case of oil pipeline inspection since the nonhomogeneous wax products inside the oil pipe can have a significant attenuating effect on ultrasonic signals and the ultrasonic method cannot cope with thin wall pipes [8]. In general, a combination of two or even more methods may be required for the complete inspection of an object. This does not imply that they may be regarded as being alternative techniques because one of the methods can be used to complement another or to verify the findings of the other. Whatever methods are used, even when pre-specified, the test specimen should first be thoroughly inspected by eye and by touch because valuable equipment and time may be wasted in locating defects that could easily be identified with the unaided eye and hand in the first instance.

B. Electromagnetic NDE

Traditional electromagnetic NDE methods include magnetic particle inspection, the magnetic flux leakage method, eddy current methods, DC and AC potential drop methods, and the microwave method. Magnetic particle and magnetic flux methods are normally used only for testing ferromagnetic

materials. The eddy current methods are normally restricted to the testing of good electrical conductors. Microwave testing is usually restricted to examining dielectric materials but potential drop methods can be used for testing semiconductors as well as good electrical conductors. These methods cover a wide range of frequencies from DC to microwave. However, the common industrial techniques are limited to active DC, residual and eddy current forms of excitation; all low frequency phenomena for which displacement current effects can be neglected [6]. These can best be described by their relation on the B/H characteristic curve as shown in Figure 1.2.

In the active magnetic flux leakage test [9-12], a test specimen is magnetized by passing an appropriate value of DC current through it, thus setting up a magnetic field governed by the Maxwell-Ampere law.

$$\oint_c \bar{H} \cdot d\bar{l} = \iint_s \bar{J} \cdot d\bar{s} \tag{1.1}$$

The presence of a defect in a magnetized ferromagnetic material results in a redistribution of magnetic flux lines in the vicinity of the flaw, causing some of these flux lines to leak out into the surrounding medium. This is because the flaws represent an increase in reluctance to the magnetic flux lines [13]. In the course of excitation, each point in the specimen is magnetized to different H values (points 'A' through 'C') along the initial magnetization curve in Figure 1.2.a).

When the driving current is removed, the working points of each internal element relax to either a remanent flux density point or, in the case of those elements close to an open defect, to a point in the second quadrant of the material's B/H loop (Figure 1.2.b). A defect can then be viewed as a permanent magnet with residual leakage flux from the defect surfaces

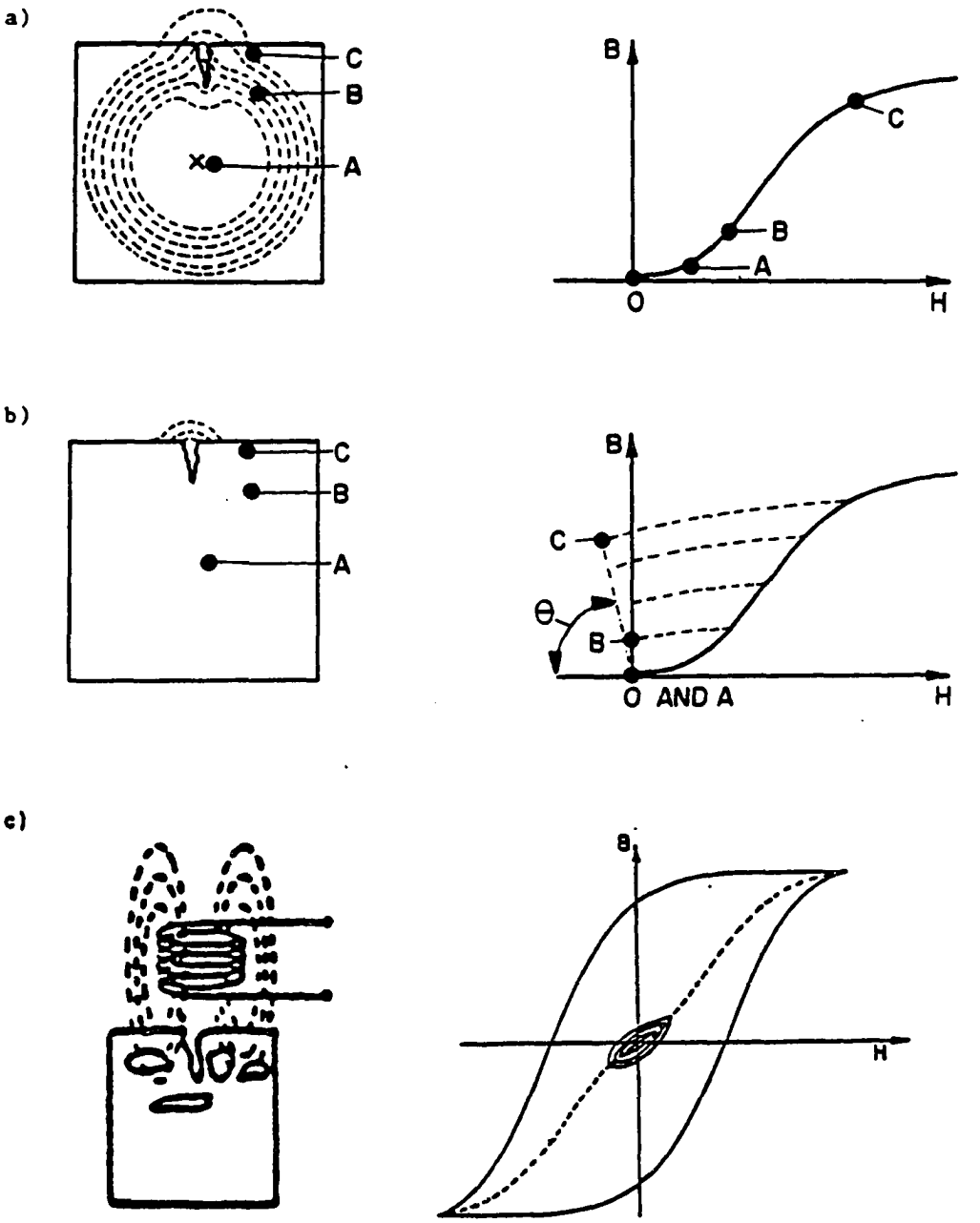

Figure 1.2. Classification of low frequency electromagnetic NDE methods; a) Active magnetic flux leakage field, b) Residual leakage field, c) Eddy current (after Lord [6] and Heath [15])

extending into the surrounding atmosphere [13]. The treatment of this residual leakage field requires a careful consideration of the demagnetization process [14-17].

Both the active and residual leakage fields can be picked up by scanning the surface with any flux sensitive transducer such as a Hall element [18,19], magnetic tape [20,21], or a coil [22]. Traditionally, magnetic particles have been used for residual cases because of their inherent sensitivity and the simplicity of the test, but the results tend to be qualitative rather than quantitative and do not lend themselves readily to automation in the signal processing sense [13]. A typical Hall probe active leakage field profile obtained by measuring the normal component of the leakage fields around a rectangular slot is given in Figure 1.3.

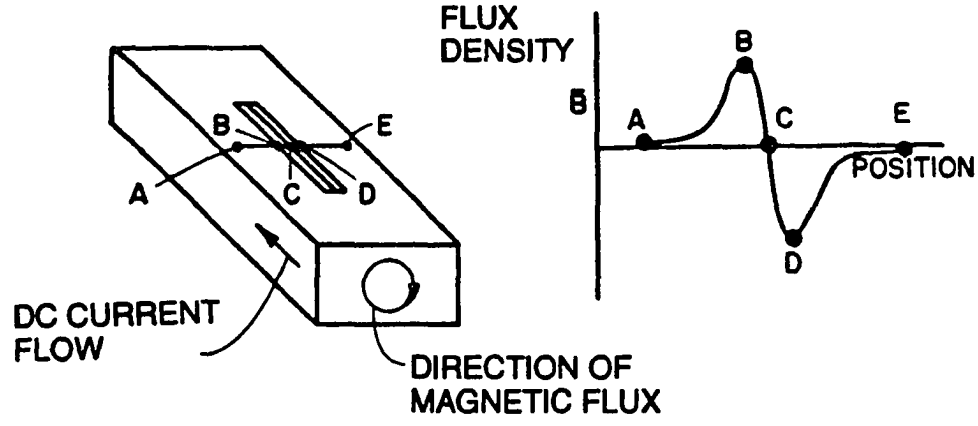

Figure 1.3. Active leakage field profile around a rectangular slot

In the active magnetic flux leakage test, care has to be taken to ensure that the direction of the resultant field is normal to the defect orientation. Another difficulty is the problem associated with handling the high DC current needed to magnetize large ferromagnetic specimens. To eliminate such problems, many techniques have been developed for inducing a magnetic field within a specimen by non-contacting means [23-26]. These non-contacting methods are also very helpful in saving inspection time. One of the techniques developed is the use of a variable reluctance probe [26]. The explanation of this probe is given in section A, Chapter II.

In eddy current methods [2,4,27-31], a low frequency (typically below 10 MHz) electromagnetic field produced by a coil carrying an alternating current, forms the probing source. The excitation levels are usually low and therefore for ferromagnetic materials, the operating point is around the origin of the B/H curve (Figure 1.2.c). When the coil is brought close to an electrically conducting test object, the time-varying magnetic field interacts with the test object according to the Maxwell-Faraday law,

$$\oint_c \bar{E} \cdot d\bar{l} = -\iint_s \dot{\bar{B}} \cdot d\bar{s} \tag{1.2}$$

thus inducing eddy currents in the medium. These secondary currents produce their own magnetic field which opposes the changes in primary field in accordance with Lenz's law. In the case of a nonferromagnetic specimen, this results in a reduction in the net flux linkages associated with the coil which, by definition, reduces the inductance of the coil. The resistance of the coil, on the other hand, increases because of eddy current losses within the material. The impedance of the excitation coil in air would therefore be different from that of the coil in the vicinity of the specimen. For

ferromagnetic materials, counteracting the decrease in inductance due to the influence of eddy currents induced in the specimen is the increase in inductance owing to the higher permeability of the material. The latter effect is more predominant and consequently the inductance of the coil increases when it is brought close to a ferromagnetic specimen. The change in inductance is accompanied by an increase in resistance due to the eddy current losses. Since the eddy current distribution is influenced by discontinuities or anomalies in the material thereby changing the total flux linkages and altering the impedance of the coil, all the electromagnetic properties of the test specimen are reflected back into the impedance of the coil. The changes in the complex probe impedance can be measured by an appropriate AC bridge as shown in Figure 1.4 and these measurement can be analyzed to estimate the surface and bulk properties of the specimen.

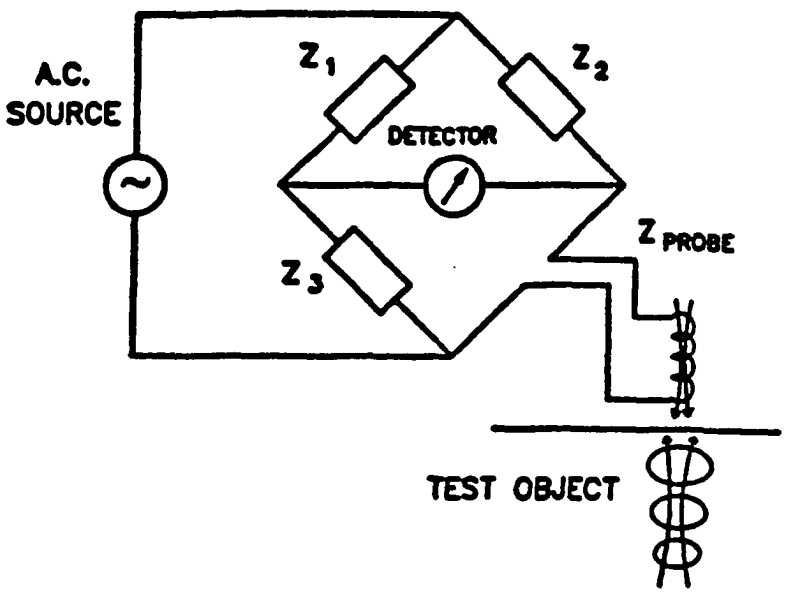

Figure 1.4. Measurement of eddy current probe impedance changes (after Udpa [31])

In practice, the variation of impedance is often displayed on a two dimensional complex plane. Since the horizontal and vertical data can be interpreted as the resistive and reactive components respectively of the complex impedance under steady state AC conditions, the eddy current test signal obtained is referred to as the impedance plane trajectory. Figure 1.5 shows the liftoff impedance plane trajectories of a coil over nonferromagnetic and ferromagnetic specimens [32].

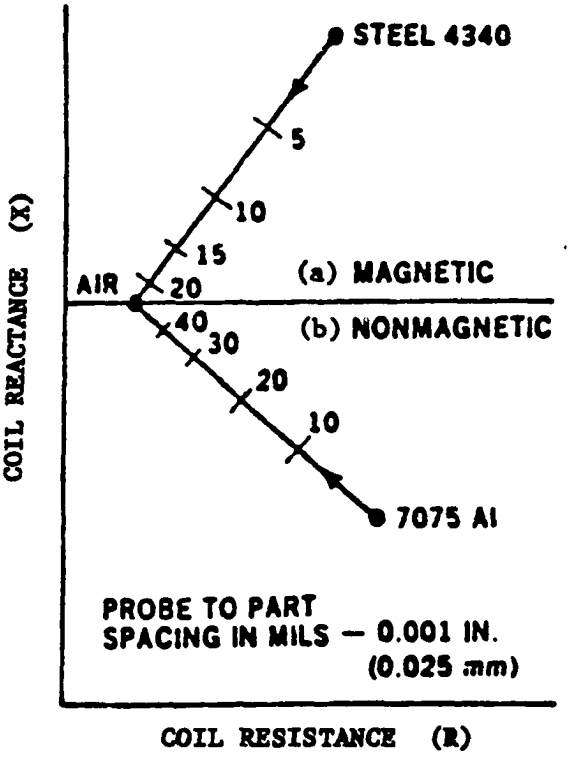

Figure 1.5. Liftoff impedance plane trajectory of a coil over a
a) Ferromagnetic specimen,
b) Nonferromagnetic specimen
(after Hagemaier [32])

However, there are some difficulties in using an absolute coil. The factors that affect the eddy current characteristics are not only material and dimensional properties but also coil properties such as magnitude and frequency of the excitation current, geometry of the coil, liftoff, and core material properties. This abundance of properties affecting the test means that the effects of multiple properties may be superimposed. Isolating the effect of one particular property can be very difficult. The coil impedance changes due to defects are often very small compared to the quiescent value of the coil impedance and these are superimposed, so that it can also be difficult to detect such small changes. Changes in the coil parameters due to environmental effects (e.g. temperature variations) can often mask changes due to defects, making signal interpretation very difficult. For this reason, many methods have been developed, among them the use of phase sensitive techniques [33], pulsed excitation [34,35], and multi-frequency and multi-parameter methods [36,37]. A variation of the absolute probe, which also overcomes these difficulties, is the differential eddy current probe and the details of this probe are given in section B, Chapter II.

Another difficulty in eddy current testing is due to the skin effect phenomenon. The skin effect restricts the deep penetration of eddy currents into conducting, ferromagnetic materials so that the conventional eddy current method is classified as a surface defect detection technique. In the testing of underground pipelines, where an inner diameter (I.D.) eddy current probe is preferred due to the limitation of accessibility, this effect may limit the eddy current method to the detection of I.D. defects and prevent the detection of outer diameter (O.D.) defects if the wall thickness of the pipe is

large enough. For this reason, the magnetic saturation technique using a permanent magnet has been developed to reduce the relative permeability of the tube to unity and increase the penetration depth [38]. Another breakthrough is the use of the remote field eddy current technique which is equally sensitive to both I.D. and O.D. defects. The remote field eddy current probe is explained in section C, Chapter II.

All the methods to be discussed in this dissertation employ non-contacting probes and they are the variable reluctance probe (active magnetic flux leakage method), the differential eddy current probe and the remote field eddy current probe (eddy current methods). These probes have been used in heat exchanger tubing and oil/gas pipeline inspection, so that the geometries of interest are axisymmetric.

C. Velocity Effects of Electromagnetic NDE Probe

The fact that most electromagnetic NDE tests can be carried out in a noncontact way permits rapid, moving inspection. Traditionally, in-line inspection of oil and gas pipeline is accomplished by a pig [39] which consists of permanent magnets to magnetize the pipe, measuring equipment and signal recording devices. This pig is pumped from one compressor station to the next, which may be up to 100 Km away [40,41]. Typical pig speeds used in pipeline inspection are from 4 to 5 meters per second in the magnetic flux leakage method [8]. Even though eddy current methods do not use high speed (up to 1 to 2 feet per second), the remote field eddy current probe for oil and gas pipeline inspection [41-44], is expected to use high speeds for testing miles

of long pipelines. However, employing these fast speeds requires careful study as moving magnetic fields induce $\sigma\overline{V}\times\overline{B}$ currents (motional induction) in all exposed conducting surfaces, thus affecting the NDE signals. For example, the magnetic flux leakage method, which is mainly concerned with the inspection of ferromagnetic material, is known to be oversensitive to the velocity of the inspection vehicle [8]. To model actual field testing situations, it is therefore necessary to include such probe velocity effects in the energy/defect interaction models for correct interpretation of the NDE signals.

The investigation of probe velocity effects was a part of the parameter variation studies in the AGA (American gas association) project on the remote field eddy current effect [43]. Recently, GRI (The Gas Research Institute) has established an NDE research and development program on the characterization of magnetic flux leakage indications recorded during in-line inspection. The first task is the identification and investigation of the effects of operational variables, including the test rig velocity [45]. Work has been done on probe velocity effects in NDE [40,46-55]. However, most research on moving magnetic field problems has been carried out in other areas rather than NDE, such as electric machinery [56-62], electromagnetic levitation [63-78], electromagnetic launcher [78-81], and electromagnetic brakes [82,83]. A review of previous approaches should, therefore, include their treatment of motional induction phenomena. Before this, a discussion of the numerical methods is in order since a majority of the reports resort to numerical techniques for their analysis.

D. General Considerations on Numerical Methods

Basic electromagnetic NDE phenomena can be fully described by the classical Maxwell equations [84,85]. Magnetostatic NDE such as magnetic particle, magnetic flux leakage, perturbation, variable reluctance and DC potential drop methods are described by either Laplace or Poisson equations, all elliptic partial differential equations. Quasi-static NDE includes single frequency, multi-frequency, pulsed and remote field eddy current techniques and all operate at excitation frequencies well below the region where displacement current densities are a factor, thus resulting in a parabolic diffusion equation. In a steady state AC situation, the parabolic governing equation can be reduced to an elliptic partial differential equation by using phasor notation. At microwave frequencies, a hyperbolic wave equation governs microwave interactions with non-conducting materials such as ceramics and composites. However, closed form solutions to the above equations are available only for very simple shapes or under simplifying assumptions. The applications associated with NDE problems such as frequency dependency, nonlinear material properties, and complex boundaries render such analytical approaches impossible.

Considering inverse problems, ideal training data are those from experiments using defects of known sizes and shapes. In reality, the optimization of a new test requires a series of experiments, often too difficult or expensive to replicate in a laboratory environment. Also, many variables involved in a test make even the simplest test hard to design.

Some numerical methods are however inherently flexible and capable of producing training data in which material nonlinearities and awkward boundaries are already taken into account. They are also of great value in the design of NDT instrumentation and the choice of its optimum operating conditions. Most importantly, they provide valuable insight into the underlying physics involved in the energy/defect interaction. One example of this is the interpretation of remote field eddy current phenomena [41]. Remote field eddy current technique has been used for more than 30 years and the interpretation of experimental observations had been based on an hypothesis until the early 1980s. The hypothesis states that there are two possible energy-coupling mechanisms between the exciter coil and an internal detector; one is direct coupling near the exciter and the other is indirect coupling occurs beyond about 1.8 pipe diameters from the exciter as a result of the through-transmission of eddy currents. This hypothesis was later confirmed and new phenomena ('potential valley' and 'phase knot' explained in section C, Chapter II) were found inside the pipe wall by the application of the finite element method in a relatively short time [41,43]. Experimental means would never have found such phenomena inside the pipe wall.

There are several numerical methods that are in use in electromagnetic NDE. The oldest is the finite difference method where domains and differential operators are replaced by a discrete grid of nodes and difference quotients using the Taylor series expansion. The formulated difference equations are solved usually by an iterative relaxation scheme to obtain the solution at each node [86]. The method suffers from a drawback in that

rectangular grids tend to be inefficient when irregular geometries are encountered. Increasing the mesh density does not minimize the error beyond a certain lower bound in some cases [87]. Moreover, open boundaries have to be modeled by a closed boundary with artificial boundary conditions.

In contrast to analytical mathematics where differentiation is usually considered simpler than integration, in numerical analysis, differentiation is more difficult to handle than integration because of stability considerations [31]. Based on this observation, the finite element method replaces the problem of differentiation by one of minimizing the integration of a functional or a weighted residual. The solution region is discretized into elements and within each element, the unknown function is approximated by an interpolating polynomial. This approximation is substituted into the functional or weighted residual and then minimized with respect to every nodal value. Actual minimization is performed element by element for convenience instead of node by node. These individual element equations are combined into a single global matrix equation. Any of the direct solution techniques utilizing the banded nature of the matrix or the iterative solution techniques utilizing the sparse nature of the matrix can be used.

The method is flexible and able to model relatively realistic defects and nonlinear material properties, but as is true of all domain methods it has some difficulties regarding mesh discretization and boundary conditions, especially for large, intricately-shaped 3-D geometries containing relatively small defect shapes [88] and open boundaries. To avoid the excessive requirement of computer resources, many techniques have been developed such as zooming [89], transform of infinite domain [90], infinite elements [91-

94], ballooning [95], and various formulations utilizing scalar potentials [30,96-102]. The problems encountered in the solution of probe velocity effects are somewhat similar to those difficulties, in that spurious oscillations occur in the solution if the element size is larger than a certain small limit [50]. One of the objectives of this dissertation is to remove such oscillations when an element size larger than the limit is used.

Another method which has attracted attention due to its few equations for solution (in view of the reduction in dimensionality by 1, such as from a volume to a surface or from a surface to a boundary line) and ease in treating open boundary problems, is the boundary integral method [86,103-105]. The first goal is to generate an equation containing integrals over the boundary of the domain of interest. This can be achieved by the application of Green's second identity, for example, in two dimensions,

$$\iint_S (G\nabla^2 A - A\nabla^2 G)ds = \int_L (G\frac{\partial A}{\partial n} - A\frac{\partial G}{\partial n})dL \tag{1.3}$$

where n is the normal direction on L, and A and G are substituted for the unknown function and the free space Green's function, respectively. Another approach is to use a weighted residual formulation and apply integration by parts and Green's theorem twice. The Green's function is again used as a weighting function. Both methods result in the same boundary integral equation. This equation is solved by a numerical technique, called the boundary element method. Boundaries, whether a surface or a line, are discretized into elements and if there is a source term, the interior of the boundary (whether a volume or a surface) also has to be subdivided into a second mesh to define the source so that it can be numerically calculated.

From the solutions of A and $\partial A/\partial n$ or any given values at the surface, it is possible to obtain, by integration, the solution at any point in space.

The limitations of this method are such that it can be applied only to those problems whose Green's function can be found, the matrix is fully populated and unsymmetric so that storage demands are heavy on the computing environment. The work involved increases with the number of points of interest and when inhomogeneous material is encountered. Also, some difficulties are expected in handling nonlinear, anisotropic materials as the Green's formulation presupposes the principles of superposition. Thus, it is in three-dimensional constant coefficient problems that the boundary element method strongly challenges the finite element method.

From an NDE perspective, the choice of numerical method depends on the NDE technique used. Many NDE applications require solutions at only a few points. In this case, the boundary integral approaches are very efficient. This is particularly obvious for the potential drop method [106-108] where only two field points are needed for an estimation of the potential drop. The comment also holds for other electromagnetic NDE methods, as the active sensor volume tends to be small compared to the overall testing geometry. However, if a major objective is to gain a fuller understanding of the underlying physics from the associated field distributions, finite element solutions are very useful in that they give full field solutions [85]. Perhaps the best choice may be the hybrid finite element-boundary integral methods [109-111] which exploit the advantages of both methods. That is, the boundary integral equations are used in the exterior and the finite element equations in the interior of a problem, with some kind of matching at the common

boundary. Such an approach could well combine the 3-D modeling capability of the boundary integral technique with the power of the finite element method to handle nonlinearities and anisotropy.

E. Review of Related Literature

The geometries related with NDE research are more complex than electric machines or other devices since they include material inhomogeneities. For example, the rail geometry of a magnetic levitation vehicle is uniform while the geometry to be modeled in steam generator tubing inspection is not uniform due to defects and support plates. This is shown in Figure 1.6.

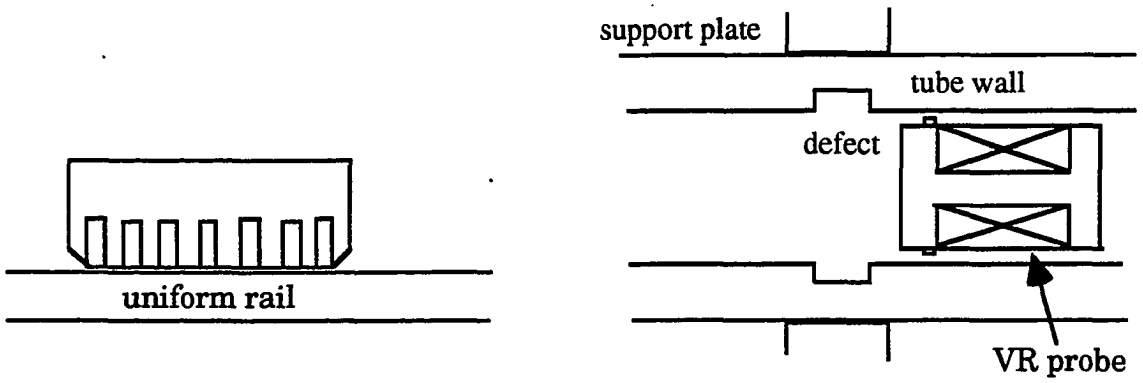

Magnetic levitation vehicle	Inspection of steam generator tubing
Uniform geometry	Non-uniform geometry
Steady state situation	Transient situation

Figure. 1.6. Comparison of uniform and non-uniform geometries

When the testing material has uniform geometry, the distribution of motionally induced current is always the same regardless of the probe position, and thus time, unless the probe velocity changes. This corresponds to a steady state situation. However, if the testing material is not uniform, the distribution of motionally induced current will be different at each probe position, thus at each time. This corresponds to a transient situation if DC or low frequency AC is used as an excitation.

The same observations are made in the literature [70,73,83] where it is noted that the steady state solution is possible only in cases in which the moving member is homogeneous and of constant cross section in the direction of motion. An application which did not consider the difference in geometries, can be found in the example of Enokizono's paper [112] where a boundary element formulation for a steady state governing equation is applied to an NDT geometry with a defect. A correct application is discussed in Jayawant's book [76] on electromagnetic levitation and suspension techniques. In the case of a magnetic suspension system, transducers are required for the measurement of position, velocity and acceleration. One of the transducers used is the inductive transducer which shows an overcompensated response when a step change in the rail geometry is encountered. Jayawant [76] explains this phenomena as the effect of the eddy currents induced in the rail being superimposed on the straightforward increase of inductance arising out of airgap reduction. The situation and response shown in Figure 1.7, clearly indicate the transient behavior even though such a response is not desirable for the measurement of air gap distance. Therefore, the study of NDE probe velocity effects should take any

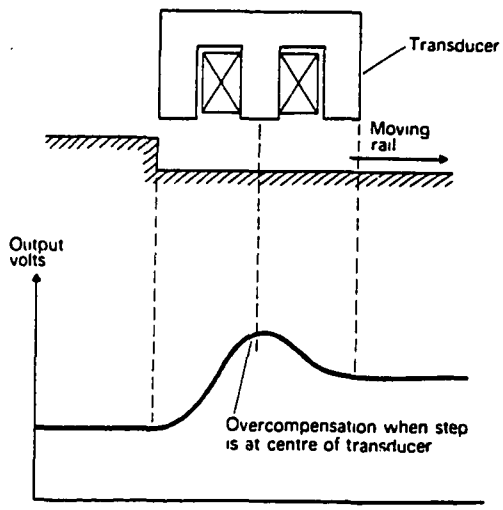

Figure 1.7. Response of an inductive position transducer to a step in the rail (after Jayawant [76])

geometry difference into account. Unfortunately, there has been almost no study on probe velocity effects with non-uniform geometries. However, since the steady state analysis of a uniform geometry can provide background knowledge when relative motion is involved and the transient analysis in that situation can readily be used for the nonuniform geometry, those studies are reviewed.

1. Steady State Analysis

In the inspection of an object with uniform geometry by the eddy current methods of NDE, the governing steady state equation for probe velocity effects can be written as

$$\nabla \times \frac{1}{\mu}(\nabla \times \bar{A}) = \bar{J}_s - j\omega\sigma\bar{A} + \sigma\bar{V} \times (\nabla \times \bar{A}) \tag{1.4}$$

where μ, $\overline{A}$, $\overline{J_s}$, ω and σ are the magnetic permeability, magnetic vector potential, applied current density, excitation frequency and the electrical conductivity, respectively. Since the derivation of the governing equation is given in Chapter IV, it is shown here without proof. The motional induction term appears as the first order spatial derivative. The governing equation is that form of convective diffusion equation which is not self-adjoint and has an unsymmetric operator due to the motional induction term. In this case, diffusion and convection effects compete with each other to govern the ensuing solution behavior [113]. It is well known that the standard domain numerical approaches, such as the finite difference method and the finite element method, show spurious oscillatory results for high magnetic Reynolds numbers ($R_m = \mu\sigma Vh$). To suppress such oscillations, many techniques have been developed. These various techniques for solving convective diffusion equations by the finite element method and the boundary element method are classified into several groups for convenience.

Mesh refinement

Employing the standard Galerkin formulation for 1-D, DC case of equation (1.4), the elemental matrix for an element of length h is given by

$$\begin{bmatrix} \frac{1}{\mu h} - \frac{\sigma V}{2} & -\frac{1}{\mu h} + \frac{\sigma V}{2} \\ -\frac{1}{\mu h} - \frac{\sigma V}{2} & \frac{1}{\mu h} + \frac{\sigma V}{2} \end{bmatrix} \tag{1.5}$$

where V is the probe velocity. As mentioned earlier, the matrix is unsymmetric and if the convection term is larger than the diffusion term, spurious oscillations occur [114]. Therefore, the condition for oscillation-free results is $1/\mu h > \sigma V/2$. This leads to $h < 2/\mu\sigma V$, the basis of mesh refinement. It also shows that the cell magnetic Reynolds number, defined as $R_m = \mu\sigma Vh$, should be less than 2. In some literature [74], the cell Peclet number instead of the cell magnetic Reynolds number is defined for the same purpose, or sometimes, it is defined as one half of the cell magnetic Reynolds number [71,73]. However, for certain situations, the refinement necessary is so excessive that the required computer resources are unusually large.

Self-adjoint transformation

The variational principle always produces a symmetric matrix. This symmetry is indeed a precondition for the existence of a variational principle and the equivalence between the variational principle and the Galerkin method can be established only under this condition [115]. The strange results of Ida's paper [116] are due to neglecting this fact where an energy functional that cannot be defined for the motional induction term was used with an upwinding quadrature point [117].

The governing equation is not self-adjoint, so it is not symmetric. Therefore, an energy functional approach requires it to be made self-adjoint. Usually, this can be done by multiplying some exponential factor to the governing equation [118]. Hulbert uses this procedure [119], and the exponential factor appears in the functional. Guymon et al. [120,121]

introduce another transformation that does not involve exponentials in the functional. Such a transformation is

$$\eta = A \exp\left[-\frac{\mu\sigma Vh}{2}\right] \tag{1.6}$$

The equation is first solved for η and then transformed back to find A. However, in general, the presence of the exponential factor with large R_m can make the inverse transformation ill-conditioned [122]. Also, most computers have certain limiting values for the argument of exponential functions. Thus, this technique is limited to highly diffusion-dominant transport equations only [123].

Upwinding technique (Petrov-Galerkin method)

The upwind scheme has its roots in the behavior of a convection dominant fluid. In such cases, a fluid property is determined to a large extent by the property prevailing immediately upstream [124]. Hence, the name, upwind. In the finite difference method (FDM), the combination of an upwind scheme for the convection term and a central difference scheme for the diffusion term has been used for stable results, but with some disadvantages in accuracy [125]. In the finite element method (FEM), upwinding corresponds to a weighted residual method. The standard (Bubnov) Galerkin method uses the shape function (N_i) as a weighting function (W_i) and reproduces central difference formulas with their inherent oscillatory behavior. On the other hand, the upwind scheme for FEM [126,127] uses a new, asymmetric weighting function which is biased to the upstream condition. It is also called the Petrov-Galerkin method. Figure 1.8 shows the

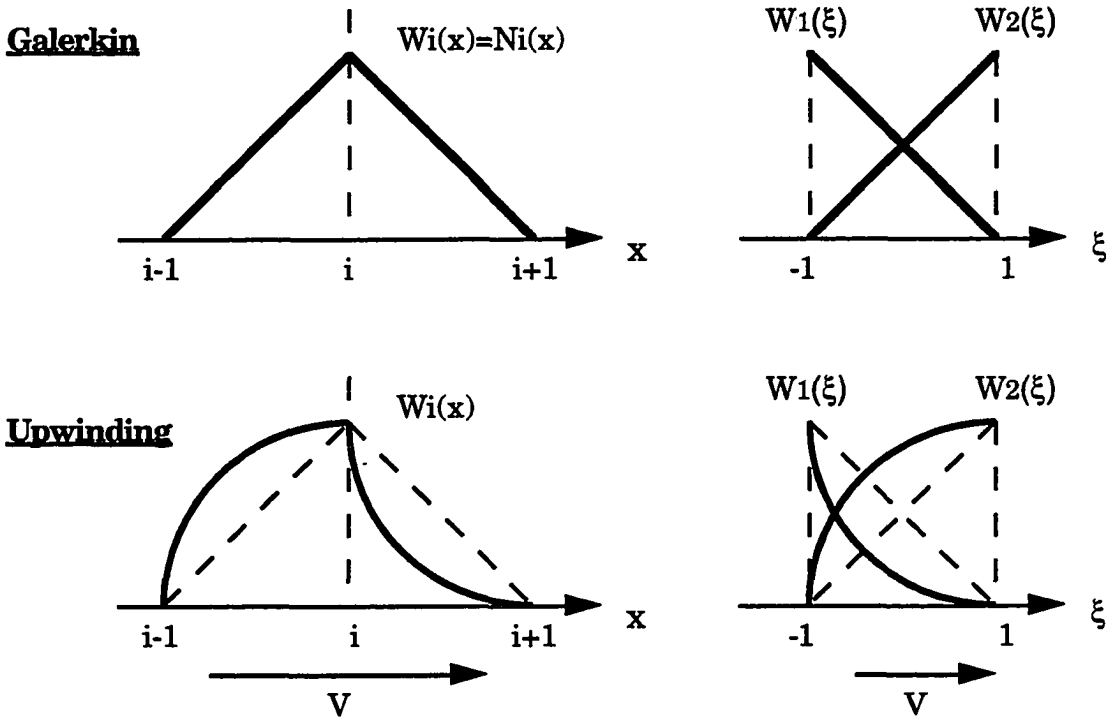

$$W_i(x,\alpha) = \begin{cases} N_i(x) + \alpha F(x) \text{ for element } (i-1);\ i \\ N_i(x) - \alpha F(x) \text{ for element } i;\ (i+1) \end{cases}$$

where $F(x) = \beta N_1(x) N_2(x)$ and $\int_0^h F(x)dx = \frac{1}{2}h$

Figure 1.8. Comparison of weighting functions

difference between the two weighting functions. Here, F(x) is some positive function, such that F(x) is zero at nodes and, for each element, satisfies the following condition.

$$\int_0^h F(x)dx = \frac{1}{2}h \tag{1.7}$$

Usually, these conditions are satisfied by using the shape functions, $N_1(x)$ and $N_2(x)$, and the coefficient, β, is decided by equation (1.7). α is the scaling

factor ranging from 0 (no upwind, standard Galerkin method) to 1 (full upwind, same as FDM), and is positive if the velocity is positive and negative if the velocity is negative. The optimal value of α is given as [126]

$$\alpha_{opt} = \left[\mathrm{Coth}\frac{R_m}{2}\right] - \frac{2}{R_m} \tag{1.8}$$

This optimal value can be controlled for each element to minimize the error.

The introduction of such a weighting function results in the additional artificial diffusion, i.e. an equivalent increase in the magnetic reluctivity by the amount of $\alpha\sigma Vh/2$ [128,129], thus reducing the magnetic Reynolds number, R_m, and stabilizing the solution, but at the cost of accuracy [74,130]. In other words, the upwinding process is equivalent to that of adding the artificial diffusion term to the coefficient of the second order derivative and applying the standard Galerkin method using linear, equal sized elements [129].

There is an alternative algorithm [117,128,131] based upon numerical quadrature techniques. The evaluation of the weighted residual integrals usually uses some quadrature rules. In this case, an inexact quadrature point displaced from the normal quadrature point, with the standard Galerkin formulation is used in evaluating the motional induction term. The location of the point on a local coordinate ($-1 \le \xi \le 1$) plays the same role as α in the previous approach. This formulation is simpler to implement and computationally more efficient. This upwinding technique seems to be the most popular approach for the motional induction problems as evidenced by the number of papers [46,51,52,54,71-75,79,80,82,83,132].

Techniques in the boundary element method (BEM)

The techniques used in BEM are basically the same as that of the self-adjoint transformation. In order to establish the boundary integral equation, a fundamental solution (i.e. Green's function) is necessary. In the process of finding it, some [133,134] transform the governing equation into self-adjoint form, while others [135-137] make the adjoint equation of the governing equation self-adjoint. Both transformations are the same except the sign change due to the adjoint relation. In any case, the final solutions are based on the fundamental solutions of the self-adjointed equations. This guarantees unconditionally stable solutions in the space domain. Again, ill-conditioning due to the exponential factor poses difficulties [137] and the same restriction on the size of the exponential argument applies as in the case of the self-adjointed variational FEM approach.

2. Transient Analysis

So far, steady state analysis in the uniform geometry has been discussed where the governing equations are based on a fixed coordinate system. In transient analysis, one can use the governing equation from the moving coordinate system where the $\overline{V} \times \overline{B}$ term does not appear in the equation. This looks promising since the motional induction term causes all the spurious oscillations. But, this approach involves extensive pre-processing and is laborious since the movement is taken into account by a moving mesh. That is, several meshes have to be created, one for each position, and then each solved in turn. Local remeshing is also possible to retain the same

mesh topology as long as is practical, and then re-mesh, joining nearest nodes on the moving interface. The idea is shown in Figure 1.9. The specific part in the obtained matrix which corresponds to the distorted mesh is recalculated at each time step [58]. This can produce distorted elements and loss of accuracy so that this technique should be used only for time periodic or transient movements and limited displacement [138].

In some rotating electrical machines working under unbalanced conditions or supplied by nonsinusoidal current, transient dynamic analysis is necessary. In order to avoid the above mentioned difficulties, Hoole [59] proposes a rotating adaptive mesh by applying the Delaunay criterion for optimality, Razek et al. [56,57] model the airgap using a Fourier technique and then couple to both rotor and stator, and Rodger et al. [60] and Marechal et al. [139] couple two boundaries with different numbers and locations of nodes by using Lagrangian multipliers while ensuring the natural continuity conditions of the physical quantities.

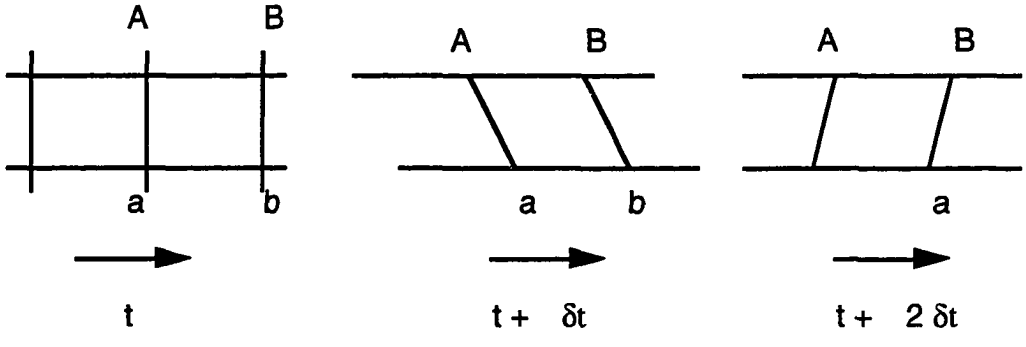

Figure. 1.9. Local remeshing of moving problems

There are a few transient analyses with governing equations from the fixed coordinate system. The upwinding techniques, originally developed from the steady state equation, are used with a time step algorithm [71,75,79]. A major criticism of this approach relates to excessive numerical dissipation [140]. Aldefeld [141] solves the two-dimensional diffusion equation with a nonperiodic source by the finite difference method. Forward time differencing is used for the motional induction term and backward time differencing for the other terms. This makes the matrix symmetric, but causes an additional error. The same methodology can be deduced from Muramatsu et al.'s work [70], where equations from the moving coordinate system and the fixed coordinate system are compared. They show that, in transient analysis, the velocity term can be obtained from the temporal derivative term of the moving coordinate system. According to this derivation, the velocity term has to be treated at the old time level, i.e. forward time differencing. Since the backward time difference method is used for all the other terms, these apparently different approaches are basically the same except that the former used FDM and the latter used FEM for spatial calculations.

Similar time step algorithms can be found in the literature of fluid mechanics. Donea [142,143] uses a Taylor-Galerkin method based on forward time stepping and an artificial diffusion-like term appears in the finite element formulation. In this formulation, however, the artificial diffusion term is thought of as part of the difference approximation. Zienkiewicz et al. [140,144,145] employ the method of characteristics and derive a similar, but more versatile time step method and an artificial diffusion term, which has

the same form as Donea's. The relationship between this time dependent artificial diffusion term and that found in the upwinding technique shows that the degree of upwinding, α, is equivalent to the grid Courant number. Leismann and Frind [146] introduce an arbitrary artificial diffusion term into the governing equation *a priori*, and use separate, unknown time weighting factors for the various terms. Errors are then investigated by choosing the midpoint between the old and new time levels as the origin of Taylor series. In the process of minimizing the errors, the expression for the artificial diffusion term is chosen and found to be the same as the former cases. Proper time weighting factors are also chosen in this process. Although their purpose is to achieve a symmetric matrix, this method can well be adapted to the study of probe velocity effects for electromagnetic NDE. This dissertation, thus, adopts Leismann and Frind's method and investigates the relationships with other methods.

F. Scope of the Dissertation

This dissertation is concerned with probe velocity effects for electromagnetic NDE. The variable reluctance probe exemplifying active magnetic flux leakage methods, the differential eddy current probe and the remote field eddy current probe exemplifying diffusion methods are considered for uniform axisymmetric geometries. For non-uniform geometries, transient analysis is required as explained earlier. However, output NDE signals in eddy current methods are such variables as impedance and phase that can only be defined under AC steady state

conditions. Therefore, only the variable reluctance probe is considered for non-uniform geometries.

Chapter II presents a detailed description of the three probes to be modeled and their applications without considering velocity effects.

Chapter III explains the use of the finite element method for spatial discretization and the finite difference method for temporal discretization, also without the motional induction term.

Starting with the Galilean transformation, the governing equation for probe velocity effects is derived and its characteristics and similarity with the convective diffusion equation found in fluid dynamics are explained in Chapter IV. The magnetic Reynolds number and the treatment of the motional induction term are also discussed.

In Chapter V, the upwinding finite element formulation is explained and probe velocity effects in the uniform NDE geometries are studied for the three probe cases.

Chapter VI compares various time step algorithms and results obtained by applying two of the algorithms, namely Donea's method and Leismann and Frind's method, are compared.

Chapter VII summarizes the work described in the dissertation and presents conclusions based on the numerical modeling experiences. Areas for future work are also included in this chapter, followed by a comprehensive list of references.

CHAPTER II

ACTIVE LEAKAGE FIELD AND EDDY CURRENT PROBES

One of the advantages of electromagnetic NDE methods, particularly those associated with magnetic flux leakage (MFL) and eddy current (EC) inspection, is that the probe does not need to contact the testing specimen. Thus, it allows for rapid moving inspection. For this reason, three kinds of noncontacting probes used in the inspection of axisymmetric geometries, are selected for the study of the probe velocity effect. These are the variable reluctance (VR) probe, the differential eddy current probe, and the remote field eddy current (RFEC) probe. The VR probe and the differential eddy current probe have been used for detecting the presence of magnetite and denting of steam generator tubes in pressurized water reactors [26,147,148] and the RFEC probe have been used for the measurement of wall thickness of oil well casing and pipelines [41-44]. However, these probes are also capable of detecting isolated pits and cracks [40,42,147]. Although a real MFL pig, which operates at high speeds to inspect steel pipelines, employs permanent magnets to induce a magnetic field from inside the tube, the basic principle of operation is the same as that of the VR probe. The VR probe is selected to study the probe velocity effect for MFL inspection because of this reason and the abundance of previous work experience on the probe [13,26,53,84,149-153]. The three probes are introduced in this chapter, but without considering probe velocity effects.

A. Variable Reluctance Probe for Active MFL Inspection

The nuclear power industry is concerned with the examination of steam generator tubing. Steam generators form an important link between the primary and secondary loops in a nuclear power plant. Heat generated by the nuclear reactor is absorbed by the primary coolant (water in the case of pressurized water reactors) and circulates through a number of Inconel tubes within the steam generator. The heat is transferred to a mixture of high pressure steam in the secondary loop which, in turn, drives the turbines. The heat exchanger tubes are supported by carbon steel support plates at regular intervals. A simplified schematic diagram of a nuclear power plant cooling system and a cross section of a steam generator are shown in Figures 2.1 and 2.2. Due to their intimate contact with the mixture of steam and water, the support plates tend to corrode over a period of time and the crevice gap between the support plate and the tube becomes packed with magnetite and other byproducts of corrosion. This eventually leads to denting and damage of tubes. Since damaged tubes result in contamination of the secondary coolant by the radioactive primary coolant, they represent a safety hazard and consequently damaged tubes are often plugged, leading to reduced operational efficiency and attendant loss of revenue. Early detection of magnetite buildup in the crevice gap region is, therefore, imperative if tube plugging is to be avoided and in order to take remedial measures such as chemical flushing of the steam generator [26,29].

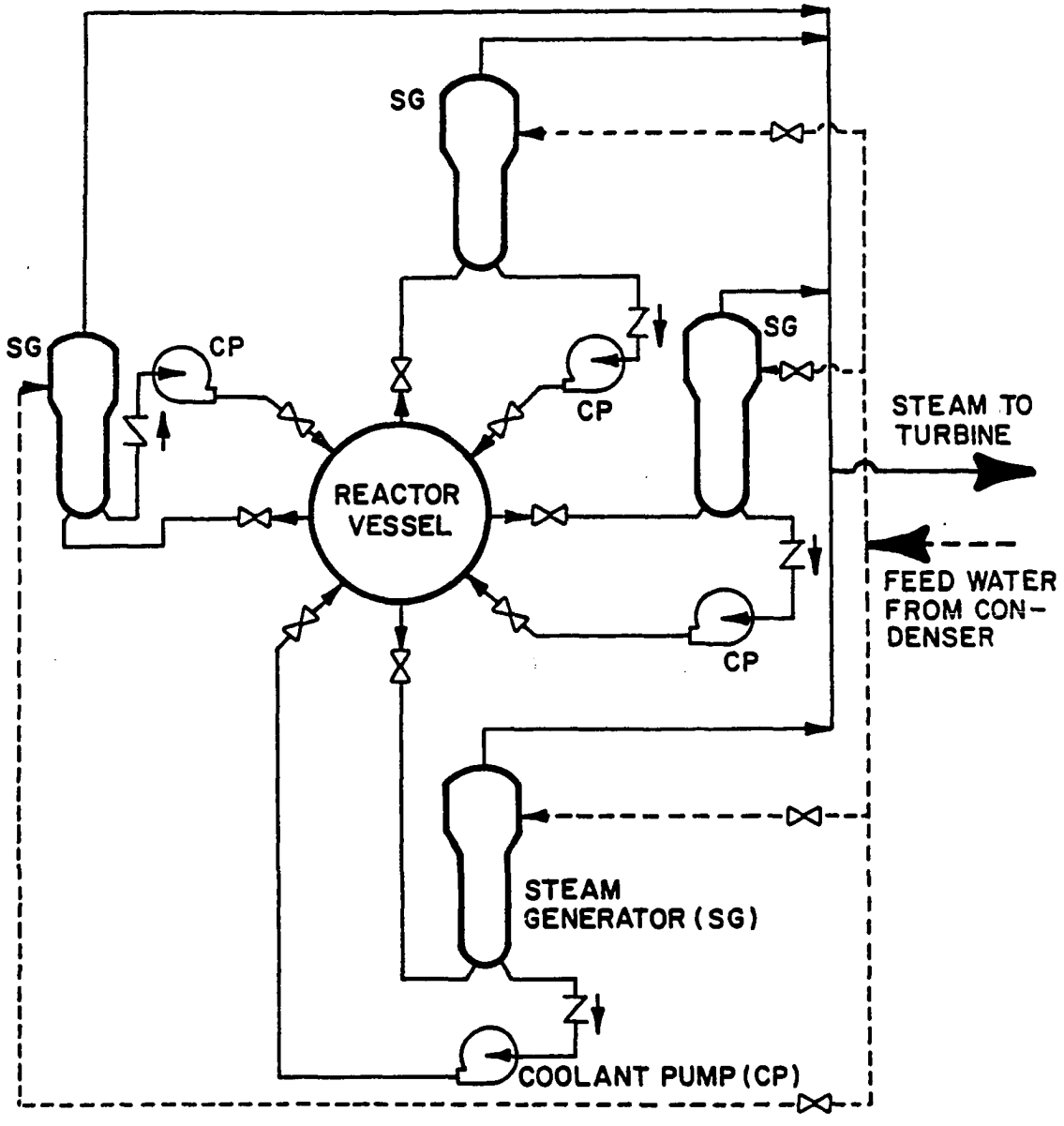

Figure 2.1. Simplified schematic diagram of a nuclear power plant cooling system (after Lord [147])

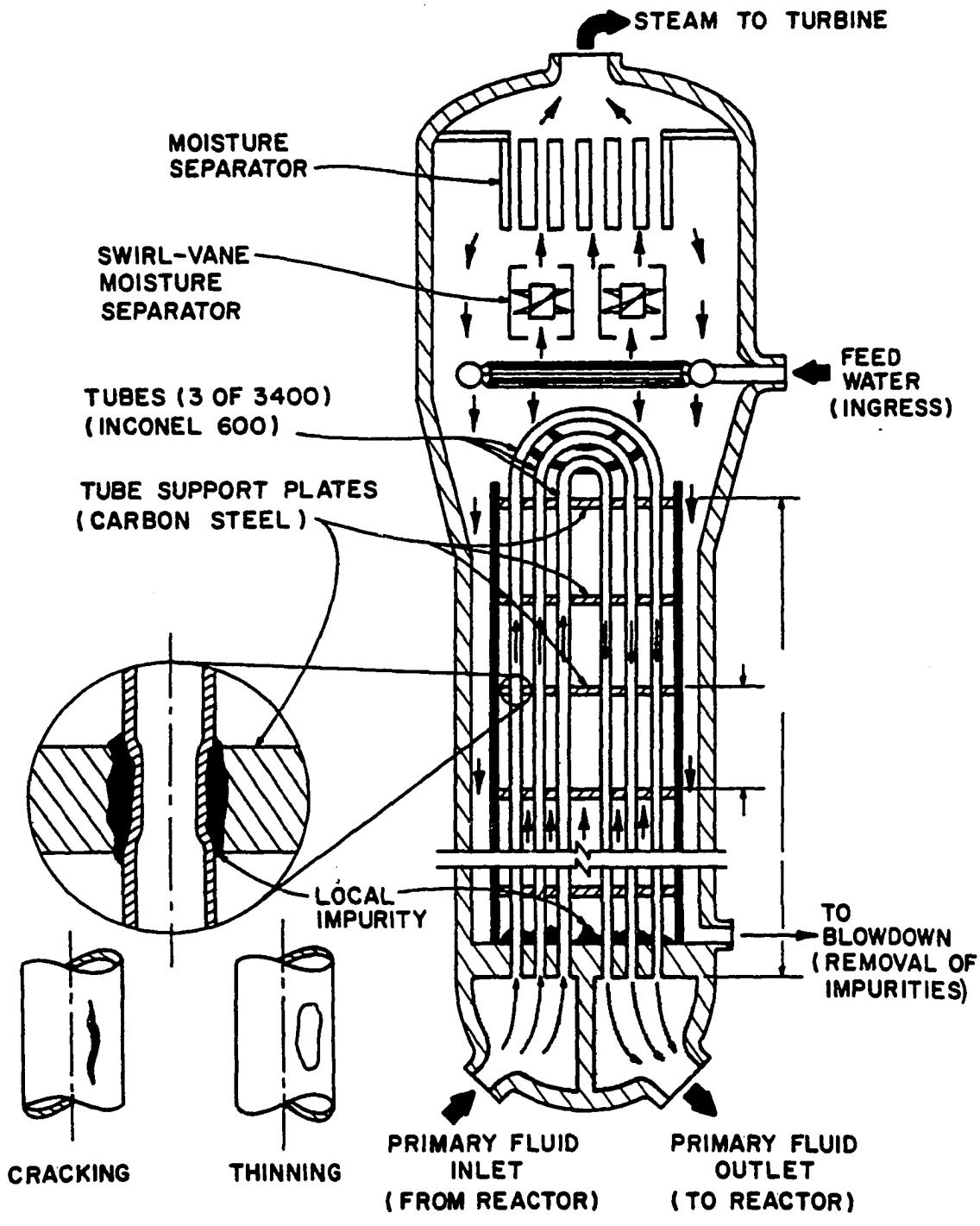

Figure 2.2. Cross section of a steam generator (after Lord [26])

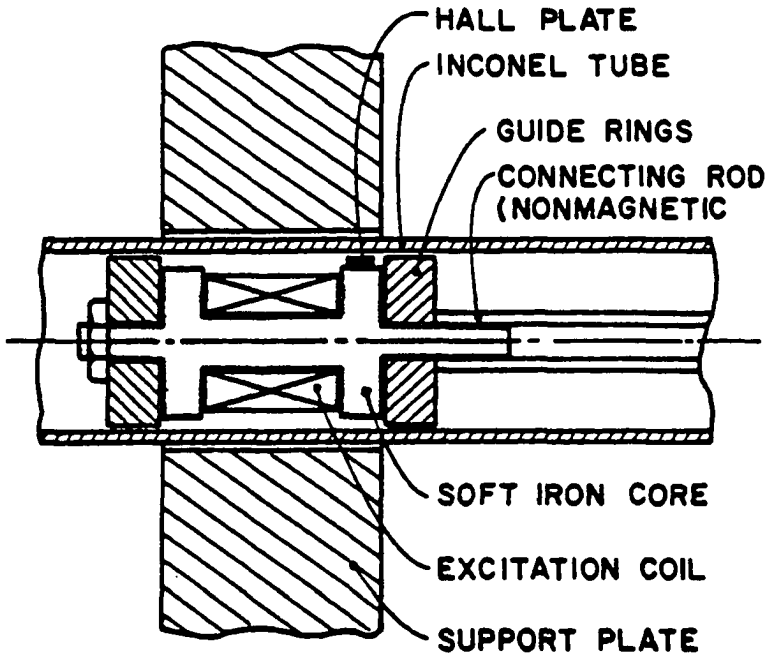

Figure 2.3. A simple variable reluctance probe (after Satish [29])

The VR probe was developed to detect and measure crevice gap clearance (distance between the tube and support plate), magnetite buildup and support plate defects. The basic premise is that all such anomalies would affect the reluctance of a simple bobbin type of VR probe carrying a dc excitation winding and a Hall plate mounted on the periphery of the bobbin (Figure 2.3). The reluctance of a magnetic circuit is given by

$$\Re = \frac{l}{\mu_r \mu_o A} \tag{2.1}$$

where l is the effective length of the flux paths and A the corresponding cross-sectional area. Because of the relative permeability term μ_r, flux paths through air have a much higher reluctance than those through

ferromagnetic support plates, consequently length or area variations in an air gap can be monitored directly by measuring the strength of the magnetic field. Figure 2.4 shows the flux distributions for different positions of the probe with respect to the support plate.

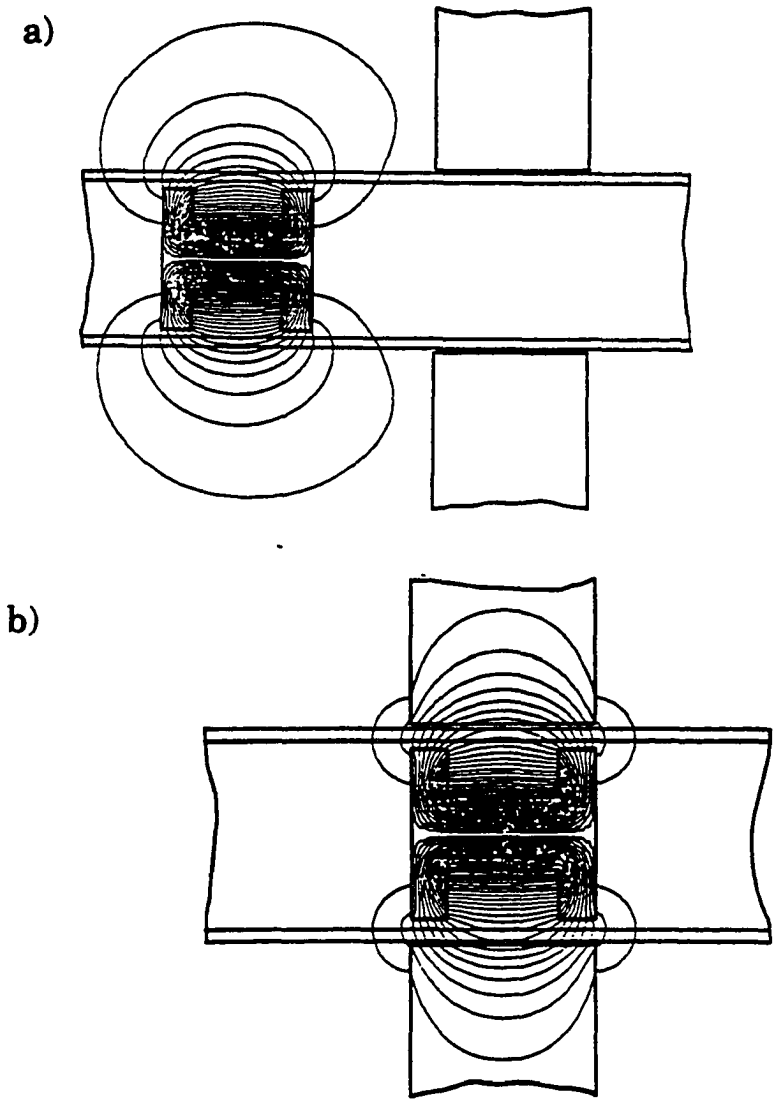

Figure 2.4. Flux distributions when the VR probe is
a) away from a support plate,
b) aligned with a support plate
(after Lord [26])

When the probe is away from the support plate, it experiences maximum reluctance as all the flux paths are in air, thus the probe flux is at a minimum. With the probe positioned directly under the support plate, the probe experiences reduced reluctance due to the higher permeability of the support plate, thus the probe flux level increases. A typical Hall plate signal obtained by passing the probe past a clean support plate is shown in Figure 2.5. The probe is initially calibrated by passing it through a calibration rig consisting of a number of accurately machined crevice gaps of known dimensions and obtaining a relationship between the probe output and crevice gap width. Repeated tests with different support plates have shown that the magnitude of the probe signal is related directly to the crevice gap clearance [26]. This relationship is used later to determine the dimensions of crevice gaps in a steam generator.

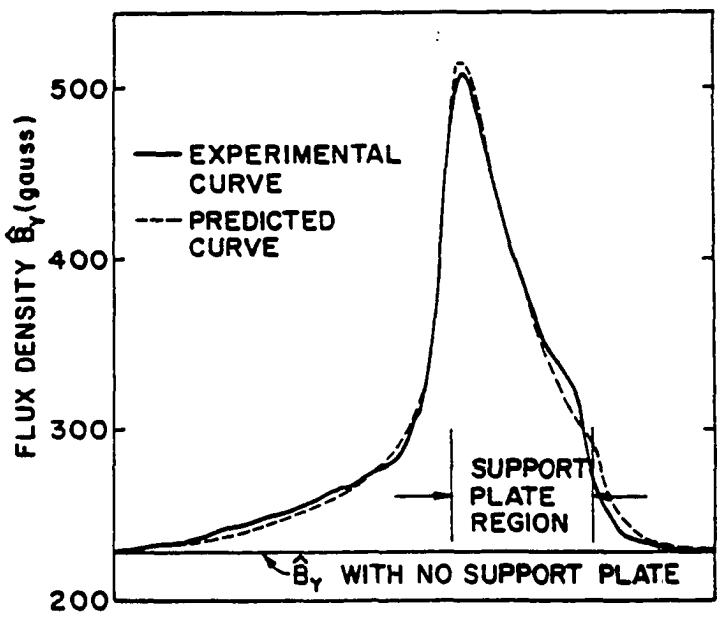

Figure 2.5. Typical variable reluctance probe signal obtained from the magnetite free crevice gap and the defect free support plate (after Lord [26])

The VR probe suffers from several disadvantages chief of which is the poor temperature sensitivity characteristic of Hall plates as well as their tendency to drift with time. This necessitates frequent calibration unless automatic calibration procedures are incorporated within the system. In addition, the probe is not sensitive to defects in the inconel steam generator tube because of the fact that the tube is nonmagnetic.

The governing equation for this VR probe is an elliptic Poisson equation expressed by

$$\nabla \times \frac{1}{\mu}(\nabla \times \bar{A}) = \bar{J}_s \tag{2.2}$$

where μ is the permeability, $\overline{A}$ is the magnetic vector potential, and $\overline{J_S}$ is the DC source current density. The output NDE signal sought is the normal component of magnetic flux density, usually obtained by a Hall plate.

B. Differential Eddy Current Probe

A typical differential eddy current probe used in PWR steam generator tube inspection is shown in Figure 2.6 [147,154]. In this method, two identical

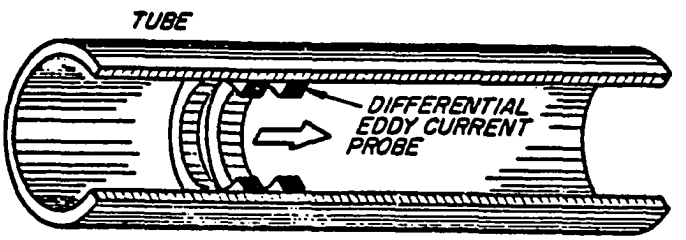

Figure 2.6. Typical differential eddy current (EC) probe used for inspecting tubes (after Satish [29])

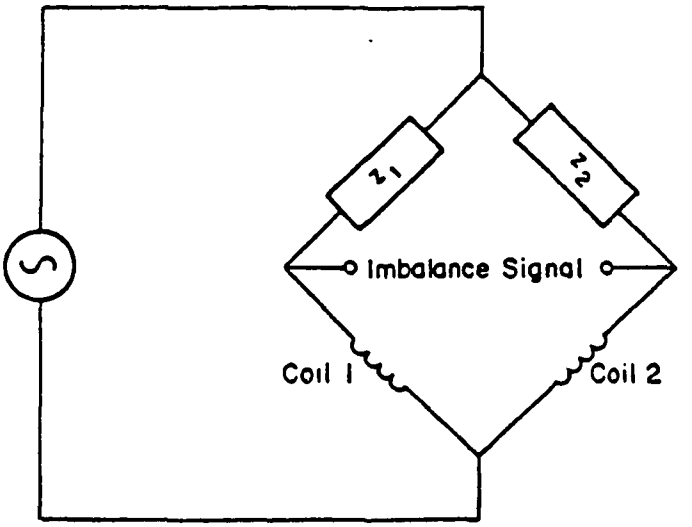

Figure 2.7. AC bridge used for measuring changes in differential EC probe impedance

coils mounted on a common axis as the tube but spaced apart by a small distance, form the two arms of a bridge circuit (Figure 2.7) which is initially nulled with the probe located in a defect-free segment of the tube. When the coil arrangement is moved past a narrow axisymmetric O.D. defect for example, whose width is considerably less than the spacing between the coils, the leading coil faces the defect first, and the presence of the defect causes a variation in the coil impedance which in turn causes an imbalance in the bridge circuit. The bridge error signal, which is linked to the difference between the impedance of the two coils, is then used to obtain a trajectory OAO in the diagram shown in Figure 2.8. Similarly, when the trailing coil faces the defect, the change in impedance causes an imbalance in the bridge circuit. But, this time, the imbalance signal is in an opposite direction relative to that caused by the leading coil so that the trajectory OBO is obtained. During the intervening period when neither of the coils face the

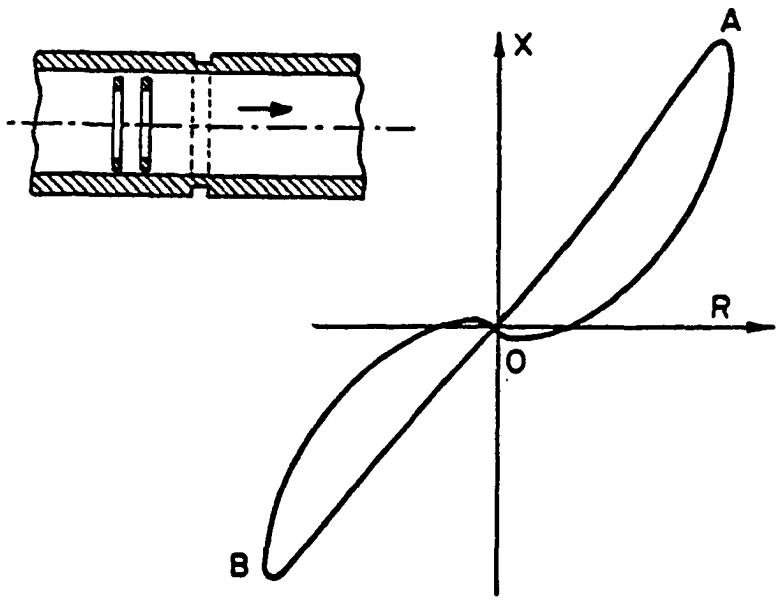

Figure 2.8. Impedance plane trajectory obtained with differential EC probe for a narrow axisymmetric O.D. defect

defect, the impedance trajectory remains stationary at the origin, O. Differential eddy current probe flux distributions for different positions of the probe with respect to the support plate are shown in Figure 2.9.

The differential nature of the probe makes the arrangement relatively insensitive to environmental effects. In addition, the differential connection results in the cancellation of the quiescent value of the coil impedance thereby highlighting the variations rather than the absolute value of the impedance. This makes measurement relatively easy. The differential probe, however, suffers from a disadvantage in that in the case of a long uniform defect running along the length of the tube, the changes in the differential

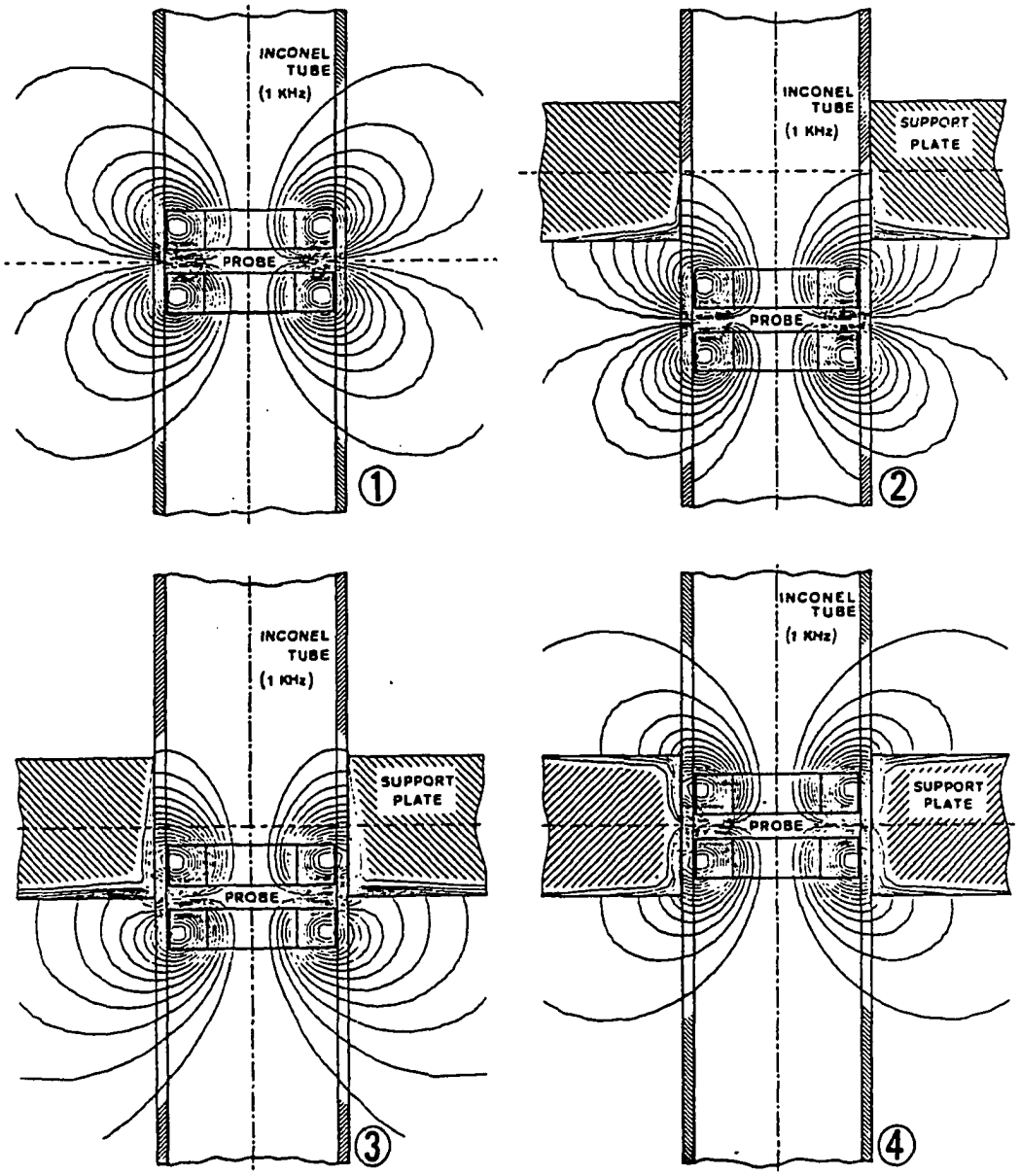

Figure 2.9. Flux distributions as the differential EC probe enters a support plate (1 KHz excitation frequency) (after Lord [147])

impedance occur only at the ends of the defect. This may be misinterpreted as two small defects instead of one long defect [29]. Another common difficulty in eddy current testing is due to the skin effect phenomenon. The skin effect equation [155], derived from Maxwell's equation and by using the solenoidal property of steady currents ($\nabla \cdot \bar{J} = 0$), can be written as

$$\nabla^2 \bar{J} = \mu\sigma \frac{\partial \bar{J}}{\partial t} \tag{2.3}$$

where σ is the conductivity. This equation describes mathematically, the tendency for eddy currents to stay at the surface of conductors. As a simple example, in the case of an infinite AC current sheet over a conducting half-space, the current density solution to equation (2.3) is given by

$$J = J_o \exp(-\frac{x}{\delta}) \sin(\omega t - \frac{x}{\delta}) \tag{2.4}$$

where $\omega = 2\pi f$ is the angular frequency, J_o is the current density at the surface of the half-space, and δ is the depth of penetration or skin depth

$$\delta = \frac{1}{\sqrt{\pi f \mu \sigma}} \tag{2.5}$$

at which the current density drops to 36.8% of the value at the surface, J_o and the phase of the current density lags that of J_o by one radian. Although the exact value is not known for complex NDE geometries, the skin depth for a half-space of aluminum is estimated as 2.59×10^{-3} meters for an excitation frequency of 1 KHz, using the above expression. The corresponding value for steel is 5×10^{-4} meters. Therefore, eddy current methods are limited to the detection of flaws close to the surface even though low excitation frequencies may help extend the penetration depth to a certain degree.

The governing equation in this case, where the displacement current term can be negligible due to low operating frequencies (up to few MHz), is a parabolic diffusion equation given by

$$\nabla \times \frac{1}{\mu}(\nabla \times \bar{A}) = \bar{J}_s - \sigma \frac{\partial \bar{A}}{\partial t} \tag{2.6}$$

where $\overline{J_S}$ is an AC source current density. In a linear, isotropic, AC steady state case, it reduces to an elliptic partial differential equation,

$$\nabla^2 \bar{A} = -\mu \bar{J}_s + j\omega\sigma\mu\bar{A} \tag{2.7}$$

by using phasor notation and the Coulomb gauge, which is automatically satisfied in axisymmetric cases. The output NDE signal sought is the differential impedance and the impedance plane trajectory that is formed as the differential EC probe passes the defect.

C. Remote Field Eddy Current (RFEC) Probe

The first known reference to the RFEC probe is in a 1951 patent by W. R. MacLean [156]. This reference went unnoticed or unappreciated for many years. The first application came in the late 1950s when it was applied to the downhole inspection of oil well casing pipe by T. R. Schmidt at Shell Development Corporation. In the early 1960s, the technique was applied to pipeline inspection and an intelligent pig, which was equipped with power, measurement, and recording devices, was built to be run through a pipeline. The pig was pumped through the pipeline and special launching and retrieving traps were used between pumping stations to insert and recover

the device, which might travel 80 Km or more. Even though the technique has been used for about 30 years, there was little information on the physics underlying this phenomenon and the experimental observations were explained by a hypothesis, as mentioned in Chapter I. This hypothesis was confirmed by the finite element analysis of W. Lord and his NDE group at Colorado State University [41,43,157].

The RFEC method shows more promise than conventional eddy current methods for oil and gas pipeline inspection due to the increased sensitivity to inner and outer pipe wall inhomogeneities. Conventional eddy current methods are limited to surface inspection because of the skin effect phenomenon. Even though the fundamental physical principles governing both methods are one and the same (that of electromagnetic induction), the differences in operating frequencies in the two methods result in field patterns that have different characteristic properties.

Figure 2.10 shows the RFEC probe where an excitation coil and a sensor coil are positioned several (about 3 to 4) pipe diameters apart. Figure 2.11

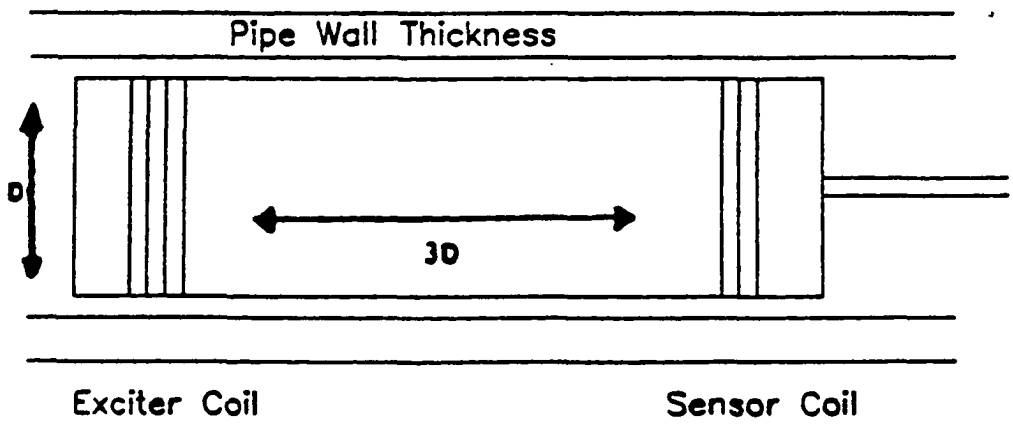

Figure 2.10. Remote field eddy current (RFEC) probe

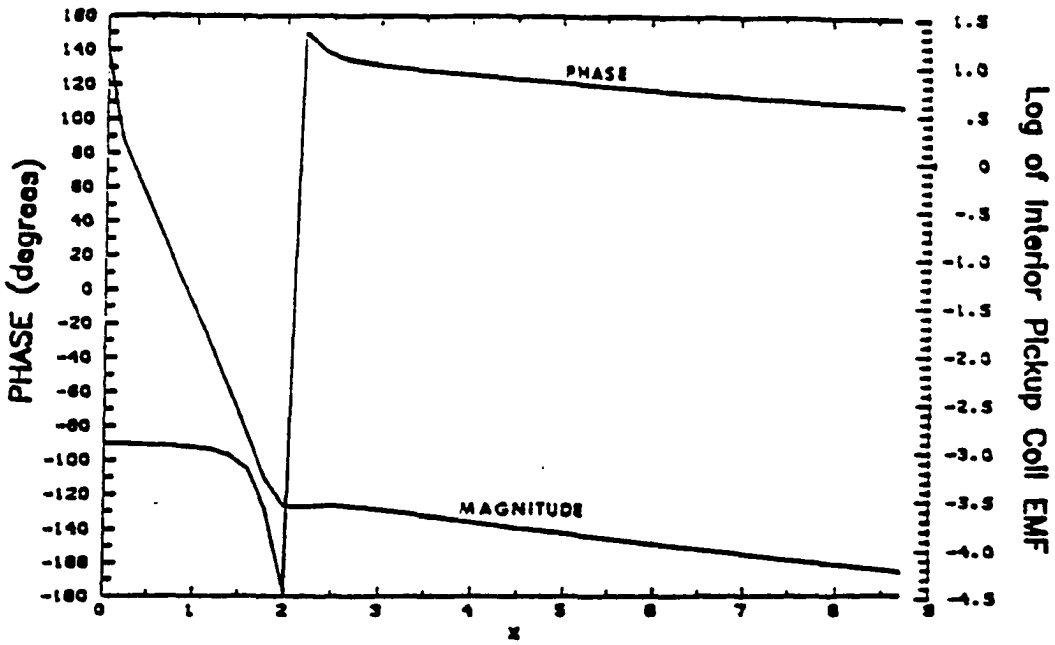

Figure 2.11. Typical RFEC magnitude and phase characteristics without defects (after Nath [159])

shows that the magnitude of sensor coil voltage changes rapidly with distance from the exciter coil until approximately two pipe diameters, after which the change is much slower. Sensor coil phase angle (relative to that of the exciter coil) also changes abruptly in the same region. Figures 2.12 and 2.13 show the existence of a magnetic potential valley (where RMS magnetic vector potential values are zero) and a phase knot (where the phase of magnetic vector potential is undefined) in this transition region. In Figure 2.12, the RMS magnetic vector potential magnitude is plotted on a logarithmic scale in order to show details of the remote field. These effects occur where outwardly directed energy from the exciter coil meets inwardly directed energy from the outer tube region. In the exciter coil region, the skin effect is

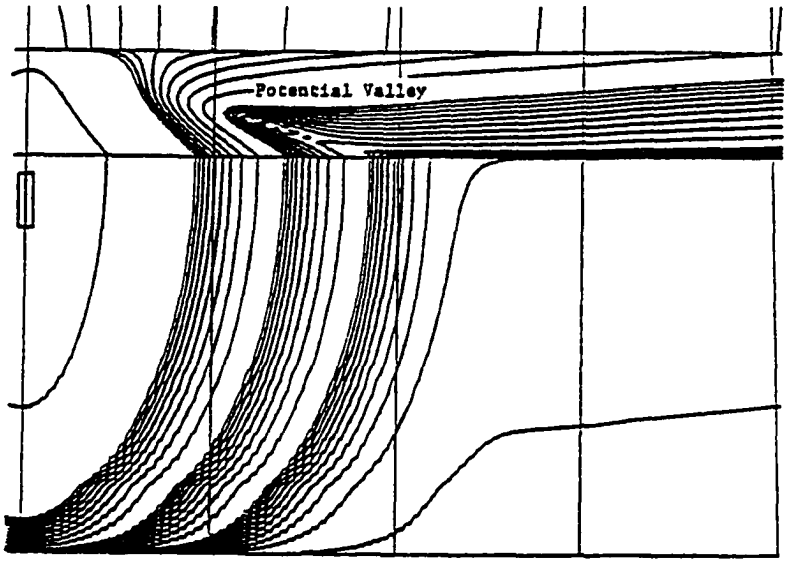

Figure 2.12. Existence of potential valley in the transition region (after Lord [155])

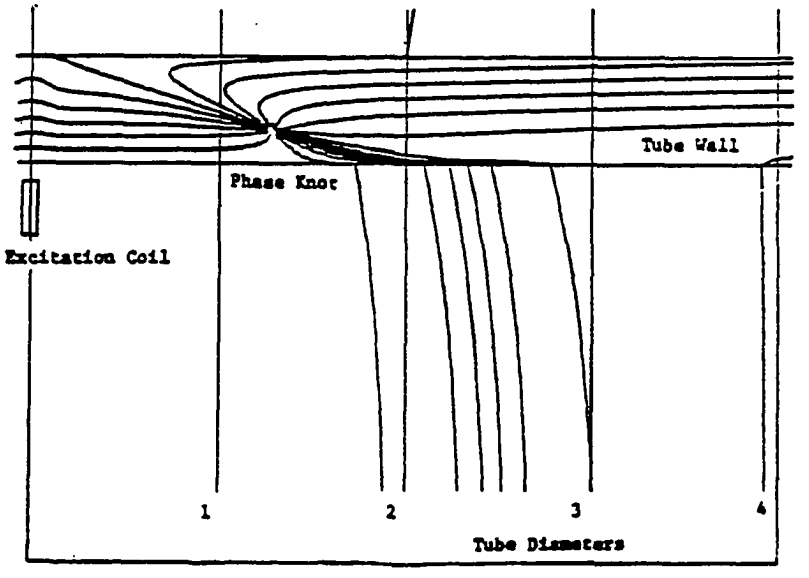

Figure 2.13. Existence of phase knot in the transition region (after Lord [155])

from tube I.D. to O.D., whereas in the remote field region the skin effect is from O.D. to I.D. In this way, the RFEC probe is sensitive to both external and internal tube flaws, a characteristic not normally associated with conventional eddy current NDE [157-159]. Figure 2.14 show flux plots for O.D. and I.D. pipe slots in the remote field regions, from which it can be seen that a sensor coil passing through such fields would give rise to similar signals.

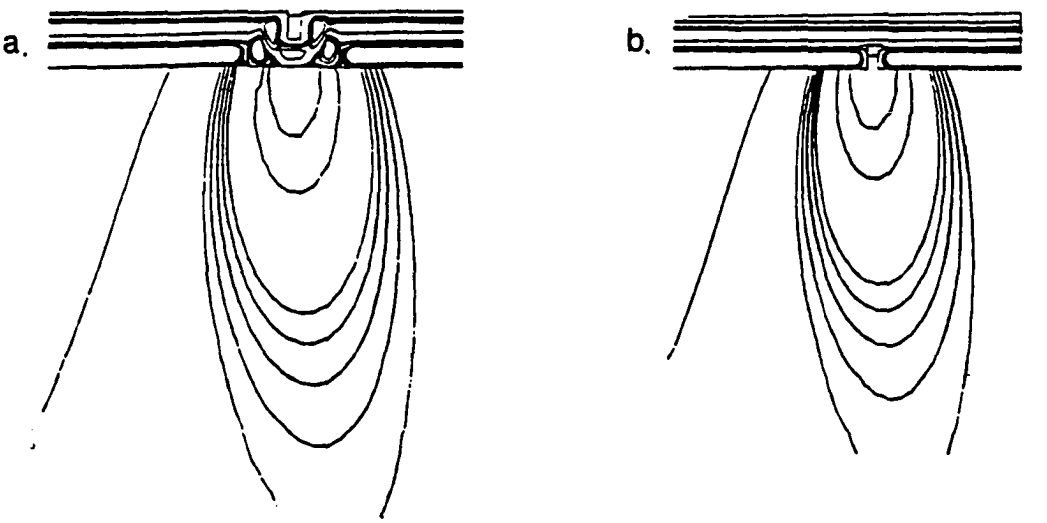

Figure 2.14. Flux contours for a) outer diameter slot, b) inner diameter slot at 160 Hz (after Lord et al. [157])

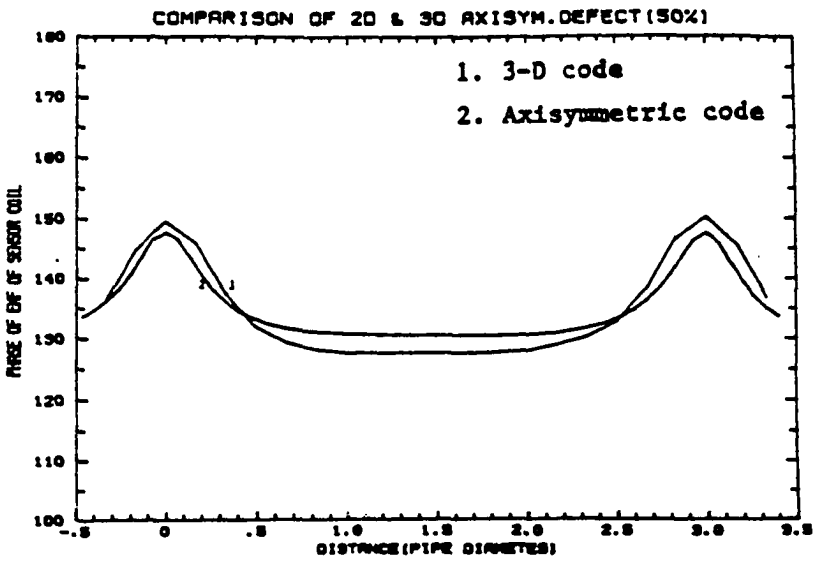

Figure 2.15. Steady state AC phase difference between the exciter coil and the sensor coil (after Lord [84])

Since the sensor coil voltage is very low (microvolt range) but the phase is sensitive to both I.D. and O.D. defects, the steady state AC phase differences between both coil voltages are also monitored. Figure 2.15 shows this phase difference plot. The double bump phenomenon associated with defect detection has a spacing equal to that of the exciter to sensor coil distance.

The governing equation is the same as that for a conventional eddy current probe. In the RFEC case, the typical operating frequency lies between 20 to 200 Hz [41]. The output NDE signals sought are the magnitude and phase of the sensor coil emf or the phase difference between the two coils. The disadvantage of this method is that signal analysis is more complex because of double signals from a single defect and hence, I.D./O.D. defect discrimination is very difficult [160]. To differentiate I.D. and O.D. defect signals, a new signal processing technique is proposed by Udpa et al. [161]..

CHAPTER III
NUMERICAL METHODS

This chapter explains the numerical methods used in this dissertation, but for introductory purposes, the motional induction term is not included in the governing equation. The finite element method (FEM) and the finite difference method (FDM) are used for spatial and time discretizations, respectively.

The governing equation to be considered in the explanation of FEM is an elliptic partial differential equation, which governs steady state problems. For the magnetic flux leakage method of NDE, the governing equation in steady state magnetostatic situations is a Poisson equation,

$$\nabla \times \frac{1}{\mu}(\nabla \times \bar{A}) = \bar{J}_s \tag{3.1}$$

For the eddy current method of NDE, the governing equation for AC steady state situations becomes the elliptic diffusion equation,

$$\nabla \times \frac{1}{\mu}(\nabla \times \bar{A}) = \bar{J}_s - j\omega\sigma\bar{A} \tag{3.2}$$

Since both are elliptic partial differential equations, the treatment in the finite element formulation is the same except that the variables in equation (3.1) are real numbers, while the variables in equation (3.2) are complex numbers since they are phasor vector quantities. The explanation in this chapter is, for simplicity, concentrated on equation (3.1).

When the physical process is governed by a parabolic partial differential equation, which represents the transient situation, the finite difference

method is used for time discretization. The causes of the transient situation are due to either nonsinusoidal sources or turn-on/off transients. Furthermore, if the probe movement is considered, unbalanced and/or non-uniform geometrical conditions also cause the transient situation as mentioned in Chapter I. For both the magnetic flux leakage method and the eddy current method, the governing equation in the transient situation is the parabolic diffusion equation,

$$\nabla \times \frac{1}{\mu}(\nabla \times \bar{A}) = \bar{J}_S - \sigma \frac{\partial \bar{A}}{\partial t} \tag{3.3}$$

In this case, all the variables are real numbers. The explanation of FDM for time discretization is, therefore, based on equation (3.3). For spatial discretization, FEM is still used.

In this dissertation, only axisymmetric geometries are considered. These axisymmetric models deal with coils moving within tubes where $\overline{A}$ and $\overline{J_S}$ have only θ components that are invariant in that direction. Consequently, all analysis can be done in a two dimensional r-z plane. In linear, isotropic, axisymmetric problems, the curl-curl expression in the above equations can be written as

$$\nabla \times \frac{1}{\mu}(\nabla \times \bar{A}) = -\frac{1}{\mu}\left(\frac{\partial^2 A_\theta}{\partial r^2} + \frac{1}{r}\frac{\partial A_\theta}{\partial r} - \frac{A_\theta}{r^2} + \frac{\partial^2 A_\theta}{\partial z^2}\right)\hat{\theta} \tag{3.4}$$

A. Finite Element Method for Spatial Discretization

The essential ideas of FEM began to appear in publications principally during the 1940s [162-166]. However, the modern finite element concept

which is used today was established by Turner et al. [167] in 1956, and the term 'finite element' first appeared in Clough's paper in 1960 [168]. Finite element analysis has its origin in the fields of structural analysis. In 1965, Zienkiewicz and Cheung [169] broadened the scope of FEM tremendously by demonstrating that it is applicable to all field problems that could be placed in variational form [170]. From the mid-1960s, the FEM spread beyond the original confines of structural analysis to many other fields such as heat transfer, acoustics, fluid mechanics and electromagnetics. The earlier applications of the method in electrical problems were made by Winslow [171] in 1967, and by Silvester [172] as well as Ahmed and Daly [173] in 1969. The method has since been used in a variety of applications. Silvester and Chari [174] solved electromagnetic field problems in electrical machines. Anderson [175] used the method for obtaining transformer leakage profiles. Chari [176] was the first to use the method for determining the solution to the eddy current problem. Brauer [177] used the method to study alternating magnetic fields and induced currents in transformers. The pioneering work in the area of electromagnetic NDE was made by Lord [178-180].

1. Finite Element Discretization and Interpolation

The first step in FEM is to discretize the solution region into finite elements. The element can have a variety of shapes. It may be triangular or quadrilateral for 2-D problems, tetrahedral or polyhedral for 3-D problems. In axisymmetric problems, the element is developed by revolving a triangle or a quadrilateral through 360 degrees. Each element has a certain number of

nodes. If only the vertices of the element are used as nodes (straight side), it is a linear element. If there are mid nodes between two vertices, it is a higher order element which can handle curved boundaries better. The final solutions are found at these discrete node points. The discretization of the solution region is therefore very important since the number of nodes as well as their locations have an impact on the solution. In general, small, dense elements must be used in regions where high gradients of the solution are expected. Also, other considerations are required such that the boundaries of an element must coincide with material interfaces and that the material properties, current density and flux density are assumed to be constant within the element.

Once the element shape is chosen, the next step is to approximate a continuous function for the solution by a discrete model that is composed of a set of piecewise continuous functions defined over the element. The most popular form of the element function is the polynomial. The order of the polynomial is related to the number of nodes per element. The polynomial can be alternatively expressed as a linear combination of interpolation (or shape) functions and the unknown nodal values. This polynomial expression is called a Lagrange interpolation polynomial [170]. Generally, a polynomial or a function is said to be interpolatory if it is defined to be equal to particular values at a number of specific and separate nodes. The shape functions themselves are also interpolatory because each one is defined to be equal to unity at one node and zero at other nodes. This interpolation property characterizes almost all finite element shape functions used for second order differential equations.

There is another way of finding these shape functions. For some elements like the triangle or tetrahedron, area coordinates or volume coordinates can be used to find them. If these elements are linear, they are simplex elements. The advantages of simplex elements are the existence of closed form expressions for integration and the satisfaction of the continuity condition between elements. For the other types, such as higher order elements or quadrilateral elements, the integration should be carried out by numerical methods and a mapping technique is required to maintain continuity between adjacent elements.

In this dissertation, linear rectangular axisymmetric elements are used. The shape of the element is shown in Figure 3.1. However, it is not well suited for approximating curved boundaries. In order to generalize the code, a general quadrilateral element whose sides are not necessarily parallel to the global coordinate system is assumed.

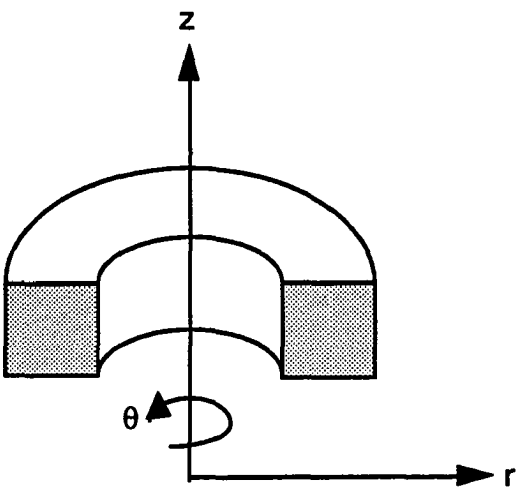

Figure 3.1. Rectangular axisymmetric finite element

Since there are four nodes in the quadrilateral element, it is possible to use an approximating function having four parameters such as

$$A(r,z) = a_1 + a_2 r + a_3 z + a_4 rz \tag{3.5}$$

However, there is a serious problem of continuity of the function between elements. Along any of the sides of such an element, both r and z would be changing values. The equation for any side could be expressed as

$$z = b_1 + b_2 r \tag{3.6}$$

Now, if equation (3.6) is substituted into equation (3.5), we have

$$A(r,z) = a_1 + a_2 r + a_3 (b_1 + b_2 r) + a_4 r(b_1 + b_2 r) \tag{3.7}$$

Without carrying out the algebra, it is at once evident that the function A(r,z) varies quadratically with r along the boundary being considered. Because there are only two nodes along any boundary, they can not be used to completely determine this quadratic function. That is, the function also depends on at least one more nodal point value not part of the boundary. This means that there is no way to guarantee continuity of the function across element boundaries. To overcome such a difficulty, a mapping technique is used and this type of element is called the isoparametric element [114].

2. Isoparametric Elements

Let us first consider the rectangular element whose sides are parallel to the local u and v axes as shown in Figure 3.2. The parent element in the u-v plane is to be mapped onto the r-z plane. The parent element for quadrilaterals is chosen to be a bi-unit square for convenience in applying the

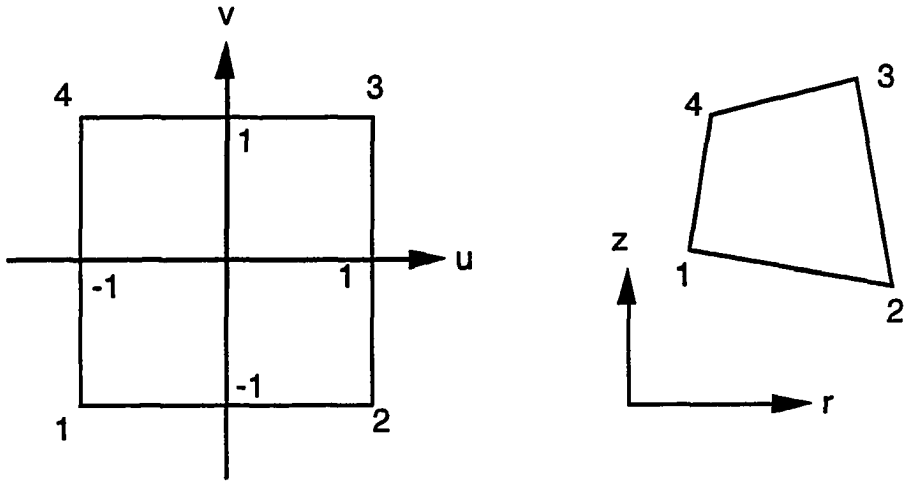

Figure 3.2. A parent element and a real element

Gaussian quadrature formulas, which integrate from -1 to 1. This parent element can be regarded as either the bilinear element of the Lagrange family or the linear element of the serendipity family [170]. The difference between these two families is in the existence of nodes inside the element. Since the shape functions of 2-D Lagrange elements are formed merely by the product of 1-D Lagrange interpolation functions, there have to be some nodes inside the 2-D element whenever a 1-D element is not linear. In this case of a linear quadrilateral parent element, however, there is no difference between the two families. Now, if the 1-D element as shown in Figure 3.3 is

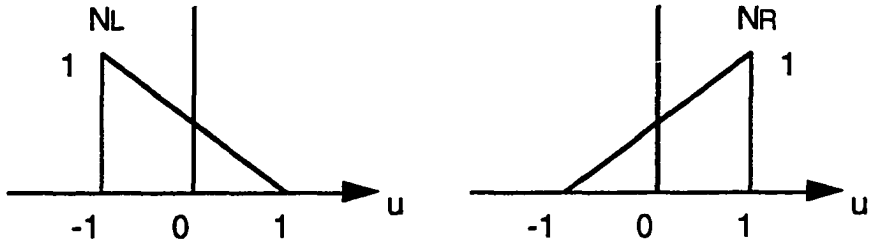

Figure 3.3. Shapes functions in 1-D parent element

considered, the shape functions for the left and right nodes can be written as

$$N_L(u) = \frac{1-u}{2} \tag{3.8}$$

$$N_R(u) = \frac{1+u}{2} \tag{3.9}$$

since these shape functions must satisfy the interpolation property, $N_L = 1$, $N_R = 0$ at $u = -1$ and $N_L = 0$, $N_R = 1$ at $u = 1$. Then, the approximating function in that element can be written as

$$A(u) = [\, N_L(u) \quad N_R(u) \,] \begin{Bmatrix} A_L \\ A_R \end{Bmatrix} \tag{3.10}$$

where A_L and A_R are the unknown nodal values on the left and on the right, respectively. This shows the form of the Lagrange interpolation polynomial mentioned in the previous subsection. From the above 1-D shape functions, 2-D shape functions can easily be found. Following the node numbering in Figure 3.2,

$$N_1(u,v) = \frac{1}{4}(1-u)(1-v) \tag{3.11}$$

$$N_2(u,v) = \frac{1}{4}(1+u)(1-v) \tag{3.12}$$

$$N_3(u,v) = \frac{1}{4}(1+u)(1+v) \tag{3.13}$$

$$N_4(u,v) = \frac{1}{4}(1-u)(1+v) \tag{3.14}$$

These functions vary linearly along any side of the element simply because either u or v is constant. Therefore, two adjacent rectangular elements sharing the same two nodal values of the dependent variable would create a continuous approximation of that dependent variable everywhere along the

common boundary. Hence, a mesh made up of these elements could be used to produce the necessary approximation which would be continuous throughout the mesh. However, a mesh of rectangular elements is very limited in its use. Therefore, it is mapped into the r-z plane with a continuous mapping function so that it will be continuous in the r-z plane. Since the shape function itself is continuous, it is used as the mapping function. Hence, the same set of parameters is used for both approximation and mapping - thus the term, isoparametric elements. For example, an approximating function A in the r-z plane can be written as follows.

$$A(r,z) = A(\, r(u,v),\, z(u,v)\,) = A(u,v) = [\, \mathbf{N}\,(u,v)\,] \begin{Bmatrix} A_1 \\ A_2 \\ A_3 \\ A_4 \end{Bmatrix} \tag{3.15}$$

where $[\mathbf{N}] = [\, N_1 \;\; N_2 \;\; N_3 \;\; N_4\,]$ and A_i is the unknown value at node i. Thus, A at point (u,v) is equal to A at point (r,z) and the position (r,z) are determined from,

$$r(u,v) = [\, \mathbf{N}\,(u,v)\,] \begin{Bmatrix} r_1 \\ r_2 \\ r_3 \\ r_4 \end{Bmatrix} \quad , \quad z(u,v) = [\, \mathbf{N}\,(u,v)\,] \begin{Bmatrix} z_1 \\ z_2 \\ z_3 \\ z_4 \end{Bmatrix} \tag{3.16}$$

where r_i and z_i are the coordinates of the node i at r-z plane.

The mapping concept is very useful not only for the inter-elemental continuity but also for the numerical integration. Since there is no closed form expression for the integration in the case of quadrilateral element, numerical integration techniques such as the Gaussian quadrature formula have to be used. In most quadrature formulations, the interval of integration is from -1 to 1 or from 0 to 1. The quadrature points are therefore given within those ranges. Since the parent element used in the isoparametric mapping is

defined within the same ranges, it is very convenient to use the given quadrature points directly. The Gaussian quadrature formula is to be explained later in this chapter.

3. Various Methods for Finite Element Formulation

Most commonly used methods for deriving finite element formulations are the weighted residual method, and the variational method which is based on the minimization of the energy functional. These two methods can be shown to be equivalent if the governing equation is self-adjoint . To show this in the simpler manner, the two dimensional version of equation (3.1) is considered, where $\overline{A}$ and $\overline{J_s}$ have only z components, and a more general formulation known as the weak formulation [114] is introduced.

Self-adjoint equation

Self-adjointness means that two equations are equal to their adjoints [181]. For a second order differential operator, α,

$$\alpha\,[y(x)] = a_2(x)\,y'' + a_1(x)\,y' + a_0(x)\,y \tag{3.17}$$

where $y' = \frac{dy}{dx}$ and $y'' = \frac{d^2y}{dx^2}$, its adjoint is defined by

$$\begin{aligned}\overline{\alpha}\,[y(x)] &= [a_2(x)\,y]'' - [a_1(x)\,y]' + a_0(x)\,y \\ &= a_2\,y'' + (2a_2' - a_1)\,y' + (a_2'' - a_1' + a_0)\,y\end{aligned} \tag{3.18}$$

Thus, equation (3.17) is self-adjoint if and only if

$$a_2'(x) = \frac{d}{dx}a_2(x) = a_1(x) \tag{3.19}$$

This self-adjointness condition shows that any second order differential operator of the form

$$\frac{d}{dx}\left[a_2(x)\frac{dy}{dx}\right] + a_0(x)\,y \tag{3.20}$$

is necessarily self-adjoint. In the finite element formulation, the self-adjoint equation always produces a symmetric matrix and this symmetry is a precondition for the existence of a variational principle [115]. Since equations (3.1), (3.2), and (3.3) do not have the first order spatial derivative term, they are self-adjoint provided that the permeability is a constant.

Galerkin weighted residual method

A residual is a function which results when an approximation of the solution is substituted into the governing equation. The two dimensional linear isotropic version of equation (3.1) is

$$\nu\left[\frac{\partial^2 A}{\partial x^2} + \frac{\partial^2 A}{\partial y^2}\right] = -J_s \tag{3.21}$$

where A and J_s are, in fact, z-components of the vectors $\overline{A}$ and $\overline{J_s}$ (i.e. $\overline{A} = A\hat{z}$, and $\overline{J_s} = J_s\hat{z}$) and ν is the reluctivity, i.e. a reciprocal of the permeability. If $A(x,y;A_i)$ is an approximation function for the solution, where A_i are the unknown parameters such as coefficients of the approximating polynomial or unknown nodal values of the interpolatory form expression, then the residual becomes

$$R(x,y;A_i) = \nu\left[\frac{\partial^2 A(x,y;A_i)}{\partial x^2} + \frac{\partial^2 A(x,y;A_i)}{\partial y^2}\right] + J_s \tag{3.22}$$

The residual depends not only on x and y but also on the yet undetermined parameters, A_i. If the approximation is accurate, the residual is identically zero. Conversely, if a particular approximation makes the residual deviate only slightly from zero, then the approximation is probably very close to the exact solution. Therefore, a technique for minimizing the residual error is employed because it tends to minimize the solution error, simultaneously. The technique is to make the weighted average of the residual zero. That is, a certain weighting function is multiplied to the residual, integrated over the solution region (element by element) and then, set to zero. Depending on the choice of the weighting function, various weighted residual methods result such as collocation, subdomain, least-square and Galerkin's methods [170]. The Galerkin weighted residual method uses each of the shape functions as the weighting function and this can be shown, for a quadrilateral element, as follows,

$$\iint_D N_1(x,y)R(x,y;A_1,A_2,A_3,A_4)dxdy = 0$$

$$\iint_D N_2(x,y)R(x,y;A_1,A_2,A_3,A_4)dxdy = 0$$

$$\iint_D N_3(x,y)R(x,y;A_1,A_2,A_3,A_4)dxdy = 0$$

$$\iint_D N_4(x,y)R(x,y;A_1,A_2,A_3,A_4)dxdy = 0 \qquad (3.23)$$

where D is the domain of the problem. These are four independent equations for the four parameters: A_1, A_2, A_3, and A_4.

Variational method

The variational approach uses an energy functional which is an integral equation comprised of the terms describing the energy within the system to be solved. This energy functional attains a minimum value corresponding to the true solution. That is, if the energy functional is calculated using the exact solution of the governing differential equation, its value will be lower than that calculated using any other approximation. Thus, if we had a family of approximating functions in which the exact solution was hidden, it could be found by simply determining which one of the approximating functions gave the lowest value for the energy functional. Furthermore, if the correct answer were not contained in the family, it could be assumed that the function which gave the lowest energy functional would be the best approximation to the exact solution. Considering this assumption and the interpolatory expression of the polynomial, the best nodal approximation can be found by taking the derivative of the energy functional with respect to the unknown at each node and setting it to zero, or equivalently by taking the variation of the energy functional due to the variation of the unknown at each node and setting it to zero. Instead of performing this process over the entire region, it is done element by element for convenience and then summing the contribution of each individual element. The equivalence between the energy functional and the governing equation is shown later by using the variational calculus.

A general energy functional over the domain D of electromagnetic field problems, can be written as

$$F = \int_D (\text{stored energy} - \text{input energy} + \text{dissipated energy})\, dv \qquad (3.24)$$

where the stored energy is due to the magnetic field, the input energy is derived from impressed current densities and the dissipated energy arises from the eddy current densities in the conducting parts of the geometry [30]. Therefore, the energy functional for the two dimensional version of equation (3.1), i.e. for the two dimensional linear isotropic magnetostatic flux leakage problem, can be written as

$$F(A)=\iint_D\left[\frac{\nu}{2}\left\{\left(\frac{\partial A}{\partial x}\right)^2+\left(\frac{\partial A}{\partial y}\right)^2\right\}-J_s A\right]dxdy \tag{3.25}$$

and that for the two dimensional version of equation (3.2), i.e. for the two dimensional linear isotropic AC steady state, eddy current problem, can be written as

$$F(A)=\iint_D\left[\frac{\nu}{2}\left\{\left(\frac{\partial A}{\partial x}\right)^2+\left(\frac{\partial A}{\partial y}\right)^2\right\}-J_s A+\frac{j\omega\sigma}{2}A^2\right]dxdy \tag{3.26}$$

The same form of energy functional can be written within an element and the elemental equations are obtained by taking the derivative or the variation of the element energy functional and setting it to zero. These elemental equations are summed up to form a global equation and then solved for the final solution, A.

In many problems, only the differential equations and their boundary conditions are available and the energy functional does not always exist for every differential equation. Since Galerkin's method does not require an energy functional, it is sometimes more convenient. For example, the

governing equation for moving magnetic fields includes a motional induction term which appears as the first order spatial derivative. The coefficient of this term does not allow us to write the governing equation in the form of equation (3.20). Therefore, this term makes the governing equation nonself-adjoint. In this case, the energy functional is not known so that the variational approach can not be applied unless the governing equation is transformed to the self-adjoint form. Galerkin's method is, therefore, very useful in this respect.

Equivalence of Galerkin's method and the variational method via the weak formulation

There is an intermediate formulation, known as the weak formulation [114], between Galerkin's method and the variational method. By using this method, the equivalence of the two methods will be shown.

Let's consider equation (3.21). The function A(x,y) is assumed to satisfy the equation for all values of x and y. Therefore, we know that

$$B(x,y)\left[\nu\left\{\frac{\partial^2 A(x,y)}{\partial x^2}+\frac{\partial^2 A(x,y)}{\partial y^2}\right\}+J_s\right]=0 \tag{3.27}$$

must also be satisfied for all values of x and y, and that this must be true regardless of the function B(x,y). Finally, we can state that

$$\iint_D B(x,y)\left[\nu\left\{\frac{\partial^2 A(x,y)}{\partial x^2}+\frac{\partial^2 A(x,y)}{\partial y^2}\right\}+J_s\right]dxdy=0 \tag{3.28}$$

must be satisfied for all functions B(x,y) if A(x,y) is the true solution. Integrating the above integral by parts, we have

$$-\iint_D\left[\nu\frac{\partial}{\partial x}\left(\frac{\partial A}{\partial x}B\right)+\nu\frac{\partial}{\partial y}\left(\frac{\partial A}{\partial y}B\right)\right]dxdy+\iint_D\left[\nu\frac{\partial A}{\partial x}\frac{\partial B}{\partial x}+\nu\frac{\partial A}{\partial y}\frac{\partial B}{\partial y}-J_sB\right]dxdy=0 \quad (3.29)$$

The first term in equation (3.29) can be reduced to an integral over the boundary of the area. This is accomplished with the aid of the 2-D divergence theorem or equivalently, Green's theorem for line integrals [170],

$$\iint\left[\frac{\partial P}{\partial x}+\frac{\partial Q}{\partial y}\right]dxdy=\oint\left[Pn_x+Qn_y\right]ds \quad (3.30)$$

Using equation (3.30), the first integral in equation (3.29) can be written as

$$-\oint_{D_s}\left[\nu\frac{\partial A}{\partial x}Bn_x+\nu\frac{\partial A}{\partial y}Bn_y\right]ds \quad (3.31)$$

This term allows us to specify boundary conditions. If the arbitrary function, B(x,y), is limited to only those functions which are zero at the boundary, this term disappears. Thus, we have

$$\iint_D\left[\nu\frac{\partial A}{\partial x}\frac{\partial B}{\partial x}+\nu\frac{\partial A}{\partial y}\frac{\partial B}{\partial y}-J_sB\right]dxdy=0 \quad (3.32)$$

The function A(x,y) must satisfy the above integral equation for all functions B(x,y) which are zero at the boundary. In this process, the existence of the second order derivative at all points has reduced to the first order derivative. Hence, the above integral formulation places a weaker demand on the function for which we are looking. Thus, the name, weak formulation.

Now, consider equation (3.28). If an approximating function for A(x,y) is substituted in that equation, the terms in the bracket become the residual,

and B(x,y) corresponds to the weighting function. When the shape functions are used for B(x,y), we have the Galerkin weighted residual method. That is, the weak formulation is basically equivalent to Galerkin's method.

The next task is to show the equivalence of the weak formulation and the variational method. In doing so, some knowledge of the variational calculus [182] is needed, so that three basic operations are given without proof.

$$\delta \frac{dy}{dx} = \frac{d}{dx}(\delta y) \tag{3.33}$$

$$\delta \int y \, dx = \int \delta y \, dx \tag{3.34}$$

$$\delta F = \frac{dF}{dy} \delta y \tag{3.35}$$

Now, consider the energy functional given in equation (3.25). Since the variation of the energy functional with respect to A has to be zero, the variation is taken first.

$$\delta F(A) = \delta \iint_D \left[\frac{\nu}{2} \left\{ \left(\frac{\partial A}{\partial x} \right)^2 + \left(\frac{\partial A}{\partial y} \right)^2 \right\} - J_s A \right] dxdy \tag{3.36}$$

Using the above basic operations, equation (3.36) can be reduced to

$$\delta F(A) = \iint_D \left[\nu \frac{\partial A}{\partial x} \frac{\partial}{\partial x}(\delta A) + \nu \frac{\partial A}{\partial y} \frac{\partial}{\partial y}(\delta A) - J_s \delta A \right] dxdy = 0 \tag{3.37}$$

Now, compare equations (3.37) with (3.32). Clearly, equation (3.32) can be obtained by substituting B for δA in equation (3.37). If A is known at the boundary, δA is zero there, which satisfies the requirement of B. This means

that the variational method is equivalent to the weak formulation. At last, according to the syllogism, we can say that the variational method is equivalent to Galerkin's method. Furthermore, in an elemental integration, δA can be expressed using the interpolatory form as

$$\delta A = [\,\mathbf{N}\,] \begin{Bmatrix} \delta A_1 \\ \delta A_2 \\ \delta A_3 \\ \delta A_4 \end{Bmatrix} \tag{3.38}$$

which includes the shape functions. Therefore, the equivalence of the two methods may be noted directly.

The last task in this subsection is to show the equivalence of the energy functional and the governing equation. Starting from equation (3.37) and integrating by parts,

$$\frac{\partial A}{\partial x}\frac{\partial}{\partial x}(\delta A) = \frac{\partial}{\partial x}\left(\frac{\partial A}{\partial x}\delta A\right) - \frac{\partial^2 A}{\partial x^2}\delta A \tag{3.39}$$

This allows us to write the variation as

$$\begin{aligned} \delta F = \iint_D \left[\nu \frac{\partial}{\partial x}\left(\frac{\partial A}{\partial x}\delta A\right) + \nu \frac{\partial}{\partial y}\left(\frac{\partial A}{\partial y}\delta A\right)\right] dxdy \\ - \iint_D \left[\nu \frac{\partial^2 A}{\partial x^2}\delta A + \nu \frac{\partial^2 A}{\partial y^2}\delta A + J_s \delta A \right] dxdy = 0 \end{aligned} \tag{3.40}$$

The first term can be written as an integration over the boundary of the area by applying Green's theorem as we did in the weak formulation and it disappears. Then, we are left with

$$\delta F = -\iint_D \left[\nu \frac{\partial^2 A}{\partial x^2} + \nu \frac{\partial^2 A}{\partial y^2} + J_s \right] (\delta A) dxdy \tag{3.41}$$

If A satisfies the governing differential equation, the term in the bracket is identically zero, and the above integral is zero for any variation δA. Likewise, if equation (3.41) is zero, i.e. the variation of the energy functional with respect to any variation δA is zero, we must say that the term in the bracket is zero. This means that the governing equation (3.21) is satisfied. Therefore, we can conclude that minimizing the energy functional is equivalent to the governing equation.

4. Finite Element Formulation using Weak Formulation

Now consider our original axisymmetric problem. Since the extension to the eddy current problem is very easy, only the magnetic flux leakage method is considered here. In linear isotropic problems, the governing equation (3.1) becomes

$$\nu\frac{\partial}{\partial r}\left\{\frac{1}{r}\frac{\partial}{\partial r}(rA)\right\}+\nu\frac{\partial}{\partial z}\left\{\frac{1}{r}\frac{\partial}{\partial z}(rA)\right\}=-J_s \tag{3.42}$$

Since the problem is axisymmetric, the magnetic vector potential and the source current density vector have only θ components and thus, A and J_s are scalar quantities. By applying the weak formulation, we have

$$\int_v \delta A\left[\nu\frac{\partial}{\partial r}\left\{\frac{1}{r}\frac{\partial}{\partial r}(rA)\right\}+\nu\frac{\partial}{\partial z}\left\{\frac{1}{r}\frac{\partial}{\partial z}(rA)\right\}+J_s\right]dv=0 \tag{3.43}$$

Integration by parts gives

$$\int_v \nu\left[\frac{\partial}{\partial r}\left\{\delta A\frac{1}{r}\frac{\partial}{\partial r}(rA)\right\}+\frac{\partial}{\partial z}\left\{\delta A\frac{1}{r}\frac{\partial}{\partial z}(rA)\right\}\right]dv$$

$$-\int_v\left[\nu\frac{1}{r}\frac{\partial}{\partial r}(rA)\frac{\partial\delta A}{\partial r}+\nu\frac{\partial A}{\partial z}\frac{\partial\delta A}{\partial z}-\delta AJ_s\right]dv=0 \qquad (3.44)$$

As we have seen earlier, the first term is supposed to transform to the lower integral. However, in the cylindrical coordinate system, the first term is not complete for applying Green's theorem, so that we manipulate as follows,

$$\int_v \nu\left[\frac{\partial}{\partial r}\left\{\delta A\frac{1}{r}\frac{\partial}{\partial r}(rA)\right\}+\frac{1}{r}\left\{\delta A\frac{1}{r}\frac{\partial}{\partial r}(rA)\right\}+\frac{\partial}{\partial z}\left\{\delta A\frac{1}{r}\frac{\partial}{\partial z}(rA)\right\}\right]dv$$

$$-\int_v\left[\nu\frac{1}{r}\frac{\partial}{\partial r}(rA)\frac{\partial\delta A}{\partial r}+\nu\frac{1}{r}\left\{\delta A\frac{1}{r}\frac{\partial}{\partial r}(rA)\right\}+\nu\frac{\partial A}{\partial z}\frac{\partial\delta A}{\partial z}-\delta AJ_s\right]dv=0 \qquad (3.45)$$

Then, using Green's theorem, the first term can be transformed to a surface integral.

$$\oint_S \nu\delta A\left\{\frac{1}{r}\frac{\partial}{\partial r}(rA)n_r+\frac{\partial A}{\partial z}n_z\right\}ds=\oint_S \nu\delta A\frac{\partial A}{\partial n}ds \qquad (3.46)$$

If the Dirichlet boundary condition is used, the value at the boundary is already known, so that the variation, δA is zero. If the Neumann boundary condition is given, then $\frac{\partial A}{\partial n}$ is zero, and we are left with only the second term in equation (3.45). The integration of this second term is performed element by element, and later elemental contributions will be summed up. Since the elemental integration has the same form, we can write it in matrix form,

$$\int_{v_e} \nu\left[\delta\left(\frac{\partial A}{\partial r}+\frac{A}{r}\right)\quad\delta\left(\frac{\partial A}{\partial z}\right)\right]\begin{bmatrix}\frac{\partial A}{\partial r}+\frac{A}{r}\\ \frac{\partial A}{\partial z}\end{bmatrix}dv-\int_{v_e}\delta AJ_s dv=0 \qquad (3.47)$$

Now, we want to substitute A for its approximation defined in an element as

$$A = [\mathbf{N}]\{\mathbf{A}\}_e = [N_1 \quad N_2 \quad N_3 \quad N_4]\begin{Bmatrix} A_1 \\ A_2 \\ A_3 \\ A_4 \end{Bmatrix} \tag{3.48}$$

and also, we will use the following notations.

$$\{\nabla \mathbf{A}\} = \begin{Bmatrix} \dfrac{\partial A}{\partial r} + \dfrac{A}{r} \\ \dfrac{\partial A}{\partial z} \end{Bmatrix} = \begin{Bmatrix} \dfrac{\partial}{\partial r} + \dfrac{1}{r} \\ \dfrac{\partial}{\partial z} \end{Bmatrix} [\mathbf{N}]\{\mathbf{A}\}_e$$

$$= \begin{bmatrix} \dfrac{\partial N_1}{\partial r} + \dfrac{N_1}{r} & \dfrac{\partial N_2}{\partial r} + \dfrac{N_2}{r} & \dfrac{\partial N_3}{\partial r} + \dfrac{N_3}{r} & \dfrac{\partial N_4}{\partial r} + \dfrac{N_4}{r} \\ \dfrac{\partial N_1}{\partial z} & \dfrac{\partial N_2}{\partial z} & \dfrac{\partial N_3}{\partial z} & \dfrac{\partial N_4}{\partial z} \end{bmatrix} \begin{Bmatrix} A_1 \\ A_2 \\ A_3 \\ A_4 \end{Bmatrix} = [\nabla \mathbf{N}]\{\mathbf{A}\}_e \tag{3.49}$$

After substituting the above notations, equation (3.47) becomes

$$\int_{v_e} \delta\{\mathbf{A}\}_e^T \left[\nu [\nabla \mathbf{N}]^T [\nabla \mathbf{N}]\{\mathbf{A}\}_e - J_s [\mathbf{N}]^T \right] dv = 0 \tag{3.50}$$

Since this equation must be satisfied for any variation δA, we can write the elemental matrix equation as follows.

$$[\mathbf{S}]_e \{\mathbf{A}\}_e = \{\mathbf{Q}\}_e \tag{3.51}$$

where

$$[\mathbf{S}]_e = \int_{v_e} \nu [\nabla \mathbf{N}]^T [\nabla \mathbf{N}] dv \tag{3.52}$$

$$\{\mathbf{Q}\}_e = \int_{v_e} J_s [\mathbf{N}]^T dv \tag{3.53}$$

Note here that even though the integration is for volume,

$$dv = r\, dr\, dz\, d\theta \tag{3.54}$$

the integrands are independent of θ. Therefore, the portion of the volume integral, $d\theta$, is cancelled on both sides of equation (3.51) and this effectively results in an area integration. The value of r is found by using the centroidal value of an element. The evaluation of equations (3.52) and (3.53) requires integration of the shape functions and equation (3.52) further requires differentiation of the shape functions with respect to the original coordinates, r and z.

First, consider the differentiation. Since the shape functions are written in terms of local u and v coordinates due to the mapping used in the isoparametric element, direct differentiation with respect to r and z is not possible. Therefore, the chain rule of differentiation is used to obtain

$$\begin{aligned}\frac{\partial N_i}{\partial r} &= \frac{\partial N_i}{\partial u}\frac{\partial u}{\partial r} + \frac{\partial N_i}{\partial v}\frac{\partial v}{\partial r} \\ \frac{\partial N_i}{\partial z} &= \frac{\partial N_i}{\partial u}\frac{\partial u}{\partial z} + \frac{\partial N_i}{\partial v}\frac{\partial v}{\partial z}\end{aligned} \tag{3.55}$$

or in matrix notation,

$$\begin{Bmatrix} \frac{\partial N_i}{\partial r} \\ \frac{\partial N_i}{\partial z} \end{Bmatrix} = \begin{bmatrix} \frac{\partial u}{\partial r} & \frac{\partial v}{\partial r} \\ \frac{\partial u}{\partial z} & \frac{\partial v}{\partial z} \end{bmatrix} \begin{Bmatrix} \frac{\partial N_i}{\partial u} \\ \frac{\partial N_i}{\partial v} \end{Bmatrix} \tag{3.56}$$

Now, we use the following notations,

$$\left[\mathbf{J}\left(\frac{u,v}{r,z}\right)\right] = \begin{bmatrix} \frac{\partial u}{\partial r} & \frac{\partial u}{\partial z} \\ \frac{\partial v}{\partial r} & \frac{\partial v}{\partial z} \end{bmatrix} \tag{3.57}$$

$$\left[\mathbf{J}\left(\frac{r,z}{u,v}\right)\right]=\begin{bmatrix}\frac{\partial r}{\partial u} & \frac{\partial r}{\partial v}\\ \frac{\partial z}{\partial u} & \frac{\partial z}{\partial v}\end{bmatrix} \tag{3.58}$$

Note that equation (3.56) becomes

$$\begin{Bmatrix}\frac{\partial N_i}{\partial r}\\ \frac{\partial N_i}{\partial z}\end{Bmatrix}=\left[\mathbf{J}^T\left(\frac{u,v}{r,z}\right)\right]\begin{Bmatrix}\frac{\partial N_i}{\partial u}\\ \frac{\partial N_i}{\partial v}\end{Bmatrix} \tag{3.59}$$

where we have used the notation

$$\left[\mathbf{J}^T\left(\frac{u,v}{r,z}\right)\right]=\left[\mathbf{J}\left(\frac{u,v}{r,z}\right)\right]^T \tag{3.60}$$

We note also that the differentials transform as

$$\begin{Bmatrix}dr\\ dz\end{Bmatrix}=\left[\mathbf{J}\left(\frac{r,z}{u,v}\right)\right]\begin{Bmatrix}du\\ dv\end{Bmatrix}$$

and

$$\begin{Bmatrix}du\\ dv\end{Bmatrix}=\left[\mathbf{J}\left(\frac{u,v}{r,z}\right)\right]\begin{Bmatrix}dr\\ dz\end{Bmatrix} \tag{3.61}$$

Hence,

$$\left[\mathbf{J}\left(\frac{u,v}{r,z}\right)\right]=\left[\mathbf{J}\left(\frac{r,z}{u,v}\right)\right]^{-1} \tag{3.62}$$

This allows us to rewrite equation (3.59) as

$$\begin{Bmatrix}\frac{\partial N_i}{\partial r}\\ \frac{\partial N_i}{\partial z}\end{Bmatrix}=\left[\mathbf{J}^T\left(\frac{r,z}{u,v}\right)\right]^{-1}\begin{Bmatrix}\frac{\partial N_i}{\partial u}\\ \frac{\partial N_i}{\partial v}\end{Bmatrix} \tag{3.63}$$

Now, consider the integrand of equation (3.52). It is convenient to divide the integrand into several terms.

$$[\nabla \mathbf{N}]^T[\nabla \mathbf{N}]$$

$$= \begin{bmatrix} \frac{\partial N_1}{\partial r}+\frac{N_1}{r} & \frac{\partial N_1}{\partial z} \\ \frac{\partial N_2}{\partial r}+\frac{N_2}{r} & \frac{\partial N_2}{\partial z} \\ \frac{\partial N_3}{\partial r}+\frac{N_3}{r} & \frac{\partial N_3}{\partial z} \\ \frac{\partial N_4}{\partial r}+\frac{N_4}{r} & \frac{\partial N_4}{\partial z} \end{bmatrix} \begin{bmatrix} \frac{\partial N_1}{\partial r}+\frac{N_1}{r} & \frac{\partial N_2}{\partial r}+\frac{N_2}{r} & \frac{\partial N_3}{\partial r}+\frac{N_3}{r} & \frac{\partial N_4}{\partial r}+\frac{N_4}{r} \\ \frac{\partial N_1}{\partial z} & \frac{\partial N_2}{\partial z} & \frac{\partial N_3}{\partial z} & \frac{\partial N_4}{\partial z} \end{bmatrix}$$

$$= \left\{ \begin{bmatrix} \frac{\partial N_1}{\partial r} & \frac{\partial N_1}{\partial z} \\ \frac{\partial N_2}{\partial r} & \frac{\partial N_2}{\partial z} \\ \frac{\partial N_3}{\partial r} & \frac{\partial N_3}{\partial z} \\ \frac{\partial N_4}{\partial r} & \frac{\partial N_4}{\partial z} \end{bmatrix} + \begin{bmatrix} \frac{N_1}{r} & 0 \\ \frac{N_2}{r} & 0 \\ \frac{N_3}{r} & 0 \\ \frac{N_4}{r} & 0 \end{bmatrix} \right\} \left\{ \begin{bmatrix} \frac{\partial N_1}{\partial r} & \frac{\partial N_2}{\partial r} & \frac{\partial N_3}{\partial r} & \frac{\partial N_4}{\partial r} \\ \frac{\partial N_1}{\partial z} & \frac{\partial N_2}{\partial z} & \frac{\partial N_3}{\partial z} & \frac{\partial N_4}{\partial z} \end{bmatrix} + \begin{bmatrix} \frac{N_1}{r} & \frac{N_2}{r} & \frac{N_3}{r} & \frac{N_4}{r} \\ 0 & 0 & 0 & 0 \end{bmatrix} \right\}$$

$$= \begin{bmatrix} \frac{\partial N_1}{\partial r} & \frac{\partial N_1}{\partial z} \\ \frac{\partial N_2}{\partial r} & \frac{\partial N_2}{\partial z} \\ \frac{\partial N_3}{\partial r} & \frac{\partial N_3}{\partial z} \\ \frac{\partial N_4}{\partial r} & \frac{\partial N_4}{\partial z} \end{bmatrix} \begin{bmatrix} \frac{\partial N_1}{\partial r} & \frac{\partial N_2}{\partial r} & \frac{\partial N_3}{\partial r} & \frac{\partial N_4}{\partial r} \\ \frac{\partial N_1}{\partial z} & \frac{\partial N_2}{\partial z} & \frac{\partial N_3}{\partial z} & \frac{\partial N_4}{\partial z} \end{bmatrix} + \begin{bmatrix} \frac{\partial N_1}{\partial r} & \frac{\partial N_1}{\partial z} \\ \frac{\partial N_2}{\partial r} & \frac{\partial N_2}{\partial z} \\ \frac{\partial N_3}{\partial r} & \frac{\partial N_3}{\partial z} \\ \frac{\partial N_4}{\partial r} & \frac{\partial N_4}{\partial z} \end{bmatrix} \begin{bmatrix} \frac{N_1}{r} & \frac{N_2}{r} & \frac{N_3}{r} & \frac{N_4}{r} \\ 0 & 0 & 0 & 0 \end{bmatrix}$$

$$+ \begin{bmatrix} \frac{N_1}{r} & 0 \\ \frac{N_2}{r} & 0 \\ \frac{N_3}{r} & 0 \\ \frac{N_4}{r} & 0 \end{bmatrix} \begin{bmatrix} \frac{\partial N_1}{\partial r} & \frac{\partial N_2}{\partial r} & \frac{\partial N_3}{\partial r} & \frac{\partial N_4}{\partial r} \\ \frac{\partial N_1}{\partial z} & \frac{\partial N_2}{\partial z} & \frac{\partial N_3}{\partial z} & \frac{\partial N_4}{\partial z} \end{bmatrix} + \begin{bmatrix} \frac{N_1}{r} & 0 \\ \frac{N_2}{r} & 0 \\ \frac{N_3}{r} & 0 \\ \frac{N_4}{r} & 0 \end{bmatrix} \begin{bmatrix} \frac{N_1}{r} & \frac{N_2}{r} & \frac{N_3}{r} & \frac{N_4}{r} \\ 0 & 0 & 0 & 0 \end{bmatrix} \quad (3.64)$$

If we define

$$[\mathbf{N}'(r,z)] = \begin{bmatrix} \frac{\partial N_1}{\partial r} & \frac{\partial N_2}{\partial r} & \frac{\partial N_3}{\partial r} & \frac{\partial N_4}{\partial r} \\ \frac{\partial N_1}{\partial z} & \frac{\partial N_2}{\partial z} & \frac{\partial N_3}{\partial z} & \frac{\partial N_4}{\partial z} \end{bmatrix}$$

$$= \begin{bmatrix} \frac{\partial u}{\partial r} & \frac{\partial v}{\partial r} \\ \frac{\partial u}{\partial z} & \frac{\partial v}{\partial z} \end{bmatrix} \begin{bmatrix} \frac{\partial N_1}{\partial u} & \frac{\partial N_2}{\partial u} & \frac{\partial N_3}{\partial u} & \frac{\partial N_4}{\partial u} \\ \frac{\partial N_1}{\partial v} & \frac{\partial N_2}{\partial v} & \frac{\partial N_3}{\partial v} & \frac{\partial N_4}{\partial v} \end{bmatrix} = \left[\mathbf{J}^T\left(\frac{r,z}{u,v}\right)\right]^{-1} [\mathbf{N}'(u,v)] \qquad (3.65)$$

and use simplified notations such as $\frac{\partial \mathbf{N_i}}{\partial r}$ and $\frac{\mathbf{N_j}}{r}$, where **i** = 1, 2, 3, 4, and **j** = 1, 2, 3, 4, then equation (3.64) can be written as

$$[\mathbf{N}'(u,v)]^T \left[\mathbf{J}\left(\frac{r,z}{u,v}\right)\right]^{-1} \left[\mathbf{J}^T\left(\frac{r,z}{u,v}\right)\right]^{-1} [\mathbf{N}'(u,v)] + \frac{\partial \mathbf{N_i}}{\partial r}\frac{\mathbf{N_j}}{r} + \frac{\mathbf{N_i}}{r}\frac{\partial \mathbf{N_j}}{\partial r} + \frac{\mathbf{N_i}}{r}\frac{\mathbf{N_j}}{r} \qquad (3.66)$$

Since $\frac{\partial N_i}{\partial r}$ is expressed in terms of $\frac{\partial N_i}{\partial u}$ and $\frac{\partial N_i}{\partial v}$ in equation (3.63), the above equation is expressed completely in terms of u and v. Therefore, this form of integrand can be directly used for the integration with respect to u and v.

For the integration, it is necessary to determine the relationship between the differential area in the u-v plane and the corresponding differential area in the r-z plane. Consider the differentials du and dv, as two vectors in the u-v plane which are mapped into the r-z plane. The differential area is then written as $\overline{\mathrm{du}} \times \overline{\mathrm{dv}}$. To evaluate this cross-product, we must determine the r and z components of each vector. The differential du represents the displacement from the point (u,v) to the point (u+du,v) and the corresponding displacement in the r-z plane would be from the point (r,z) to the point

(r+dr,z+dz). That is, a differential change du in the u-v plane causes a differential change in the r-z plane equal to

$$dr = \frac{\partial r}{\partial u} du \quad \text{and} \quad dz = \frac{\partial z}{\partial u} du \tag{3.67}$$

Hence, these are the r and z components of the transformed vector du. Therefore, we can write

$$\overline{du} = \frac{\partial r}{\partial u} du\, \hat{r} + \frac{\partial z}{\partial u} du\, \hat{z} \tag{3.68}$$

and likewise,

$$\overline{dv} = \frac{\partial r}{\partial v} dv\, \hat{r} + \frac{\partial z}{\partial v} dv\, \hat{z} \tag{3.69}$$

The differential area can now be written as

$$\overline{du} \times \overline{dv} = \left(\frac{\partial r}{\partial u}\frac{\partial z}{\partial v} - \frac{\partial z}{\partial u}\frac{\partial r}{\partial v} \right) du\, dv$$

$$= \begin{vmatrix} \frac{\partial r}{\partial u} & \frac{\partial r}{\partial v} \\ \frac{\partial z}{\partial u} & \frac{\partial z}{\partial v} \end{vmatrix} du\, dv = \left| \mathbf{J}\left(\frac{r,z}{u,v} \right) \right| du\, dv \tag{3.70}$$

where $\mathbf{J}$ is the Jacobian matrix as shown earlier in equation (3.58), and $|\mathbf{J}|$ is its determinant. The mapping is acceptable only when this determinant of the Jacobian is larger than zero [170]. The value of this determinant tells us the amount of local expansion or contraction of the coordinates due to the mapping.

The integral in equation (3.52) can now be evaluated as

$$[\mathbf{S}]_e = \int_{-1}^{1}\int_{-1}^{1} v\left[[\mathbf{N}'(u,v)]^T\left[\mathbf{J}\left(\frac{r,z}{u,v}\right)\right]^{-1}\left[\mathbf{J}^T\left(\frac{r,z}{u,v}\right)\right]^{-1}[\mathbf{N}'(u,v)]\right]|\mathbf{J}|r_c\,dudv$$

$$+ \int_{-1}^{1}\int_{-1}^{1} v\left[\frac{\partial \mathbf{N_i}}{\partial r}\frac{\mathbf{N_j}}{r} + \frac{\mathbf{N_i}}{r}\frac{\partial \mathbf{N_j}}{\partial r} + \frac{\mathbf{N_i}}{r}\frac{\mathbf{N_j}}{r}\right]|\mathbf{J}|r_c\,dudv \qquad (3.71)$$

where r_c is the centroidal value of an element which can be written as

$$r_c = \frac{r_1 + r_2 + r_3 + r_4}{4} \qquad (3.72)$$

Similarly, the integral in equation (3.53) can be evaluated as

$$\{\mathbf{Q}\}_e = \int_{-1}^{1}\int_{-1}^{1} J_s[\mathbf{N}]^T|\mathbf{J}|r_c\,dudv \qquad (3.73)$$

Actual integration is performed numerically by using the Gaussian quadrature formula. If we let I(u) represent the integrand, any of the 1-D integrals from -1 to 1 may be evaluated as follows,

$$\int_{-1}^{1} I(u)du \cong \sum_{l=1}^{n} W_{nl} I(u_{nl}) \qquad (3.74)$$

where W_{nl} are weight factors and u_{nl} are points at which the integrand is evaluated. The u_{nl} are called quadrature points. The values for the weight factors and the quadrature points depend on the quadrature formulas. The simplest formulas are the equally spaced, closed Newton-Cotes rules, such as the trapezoidal rule and Simpson's rule. If n is even, these rules integrate exactly a polynomial of degree n-1; if n is odd, they integrate exactly a polynomial of degree n. The Gauss quadrature rules are more precise than the Newton-Cotes rules. For n points in equation (3.74), the Gauss rules

Table 3.1. Gauss quadrature points and weights in 1-D problems

Number of Gauss points, n	Gauss points, u_{nl}	Weights, W_{nl}
1	$u_{11} = 0$	$W_{11} = 2$
2	$u_{21} = -\frac{1}{\sqrt{3}}$ $u_{22} = -\frac{1}{\sqrt{3}}$	$W_{21} = 1$ $W_{22} = 1$
3	$u_{31} = -\sqrt{\frac{3}{5}}$ $u_{32} = 0$ $u_{33} = -\sqrt{\frac{3}{5}}$	$W_{31} = \frac{5}{9}$ $W_{32} = \frac{8}{9}$ $W_{33} = \frac{5}{9}$

integrate exactly a polynomial of degree 2n-1. However, there is no simple answers for what order quadrature rule should be used. Enokizono et al. [112] even used one thousand quadrature points for a 2-D problem. A few sample values for the weights and the quadrature points are shown in Table 3.1. It might be noted that for each integration order, the sum of the weights equals 2, the length of the interval of integration.

Since the area integrals are over the bi-unit square, they may be treated as two separate 1-D integrals, each over an interval from -1 to +1, and hence the 1-D Gaussian quadrature formulas can be used for each integration. Thus, letting I(u,v) represent the integrand, any of the area integrals can be evaluated as follows,

$$\int_{-1}^{1}\int_{-1}^{1} I(u,v)\,du\,dv \cong \int_{-1}^{1}\left(\sum_{l=1}^{n} W_{nl} I\left(u_{nl},v\right)\right)dv = \sum_{k=1}^{n}\sum_{l=1}^{n} W_{nk} W_{nl} I\left(u_{nl},v_{nk}\right) \qquad (3.75)$$

The sampling points now form a 2-D array, as shown in Table 3.2, and the weights are the products of the 1-D weights. Since these rules are the extension of 1-D cases, they integrate exactly all the terms associated with the Lagrange family of elements which involve the products of 1-D polynomials, but they are not optimally efficient for the serendipity elements except, of course, the linear element.

With the aid of isoparametric mapping and Gaussian quadrature rules, differentiation and integration are carried out for each element, contributions from each element are summed up, and finally, a global matrix equation is obtained.

In general, the coefficient matrix, which is often called the stiffness matrix due to the terminology used in structural analysis, has all the information about the geometry and material properties. As we can predict in the form of equation (3.52), the stiffness matrix is symmetric for the Poisson equation. However, if we consider the probe velocity effect, the matrix is not symmetric due to the presence of the motional induction term. The right hand side vector contains information about the source. The stiffness matrix has some nice features such as bandedness, sparsity and diagonal dominance. The bandwidth is dependent upon the mesh and can be seen as the largest difference in node numbers of a single element, plus one. Therefore, effective numbering of nodes can drastically reduce the bandwidth thus reducing computer resources and solution time. The banded nature of the matrix can be utilized in the direct solution methods and the sparsity can be utilized in the iterative solution methods. Of course, if it exists, the symmetric property of the matrix is very helpful in both methods. Extensive

Table 3.2. Gauss quadrature points and weights in 2-D problems

n	Number of Gauss points, nxn	Gauss points, (u_{nl}, v_{nl})	Weights, $W_{nk} \times W_{nl}$
1	1	$(0, 0)$	4
2	4	$(-\frac{1}{\sqrt{3}}, -\frac{1}{\sqrt{3}})$	1
		$(-\frac{1}{\sqrt{3}}, \frac{1}{\sqrt{3}})$	1
		$(\frac{1}{\sqrt{3}}, -\frac{1}{\sqrt{3}})$	1
		$(\frac{1}{\sqrt{3}}, \frac{1}{\sqrt{3}})$	1
3	9	$(-\frac{\sqrt{3}}{\sqrt{5}}, -\frac{\sqrt{3}}{\sqrt{5}})$	$\frac{25}{81}$
		$(-\frac{\sqrt{3}}{\sqrt{5}}, 0)$	$\frac{40}{81}$
		$(-\frac{\sqrt{3}}{\sqrt{5}}, \frac{\sqrt{3}}{\sqrt{5}})$	$\frac{25}{81}$
		$(0, -\frac{\sqrt{3}}{\sqrt{5}})$	$\frac{40}{81}$
		$(0, 0)$	$\frac{64}{81}$
		$(0, \frac{\sqrt{3}}{\sqrt{5}})$	$\frac{40}{81}$
		$(\frac{\sqrt{3}}{\sqrt{5}}, -\frac{\sqrt{3}}{\sqrt{5}})$	$\frac{25}{81}$
		$(\frac{\sqrt{3}}{\sqrt{5}}, 0)$	$\frac{40}{81}$
		$(\frac{\sqrt{3}}{\sqrt{5}}, \frac{\sqrt{3}}{\sqrt{5}})$	$\frac{25}{81}$

survey of various solution techniques can be found in reference 30. In this dissertation, the Gaussian elimination technique is used. The technique decomposes the matrix into three matrices. A simple forward and backward substitution allows solution for the vector potential at each node point.

To impose a boundary condition, such as the Dirichlet boundary condition on the center axis and the distant boundaries in our axisymmetric problems, a blasting technique [114] is used. That is, the diagonal elements of the stiffness matrix which correspond to the specified boundary points are blasted or multiplied by a very large factor. The factor is many orders of magnitude larger than the values of the elements being dealt with in the matrix. The corresponding right hand side is replaced by the known value multiplied by the new large diagonal term. Thus, the other elements in the same row become effectively zero and the specified boundary value is enforced for that node. This technique can easily be integrated into the finite element program. The concept of this technique is very similar to the penalty function of the modified variational principle [118]. When minimizing the functional, subject to the unknowns obeying an additional differential relationship, a new functional is formed by including the integration of this constraint squared and multiplied by the penalty number. By using a large penalty number, this constraint can be achieved.

5. Postprocessing

The final step in the finite element method is postprocessing. When the FEM is used for modeling magnetic NDE methods, solutions are obtained in

the form of magnetic vector potentials. The purpose of postprocessing is to use the computer to interpret the results. Flux density (or Hall plate signal), coil impedance, eddy current densities, emf, phase, etc. can be calculated from the resulting magnetic vector potential values. Also, equipotential plots can be drawn. Indeed, plotting is a good way to judge the correctness of the solution and provides better understanding of energy/defect interactions. In this subsection, the output signals of the NDE methods selected in this dissertation are explained.

Hall plate signal of the variable reluctance probe

The Hall plate signal is in fact a normal component of the flux density. From Figure 2.3, the normal component can be identified as the r-component. The expression of flux density in terms of magnetic vector potential can be obtained from the definition of the magnetic vector potential,

$$\overline{B} = \nabla \times \overline{A}$$

$$= \begin{vmatrix} \frac{1}{r}\hat{r} & \hat{\theta} & \frac{1}{r}\hat{z} \\ \frac{\partial}{\partial r} & 0 & \frac{\partial}{\partial z} \\ 0 & rA & 0 \end{vmatrix} = \left(-\frac{\partial A}{\partial z}\right)\hat{r} + \left(\frac{A}{r} + \frac{\partial A}{\partial r}\right)\hat{z} = B_r\hat{r} + B_z\hat{z} \qquad (3.76)$$

where the axisymmetric nature of the problem makes $\frac{\partial}{\partial \theta}$, the r-component and z-component of $\overline{A}$ zero. To find B_r for the Hall plate signal, the differentiation of A, i.e. the θ–component of $\overline{A}$, with respect to z is necessary. However, since isoparametric mapping is used, the spatial derivative $\frac{\partial}{\partial z}$ was already calculated during the finite element formulation process. Equation

(3.63) defines the derivatives of the shape functions with respect to r and z. These are the transformed derivatives from the local u-v coordinate system to the r-z coordinate system. Since the shape functions at their corresponding nodes have a value of 1, and 0 elsewhere, the derivatives in equation (3.63) can be considered as spatial derivatives and used to evaluate the flux density components. For each element, the derivative with respect to z is calculated during the numerical integration over the element and stored in a special array. The $\frac{\partial A}{\partial z}$ is then calculated simply by multiplying the derivative at each node to the value of A at each node. This calculation gives the B_r value at each node, but the Hall plate was assumed to take an element. Therefore, an average of the four nodal values of the element is used as the Hall plate signal.

Differential impedance of the differential eddy current probe

Although the finite element formulation of the eddy current method is not explained specifically in this chapter, it is almost the same as that of the magnetic flux leakage method. Therefore, we can assume that the complex valued magnetic vector potential solutions for the eddy current problem are already obtained.

There are, in general, two ways of finding the impedance of the coil. One is to use Faraday's law by interpreting the emf induced in the coil as the integration of the emf-producing field $\overline{E}$ all the way around the coil. In this case, the magnetic vector potential solutions of the finite element analysis are directly used for the calculation of coil impedance. For this reason, the phase information with respect to the source can be directly obtained. Palanisamy

[28] and Satish [29] use this method based on centroidal values of r and A. To avoid an error associated with these centroidal values, Udpa [31] performed an integration over the source coil region incorporated into the finite element model by obtaining a closed form expression for the integrand.

One other method uses the energy of the system. This method is more accurate than the direct use of the potential solution and it is proved by Hoole [104] as follows. Consider equation (3.25). This equation can be rewritten as

$$F = \iint \left\{ \frac{\nu}{2} (\nabla A)^2 - J_s A \right\} dR \tag{3.77}$$

Now, take a small variation of A, i.e. $A \rightarrow A + k\eta$, where k is a small constant less than 1, and η is a function of the coordinate variables. Then, we have

$$F + \delta F = \iint \left[\frac{\nu}{2} \{ \nabla (A + k\eta) \}^2 - J_s (A + k\eta) \right] dR \tag{3.78}$$

Subtracting equation (3.77) from equation (3.78),

$$\delta F = \iint \left[\nu k (\nabla A \cdot \nabla \eta) + k^2 (\nabla \eta)^2 - J_s k \eta \right] dR \tag{3.79}$$

Now, if we integrate the identity,

$$\nabla \cdot (\eta \nabla A) = \eta \nabla^2 A + \nabla A \cdot \nabla \eta \tag{3.80}$$

over the region of solution R and apply the divergence theorem to the left hand side,

$$\int \eta \nabla A \cdot d\bar{S} = \iint \left(\eta \nabla^2 A + \nabla A \cdot \nabla \eta \right) dR \tag{3.81}$$

Putting this into equation (3.79), we get

$$\delta F = \int \nu k \eta \frac{\partial A}{\partial n} dS - \iint k \eta \left(\nu \nabla^2 A + J_s \right) dR + \iint k^2 \nu (\nabla \eta)^2 dR \tag{3.82}$$

As mentioned earlier, the first integral vanishes because of the boundary conditions and the second term vanishes when the governing equation is satisfied. The last term is positive and of order k^2, which shows that the functional is at a minimum and also that when the changes in A are of order k, changes in the functional are even smaller and of order k^2. Therefore, energy is of one higher order of accuracy than potential.

For the impedance calculation, we can associate inductance with the stored energy and resistance with the dissipated energy [30]. The stored energy can be written as

$$W = \int_v \frac{1}{2}\overline{B}\cdot\overline{H}dv = \sum_{i=1}^{N}\frac{1}{2}v_i\left[B_{ri}^2 + B_{zi}^2\right]v_i$$

$$= \sum_{i=1}^{N} v_i\left[\left\{\left(\frac{\partial A}{\partial z}\right)_{ci}\right\}^2 + \left\{\frac{A_{ci}}{r_{ci}} + \left(\frac{\partial A}{\partial r}\right)_{ci}\right\}^2\right]\pi r_{ci}\Delta_i \qquad (3.83)$$

where

N is the total number of elements,

Δ_i is the elemental area on the r-z plane,

$v_i = 2\pi r_{ci}\Delta_i$ is the element volume,

subscript ci means the centroidal value of element i.

Again, the derivatives are calculated at each node as explained earlier and averaged centroidal values of elements are used in the above equation. Another familiar expression for the stored energy is

$$W = \frac{1}{2} L I_s^2 \qquad (3.84)$$

where L is the inductance of the coil and I_s the current in the coil. Therefore, the inductance, L, can be obtained from equation (3.83) and (3.84).

The calculation of the resistive part of the system is based on the eddy current distribution. The dissipated energy can be written as

$$P = \int_v \bar{J}_e \cdot \bar{E}_e dv = \sum_{i=1}^{N} \frac{1}{\sigma_i} \left| (J_e)_{ci} \right|^2 v_i$$

$$= \sum_{i=1}^{N} \omega^2 \sigma_i |A_{ci}|^2 2\pi r_{ci} \Delta_i \qquad (3.85)$$

where

$\overline{J_e} = J_e \hat{\theta}$ is the eddy current density,

$(J_e)_{ci} = -j\omega\sigma_i A_{ci}$ is the centroidal eddy current density of element i,

$\overline{E_e}$ is the emf-producing field associated with $\overline{J_e}$,

ω is the angular frequency.

The coil resistance now becomes

$$R = \frac{P}{I_s^2} \qquad (3.86)$$

and finally, the coil impedance can be written as

$$Z = R + j\omega L = \frac{1}{I_s^2} \left(P + j\omega 2W \right) \qquad (3.87)$$

Although this energy approach is more accurate, there are some drawbacks. Because energy calculations involves squared terms and absolute values of the magnetic vector potential, the original information regarding phase with respect to the source is lost. Also, it is impossible to

calculate the impedance of each coil in a differential probe. That is because the energy is found from the total energy and therefore yields the total impedance regardless of the number of coils, their shapes or their locations in the solution region. To avoid the latter difficulty, the impedance of an absolute coil is calculated for all the positions of each coil in the differential probe and then, the differential impedance is found by taking the difference between the two absolute impedances that correspond to the positions of the two coils in the differential probe.

Induced emf of the remote field eddy current probe

Unlike the differential eddy current probe, the remote field eddy current probe has a separate sensor coil and the output NDE signal sought is the magnitude and phase of the emf induced in that coil. The induced emf, V, is given by Faraday's law,

$$V = - N_t \frac{d\phi}{dt} \tag{3.88}$$

where N_t is the number of turns in the sensor coil and ϕ is the total magnetic flux across the sensor coil. The total magnetic flux is given by

$$\phi = \iint \overline{B} \cdot d\overline{S} = \iint (\nabla \times \overline{A}) \cdot d\overline{S} = \oint \overline{A} \cdot d\overline{l} \tag{3.89}$$

The last step is due to Stoke's theorem. Then, for a circular coil of radius r,

$$\phi = \oint_{\theta} \overline{A} \cdot r d\overline{\theta} = 2\pi r A \tag{3.90}$$

since $\overline{A} = A\hat{\theta}$. Therefore, the induced emf under the AC steady state condition is

$$V = - j\omega N_t 2\pi r A \tag{3.91}$$

where ω is the angular frequency of the current source. Again, the centroidal values of r and A of the elements that correspond to the sensor coil area are used in the above calculation. For example, suppose the centroidal values of r and A of a coil element i are r_{ci} and A_{ci}, respectively, and the number of turns associated with each coil element is the same, then the total emf is

$$V = - N_t \sum_{i=1}^{M} j2\pi\omega r_{ci} A_{ci} \tag{3.92}$$

where M is the total number of elements in the sensor coil area. Note that the emf and A_{ci} are, in fact, complex phasor values. Therefore, we can write V = a + jb. In the time domain, this can be written as

$$V = \sqrt{a^2+b^2}\,\sin\{\omega t + TAN^{-1}(\frac{b}{a})\} \tag{3.93}$$

Hence the peak value of the induced emf is $\sqrt{a^2+b^2}$, and the phase angle is $TAN^{-1}(\frac{b}{a})$.

B. Finite Difference Method for Temporal Discretization

There are situations where the excitation is nonsinusoidal such as a pulsed excitation, or the steady state can not be defined due to non-uniform geometries in the case of the moving magnetic fields as mentioned in

Chapter I. In these cases, the unknown magnetic vector potential, A, is a function of time so that the time dependent transient analysis is necessary. The A in the case of sinusoidal excitation is in fact a function of time, but under the sinusoidal steady state conditions the phasor variable, which is not time dependent, can be used . If the unknown variable is a function only of time, the ordinary differential equation results and this kind of problem is called the initial-value problem. Compared to the requirement of boundary conditions on all sides of the solution domain in the boundary-value problem, the initial-value problem requires only an initial condition at a certain time and marches forward indefinitely into the future. Equation (3.3), however, involves several spatial derivative terms as well as a temporal derivative term. Therefore, the A is a function of both time and space, and the equation is a partial differential equation. Specifically, it is a parabolic partial differential equation since the time derivative is first order. This kind of problem is called the mixed initial-value/boundary-value problem [170]. In this case, not only the initial condition but also boundary conditions are required.

All the numerical methods are capable of dealing with transient problems. In the boundary element method, however, the transient analysis is not a common practice [105]. Although the finite element method can handle the time discretization in a similar way to the spatial discretization [170,183], the most popular method is the finite difference method. In this dissertation, therefore, the finite difference method is used for time discretization.

1. Derivation of Elemental Matrix Equation

Since A is a function of three variables, r, z, and t, the approximation of A might be written as

$$A(r,z,t) = [\mathbf{N}(r,z,t)]\{\mathbf{A}\} \tag{3.94}$$

that is, the shape functions are now also a function of time. However, this approach has some difficulties. Because of the time axis, 3-D elements are required and the 'boundary' condition at t = ∞ is missing. One way to resolve this lack of boundary condition is to first calculate the steady state solution. Anyway, the dimensional increase in elements and the requirement of pre-calculation for the boundary condition makes this approach unattractive.

Instead of putting all the independent variables in the shape functions, {A} can be made time dependent so that the shape functions remain the same as in the former boundary-value problem. That is,

$$A(r,z,t) = [\mathbf{N}(r,z)]\{\mathbf{A}(t)\} \tag{3.95}$$

This is the classical separation of variables technique, sometimes also referred to as the method of Kantorovich. At this point, compare equations (3.3) and (3.1). The only difference is the time derivative term, $-\sigma\frac{\partial \overline{A}}{\partial t}$, in equation (3.3). This term is treated as a function independent of $\overline{A}$ in this formulation. Since the shape functions have not changed from the earlier development for equation (3.1), the elemental matrix $[\mathbf{S}]_e$ and $\{\mathbf{Q}\}_e$ of equations (3.52) and (3.53) can still be used without any alteration. These matrices $[\mathbf{S}]_e$ and $\{\mathbf{Q}\}_e$ correspond to the second order spatial derivative term and the

source term, respectively. Using the same weak formulation, the time derivative term becomes

$$\int_v \delta A\left(-\sigma\frac{\partial A}{\partial t}\right)dv \tag{3.96}$$

From equation (3.95), the approximation of the derivative term in an element can be written as

$$\frac{\partial A(r,z,t)}{\partial t} = \dot{A}(r,z,t) = [\mathbf{N}(r,z)]\{\dot{\mathbf{A}}(t)\}_e \tag{3.97}$$

Substituting equation (3.97) into the elemental integration of equation (3.96) gives

$$-\int_{v_e} \delta\{\mathbf{A}\}_e{}^T\left(\sigma[\mathbf{N}]^T[\mathbf{N}]\left\{\dot{\mathbf{A}}\right\}_e\right)dv \tag{3.98}$$

Combining equation (3.98) with equation (3.50) gives

$$\int_{v_e} \delta\{\mathbf{A}\}_e{}^T\left[\nu[\nabla\mathbf{N}]^T[\nabla\mathbf{N}]\{\mathbf{A}\}_e + \sigma[\mathbf{N}]^T[\mathbf{N}]\left\{\dot{\mathbf{A}}\right\}_e - J_s[\mathbf{N}]^T\right]dv = 0 \tag{3.99}$$

Since this equation must be satisfied for any variation δA, the elemental matrix equation can be written as

$$[\mathbf{S}]_e\{\mathbf{A}\}_e + [\mathbf{C}]_e\left\{\dot{\mathbf{A}}\right\}_e = \{\mathbf{Q}\}_e \tag{3.100}$$

where $[\mathbf{C}]_e = \int_{v_e} \sigma[\mathbf{N}]^T[\mathbf{N}]dv$, and $[\mathbf{S}]_e$ and $\{\mathbf{Q}\}_e$ are the same as shown in equations (3.52) and (3.53). Summation of all the elemental contributions gives the global matrix equation,

$$[\mathbf{S}]\ \{\mathbf{A}\}\ + [\mathbf{C}]\ \left\{\dot{\mathbf{A}}\right\}\ = \{\mathbf{Q}\} \tag{3.101}$$

2. Finite Difference Method for Time Stepping

In all time stepping methods, the time axis is divided into a succession of time steps beginning at time t_0. The time step size may be uniform or non-uniform. Therefore, we look for an approximate solution consisting of discrete values at the end of each time step. The discrete values are computed from a recurrence relation, which is an algebraic equation that relates the values at two or more successive times. A one step method relates the discrete values at both ends of a single time step. For example, the one step method in the n th time step has the form,

$$[\mathbf{D}]\{\mathbf{A}\}^n + [\mathbf{E}]\{\mathbf{A}\}^{n-1} = \theta_1\{\mathbf{G}\}^n + \theta_2\{\mathbf{G}\}^{n-1} \tag{3.102}$$

where the coefficient matrices [**D**] and [**E**] are known constants, which can be expressed by our [**S**] and [**C**] matrices. The coefficients θ_1 and θ_2 are also known constants and their values are related to the type of difference method such as the forward, backward, and central difference. The $\{\mathbf{G}\}^n$ and $\{\mathbf{G}\}^{n-1}$ are the source vector, $\{\mathbf{G}(t)\}$, evaluated at times t_n and t_{n-1}, respectively, and hence are also known. At the first time step, where n=1, $\{\mathbf{A}\}^1$ is obtained by using the initial condition, $\{\mathbf{A}\}^0$. At the second time step, $\{\mathbf{A}\}^2$ can be obtained by using the result, $\{\mathbf{A}\}^1$, from the former step and so forth. Phrases such as 'time-stepping' and 'time-marching' are therefore used to describe this process. A multistep method relates the discrete values corresponding to k successive time steps. Since this method requires k initial values, it is not so popular. Therefore, the one step method is employed in this dissertation.

Since only one step is considered, we consider the (n+1)th uniform time step, which carries the solution from time t_n to time t_{n+1}. There are many types of finite difference method. In the backward difference method (also known as the backward Euler rule), each of the terms in equation (3.101) is evaluated at time t_{n+1}. On the other hand, in the forward difference method (known as Euler's rule), each term is evaluated at time t_n. In both methods, however, the expression of the time derivative term is the same even if the time derivative term is evaluated at different times. That is, in the backward method,

$$\{\dot{\mathbf{A}}\}^{n+1} = \frac{\{\mathbf{A}\}^{n+1} - \{\mathbf{A}\}^{n}}{\Delta t} \tag{3.103}$$

and in the forward method,

$$\{\dot{\mathbf{A}}\}^{n} = \frac{\{\mathbf{A}\}^{n+1} - \{\mathbf{A}\}^{n}}{\Delta t} \tag{3.104}$$

To understand the difference between these two methods, consider the Taylor series. For convenience, the braces and the bold type are omitted. The unknown variable, A, is expressed by the old and new time levels in terms of its value at the point of origin of the Taylor series. If we choose the new time level, t_{n+1}, as the origin, we can write

$$A^n = A(t_{n+1} - \Delta t) = A^{n+1} - \Delta t \frac{\partial A^{n+1}}{\partial t} + \frac{\Delta t^2}{2} \frac{\partial^2 A^{n+1}}{\partial t^2} + \vartheta\left(\Delta t^3\right) \tag{3.105}$$

where $A^n = A(t_n)$. Ignoring the second and higher order error terms, we get equation (3.103). Consequently, the backward method is first order accurate.

If we choose the old time level, t_n, as the origin,

$$A^{n+1} = A(t_n + \Delta t) = A^n + \Delta t \frac{\partial A^n}{\partial t} + \frac{\Delta t^2}{2} \frac{\partial^2 A^n}{\partial t^2} + \vartheta\left(\Delta t^3\right) \tag{3.106}$$

Ignoring the second and higher order error terms, we get equation (3.104) and the forward method also becomes first order accurate.

To achieve a better accuracy, the midpoint, $t_{n+\frac{1}{2}}$, can be chosen. That is,

$$A^{n+1} = A\left[\left(t_n + \frac{\Delta t}{2}\right) + \frac{\Delta t}{2}\right] = A\left(t_n + \frac{\Delta t}{2}\right) + \frac{\Delta t}{2} \frac{\partial A\left(t_n + \frac{\Delta t}{2}\right)}{\partial t} + \frac{\Delta t^2}{8} \frac{\partial^2 A\left(t_n + \frac{\Delta t}{2}\right)}{\partial t^2} + \vartheta\left(\Delta t^3\right) \tag{3.107}$$

and

$$A^n = A\left[\left(t_n + \frac{\Delta t}{2}\right) - \frac{\Delta t}{2}\right] = A\left(t_n + \frac{\Delta t}{2}\right) - \frac{\Delta t}{2} \frac{\partial A\left(t_n + \frac{\Delta t}{2}\right)}{\partial t} + \frac{\Delta t^2}{8} \frac{\partial^2 A\left(t_n + \frac{\Delta t}{2}\right)}{\partial t^2} + \vartheta\left(\Delta t^3\right) \tag{3.108}$$

By subtracting equation (3.108) from equation (3.107), we get

$$A^{n+1} - A^n = \Delta t \frac{\partial A^{n+1/2}}{\partial t} + \vartheta\left(\Delta t^3\right) \tag{3.109}$$

Ignoring the error term gives

$$\frac{\partial A^{n+1/2}}{\partial t} = \frac{A^{n+1} - A^n}{\Delta t} \tag{3.110}$$

Again, we have the same expression for the time derivative. This is the central difference method (also known as the Crank-Nicolson method), which has second order accuracy as can be seen in equation (3.109).

There is a more general method which uses the dimensionless time weighting factor, θ. Figure 3.4 shows the variation of θ. The value of θ is

$$\theta = \frac{t - t_n}{\Delta t} \tag{3.111}$$

and with this θ, the interpolation polynomial can be written as follows.

$$\{\mathbf{A}\}^{\theta} = \{\mathbf{A}\}^{n} + \theta\left[\{\mathbf{A}\}^{n+1} - \{\mathbf{A}\}^{n}\right] = (1-\theta)\{\mathbf{A}\}^{n} + \theta\{\mathbf{A}\}^{n+1} \tag{3.112}$$

This means that the θ plays the role of local coordinate, ranging from 0 to 1, similar to the local coordinate, u, ranging from -1 to 1 as shown in Figure 3.3. If θ = 0, {**A**} is evaluated at time t_n, i.e. the forward difference method; for θ = 1, {**A**} is evaluated at time t_{n+1}, i.e. the backward difference method; and for $\theta = \frac{1}{2}$, {**A**} is evaluated at time $t_{n+\frac{1}{2}}$, i.e. the central difference method. As we have seen earlier in equations (3.103), (3.104), and (3.110), the expression for the time derivative is always the same. Therefore, it can be written as

$$\left\{\dot{\mathbf{A}}\right\}^{\theta} = \frac{\{\mathbf{A}\}^{n+1} - \{\mathbf{A}\}^{n}}{\Delta t} \tag{3.113}$$

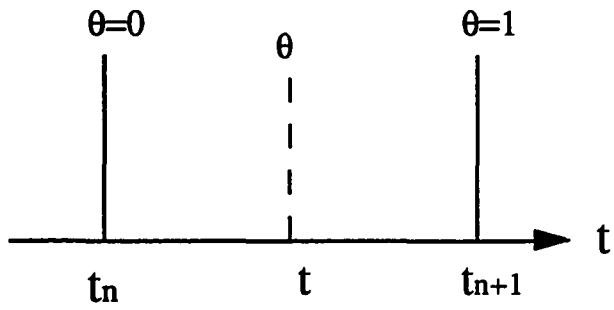

Figure 3.4. Time weighting factor over the (n+1)th time step

Using equations (3.112) and (3.113), equation (3.101) can then be written as

$$\left[\frac{1}{\Delta t}[\mathbf{C}]+\theta[\mathbf{S}]\right]\{\mathbf{A}\}^{n+1}=\{\mathbf{Q}\}^{ave}+\left[\frac{1}{\Delta t}[\mathbf{C}]-(1-\theta)[\mathbf{S}]\right]\{\mathbf{A}\}^{n} \tag{3.114}$$

where, like equation (3.112),

$$\{\mathbf{Q}\}^{ave}=(1-\theta)\{\mathbf{Q}\}^{n}+\theta\{\mathbf{Q}\}^{n+1} \tag{3.115}$$

In the above formulation, we have not associated a time superscript to either the [C] or the [S] matrices. If these matrices are explicit functions of time, then they should be evaluated at time $t+\theta\Delta t$.

Now, examine the coefficient matrix on the left hand side of equation (3.114) closely. In the backward (θ=1) or central (θ=1/2) difference methods, the matrix [S] does not disappear and the coefficient matrix is a nondiagonal matrix which requires matrix 'inversion'. Because of this, these methods are said to be implicit, meaning that the unknown, $\{\mathbf{A}\}^{n+1}$, is defined implicitly by equation (3. 114). In other words, $\{\mathbf{A}\}^{n+1}$ at any nodal point will be given implicitly in an equation involving other nodal point values of A at t_{n+1}. In this problem, fortunately, the matrices [S] and [C] are both symmetric so that this property can be used in the matrix solution algorithm.

In the forward difference method (θ=0), however, the coefficient matrix consists of only the matrix [C], which is called the mass matrix in structural engineering problems. If the finite difference method were used for spatial discretization, this matrix would be a diagonal matrix so that matrix inversion would not be necessary. The solution could be obtained explicitly and very rapidly by merely dividing the corresponding right hand side term

by the left hand side coefficient on the diagonal of the coefficient matrix. In the finite element method, unfortunately, the matrix [C] is not a diagonal matrix, thus making the equation implicit. Because of this, techniques for diagonalizing [C] are developed and are called mass lumping [118,130,170]. The procedure of mass lumping is to add all the terms in each row of [C], place the sum on the diagonal, and then replace the off-diagonal terms to zero. This lumping technique can be used only in the forward difference method and is very helpful in saving solution time considering the limitation of time step size imposed on the forward difference method. The smaller the time step, the more the recurrence calculations are required. The limitation of time step size is due to the stability consideration. Stability analysis is discussed in the next subsection.

3. Stability Analysis of Temporal Dicretization

Stability is concerned with the behavior of the solution as time goes to infinity and calls for the boundedness of all perturbations in a computed solution. It is a characteristic of the method, not of the particular problem the method is applied to. For example, the backward difference method is unconditionally stable, while the forward difference method is stable only under a certain condition. Stable or unstable behavior can be investigated by examining the free response of a system [170]. If unstable behavior exists in the free response, the oscillations in the homogeneous solution will grow very large as time increases, so that the total response will also be unstable even if the particular response were stable.

There are two methods frequently used to test for stability, the matrix (or eigenvalue) method [86,170,184] and the von Neumann method [86,184]. Consider equation (3.114). If there is an alternative solution $\{\mathbf{a}\}^n$ based on the same discretization but with a different initial condition, then the difference

$$\{\mathbf{E}\}^n = \{\mathbf{A}\}^n - \{\mathbf{a}\}^n \tag{3.116}$$

satisfies

$$\{\mathbf{E}\}^{n+1} = \left[\frac{1}{\Delta t}[\mathbf{C}] + \theta[\mathbf{S}]\right]^{-1}\left[\frac{1}{\Delta t}[\mathbf{C}] - (1-\theta)[\mathbf{S}]\right]\{\mathbf{E}\}^n = [\mathbf{B}]\{\mathbf{E}\}^n = ([\mathbf{B}])^{n+1}\{\mathbf{E}\}^0 \tag{3.117}$$

where $\{\mathbf{E}\}^0 = \{\mathbf{A}\}^0 - \{\mathbf{a}\}^0$. A stable method is one in which the effect of the perturbation $\{\mathbf{E}\}^0$ does not grow. For errors to die out or be damped as n increases, it is necessary that the norm of matrix [**B**] must be less than 1. In other words, the absolute value of the eigenvalue of [**B**] must be less than 1. Since equation (3.117) involves the number of unknowns equal to the total number of nodes in the solution region, there are many eigenvalues. Therefore, the maximum eigenvalue (also called spectral radius) has to be used to satisfy the stability condition. This is the matrix method. To find the maximum eigenvalue of the finite element model, not the exact problem, we need to solve the eigenvalue problem for the system numerically unless the approximation for that eigenvalue is used. This requirement of additional computation simply to determine the maximum eigenvalue makes the matrix method not so attractive. Hindmarsh et al. [185] compare the two methods and prefer the von Neumann method even though it ignores boundary conditions.

The von Neumann method is based on the finite discrete Fourier series expansion for the error. The method applies, in a theoretical sense, only to pure initial value problems so that it neglects the influence of boundary conditions. However, this is not a serious problem because instability is usually generated far from the boundaries [185]. Further, it applies only to linear, constant coefficient, finite difference approximations. If the linearization condition is not met, some form of local linearization is necessary. This linear property allows us to treat each Fourier component separately and use superposition to add all other components. The method also requires a difference form of equation. Therefore, we need to write the finite element equation in the form of a difference equation.

To do this, consider the 1-D version of equation (3.3) in a purely mathematical sense. Since only the free response of the system is to be examined, the source term is ignored. Then, the governing equation can be written as

$$\nu\frac{\partial^2 A}{\partial z^2} = \sigma\frac{\partial A}{\partial t} \tag{3.118}$$

The weak formulation yields

$$\int \delta A\left[\sigma\frac{\partial A}{\partial t} - \nu\frac{\partial^2 A}{\partial z^2}\right]dl = 0 \tag{3.119}$$

After integrating by parts and substituting the elemental approximation of A,

$$\int_e \{\delta\mathbf{A}\}_e{}^T[\mathbf{N}]^T\sigma[\mathbf{N}]\{\dot{\mathbf{A}}\}_e\,dl + \int_e \{\delta\mathbf{A}\}_e{}^T\left[\frac{\partial\mathbf{N}}{\partial z}\right]^T\nu\left[\frac{\partial\mathbf{N}}{\partial z}\right]\{\mathbf{A}\}_e\,dl = 0 \tag{3.120}$$

Here, the approximation of A in a 1-D linear element can be written as

$$A = [\mathbf{N}]\{\mathbf{A}\}_e = \begin{bmatrix} 1-\frac{z}{h} & \frac{z}{h} \end{bmatrix} \begin{Bmatrix} A_L \\ A_R \end{Bmatrix} \tag{3.121}$$

where h is the length of an element. Note here that the shape functions are not written for isoparametric elements. Equation (3.120) can be written in a matrix form as follows.

$$[\mathbf{C}]_e \{\dot{\mathbf{A}}\}_e + [\mathbf{S}]_e \{\mathbf{A}\}_e = 0 \tag{3.122}$$

where

$$[\mathbf{C}]_e = \int_e [\mathbf{N}]^T \sigma [\mathbf{N}] dl = \sigma \int_0^h \begin{bmatrix} 1-\frac{z}{h} \\ \frac{z}{h} \end{bmatrix} \begin{bmatrix} 1-\frac{z}{h} & \frac{z}{h} \end{bmatrix} dl = \sigma \begin{bmatrix} \frac{h}{3} & \frac{h}{6} \\ \frac{h}{6} & \frac{h}{3} \end{bmatrix} \tag{3.123}$$

$$[\mathbf{S}]_e = \int_e \left[\frac{\partial \mathbf{N}}{\partial z}\right]^T \nu \left[\frac{\partial \mathbf{N}}{\partial z}\right] dl = \nu \int_0^h \begin{bmatrix} -\frac{1}{h} \\ \frac{1}{h} \end{bmatrix} \begin{bmatrix} -\frac{1}{h} & \frac{1}{h} \end{bmatrix} = \nu \begin{bmatrix} \frac{1}{h} & -\frac{1}{h} \\ -\frac{1}{h} & \frac{1}{h} \end{bmatrix} \tag{3.124}$$

This is the elemental matrix equation. To assemble the global matrix, consider the whole solution domain shown in Figure 3.5. Suppose that the

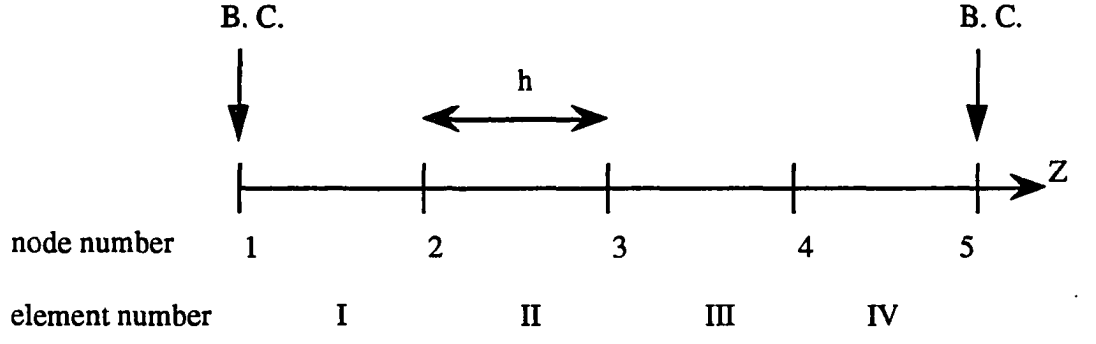

Figure 3.5. Solution domain of 1-D problem

matrix equation is expressed as follows,

$$[C]\{\dot{A}\}+[S]\{A\}=0 \tag{3.125}$$

then, the global matrices [C] and [S] become

$$[C]=\sigma\begin{bmatrix} \frac{h}{3} & \frac{h}{6} & 0 & 0 & 0 \\ \frac{h}{6} & \frac{h}{3}+\frac{h}{3} & \frac{h}{6} & 0 & 0 \\ 0 & \frac{h}{6} & \frac{h}{3}+\frac{h}{3} & \frac{h}{6} & 0 \\ 0 & 0 & \frac{h}{6} & \frac{h}{3}+\frac{h}{3} & \frac{h}{6} \\ 0 & 0 & 0 & \frac{h}{6} & \frac{h}{3} \end{bmatrix}=\sigma\begin{bmatrix} \frac{h}{3} & \frac{h}{6} & 0 & 0 & 0 \\ \frac{h}{6} & \frac{2h}{3} & \frac{h}{6} & 0 & 0 \\ 0 & \frac{h}{6} & \frac{2h}{3} & \frac{h}{6} & 0 \\ 0 & 0 & \frac{h}{6} & \frac{2h}{3} & \frac{h}{6} \\ 0 & 0 & 0 & \frac{h}{6} & \frac{h}{3} \end{bmatrix} \tag{3.126}$$

$$[S]=\nu\begin{bmatrix} \frac{1}{h} & -\frac{1}{h} & 0 & 0 & 0 \\ -\frac{1}{h} & \frac{1}{h}+\frac{1}{h} & -\frac{1}{h} & 0 & 0 \\ 0 & -\frac{1}{h} & \frac{1}{h}+\frac{1}{h} & -\frac{1}{h} & 0 \\ 0 & 0 & -\frac{1}{h} & \frac{1}{h}+\frac{1}{h} & -\frac{1}{h} \\ 0 & 0 & 0 & -\frac{1}{h} & \frac{1}{h} \end{bmatrix}=\nu\begin{bmatrix} \frac{1}{h} & -\frac{1}{h} & 0 & 0 & 0 \\ -\frac{1}{h} & \frac{2}{h} & -\frac{1}{h} & 0 & 0 \\ 0 & -\frac{1}{h} & \frac{2}{h} & -\frac{1}{h} & 0 \\ 0 & 0 & -\frac{1}{h} & \frac{2}{h} & -\frac{1}{h} \\ 0 & 0 & 0 & -\frac{1}{h} & \frac{1}{h} \end{bmatrix} \tag{3.127}$$

where, for the sake of explanation, material properties, σ and ν, are respectively assumed to be the same in the whole domain. In the global matrices, each column and row correspond to the global node number and contributions from elements are placed according to the global node numbers of the elements. For example, the contribution from the element I is placed at C(1,1), C(1,2), C(2,1) and C(2.2) since the global node numbers of that element are 1 and 2. Because the global node number 2 is also present in element II, this contribution from the element II is superimposed at C(2,2).

Now, by using the general θ-difference method, equation (3.125) can be written as

$$\left[\frac{1}{\Delta t}[\mathbf{C}]+\theta[\mathbf{S}]\right]\{\mathbf{A}\}^{n+1}=\left[\frac{1}{\Delta t}[\mathbf{C}]-(1-\theta)[\mathbf{S}]\right]\{\mathbf{A}\}^{n} \tag{3.128}$$

or using the definition of errors in equation (3.116),

$$\left[\frac{1}{\Delta t}[\mathbf{C}]+\theta[\mathbf{S}]\right]\{\mathbf{E}\}^{n+1}=\left[\frac{1}{\Delta t}[\mathbf{C}]-(1-\theta)[\mathbf{S}]\right]\{\mathbf{E}\}^{n} \tag{3.129}$$

From equations (3.126) and (3.127), we can evaluate the coefficient matrices. To write a difference form of equation, we select a node which is not at the boundary, e.g. node number 3. Then, we can write the difference equation for node k by using the elements of the k th row of the coefficient matrices.

$$\begin{aligned}&\frac{\sigma h}{6\Delta t}\left[E_{k-1}^{n+1}+4E_{k}^{n+1}+E_{k+1}^{n+1}\right]+\frac{\theta\nu}{h}\left[-E_{k-1}^{n+1}+2E_{k}^{n+1}-E_{k+1}^{n+1}\right]\\&=\frac{\sigma h}{6\Delta t}\left[E_{k-1}^{n}+4E_{k}^{n}+E_{k+1}^{n}\right]-\frac{(1-\theta)\nu}{h}\left[-E_{k-1}^{n}+2E_{k}^{n}-E_{k+1}^{n}\right]\end{aligned} \tag{3.130}$$

where the superscript and subscript denote the time level and the node number, respectively. Note that the terms inside the bracket associated with ν (i.e. corresponding to the second order spatial derivative term) show the central difference scheme. This shows that the standard Galerkin method or weak formulation always reproduces the central difference formulas when there is no time derivative term (i.e. for steady state equations) as mentioned in Chapter I, where the upwinding technique is explained.

We now have the difference form of equation. The von Neumann method assumes that the nodal errors can be represented by a finite discrete Fourier

series at each time level and such that each component is multiplied by a scalar amplification factor as the scheme proceeds to the next time level. However, because of linearity, it is possible to consider a single component. Thus, in one space dimension, we can write [86,185,186],

$$E_k^n = \xi^n e^{j\alpha kh} \tag{3.131}$$

where ξ is the amplification factor, α is the spatial frequency of the error or wave number, and $j = \sqrt{-1}$. If the method is stable, the absolute value of the amplification factor should be less than 1.

Now, substituting equation (3.131) into equation (3.130) and dividing it by E_k^n,

$$\xi = \frac{\frac{\sigma h}{3\Delta t}\left[2\cos^2\left(\frac{\alpha h}{2}\right)+1\right]-4(1-\theta)\frac{\nu}{h}\sin^2\left(\frac{\alpha h}{2}\right)}{\frac{\sigma h}{3\Delta t}\left[2\cos^2\left(\frac{\alpha h}{2}\right)+1\right]+4\theta\frac{\nu}{h}\sin^2\left(\frac{\alpha h}{2}\right)}$$

$$= 1-\frac{X}{1+\theta X} \tag{3.132}$$

where

$$X = \frac{12\nu\Delta t}{\sigma h^2}\frac{\sin^2\left(\frac{\alpha h}{2}\right)}{2\cos^2\left(\frac{\alpha h}{2}\right)+1} \tag{3.133}$$

The stability condition requires $-1 \le \xi \le 1$ for all α. Since X and θ are always positive, the upper condition is automatically satisfied. The lower condition can be rewritten as $(1-2\theta)X \le 2$. If $\theta \ge \frac{1}{2}$, this stability condition is

satisfied so that the method is unconditionally stable. Therefore, the central difference method and the backward difference method are unconditionally stable. Further study [170] shows that when the time step is very large, the central difference solutions may oscillate for many time steps, but with slow decay in the oscillations. The backward difference solutions, however, approach steady state with no oscillations at all.

If $\theta < \frac{1}{2}$, the worst case is when $\sin(\frac{\sigma h}{2}) = 1$ and this leads to the following condition,

$$\Delta t \leq \frac{\sigma h^2}{6\nu(1-2\theta)} \tag{3.134}$$

Therefore, the forward difference method is conditionally stable and the time step size should not exceed the limit given by equation (3.134).

CHAPTER IV

GOVERNING EQUATION FOR PROBE VELOCITY EFFECTS

A. Existence of Quasi-Static System in the Presence of a Moving Probe

Most electromagnetic NDE processes which operate at frequencies where the displacement current term is negligible can be described by the quasi-static form of Maxwell's equations [5]. This form of the equations is used to explain the laws of circuit theory and electromagnetic diffusion phenomena. However, it is not clear whether the quasi-static approximation is valid in the presence of a moving probe. Therefore, its validity in the presence of a moving probe is studied in this section.

The usual definitions of quasi-statics are somewhat loose. One approach to the quasi-static approximation is through the *in-vacuo* wavelength λ of the considered field which oscillates at frequency f [187]. If the characteristic dimension l of the system under investigation is much smaller than the wavelength, the exchange mechanism between electric and magnetic energy may be disregarded and it is a case of quasi-statics. That is,

$$\lambda = \frac{c}{f} >> l \tag{4.1}$$

where $c = \frac{1}{\sqrt{\mu_o \varepsilon_o}}$ is the speed of light. If this expression is rewritten using the period, $T = \frac{1}{f}$,

$$T >> \frac{l}{c} \tag{4.2}$$

Now, consider the special theory of relativity [188,189]. The time between events that happen at the same place in a reference frame is called proper time. The time interval measured in any other reference frame is always longer by a factor γ than the proper time. This is called time dilation. In a moving probe frame, the period T corresponds to the proper time. Then, the period T' measured in a stationary test object frame can be written as

$$T' = \gamma T = \frac{1}{\sqrt{1-\left(v/c\right)^2}} T \geq T \tag{4.3}$$

which is longer than the proper time T. Since the speed of light is independent of the relative motion of sources and observers according to Einstein's postulates, the inequality in equation (4.2) is satisfied in the stationary test object frame.

Time dilation is closely related to another phenomenon, length contraction. The length of an object measured in the reference frame in which the object is at rest is called its proper length. In a reference frame in which the object is moving, the measured length is shorter by a factor γ (along the direction of relative motion) than its proper length. The proper length l in the stationary test object frame is then measured as l' in the moving probe frame,

$$l' = \frac{l}{\gamma} = \sqrt{1-\left(v/c\right)^2}\, l \leq l \tag{4.4}$$

which is shorter than the proper length l. Again, by Einstein's postulates, the inequality in equation (4.2) is satisfied in the moving probe frame.

Since equation (4.2) is satisfied in both moving and stationary frames, we can conclude that the quasi-static approximation is valid in the presence of a moving probe. Even though the validity of the quasi-static approximation is shown by using the special theory of relativity, it is also valid in Galilean systems because the velocities dealt with in these systems are much slower than those in the special theory of relativity.

B. Transformation of Quasi-Static Magnetic Fields

As a prerequisite to forming a governing equation for probe velocity effects, there must be some relationships between field variables measured in a frame of reference moving with a constant velocity and the field variables measured in the stationary frame. For easy understanding of probe velocity effects, the desired governing equation needs to be formulated in the stationary reference frame. The treatment of relative motion in this dissertation is based on two postulates: (a) the equations of motion, including Maxwell's equations, are always written for a coordinate system that is moving with a constant magnitude and fixed direction; and (b) the laws of physics (e.g. Newton's laws and Maxwell's equations) are the same in every coordinate system (called invariance [188] or covariance [187,189,190]). These postulates are normally associated with the special theory of relativity but they are also valid for Galilean systems [191]. The general form of Maxwell's equations cannot be transformed consistently by means of the Galilean

transformation. The term consistent means that the equations are invariant. To be transformed consistently, a relativistic treatment is necessary such as the Lorentz transformation [187-189] or the Cerenkov transformation [187]. However, the quasi-static form of Maxwell's equations can be transformed consistently by the Galilean transformation. Furthermore, when the probe velocity is much slower than the speed of light, both Lorentz and Cerenkov transformations degenerate to the Galilean transformation, thus the relativistic terms make no significant contribution to the relatively low speed, quasi-static NDE problems. Therefore, in this dissertation, the quasi-static magnetic field equations are used from the outset and the Galilean transformation is applied. If primed variables are used for the coordinate system moving with a constant velocity, the differential equations in quasi-static magnetic field systems can be written, by using the concept of covariance, as

$$\nabla' \times \overline{H}' = \overline{J}' \tag{4.5}$$

$$\nabla' \cdot \overline{B}' = 0 \tag{4.6}$$

$$\nabla' \cdot \overline{D}' = 0 \tag{4.7}$$

$$\nabla' \times \overline{E}' = -\frac{\partial \overline{B}'}{\partial t'} \tag{4.8}$$

$$\overline{B}' = \mu' \overline{H}' \tag{4.9}$$

In this quasi-static magnetic field system, equation (4.7) expressing absence of free electric charges is of little practical value. However, this equation

plays the key role in the consistent transformation of the quasi-static form of Maxwell's equations by the Galilean transformation.

Now, consider the Galilean transformation. The field variables in electromagnetic theory are, in general, functions of space and time. Let unprimed variables represent the variables in the stationary reference frame. The transformations for field variables are obtained from the differential equations. Consequently, before the transformations are derived, the relationship between the two differential operators, ∇' and ∇, is necessary. To determine the relationship, consider two inertial coordinate systems $\bar{r}$ and $\bar{r}'$ which are moving with a constant relative velocity $\bar{V}$. The time t and t' measured by observers in the two coordinate systems are assumed to be the same according to Newtonian mechanics, which states that the time variables in any two systems moving with respect to each other have the same measure [190]. Thus,

$$t = t' \tag{4.10}$$

If the origins of the two coordinate systems are selected to coincide at t = 0, the relation between $\bar{r}$ and $\bar{r}'$ can be seen in Figure 4.1 and written as follows.

$$\bar{r}' = \bar{r} - \bar{V}t \tag{4.11}$$

Equations (4.10) and (4.11) define a Galilean transformation between the two coordinate systems. If this vector equation is rewritten at each coordinate,

$$x' = x - V_x t, \quad y' = y - V_y t, \quad z' = z - V_z t \tag{4.12}$$

Consider a scalar function f '(x,y,z,t) which can also be written as f '(x',y',z',t') by making substitutions from equations (4.10) and (4.12). The gradient of this function in the primed coordinate system is

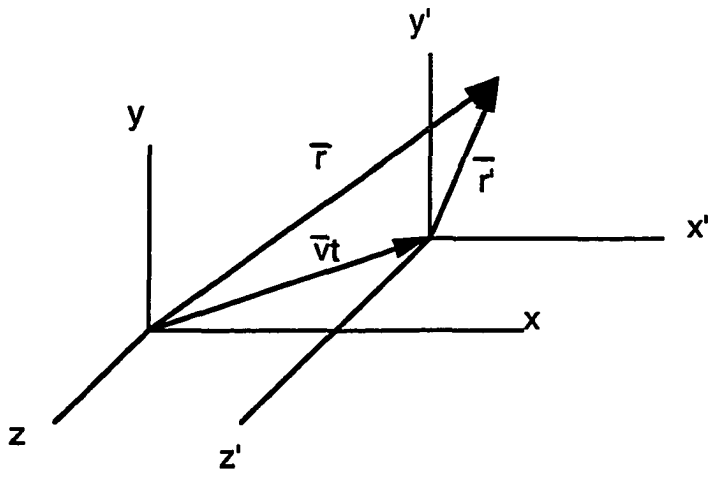

Figure 4.1. Two inertial coordinate systems in relative motion

$$\nabla' f' = \frac{\partial f'}{\partial x'}\hat{x} + \frac{\partial f'}{\partial y'}\hat{y} + \frac{\partial f'}{\partial z'}\hat{z} \tag{4.13}$$

By using the chain rule, we can write

$$\frac{\partial f'}{\partial x} = \frac{\partial f'}{\partial x'}\frac{\partial x'}{\partial x} + \frac{\partial f'}{\partial y'}\frac{\partial y'}{\partial x} + \frac{\partial f'}{\partial z'}\frac{\partial z'}{\partial x} + \frac{\partial f'}{\partial t'}\frac{\partial t'}{\partial x} \tag{4.14}$$

From equations (4.10) and (4.12) it follows that

$$\frac{\partial x'}{\partial x} = 1\,;\quad \frac{\partial y'}{\partial x} = \frac{\partial z'}{\partial x} = \frac{\partial t'}{\partial x} = 0\ ,$$

$$\frac{\partial y'}{\partial y} = 1\,;\quad \frac{\partial x'}{\partial y} = \frac{\partial z'}{\partial y} = \frac{\partial t'}{\partial y} = 0\ ,$$

$$\frac{\partial z'}{\partial z} = 1\,;\quad \frac{\partial x'}{\partial z} = \frac{\partial y'}{\partial z} = \frac{\partial t'}{\partial z} = 0 \tag{4.15}$$

Substituting equation (4.15) into equation (4.14), and by the same procedure for other terms in equation (4.13), the following relation can be established.

$$\nabla' f' = \nabla f' \tag{4.16}$$

The scalar function f ' may be a component of a vector function. Therefore, the same method can be used to establish that, for any vector function, $\overline{B'}(x',y',z',t')$, the spatial derivatives can be written as

$$\nabla' \cdot \overline{B}' = \nabla \cdot \overline{B}' \tag{4.17}$$

$$\nabla' \times \overline{B}' = \nabla \times \overline{B}' \tag{4.18}$$

The same techniques are used to establish the relation between temporal derivatives. Assume a scalar function f '(x',y',z',t') and write the temporal derivative in the unprimed system as

$$\frac{\partial f'}{\partial t} = \frac{\partial f'}{\partial t'}\frac{\partial t'}{\partial t} + \frac{\partial f'}{\partial x'}\frac{\partial x'}{\partial t} + \frac{\partial f'}{\partial y'}\frac{\partial y'}{\partial t} + \frac{\partial f'}{\partial z'}\frac{\partial z'}{\partial t} \tag{4.19}$$

It is evident from equations (4.10) and (4.12) that

$$\frac{\partial t'}{\partial t} = 1 \ , \ \frac{\partial x'}{\partial t} = -V_x \ , \ \frac{\partial y'}{\partial t} = -V_y \ , \ \frac{\partial z'}{\partial t} = -V_z \tag{4.20}$$

Substituting equation (4.20) into equation (4.19) yields

$$\frac{\partial f'}{\partial t} = \frac{\partial f'}{\partial t'} - \left(V_x \frac{\partial}{\partial x'} + V_y \frac{\partial}{\partial y'} + V_z \frac{\partial}{\partial z'} \right) f' = \frac{\partial f'}{\partial t'} - \left(\overline{V} \cdot \nabla' \right) f' \tag{4.21}$$

Using equation (4.16), equation (4.21) can be rewritten as

$$\frac{\partial f'}{\partial t'} = \frac{\partial f'}{\partial t} + \left(\overline{V} \cdot \nabla \right) f' \tag{4.22}$$

The scalar function f ' can be a component of a vector function. Thus, if a vector function, $\overline{B}'(x',y',z',t')$, is defined, the same process leads to

$$\frac{\partial \overline{B}'}{\partial t'} = \frac{\partial \overline{B}'}{\partial t} + \left(\overline{V}\cdot\nabla\right)\overline{B}' \tag{4.23}$$

Since the unprimed frame is the fixed, laboratory frame, it is clear from the left-hand side of equation (4.23) that the right-hand side is the temporal variation of the function $\overline{B}'$ for an observer moving with velocity $\overline{V}$. This derivative is also called the substantial or convective derivative and can be written in an alternative form

$$\frac{D\overline{B}'}{Dt} \equiv \frac{\partial \overline{B}'}{\partial t} + \left(\overline{V}\cdot\nabla\right)\overline{B}' \tag{4.24}$$

By using a vector identity,

$$\nabla\times\left(\overline{V}\times\overline{B}\right) = (\overline{B}\cdot\nabla)\overline{V} - (\overline{V}\cdot\nabla)\overline{B} + \overline{V}(\nabla\cdot\overline{B}) - \overline{B}(\nabla\cdot\overline{V}) \tag{4.25}$$

and since $\overline{V}$ is constant, the first and fourth terms on the right-hand side of equation (4.25) are zero, equation (4.23) can be written in a different form

$$\frac{\partial \overline{B}'}{\partial t'} = \frac{\partial \overline{B}'}{\partial t} - \nabla\times(\overline{V}\times\overline{B}') + \overline{V}(\nabla\cdot\overline{B}') \tag{4.26}$$

This equation is also derived from Faraday's law for moving media by Helmholtz [192] and others [193,194]. Using equations (4.17), (4.18) and (4.26), equations (4.5) to (4.8) can be expressed in the equivalent forms

$$\nabla \times \overline{H}' = \overline{J}' \tag{4.27}$$

$$\nabla \cdot \overline{B}' = 0 \tag{4.28}$$

$$\nabla \cdot \overline{D}' = 0 \tag{4.29}$$

$$\nabla \times \left(\overline{E}' - \overline{V} \times \overline{B}'\right) = -\frac{\partial \overline{B}'}{\partial t} \tag{4.30}$$

where equation (4.28) is used to simplify the form of equation (4.30).

Now, transformations can be made. The differential equations of quasi-static magnetic field systems in the laboratory frame are

$$\nabla \times \overline{H} = \overline{J} \tag{4.31}$$

$$\nabla \cdot \overline{B} = 0 \tag{4.32}$$

$$\nabla \cdot \overline{D} = 0 \tag{4.33}$$

$$\nabla \times \overline{E} = -\frac{\partial \overline{B}}{\partial t} \tag{4.34}$$

$$\overline{B} = \mu \overline{H} \tag{4.35}$$

It has been postulated that equations (4.27) - (4.30) describe the same physical laws as equations (4.31) - (4.34). A comparison of the two sets of equations shows that a consistent set of transformations is

$$\overline{H}' = \overline{H} \ , \ \overline{J}' = \overline{J} \ , \ \overline{B}' = \overline{B} \ , \ \overline{D}' = \overline{D} \ , \ \overline{E}' = \overline{E} + \overline{V} \times \overline{B} \ , \ \mu' = \mu \tag{4.36}$$

The transformations in equation (4.36) relate the values of electromagnetic quantities in a quasi-static magnetic field system. If the displacement

current term had been kept, the equations of two coordinate systems would have been different because of the term, $\nabla \cdot \overline{D}'$. In quasi-static magnetic field systems, this term is zero, thus there is no inconsistency. Notice that in these transformations, the conductivity and the permittivity have different values in the moving frame from those in the stationary frame. Under the Cerenkov transformation [187], however, the constitutive equations are invariant. Nevertheless, the transformation shown here agrees well with the Lorentz force expression,

$$\overline{F} = q(\overline{E} + \overline{V} \times \overline{B}) \tag{4.37}$$

Now, the relation between field variables in different frames are established. In the next section, the governing equation for probe velocity effects is discussed.

C. Governing Equation

It can be assumed, in a relative sense, that the probe is stationary and the test specimen is moving opposite to the original probe movement. This assumption is reasonable because a sensing device is located in the same moving probe so that the 'observer' thinks himself stationary and sees the test specimen moving backwards. Also, in the finite element formulation, no currents are assumed to be induced in the source coil. Therefore, the moving part has to be the test specimen. From now on, primes are omitted for convenience. Then, quasi-static, magnetic field equations are

$$\nabla \times \overline{H} = \overline{J} \tag{4.38}$$

$$\nabla \cdot \overline{B} = 0 \tag{4.39}$$

$$\nabla \cdot \overline{D} = 0 \tag{4.40}$$

$$\nabla \times \overline{E} = -\frac{D\overline{B}}{Dt} = -\frac{\partial \overline{B}}{\partial t} + \nabla \times (\overline{V} \times \overline{B}) \tag{4.41}$$

$$\overline{B} = \mu \overline{H} \tag{4.42}$$

From equation (4.39), $\overline{\mathrm{B}}$ can be expressed as the curl of the magnetic vector potential $\overline{\mathrm{A}}$, i.e.

$$\overline{B} = \nabla \times \overline{A} \tag{4.43}$$

Substituting this into equation (4.41) gives

$$\nabla \times (\overline{E} + \frac{\partial \overline{A}}{\partial t} - \overline{V} \times \nabla \times \overline{A}) = 0 \tag{4.44}$$

Since the curl of the terms within the parenthesis in equation (4.44) is zero, it can be expressed as the negative gradient of the electric scalar potential Φ, i.e.

$$\overline{E} + \frac{\partial \overline{A}}{\partial t} - \overline{V} \times \nabla \times \overline{A} = -\nabla \Phi \tag{4.45}$$

Assuming that the conducting medium is isotropic and homogeneous, we have

$$\overline{J} = \sigma \overline{E} \tag{4.46}$$

Substituting equation (4.45) into equation (4.46) gives

$$\bar{J} = -\sigma\frac{\partial \bar{A}}{\partial t} + \sigma\bar{V}\times\nabla\times\bar{A} - \sigma\nabla\Phi$$

$$= -\sigma\frac{\partial \bar{A}}{\partial t} + \sigma\bar{V}\times\nabla\times\bar{A} + \bar{J}_S \tag{4.47}$$

where $\bar{J}_S = -\sigma\nabla\Phi$ is the source current density. By using equations (4.42), (4.43), and (4.47), equation (4.38) can be rewritten as

$$\nabla\times\frac{1}{\mu}\left(\nabla\times\bar{A}\right) = \bar{J}_S - \sigma\frac{\partial \bar{A}}{\partial t} + \sigma\bar{V}\times\nabla\times\bar{A} \tag{4.48}$$

In the above equation, the magnetic vector potential is not defined uniquely since its divergence is not specified. However, in 2-D or axisymmetric problems, the Coulomb gauge, $\nabla\cdot\bar{A} = 0$, is automatically satisfied. For linear, isotropic problems, the vector identity

$$\nabla\times(\nabla\times\bar{A}) = \nabla(\nabla\cdot\bar{A}) - \nabla^2\bar{A} \tag{4.49}$$

can be used with the Coulomb gauge to obtain

$$\frac{1}{\mu}\nabla^2\bar{A} = \sigma\frac{\partial \bar{A}}{\partial t} - \sigma\bar{V}\times\nabla\times\bar{A} - \bar{J}_S \tag{4.50}$$

This is the general governing equation for transient cases. In steady state magnetostatic problems, the time derivative term vanishes, thus the governing equation becomes

$$\frac{1}{\mu}\nabla^2\bar{A} = -\sigma\bar{V}\times\nabla\times\bar{A} - \bar{J}_S \tag{4.51}$$

For AC sinusoidal steady state problems, a phasor notation

$$\overline{A} = |\overline{A}|\cos(\omega t + \phi) = \mathrm{Re}|\overline{A}|e^{j(\omega t+\phi)} \Rightarrow \overline{A}_{phasor} = |\overline{A}|e^{j\phi} \tag{4.52}$$

$$\frac{\partial \overline{A}}{\partial t} = \frac{\partial}{\partial t}\mathrm{Re}\left[\overline{A}_{phasor}e^{i\omega t}\right] = \mathrm{Re}\left[j\omega\overline{A}_{phasor}e^{i\omega t}\right] \Rightarrow j\omega\overline{A}_{phasor} \tag{4.53}$$

can be used to obtain the following governing equation.

$$\frac{1}{\mu}\nabla^2\overline{A} = j\omega\sigma\overline{A} - \sigma\overline{V}\times\nabla\times\overline{A} - \overline{J}_s \tag{4.54}$$

where the subscript indicating a phasor quantity is omitted for convenience. In axisymmetric problems with uni-directional movement in the z-direction,

$$\overline{B} = -\frac{1}{r}\frac{\partial}{\partial z}(rA)\hat{r} + \frac{1}{r}\frac{\partial}{\partial r}(rA)\hat{z} = \left(-\frac{\partial A}{\partial z}\right)\hat{r} + \left(\frac{A}{r} + \frac{\partial A}{\partial r}\right)\hat{z} \tag{4.55}$$

$$\nabla^2\overline{A} = -\nabla\times\nabla\times\overline{A} = -\begin{vmatrix} \frac{1}{r}\hat{r} & \hat{\theta} & \frac{1}{r}\hat{z} \\ \frac{\partial}{\partial r} & 0 & \frac{\partial}{\partial z} \\ -\frac{\partial A}{\partial z} & 0 & \frac{1}{r}\frac{\partial}{\partial r}(rA) \end{vmatrix} = \hat{\theta}\left[\frac{\partial}{\partial r}\left\{\frac{1}{r}\frac{\partial}{\partial r}(rA)\right\} + \frac{\partial}{\partial z}\left\{\frac{\partial A}{\partial z}\right\}\right] \tag{4.56}$$

$$\overline{V}\times\nabla\times\overline{A} = \begin{vmatrix} \hat{r} & \hat{\theta} & \hat{z} \\ 0 & 0 & V \\ -\frac{\partial A}{\partial z} & 0 & \frac{1}{r}\frac{\partial}{\partial r}(rA) \end{vmatrix} = -V\frac{\partial A}{\partial z}\hat{\theta} \tag{4.57}$$

Since $\overline{A}$ and $\overline{J}_s$ have only a θ-component, equation (4. 50) can be written as

$$\frac{1}{\mu}\left[\frac{\partial}{\partial r}\left\{\frac{1}{r}\frac{\partial}{\partial r}(rA)\right\} + \frac{\partial}{\partial z}\left\{\frac{\partial A}{\partial z}\right\}\right] = \sigma\frac{\partial A}{\partial t} + \sigma V\frac{\partial A}{\partial z} - J_s \tag{4.58}$$

equation (4.51) as

$$\frac{1}{\mu}\left[\frac{\partial}{\partial r}\left\{\frac{1}{r}\frac{\partial}{\partial r}(rA)\right\}+\frac{\partial}{\partial z}\left\{\frac{\partial A}{\partial z}\right\}\right]=\sigma V\frac{\partial A}{\partial z}-J_s \tag{4.59}$$

and equation (4.54) as

$$\frac{1}{\mu}\left[\frac{\partial}{\partial r}\left\{\frac{1}{r}\frac{\partial}{\partial r}(rA)\right\}+\frac{\partial}{\partial z}\left\{\frac{\partial A}{\partial z}\right\}\right]=j\omega\sigma A+\sigma V\frac{\partial A}{\partial z}-J_s \tag{4.60}$$

Now, compare equations (4.50) with (3.3), (4.51) with (3.1), and (4.54) with (3.2), respectively. The difference in each of the three comparisons is only the addition of the motional induction term, which can be expressed as $\sigma V\frac{\partial A}{\partial z}$ for axisymmetric problems as shown in equations (4.58) to (4.60). The presence of this term does not allow us to write equations (4.58) to (4.60) in the self-adjoint form of equation (3.20). Therefore, these equations are nonself-adjoint.

In terms of mathematical expressions, there is a close resemblance between these governing equations and those found in fluid dynamics and heat transport problems. For example, the governing equation for steady vorticity transport in two-dimensions [126] is

$$K\left(\frac{\partial^2 W}{\partial x^2}+\frac{\partial^2 W}{\partial y^2}\right)=u\frac{\partial W}{\partial x}+v\frac{\partial W}{\partial x} \tag{4.61}$$

where W is the vorticity, u and v are the flow velocity components, and K is the coefficient of kinematic viscosity [126] or the diffusivity [117]. In convective heat transport problems [127], the governing equation is written as

$$\nabla^T\cdot K\nabla\phi-\overline{V}\cdot\nabla\phi=0 \tag{4.62}$$

where K is the thermal diffusivity and $\overline{V}$ is the velocity, and ϕ is the temperature. These two equations are mathematically equivalent to equations (4.59) and (4.60). In a transient problem of thermodynamics [140],

$$\nabla^T \cdot K\nabla\phi = \frac{\partial(c\phi)}{\partial t} + \overline{V}\cdot(\nabla c\phi) - Q \tag{4.63}$$

where c is the specific heat, and Q is the rate of heat generation. This equation is equivalent to equation (4.58). Since the coefficients of the second order term are called diffusivity, such names as convective-diffusion equation and artificial diffusion are frequently used in these areas. In electromagnetics, a term reluctivity is used instead of the diffusivity and equation (4.59) does not represent diffusion phenomena. For this reason, the term 'artificial reluctivity' instead of artificial diffusion is used in this dissertation.

Even though mathematical expressions of the governing equations are the same, there is a delicate physical difference. When the moving electromagnetic probe passes a non-uniform geometry, there is only a short transient period which depends on the probe velocity (i.e. traversal time of the probe), and no steady state situation can exist. This is truly a transient case. However, in fluid problems, fluid flows continuously so that a steady state can be assumed even if the geometry is non-uniform. Also, when transient problems are solved, the moving probe requires its relocation at each time step, while in fluid and heat dynamics problems, there is no moving 'object' to be relocated. In this respect, they appear more like wave problems. The consequence of this difference is reflected on the time step size. In moving probe problems, the time step must satisfy $\Delta t = \frac{h}{\overline{V}}$, where h is the distance the

probe moves during this time step. If probe moves one element (length Δh) per time step, the grid Courant number, defined as $C = \frac{V\Delta t}{\Delta h}$, should be 1. In fluid and heat dynamics problems, there is no such restriction other than $C \leq 1$, which results from stability analysis. The same restriction on the grid Courant number can be found also in wave problems [195].

D. Results from Standard Finite Element Method

Having compared the equations in this chapter with those in Chapter III, that do not consider probe velocity effects, it is found that the difference is only the addition of the motional induction term. This means that the matrix equations developed in the previous chapter can be used without any alteration and only the additional matrix corresponding to the motional induction term is needed.

First, consider equation (4.59) for the steady state magnetic flux leakage method. Except for the motional induction term, the finite element formulation is already completed by using equation (3.42) and the resulting matrix equations are shown in equations (3.51) to (3.53). To find the additional matrix, the same weak formulation is applied to the motional induction term.

$$\int_v \delta A\left(\sigma V \frac{\partial A}{\partial z}\right) dv \tag{4.64}$$

Using equation (3.48), the approximation for the derivative of A with respect to z becomes

$$\frac{\partial A}{\partial z} = \begin{bmatrix} \frac{\partial N_1}{\partial z} & \frac{\partial N_2}{\partial z} & \frac{\partial N_3}{\partial z} & \frac{\partial N_4}{\partial z} \end{bmatrix} \begin{Bmatrix} A_1 \\ A_2 \\ A_3 \\ A_4 \end{Bmatrix} = \left[\frac{\partial \mathbf{N}}{\partial z}\right] \{\mathbf{A}\}_e \tag{4.65}$$

Substituting equation (4.65) into the elemental integration of equation (4.64) gives

$$\int_{v_e} \delta\{\mathbf{A}\}_e^T \left(\sigma V [\mathbf{N}]^T \left[\frac{\partial \mathbf{N}}{\partial z}\right] \{\mathbf{A}\}_e \right) dv \tag{4.66}$$

Combining equation (4.66) with equation (3.50) gives

$$\int_{v_e} \delta\{\mathbf{A}\}_e^T \left[\nu [\nabla \mathbf{N}]^T [\nabla \mathbf{N}] \{\mathbf{A}\}_e + \sigma V [\mathbf{N}]^T \left[\frac{\partial \mathbf{N}}{\partial z}\right] \{\mathbf{A}\}_e - J_s [\mathbf{N}]^T \right] dv = 0 \tag{4.67}$$

Since this equation must be satisfied for any variation $\delta\mathbf{A}$, the elemental matrix equation can be written as

$$[\mathbf{S}]_e \{\mathbf{A}\}_e + [\mathbf{SV}]_e \{\mathbf{A}\}_e = \left([\mathbf{S}]_e + [\mathbf{SV}]_e\right) \{\mathbf{A}\}_e = \{\mathbf{Q}\}_e \tag{4.68}$$

where $[\mathbf{SV}]_e = \int_{v_e} \sigma V [\mathbf{N}]^T \left[\frac{\partial \mathbf{N}}{\partial z}\right] dv$, which is not symmetric, and $[\mathbf{S}]_e$ and $\{\mathbf{Q}\}_e$ are shown in equations (3.52) and (3.53). Summation of all the elemental contributions gives the global matrix equation,

$$([\mathbf{S}] + [\mathbf{SV}]) \{\mathbf{A}\} = [\mathbf{SK}] \{\mathbf{A}\} = \{\mathbf{Q}\} \tag{4.69}$$

In sinusoidal steady state eddy current problems, the necessary matrix equation can easily be obtained from equation (3.101). Rewriting equation (3.101) using phasor notation,

$$[\mathbf{S}]\{\mathbf{A}\} + j\omega[\mathbf{C}]\{\mathbf{A}\} = \{\mathbf{Q}\} \tag{4.70}$$

Adding the matrix [**SV**] developed in the above for the motional induction term,

$$([\mathbf{S}] + [\mathbf{SV}] + j\omega[\mathbf{C}])\{\mathbf{A}\} = [\mathbf{SK}']\{\mathbf{A}\} = \{\mathbf{Q}\} \tag{4.71}$$

In this case, each element in the stiffness matrix is a complex number.

Note that the stiffness matrices in both cases are not symmetric because of the asymmetric [**SV**] matrix. An example of an asymmetric elemental matrix for a 1-D problem is shown in equation (1.5). This asymmetry is due to the motional induction (first order spatial derivative) term, which makes the governing equation nonself-adjoint.

In general, motional induction problems are closely related to a dimensionless parameter called the magnetic Reynolds number, $R_m = \mu\sigma V l$, where l is the characteristic length of the problem. The traditional definition of the magnetic Reynolds number in electrodynamics literature, is the ratio of the induced magnetic field to the imposed magnetic field [191] or the ratio of the magnetic convection to the magnetic diffusion[196]. In the particular case where the diffusion of flux is in the opposite direction to the direction of motion, the magnetic Reynolds number can be expressed as the ratio of the diffusion time constant to the traversal time [191]. The fundamental interpretation of the magnetic Reynolds number, however, is always the same, namely that it indicates the relative importance of the convection term ($\overline{V} \times \nabla \times \overline{A}$) to the second order term ($\nabla^2 \overline{A}$). If this number is large, the magnetic field is altered appreciably by the motion.

In the finite element method, this number is defined at each element and called the cell magnetic Reynolds number, thus $R_m=\mu\sigma Vh$ where h is the length of an element in the direction of motion. If this number is larger than 2, the solution of equations (4.69) and (4.71) shows spurious oscillatory results as explained in Chapter I. Such oscillatory results are shown in this section. In this dissertation, all probes are assumed to move to the left and in the case of uniform geometries, which allow steady state analyses, probes are located at the center of the z-axis.

Figure 4.2 show the RMS magnetic vector potential plots of the stationary remote field eddy current probe. Figure 4.2.a) shows the RMS magnetic vector potential magnitudes plotted on a logarithmic scale in order to show details of the remote field several pipe diameters away from the exciter coil. For example, the six bands of flux lines in the figure contain 90 %, 9 %, 0.9 %, 0.09 %, 0.009 %, and 0.0009 % of the total flux with corresponding coutour intervals of 10 %, 1 %, 0.1 %, 0.01 %, 0.001 %, and 0.0001 %, respectively. An ordinary equipotential plot is shown in Figure 4.2.b). The relative constant permeability and conductivity of the tube are 150 and $0.45X10^7$ mho/meter, respectively. The tube element length parallel to the direction of probe motion (z direction) is 1.27 mm.

The equipotential plots obtained by applying the standard Galerkin method to a uniform geometry problem are shown in Figures 4.3.a) and 4.3.b) at the probe velocity of 10 m/sec and 50 m/sec, respectively. The corresponding cell magnetic Reynolds numbers are 10.77 and 53.85. Even though R_m exceeds 2, Figure 4.3.a) does not show any spurious oscillations. This may be due to extremely small oscillations and limits associated with

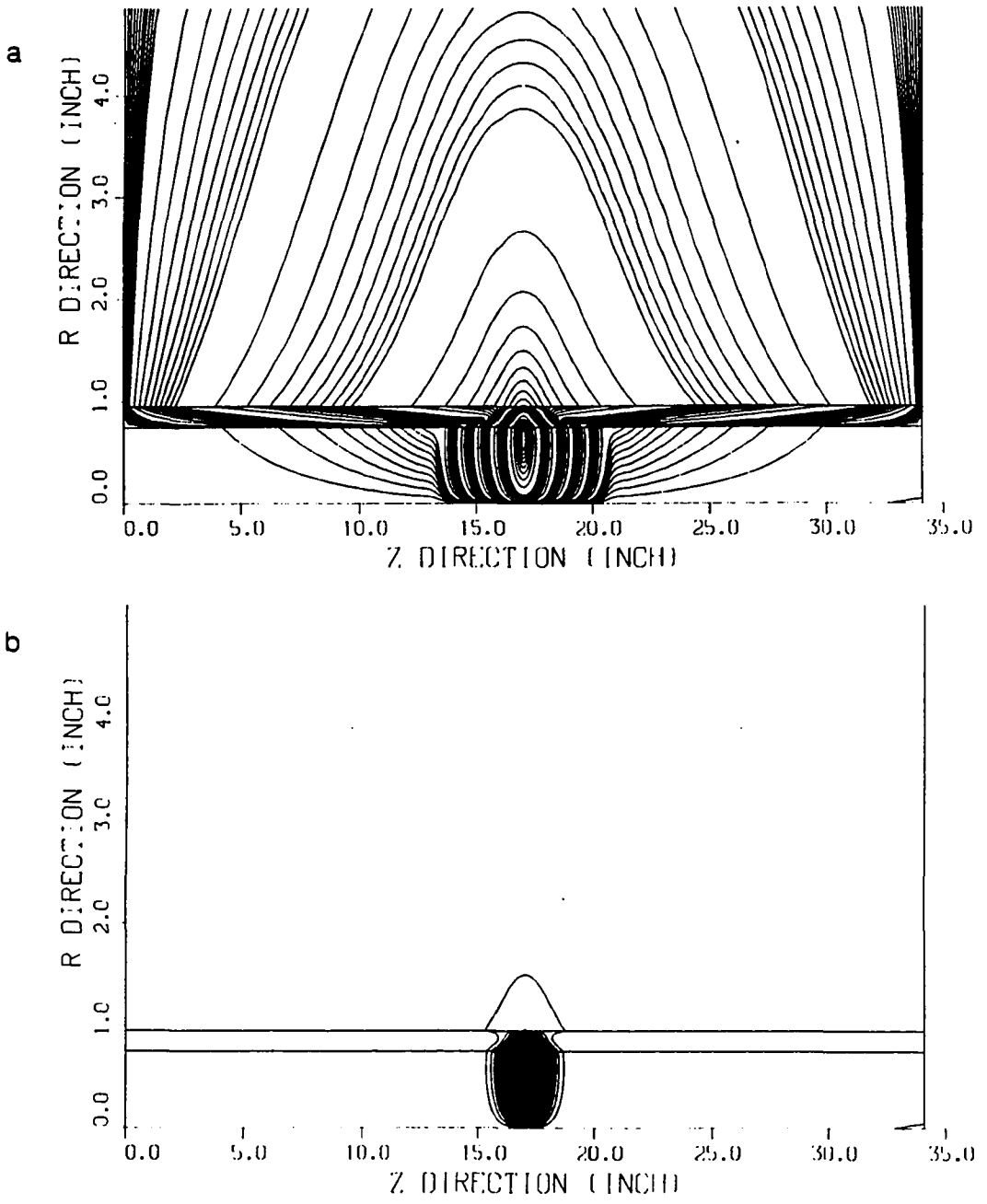

Figure 4.2. RMS magnetic vector potential magnitude plots of the stationary RFEC probe; a) logarithmic scale, b) ordinary scale

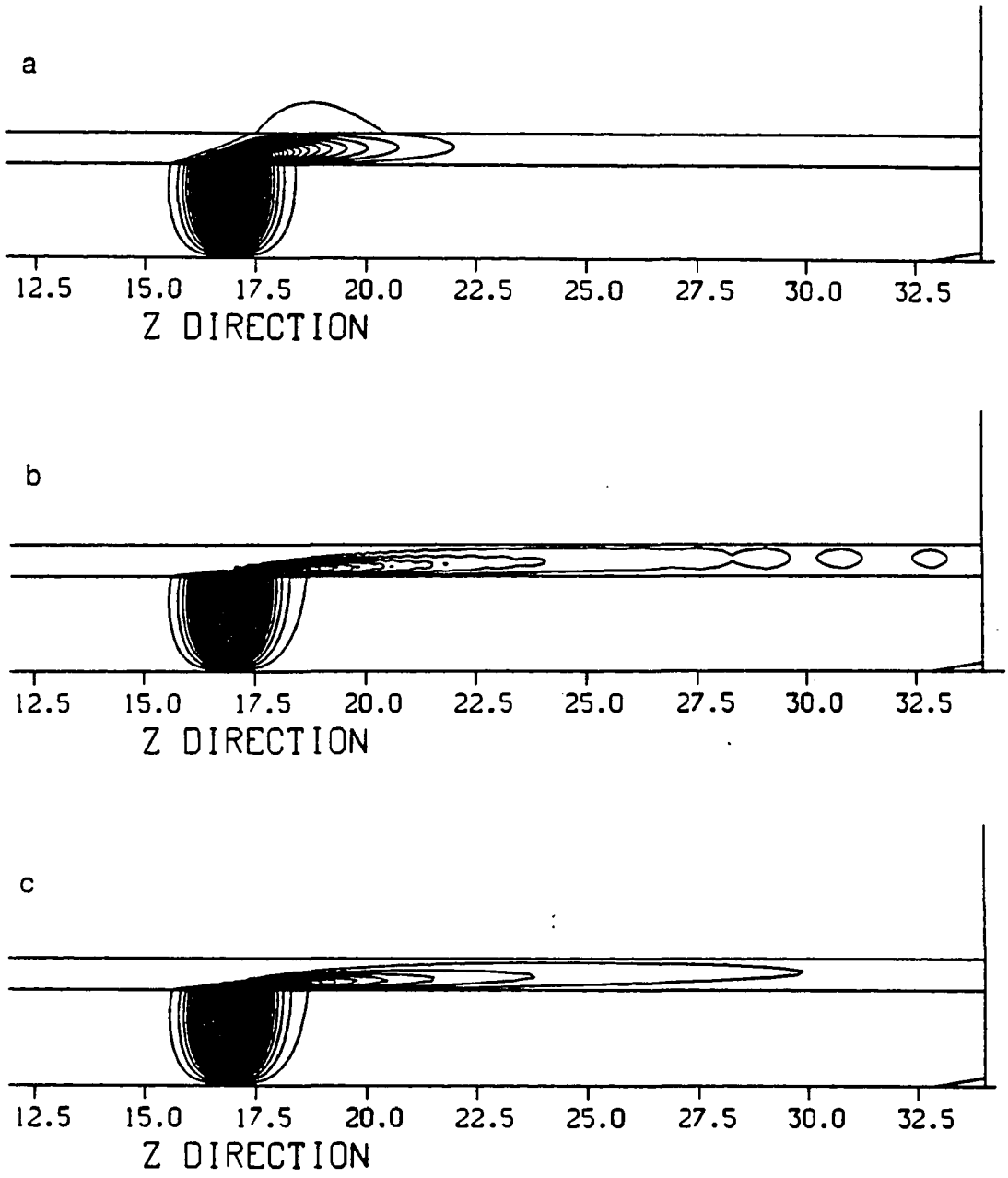

Figure 4.3. Equipotential plots of RFEC probe;
a) V=10 m/sec (R_m=10.77), standard Galerkin,
b) V=50 m/sec (R_m=53.85), standard Galerkin,
c) V=50 m/sec, upwinding technique

the plotting device. When R_m is much larger than 2, spurious oscillations can be seen as shown in Figure 4.3.b). Figure 4.3.c) shows the removal of such oscillations by applying the upwinding technique, explained in Chapter V.

Since the cell magnetic Reynolds number is composed of four variables, the material permeability (μ) and conductivity (σ), the probe velocity (V), and the element length (h), each variable can cause spurious oscillations. The oscillations due to these different variables are investigated using the variable reluctance probe applied to the uniform tube geometry. To investigate the results effectively, a graph of the magnetic vector potential values along the center line of the tube wall is chosen.

Figure 4.4 compares the results at probe velocities of 5, 50, and 100 m/sec. The relative constant permeability and conductivity of the tube are 100 and 0.6×10^7 mho/meter, respectively and the element length is 1.59 mm. Thus, the corresponding R_m are 5.99, 59.94, and 119.88. In this case, Dirichlet boundary conditions are imposed on all the boundaries. At V=50 m/sec, small oscillations exist but cannot be seen in the graph because the maximum magnitude at V=5 m/sec is too large to show such small oscillations. At V=100 m/sec, relatively large oscillations can be seen at the front edge of the probe and at the boundary behind the probe.

However, as can be seen in Figure 4.3, the fields are dragged behind the probe and at extremely high velocities, the fields may be extended beyond the boundary. In such cases, Neumann boundary conditions are more suitable. Neumann boundary conditions are also known as natural boundary conditions and no value needs to be specified on that boundary in the finite

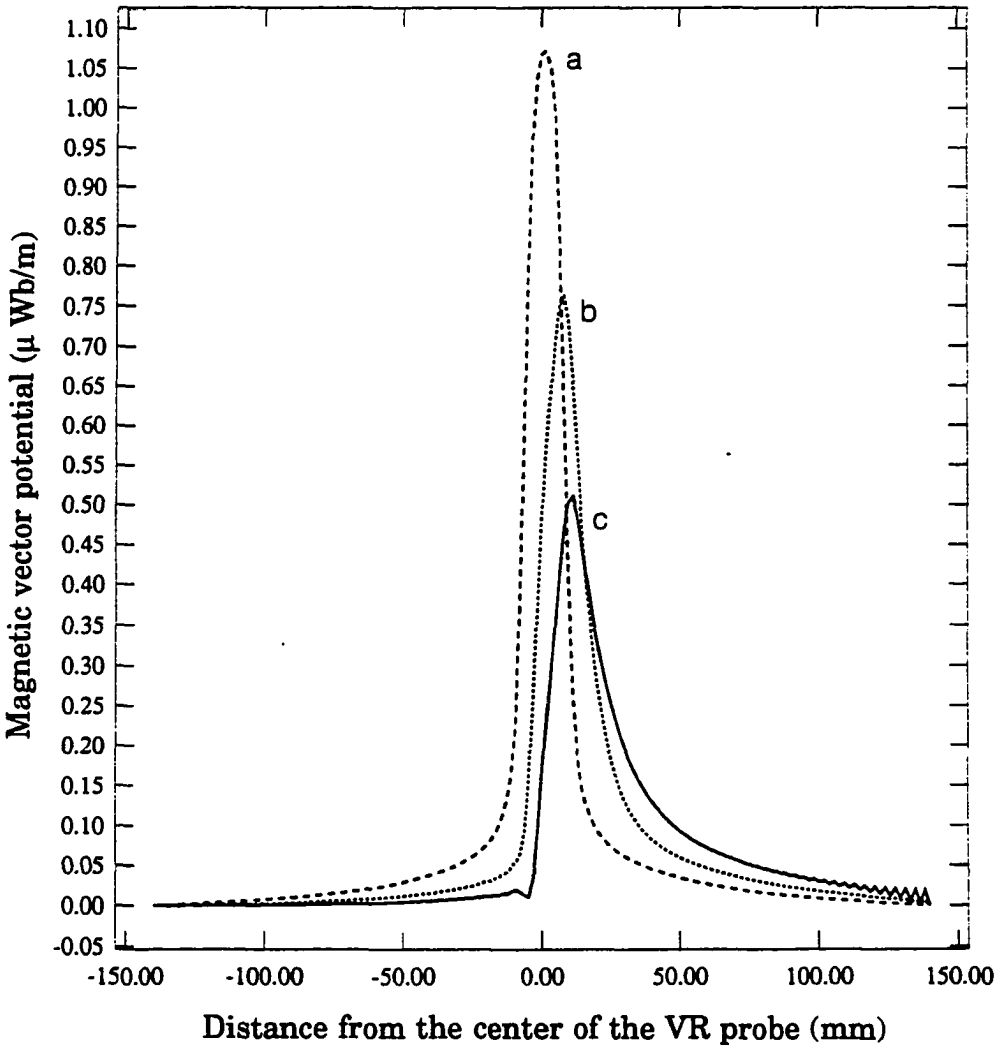

Figure 4.4. Magnetic vector potential along the center line of tube wall (VR probe, Dirichlet B.C.); a) V = 5 m/sec (R_m=5.99), b) V = 50 m/sec (R_m=59.94), c) V = 100 m/sec (R_m=119.88)

element method. The results obtained by applying Neumann boundary conditions are shown in Figure 4.5. As expected, the oscillations near the natural boundary have disappeared. However, the oscillations at the front edge of the probe still remain.

Figure 4.6 shows results from two different conductivities. In this case, the relative permeability of the tube is 100, the element length is 4.76 mm, and the probe velocity is 5 m/sec. When the conductivity of the tube is 0.6×10^7 mho/meter (R_m=17.9), no spurious oscillation occurs. If the conductivity is increased to 2×10^7 mho/meter (R_m=59.8), spurious oscillations occur again at the front edge of the probe.

Additional results show the importance of mesh discretization. In this case, the relative permeability and conductivity of the tube are 100 and 2×10^7 mho/meter, respectively and the probe velocity is 5 m/sec. If the element length is 1.59 mm (R_m=20), no spurious oscillation occurs, while the element length of 4.76 mm (R_m=59.8) is used, spurious oscillations occur at the same location as shown in Figure 4.7. This means that heavy mesh discretization is necessary to avoid spurious oscillations. In some cases, especially in 3-D problems, this requires enormous computer resources even today's computers cannot afford. To overcome this difficulty, an upwinding technique originally developed in fluid mechanics is now applied widely to moving magnetic fields problems. In Chapter V, this technique is explained and resulting oscillation-free results are shown under the same conditions as in this section.

Note that almost the same values of magnetic Reynolds number (59.94 and 59.8) are used in Figure 4.5.b) and 4.6.a), but the results are different, i.e.,

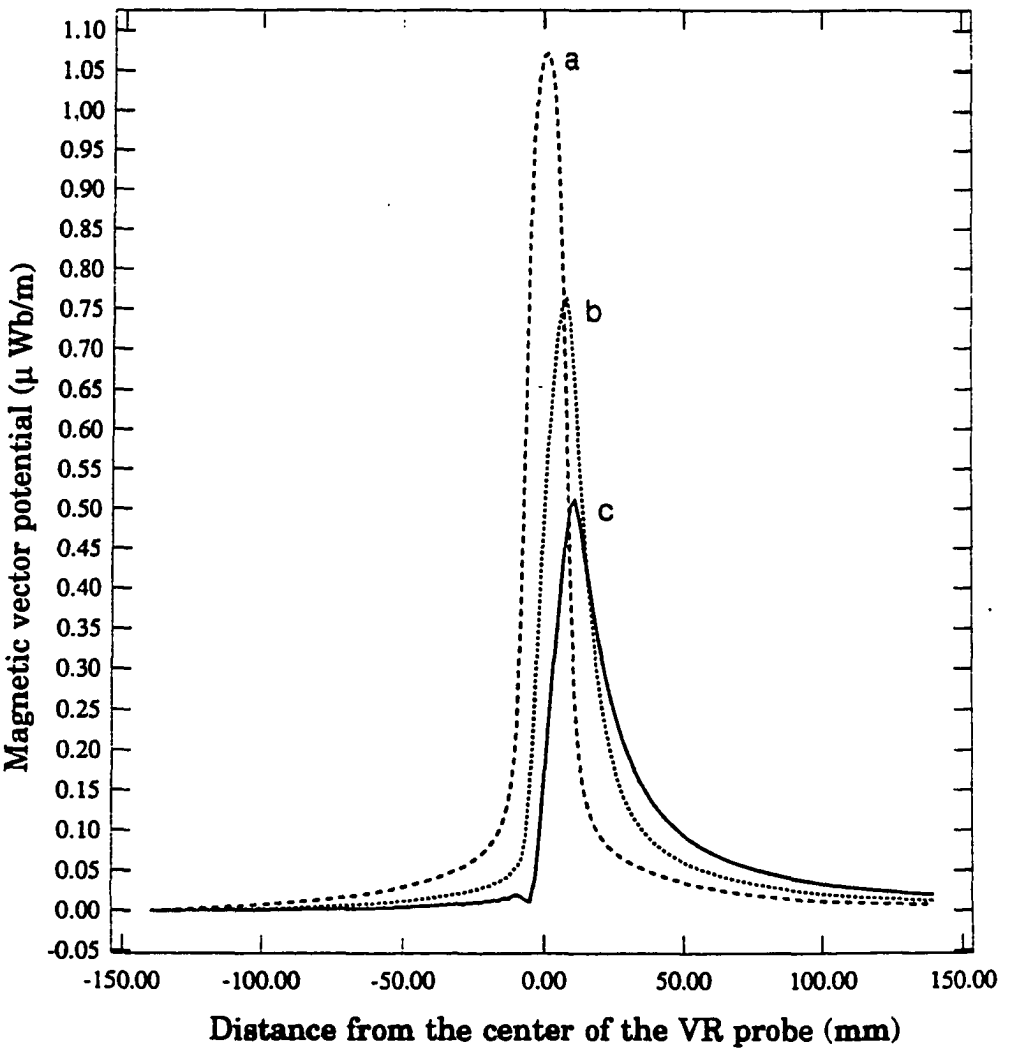

Figure 4.5. Results obtained by applying Neumann B.C.;
a) V = 5 m/sec (R_m=5.99),
b) V = 50 m/sec (R_m=59.94),
c) V = 100 m/sec (R_m=119.88)

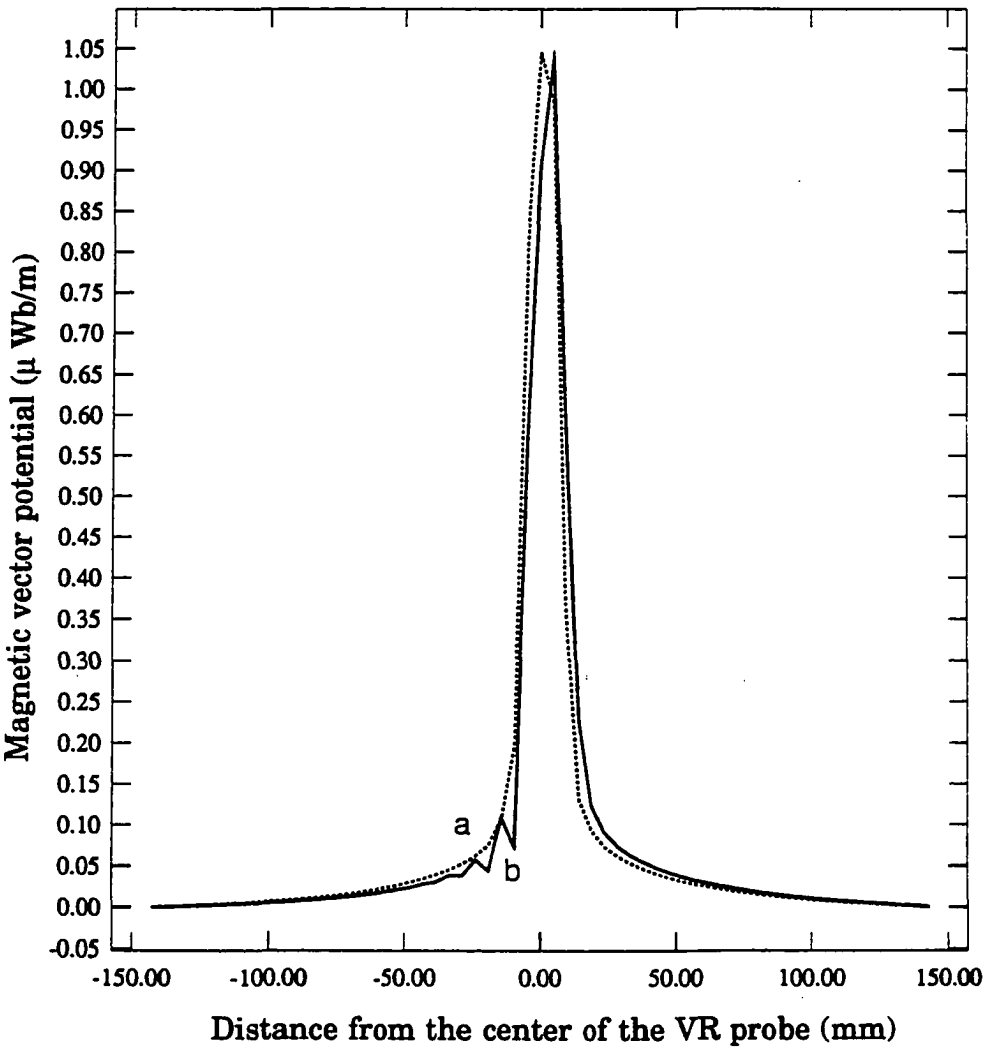

Figure 4.6. Results from two different conductivities;
a) $\sigma = 0.6 \times 10^7$ mho/meter ($R_m = 17.9$),
b) $\sigma = 2 \times 10^7$ mho/meter ($R_m = 59.8$)

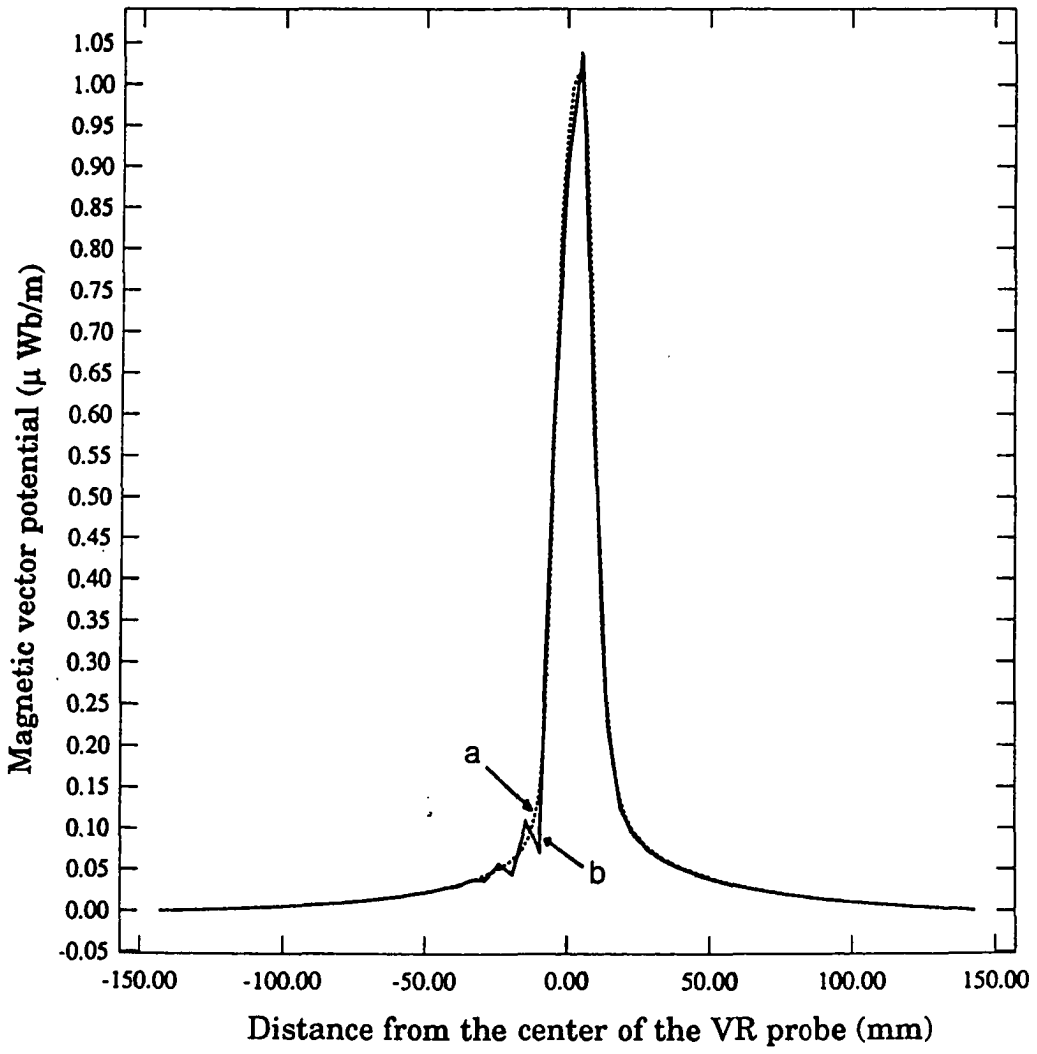

Figure 4.7. Results from two different element lengths;
a) h = 1.59 mm (R_m = 20),
b) h = 4.76 mm (R_m = 59.8)

the same cell magnetic Reynolds number does not necessarily produce the same results.

E. Treatment of Motional Induction Term

The motional induction is essentially expressed as $\overline{V} \times \overline{B}$. The treatment of this term may depend on its interpretation. In this section, the time dependent interpretation and the nonlinear interpretation with respect to the velocity are discussed.

1. Time Dependent Interpretation

The motional induction currents can exist only when the magnetic flux density, $\overline{B}$, is already present. Without prior existence of the magnetic flux, there are no motionally induced currents no matter how fast the conductor may move. Since only constant velocities are considered (even the special theory of relativity is confined to constant velocities), this means that the motional induction term must be evaluated at the old time level when a transient problem is solved.

The upwinding technique can also be viewed in close relation to this interpretation. As explained in the introduction, the upwinding technique [126,127] developed for the finite element method gives more emphasis to the upwind condition by using an asymmetric weighting function which is biased in the upwind direction. Another upwinding technique for the finite element method is based on a numerical quadrature rule [117,128,131]. When

the integral corresponding to the motional induction term is evaluated, a quadrature point, displaced in the upwind direction from the normal quadrature point, is used. The rest of the integrals are evaluated at the regular quadrature points. The upwind scheme was first developed in the finite difference method [124,125]. In the finite difference method, only the motional induction term is treated by the upwind (backward) difference scheme and the rest of the terms in the governing equation are treated by the central difference scheme. Note that these finite difference methods are used for spatial discretization, not for temporal discretization since the governing equation considered is a steady state equation. In fact, all these upwinding techniques are developed for the steady state equation. Therefore, the emphasis is given to the prior (upwind) 'position' where the probe has already passed in a moving probe problem. If a transient problem is considered, the prior position corresponds to the prior time; that is, the old time level. A notation for this interpretation can be written as

$$\overline{V} \times \overline{B}\left(t^{n-1}\right) \tag{4.72}$$

where n-1 indicates the old time level.

This interpretation agrees well with Muramatsu et al.'s work [70] even though view points are slightly different. Consider a moving coordinate system (X', Y', Z'). The governing equation to the observer moving with the coordinate system can be written, by using the concept of covariance, as

$$\nabla \times \frac{1}{\mu}\left(\nabla \times \overline{A}(X', Y', Z')\right) = \overline{J}_s - \sigma \frac{\partial \overline{A}(X', Y', Z')}{\partial t} \tag{4.73}$$

To the observer in the stationary coordinate system, this equation becomes equation (4.48). For simplicity, consider a 1-D model moving with a constant velocity in the z-direction as shown in Figure 4.8. The time derivative in equation (4.73) at a point $P(Z'_1)$ moving with the coordinate system at an instant t can be written as

$$\frac{\partial A(Z'_1)^t}{\partial t} = \frac{A(Z'_1)^t - A(Z'_1)^{t-\Delta t}}{\Delta t} \tag{4.74}$$

$$= \frac{A(z_2)^t - A(z_1)^{t-\Delta t}}{\Delta t} \tag{4.75}$$

$$= \frac{A(z_2)^t - A(z_2)^{t-\Delta t}}{\Delta t} + \frac{A(z_2)^{t-\Delta t} - A(z_1)^{t-\Delta t}}{\Delta z}\frac{\Delta z}{\Delta t} \tag{4.76}$$

$$= \frac{\partial A(z_2)}{\partial t} + V\frac{\partial A^{t-\Delta t}}{\partial z} \tag{4.77}$$

$$= \frac{\partial A(z_2)}{\partial t} + (\overline{V}\cdot\nabla)A^{t-\Delta t} \equiv \frac{DA}{Dt} \tag{4.78}$$

where z_i's are the fixed coordinates. Again, the convective derivative as shown in equation (4.24) is obtained. However, valuable information is added

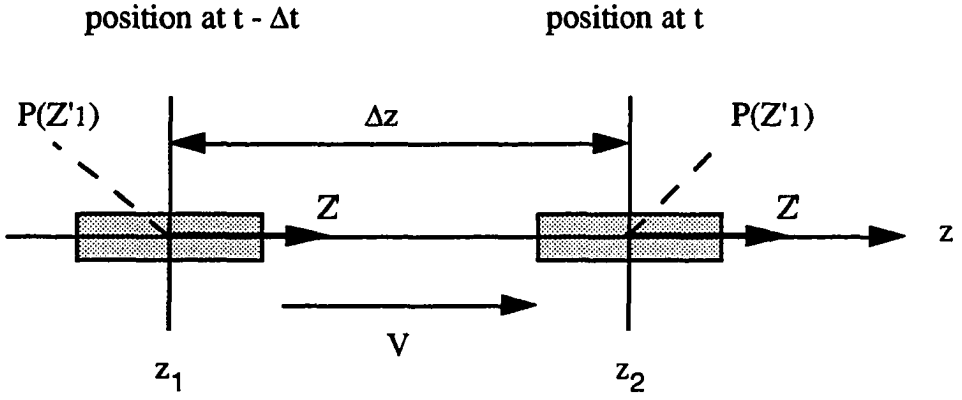

Figure 4.8. 1-D moving model with a constant velocity

from this procedure. That is, the motional induction term, $V\frac{\partial A^{t-\Delta t}}{\partial z}$, is evaluated at the old time level, (t-Δt)! Muramatsu et al. consider this term as the average flux density between z_1 and z_2 at the instant t-Δt. But, it seems more accurate to interpret this term as the motional induction term.

Other information can be extracted from this mathematical derivation. According to equations (4.74) and (4.75), the time derivative term has to be evaluated by the values of A at different positions at different time levels. This means that if the moving coordinate system is used, mesh discretization has to be updated at each time level to evaluate the time derivative term. However, in equations (4.76) to (4.78), the time derivative term is evaluated at the present position (z2) even though the time levels are different. This means that the time derivative term can be evaluated from the present mesh discretization if the problem is solved in terms of the stationary coordinate system.

This view of evaluating motional induction term at the old time level is applied in Chapter VI, where transient analyses for non-uniform geometry are discussed.

2. Nonlinear Interpretation with respect to Velocity

Another point of view is that the motional induction term is nonlinear with respect to the velocity [197]. It is based on the fact that there is no sudden step change in velocities, such as from zero to 5 m/sec. Instead, the velocity is gradually increased to the final speed. In the course of gradual increase, the magnetic flux also changes accordingly and at the higher velocity, the

motional induction currents are obtained based on this changed magnetic flux. In a simple notation, this interpretation can be expressed as

$$\Delta\overline{V}\times\overline{B}\left(\overline{V}^{n-1}\right) \tag{4.79}$$

where $\Delta\overline{V}$ is the incremental velocity step. This expression clearly shows that the motional induction term is nonlinear with respect to the velocity.

The basic equation to solve in this case is a Poisson equation. At first, the equation is solved without the motional induction term. From the result of A, the flux density, B, is calculated and then multiplied by a small increase in velocity to find the motional induction currents. Using these induced currents as the source, the Poisson equation is solved again and the result is superposed with the original result. From this superposed result, the flux density is calculated again and the same procedures are repeated until the given velocity is reached. The algorithm of this procedure is as follows.

1. Solve Poisson equation, $\nabla^2 A_k = -\mu J_s$
2. From the resulting magnetic vector potential A_k,
   find flux density, $B_k = \nabla \times A_k$
3. Find motional induction current density, $J_{ik} = \sigma\Delta V \times B_k$
4. Solve $\nabla^2 A_k' = -\mu J_{ik}$
5. Add A_k and A_k' to find A_{k+1};
   k th iteration is finished, where $k = 1, \ldots, \frac{V}{\Delta V}$.
6. Repeat step 2 to step 5 until the given velocity is reached.

If $\Delta V = V$, direct superposition results.

This algorithm is applied to the variable reluctance probe case associated with a uniform geometry. The relative permeability and conductivity of the tube material used is 100 and 0.6×10^7, respectively and the element length used is 3.8 mm. Figure 4.9 compares magnetic vector potential values along the center line of the tube wall at V = 1 m/sec (R_m=2.87). The results included are from the direct superposition ($\Delta V = 1$), the incremental calculation ($\Delta V = 0.5, 0.2, 0.1$), and the upwinding technique. All the results agree well since the probe velocity is relatively slow and thus, R_m is small enough to prevent spurious oscillations.

When the probe velocity is increased to 5 m/sec (R_m=14.36), slight discrepancies are observed at the peak as shown in Figure 4.10. The peak region is blown up in Figure 4.11. It shows that the smaller the velocity step size, the closer is the result to the upwinding result.

Figures 4.12.a) and 4.12.b) show the equipotential plots resulting from the direct superposition of motional induction fields to the main fields at the probe velocities of 20 m/sec (R_m=57.45) and 50 m/sec (R_m=143.6), respectively. As expected from the value of R_m, spurious oscillations occur. For comparison, the upwinding results are plotted in Figure 4.13.

The magnetic vector potential values along the center line of the tube wall corresponding to Figure 4.12.a) are shown in Figure 4.14 together with the upwinding result of Figure 4.13.a). The result from incremental calculation using a velocity step size of 2 m/sec is added in Figure 4.15. It shows that the incremental result not only removes the spurious oscillation of direct superposition, but also reduces the peak value towards the upwinding result. The same tendency as seen in Figure 4.11 is observed here,

again. Therefore, it can be said that the results from upwinding techniques are reliable. Also, as pointed out by Hwang and Lord [197], when the magnetic Reynolds number is very large compared to 2, the incremental calculation should be used instead of the direct superposition. A drawback of this method is that it takes numerous iterations to obtain an accurate result. Compared to this, the upwinding technique provides an efficient way of calculation.

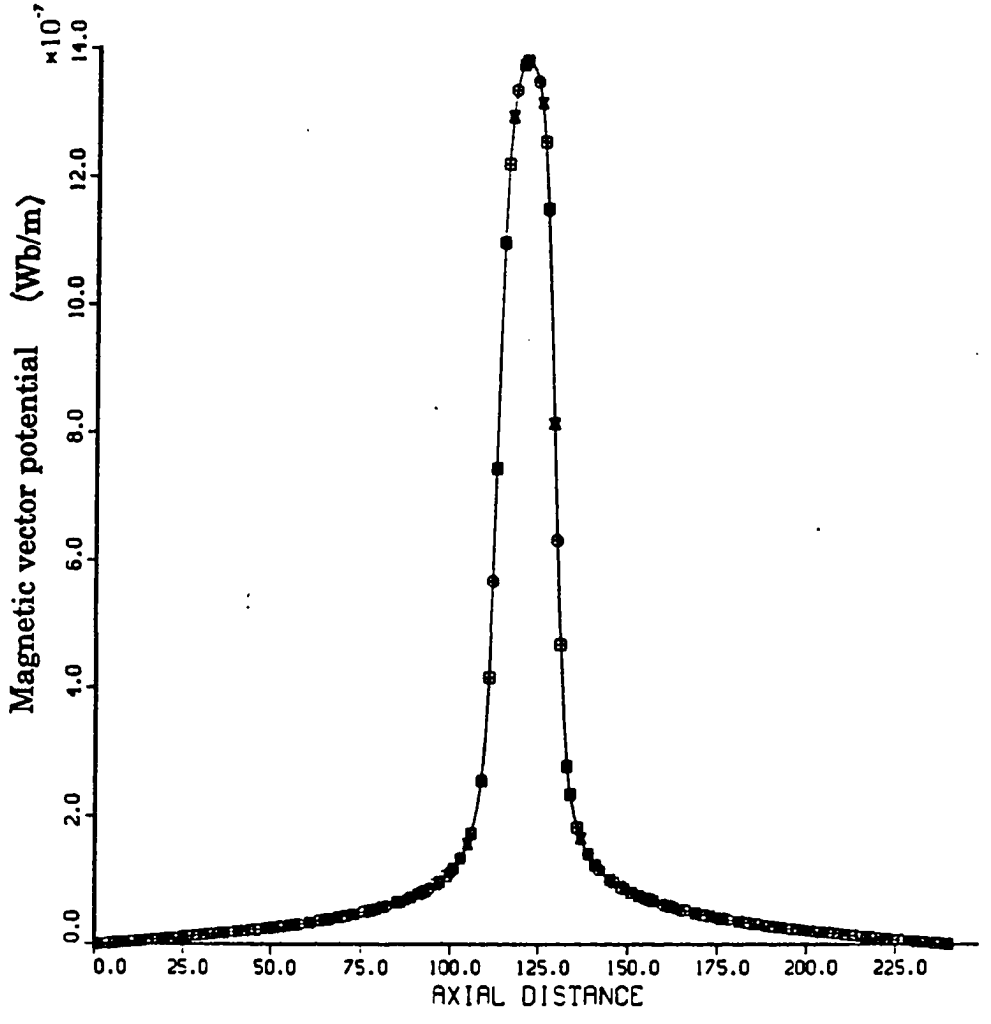

Figure 4.9. Comparison of results at V = 1 m/sec (R_m = 2.87); direct superposition, incremental calculations (ΔV = 0.5, 0.2, 0.1), and upwinding result

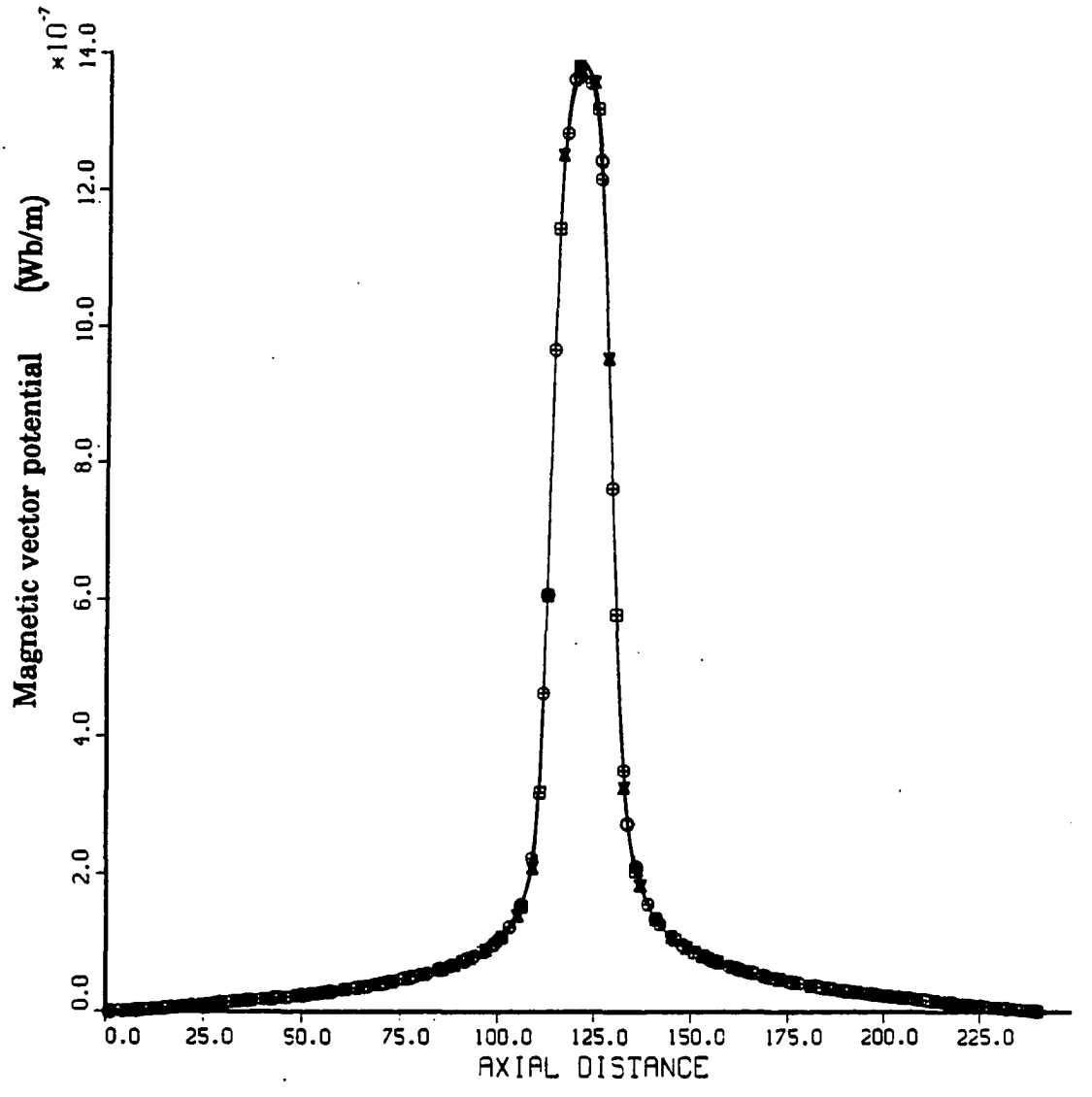

Figure 4.10. **Comparison of results at V = 5 m/sec (R_m = 14.36); direct superposition, incremental calculations (ΔV = 2.5, 0.2), and upwinding result**

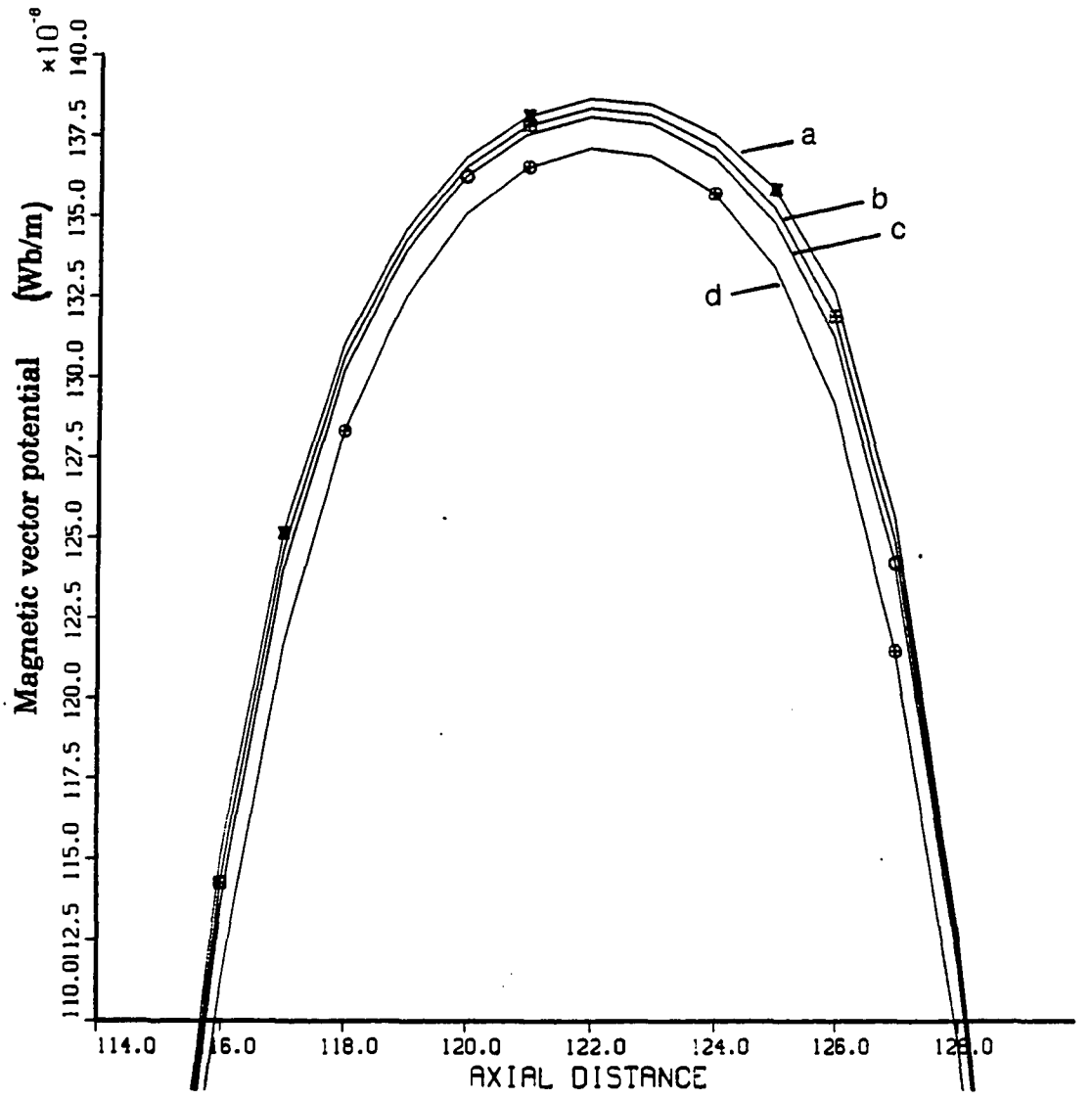

Figure 4.11. Blow up of peak region in Figure 4.10;
a) direct superposition result: ΔV = 5 m/sec,
b) incremental calculation: ΔV = 2.5 m/sec,
c) incremental calculation: ΔV = 0.2 m/sec,
d) upwinding result

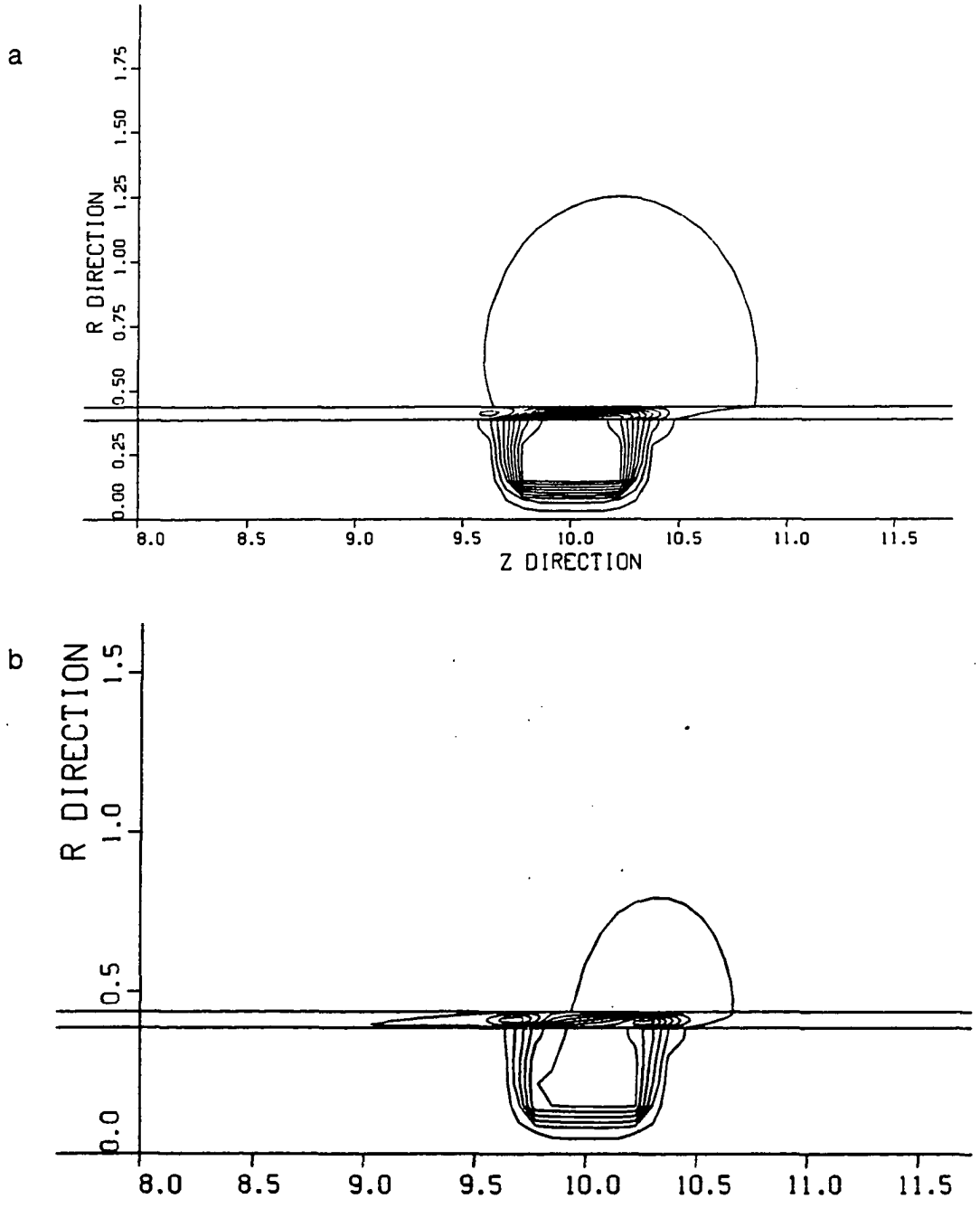

Figure 4.12. Equipotential plots of direct superposition results;
a) V = 20 m/sec (R_m = 57.45),
b) V = 50 m/sec (R_m = 143.6)

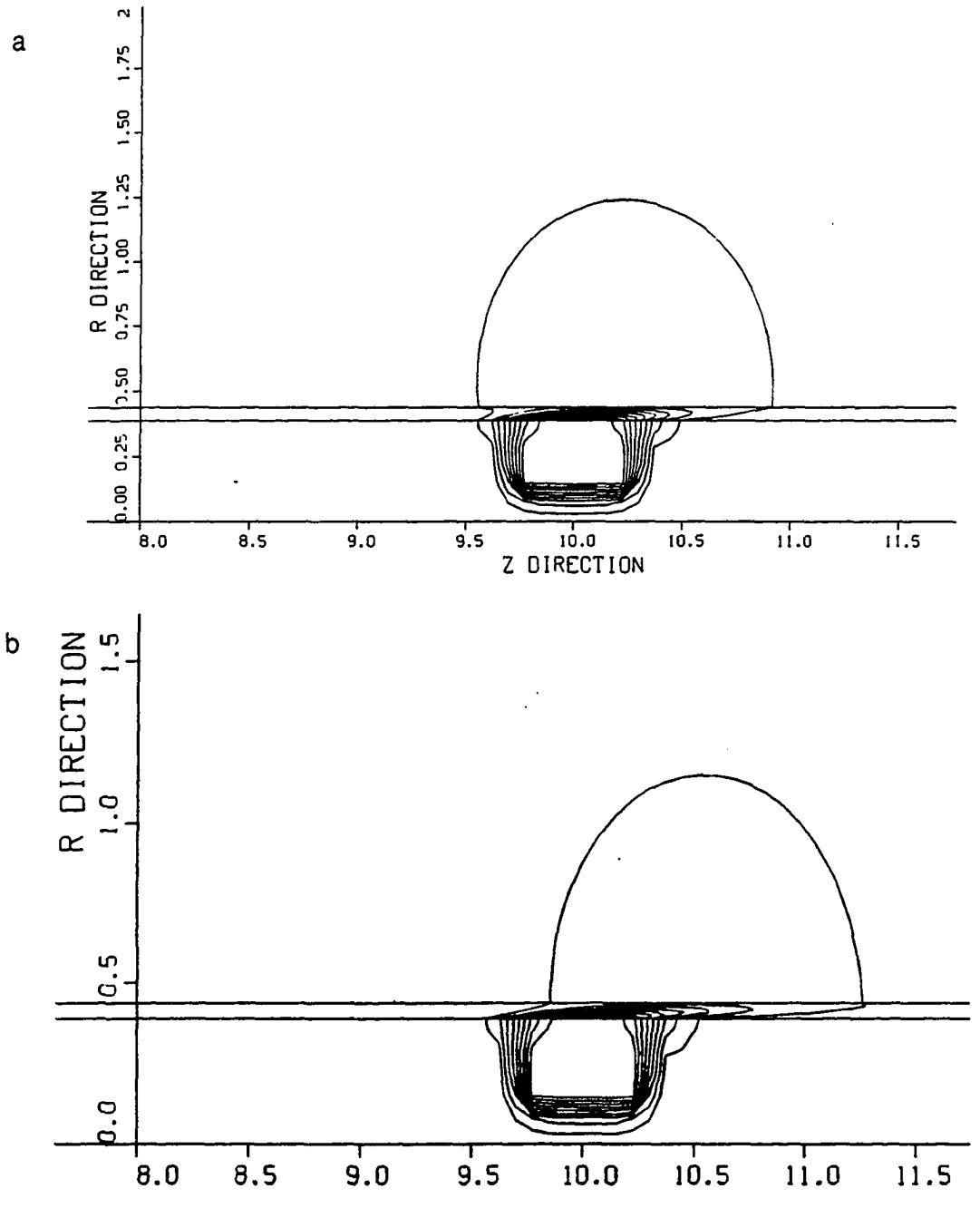

Figure 4.13. Equipotential plots of upwinding results;
a) V = 20 m/sec (R_m = 57.45),
b) V = 50 m/sec (R_m = 143.6)

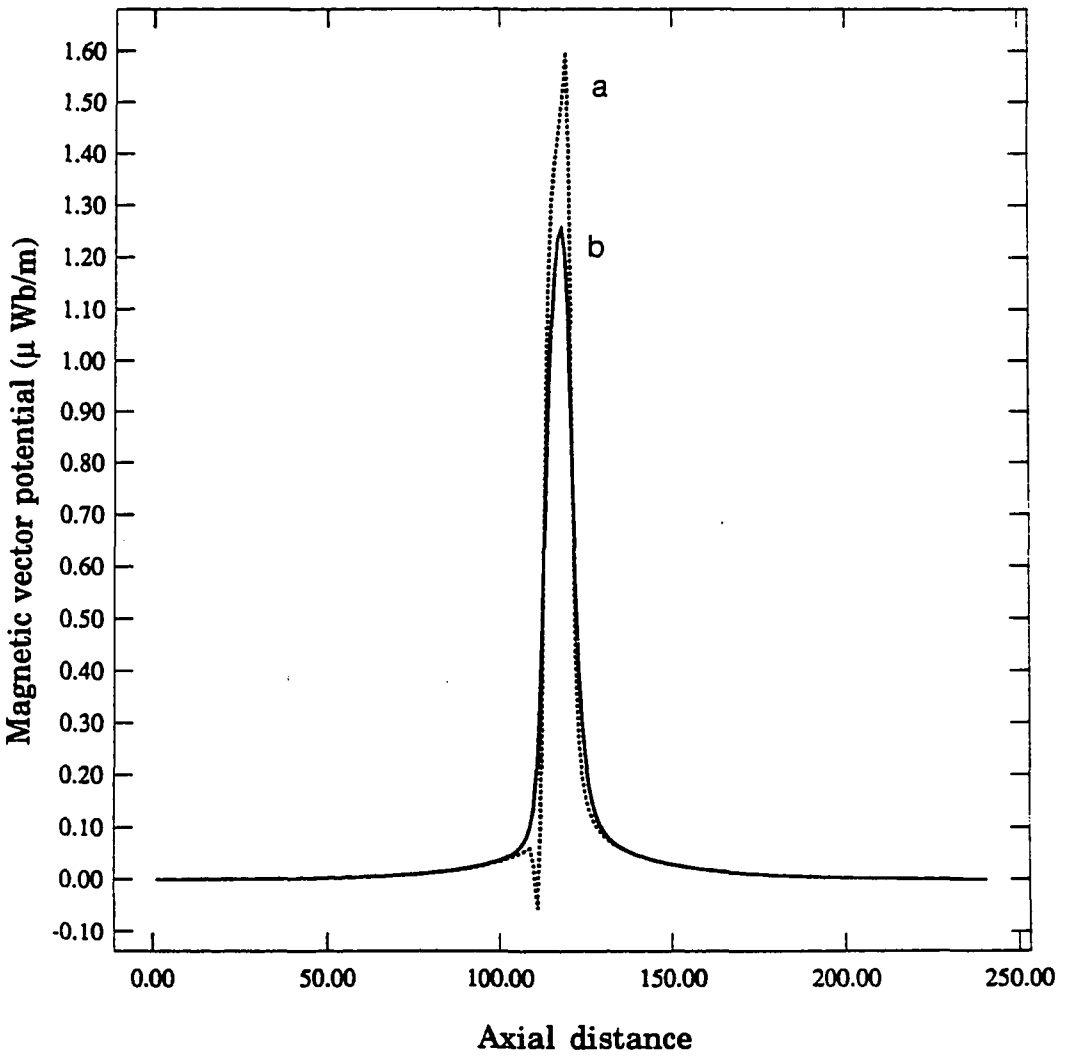

Figure 4.14. Magnetic vector potential values along the center line of the tube at V = 20 m/sec (R_m = 57.45);
a) direct superposition result, b) upwinding result

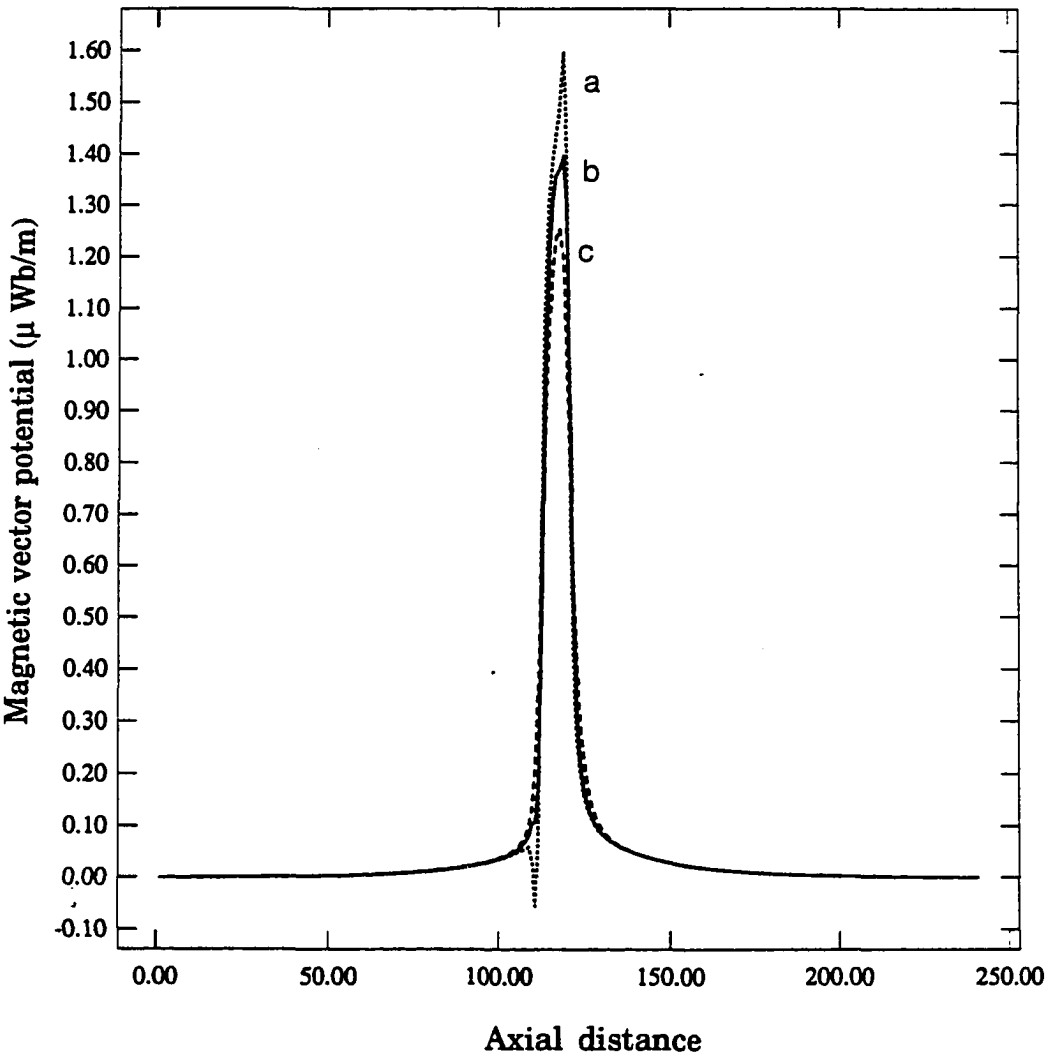

Figure 4.15. Magnetic vector potential values along the center line of the tube at V = 20 m/sec (R_m = 57.45);
a) direct superposition result (ΔV = 20 m/sec),
b) incremental calculation result (ΔV = 2 m/sec),
c) upwinding result

CHAPTER V
UNIFORM NDE GEOMETRIES

This chapter explains the upwinding technique and shows the results obtained by applying the technique to uniform NDE geometries associated with the variable reluctance (VR) probe , the differential eddy current probe, and the remote field eddy current (RFEC) probe. Each probe represents the magnetic flux leakage method, eddy current method, and RFEC method of NDE, respectively. Because of uniform, homogeneous geometries, it is not possible to obtain specific defect signals. However, this analysis is useful in that it provides general background knowledge whenever relative motion is involved. Also, it can be used to predict an optimal sensor position under moving probe conditions.

A. Upwinding Techniques

The upwinding technique was first developed in the finite difference method [124,125]. Noticing successful results of the finite difference upwind scheme, finite element researchers developed an upwinding technique for the finite element method [126,127] which uses an asymmetric weighting function biased in the upwind direction. To distinguish this technique from the standard (Bubnov) Galerkin method, it is often called the Petrov-Galerkin method because the weighting function is not the same as the shape function [118,130]. Later, an easier way of implementing the upwinding concept was

found by using a numerical quadrature rule [117,128,131]. In this section, these upwinding techniques are explained. For simplicity, the explanation is based on the 1-D version of the governing equation for steady state, magnetostatic problems. This 1-D analysis can easily be extended to a 2-D problem as long as the chosen 1-D coordinate coincides with the direction of probe movement.

Consider equation (4.59) for a uniform, homogeneous geometry. Ignoring the source current density term and writing it in 1-D form by ignoring the r-component related term, we have

$$\frac{1}{\mu}\frac{\partial^2 A}{\partial z^2} - \sigma V \frac{\partial A}{\partial z} = 0 \tag{5.1}$$

where the range of z is divided into M equal elements each of length h and the nodes are located at z = mh (m = 0,1,2,..., M). The theoretical solution to equation (5.1) is

$$A(z) = C_1 + C_2 e^{\mu\sigma V z} \tag{5.2}$$

where C_1 and C_2 can be decided by the boundary conditions.

Applying the weighted residual method to equation (5.1),

$$\int_l W^T \left[\nu \frac{\partial^2 A}{\partial z^2} - \sigma V \frac{\partial A}{\partial z} \right] dz = 0 \tag{5.3}$$

where W^T are the weighting functions. If the first term is integrated by parts,

$$\int_l W^T \nu \frac{\partial^2 A}{\partial z^2} dz = \int_l \nu \frac{\partial}{\partial z}\left[W^T \frac{\partial A}{\partial z} \right] dz - \int_l \nu \frac{\partial W^T}{\partial z}\frac{\partial A}{\partial z} dz \tag{5.4}$$

The first term on the right hand side becomes zero as seen in Chapter III. Then, we have

$$\int_l \left[\nu \frac{\partial W^T}{\partial z} \frac{\partial A}{\partial z} + \sigma V W^T \frac{\partial A}{\partial z} \right] dz = 0 \tag{5.5}$$

Since the integration is performed element by element, it can be written as

$$\sum_1^M \int_0^h \left[\nu \frac{\partial W^T}{\partial z} \frac{\partial A}{\partial z} + \sigma V W^T \frac{\partial A}{\partial z} \right] dz = 0 \tag{5.6}$$

From now on, only the elemental integration is considered. The contributions from each element are summed up after elemental matrix equations are found. Now, consider the asymmetric weighting function shown in Figure 1.8. This asymmetric weighting function of the upwinding technique is written as

$$W^T = \begin{Bmatrix} W_L \\ W_R \end{Bmatrix} = \begin{Bmatrix} N_L - \alpha F(z) \\ N_R + \alpha F(z) \end{Bmatrix} \tag{5.7}$$

where $N_L = 1 - \frac{z}{h}$ and $N_R = \frac{z}{h}$ are the shape functions for the left and right nodes of the 1-D element, and α is the degree of upwinding. Here, F(z) is some positive function, such that F(z) is zero at nodes and satisfies the condition shown in equation (1.7). These conditions are met if we use

$$F(z) = 3N_1N_2 = \frac{3}{h^2} z(h - z) \tag{5.8}$$

Therefore, the weighting function can be rewritten as

$$W^T = \begin{Bmatrix} N_L - \frac{3\alpha}{h^2} z(h-z) \\ N_R + \frac{3\alpha}{h^2} z(h-z) \end{Bmatrix} \tag{5.9}$$

From equation (5.6) and since A = [N]{A}, the derivatives of shape functions and weighting functions with respect to z are necessary. Therefore, they are written here.

$$\frac{\partial N_L}{\partial z} = -\frac{1}{h} \tag{5.10}$$

$$\frac{\partial N_R}{\partial z} = \frac{1}{h} \tag{5.11}$$

$$\frac{\partial W_L}{\partial z} = -\frac{1+3\alpha}{h} + \frac{6\alpha z}{h^2} \tag{5.12}$$

$$\frac{\partial W_R}{\partial z} = \frac{1+3\alpha}{h} - \frac{6\alpha z}{h^2} \tag{5.13}$$

The first term of the elemental integration of equation (5.6) can be evaluated as

$$\int_0^h \nu \frac{\partial W^T}{\partial z} \frac{\partial A}{\partial z} dz = \int_0^h \nu \begin{bmatrix} -\frac{1+3\alpha}{h} + \frac{6\alpha z}{h^2} \\ \frac{1+3\alpha}{h} - \frac{6\alpha z}{h^2} \end{bmatrix} \begin{bmatrix} -\frac{1}{h} & \frac{1}{h} \end{bmatrix} \begin{Bmatrix} A_1 \\ A_2 \end{Bmatrix} dz$$

$$= \int_0^h \nu \begin{bmatrix} \frac{1+3\alpha}{h^2} - \frac{6\alpha z}{h^3} & -\frac{1+3\alpha}{h^2} + \frac{6\alpha z}{h^3} \\ -\frac{1+3\alpha}{h^2} + \frac{6\alpha z}{h^3} & \frac{1+3\alpha}{h^2} - \frac{6\alpha z}{h^3} \end{bmatrix} dz \begin{Bmatrix} A_1 \\ A_2 \end{Bmatrix}$$

$$= \nu \begin{bmatrix} \frac{1}{h} & -\frac{1}{h} \\ -\frac{1}{h} & \frac{1}{h} \end{bmatrix} \begin{Bmatrix} A_1 \\ A_2 \end{Bmatrix} \tag{5.14}$$

and the second term as

$$\int_0^h \sigma V W^T \frac{\partial A}{\partial z} dz = \sigma V \int_0^h \begin{bmatrix} 1-\frac{z}{h}-\frac{3\alpha}{h^2}z(h-z) \\ \frac{z}{h}+\frac{3\alpha}{h^2}z(h-z) \end{bmatrix} \begin{bmatrix} -\frac{1}{h} & \frac{1}{h} \end{bmatrix} \begin{Bmatrix} A_1 \\ A_2 \end{Bmatrix} dz$$

$$= \sigma V \int_0^h \begin{bmatrix} -\frac{1}{h}+\frac{z}{h^2}+\frac{3\alpha}{h^3}z(h-z) & \frac{1}{h}-\frac{z}{h^2}-\frac{3\alpha}{h^3}z(h-z) \\ -\frac{z}{h^2}-\frac{3\alpha}{h^3}z(h-z) & \frac{z}{h^2}+\frac{3\alpha}{h^3}z(h-z) \end{bmatrix} dz \begin{Bmatrix} A_1 \\ A_2 \end{Bmatrix}$$

$$= \frac{\sigma V}{2} \begin{bmatrix} \alpha-1 & 1-\alpha \\ -1-\alpha & 1+\alpha \end{bmatrix} \begin{Bmatrix} A_1 \\ A_2 \end{Bmatrix} \qquad (5.15)$$

Note that the result in equation (5.14) is the same as that in equation (3.124). However, equation (3.124) is obtained when the weighting function is the same as the shape function. Therefore, we find that this asymmetric weighting function of the upwinding technique does not affect the integration of the second order spatial derivative term. The only term affected by the upwinding asymmetric weighting function is the first order spatial derivative term, that is, the motional induction term. As discussed in Chapter IV in relation to the time dependent interpretation of the motional induction term, the purpose of all the upwinding techniques is to place an emphasis on the upwind direction when the first order spatial derivative term is evaluated.

Now, combine equations (5.14) and (5.15) to obtain an elemental matrix equation,

$$\begin{bmatrix} \frac{\nu}{h}+\frac{\sigma V}{2}(\alpha-1) & -\frac{\nu}{h}+\frac{\sigma V}{2}(1-\alpha) \\ -\frac{\nu}{h}-\frac{\sigma V}{2}(1+\alpha) & \frac{\nu}{h}+\frac{\sigma V}{2}(1+\alpha) \end{bmatrix} \begin{Bmatrix} A_1 \\ A_2 \end{Bmatrix} = \begin{Bmatrix} 0 \\ 0 \end{Bmatrix} \qquad (5.16)$$

Following the same procedure as in Chapter III, the global matrix equation becomes, for example,

$$\begin{bmatrix} \frac{\nu}{h}+\frac{\sigma V}{2}(\alpha-1) & -\frac{\nu}{h}+\frac{\sigma V}{2}(1-\alpha) & 0 \\ -\frac{\nu}{h}-\frac{\sigma V}{2}(1+\alpha) & \frac{2\nu}{h}+\alpha\sigma V & -\frac{\nu}{h}+\frac{\sigma V}{2}(1-\alpha) \\ 0 & -\frac{\nu}{h}-\frac{\sigma V}{2}(1+\alpha) & \frac{\nu}{h}+\frac{\sigma V}{2}(1+\alpha) \end{bmatrix} \begin{Bmatrix} A_{i-1} \\ A_i \\ A_{i+1} \end{Bmatrix} = \begin{Bmatrix} 0 \\ 0 \\ 0 \end{Bmatrix} \qquad (5.17)$$

Now, we can write a difference equation for node i,

$$\left[-\frac{\nu}{h}-\frac{\sigma V}{2}(1+\alpha)\right]A_{i-1}+\left[\frac{2\nu}{h}+\alpha\sigma V\right]A_i+\left[-\frac{\nu}{h}+\frac{\sigma V}{2}(1-\alpha)\right]A_{i+1}=0 \qquad (5.18)$$

If we multiply $-\mu h$ to equation (5.18) and writing $R_m = \mu\sigma V h$, we have

$$\left[1+\frac{R_m}{2}(1+\alpha)\right]A_{i-1}-2\left[1+\frac{R_m}{2}\alpha\right]A_i+\left[1-\frac{R_m}{2}(1-\alpha)\right]A_{i+1}=0 \qquad (5.19)$$

If the degree of upwinding (α) is zero, as can be seen from equation (5.7), it corresponds to the standard Galerkin method. Note also that equation (5.19) gives a formula identical to that of the central difference method when α is zero, and when α is one, gives an upwind difference scheme. An exact difference solution of equation (5.19) is of the form [127]

$$A_i = C_3 + C_4\left[\frac{1+\frac{R_m}{2}(1+\alpha)}{1-\frac{R_m}{2}(1-\alpha)}\right]^i \qquad (5.20)$$

where C_3 and C_4 are constants to be determined by the boundary conditions. This solution is not oscillatory if

(i) $\alpha = 0$ (standard Galerkin method); $1 - \frac{R_m}{2} > 0 \Leftrightarrow 2 > R_m$

(ii) when $R_m \geq 2$; $1 - \frac{R_m}{2}(1-\alpha) > 0 \Leftrightarrow \alpha_{critical} \geq 1 - \frac{2}{R_m}$

Condition (i) gives the basis of mesh refinement when the standard Galerkin method is used. By equating equation (5.2) with equation (5.20), Christie et al. [126] found that the exact solution can be obtained when

$$\alpha = \coth\left(\frac{R_m}{2}\right) - \frac{2}{R_m} \tag{5.21}$$

Note that this exact solution can be obtained only in the uni-directional velocity, steady state, and constant coefficient cases. Since $R_m = \mu\sigma Vh$, α is a function of h. Therefore, we can use different sizes of elements and α can be decided for each element.

There is an important term related to the upwinding technique. This term can be found as follows. Consider equation (5.18). If the standard Galerkin method ($\alpha = 0$) were used, equation (5.18) would be

$$\left[-\frac{\nu}{h} - \frac{\sigma V}{2}\right]A_{i-1} + \frac{2\nu}{h}A_i + \left[-\frac{\nu}{h} + \frac{\sigma V}{2}\right]A_{i+1} = 0 \tag{5.22}$$

Now, compare equation (5.22) with (5.18). Equation (5.22) would be the same as equation (5.18) if ν in equation (5.22) were replaced by $\nu + \frac{\alpha\sigma Vh}{2}$. This means that if we add the term, $\frac{\alpha\sigma Vh}{2}$, to the original reluctivity (ν) and solve the new governing equation by the standard Galerkin method, we can get the same answers as upwinding results. Consequently, the upwinding technique artificially increases the reluctivity by the amount of the above

additional term to suppress spurious oscillations. This additional term is called 'artificial diffusion' in fluid mechanics, but in this dissertation, it is called 'artificial reluctivity' because of the differences in terminology. A more rigorous mathematical derivation of this term can be found in reference 128. Although this term removes spurious oscillations, it also causes a numerical dissipation. Examples of numerical dissipation are shown in the next section.

Another upwinding technique developed by Hugh [117] is based on a numerical quadrature rule. However, the upwinding quadrature point is different from the ordinary quadrature point. It is displaced in the upwind direction from the ordinary point, and used only for the integration of the motional induction term. The amount of displacement plays the same role as α, the degree of upwinding. Figure 5.1 compares the ordinary quadrature point with the upwinding, displaced quadrature point. This method is easier to implement the upwinding concept into the computer program.

The rest of this chapter shows and discusses the upwinding results for the three probe cases applied to uniform geometries. In this dissertation, the solution region is discretized into rectangular elements and the example of such discretization is shown in Figure 5.2. The heavily discretized region corresponds to the tube.

B. Results of the Variable Reluctance Probe Case

Figure 5.3 show the equipotential plots around the variable reluctance probe at V = 0 m/sec and V = 5 m/sec. It can be noticed that magnetic fields

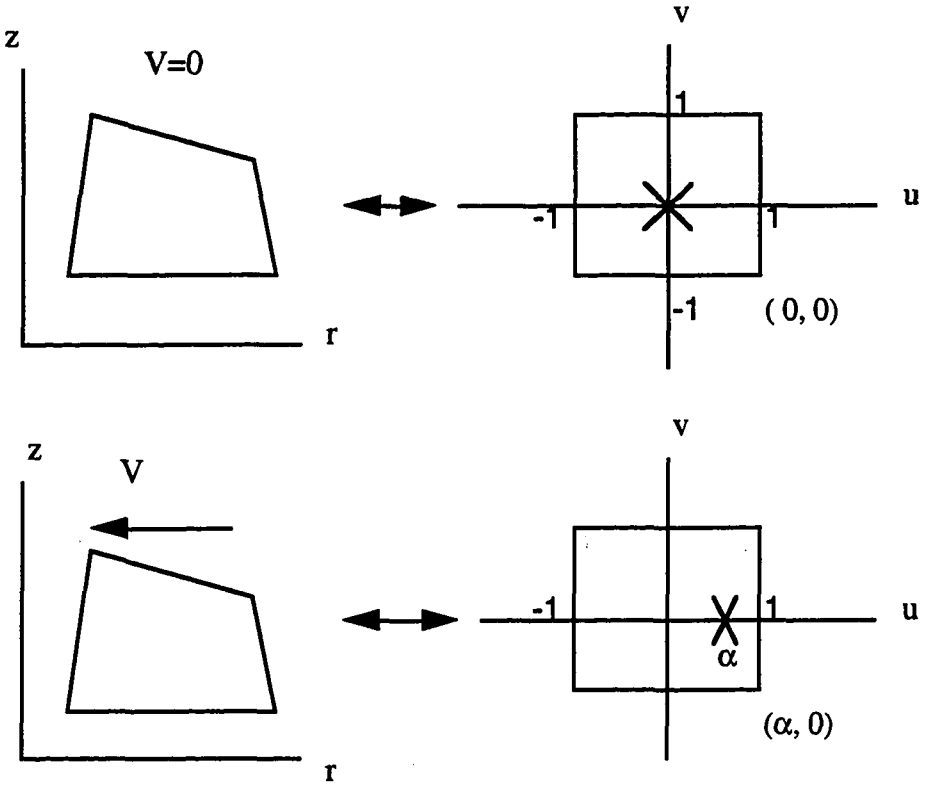

Figure 5.1. Comparison of an ordinary quadrature point and a upwinding quadrature point for motional induction term

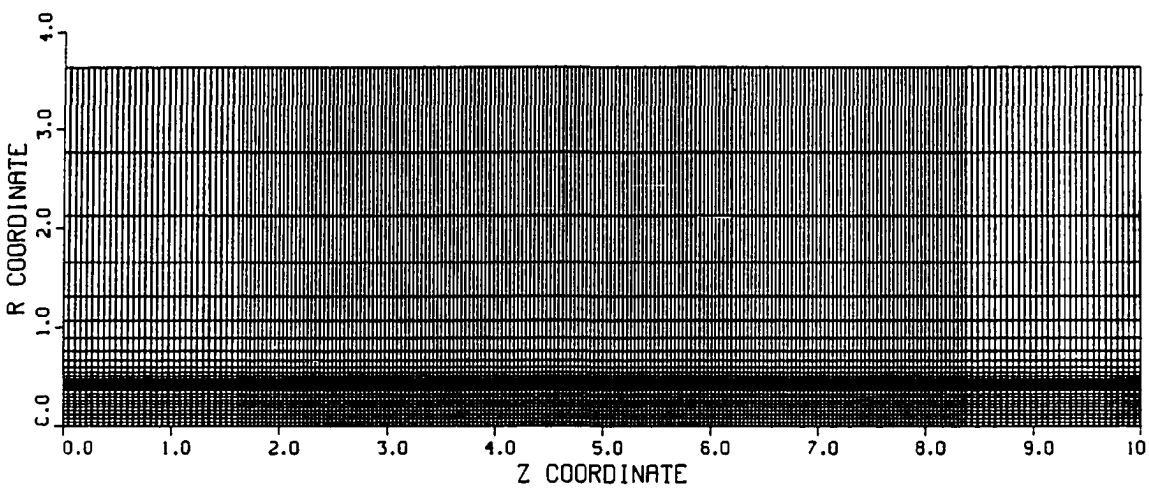

Figure 5.2. An example of mesh discretization

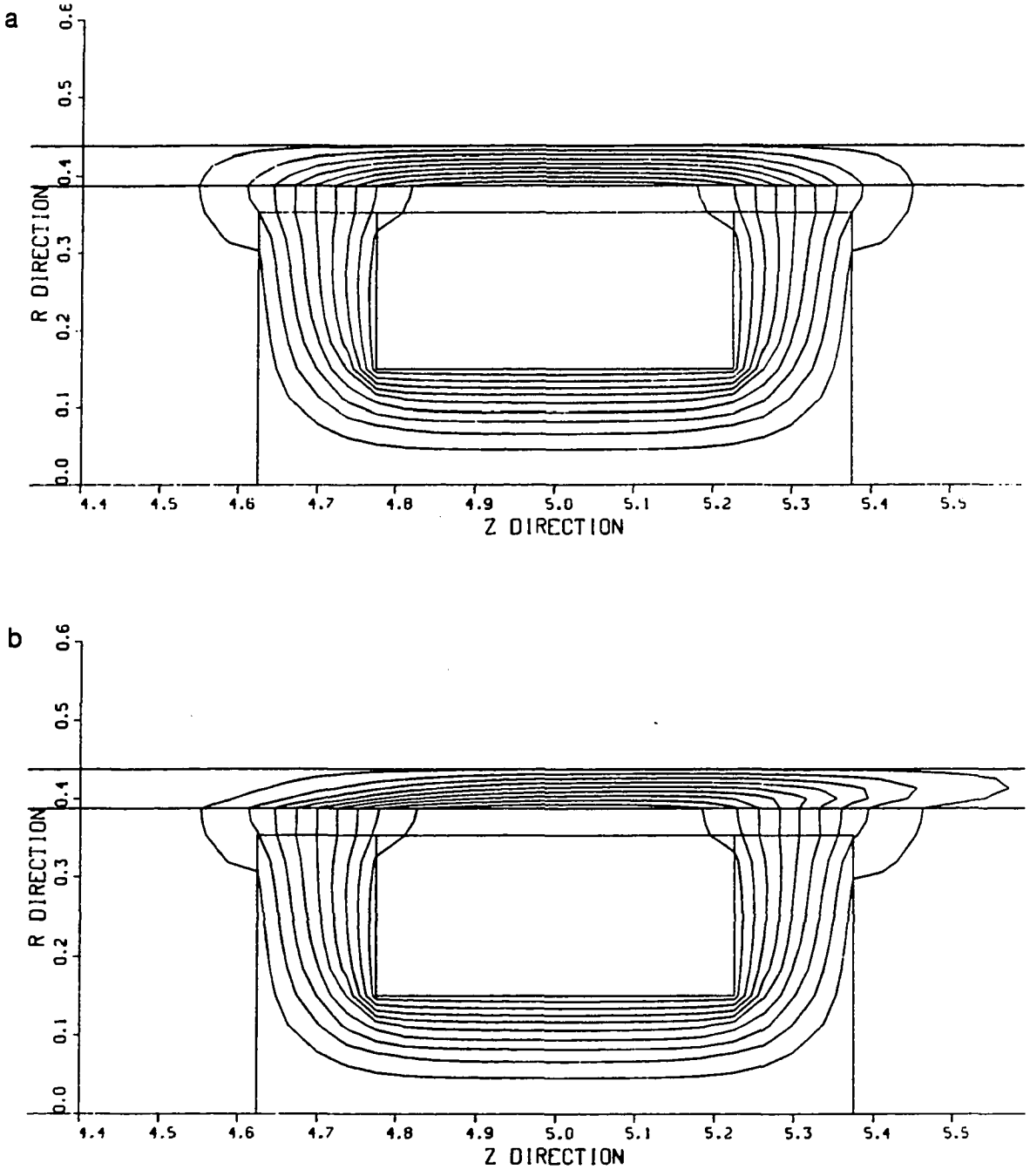

Figure 5.3. Equipotential plots around the variable reluctance probe; a) V = 0 m/sec, b) V = 5 m/sec

are dragged behind the probe and as a result, magnetic fields do not penetrate far into the front edge of the tube.

Figure 5.4 shows the upwinding results corresponding to Figure 4.4. Even though the Dirichlet boundary condition (B.C.) is used, the upwinding technique removes spurious oscillations everywhere. However, at V = 100 m/sec, a sudden drop to zero potential at the boundary behind, is noticed. This is not reasonable, so the Neumann B.C. is used for that boundary to get reasonable results as shown in Figure 5.5. Therefore, we can conclude that the natural boundary condition should be used when the probe velocity is so high that magnetic fields are expected to cross over the boundary.

Figure 5.6 compares the upwinding result with the standard Galerkin result when there is no oscillation in the standard Galerkin result (i.e. R_m is small). The relative permeability and conductivity of the tube are 100 and 0.6×10^7 mho/meter, respectively. The element length is 4.76 mm and the probe velocity is 5 m/sec. Thus, R_m is 17.9. When the conductivity is increased to 2×10^7 mho/meter (R_m = 59.8), spurious oscillations occur in the standard Galerkin result as shown in Figure 5.7. The upwinding technique removes such oscillations, but at the cost of accuracy. This can be seen in Figure 5.7. The loss of accuracy is due to the numerical dissipation associated with the artificial reluctivity term. Although small, the same numerical dissipation can be noticed in Figure 5.6. Therefore, when there is no oscillation in the standard Galerkin result, the upwinding technique should not be used. The loss of accuracy is more evident in Figure 5.8 where the standard Galerkin, non-oscillatory result obtained by using smaller elements is added (R_m = 20). Although the upwinding technique provides a

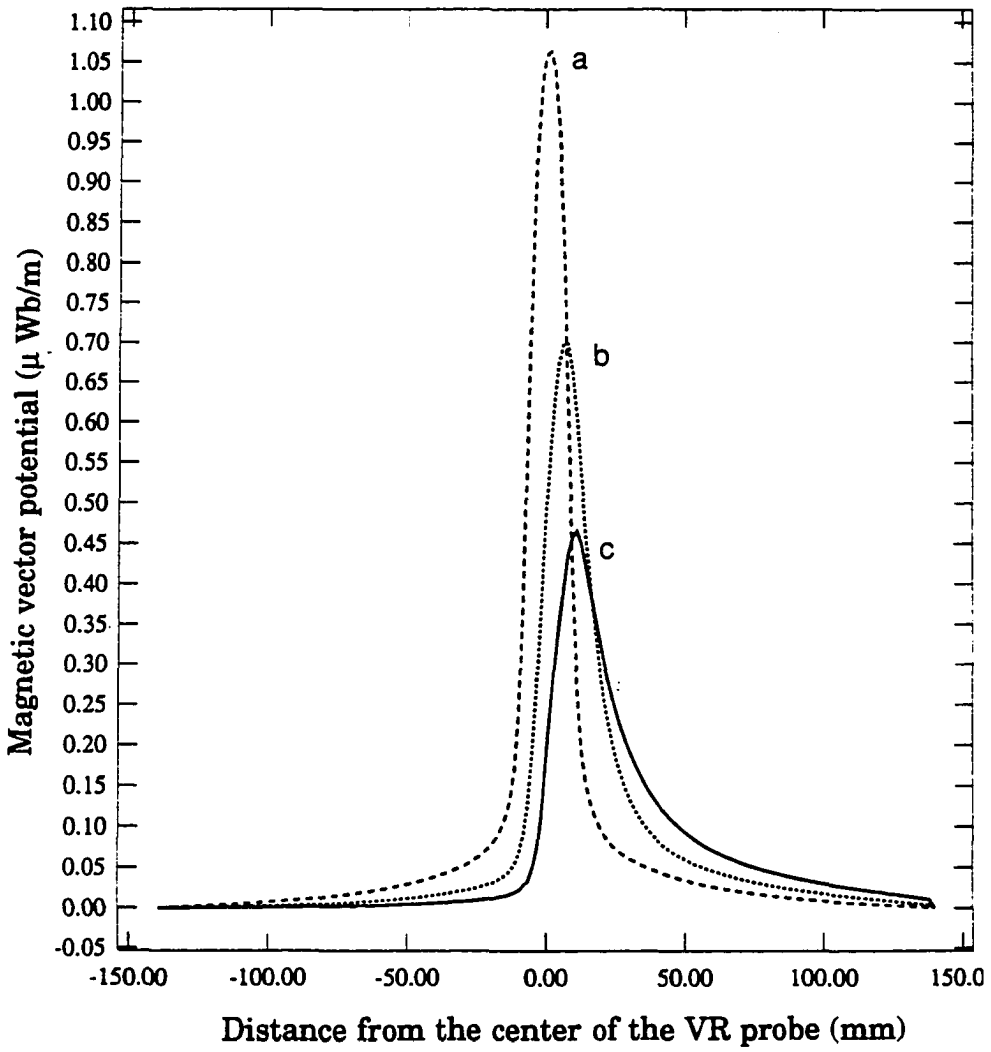

Figure 5.4. Upwinding results corresponding to Figure 4.4 (Dirichlet B.C.); a) V = 5 m/sec (R_m = 5.99), b) V = 50 m/sec (R_m = 59.94), c) V = 100 m/sec (R_m = 119.88)

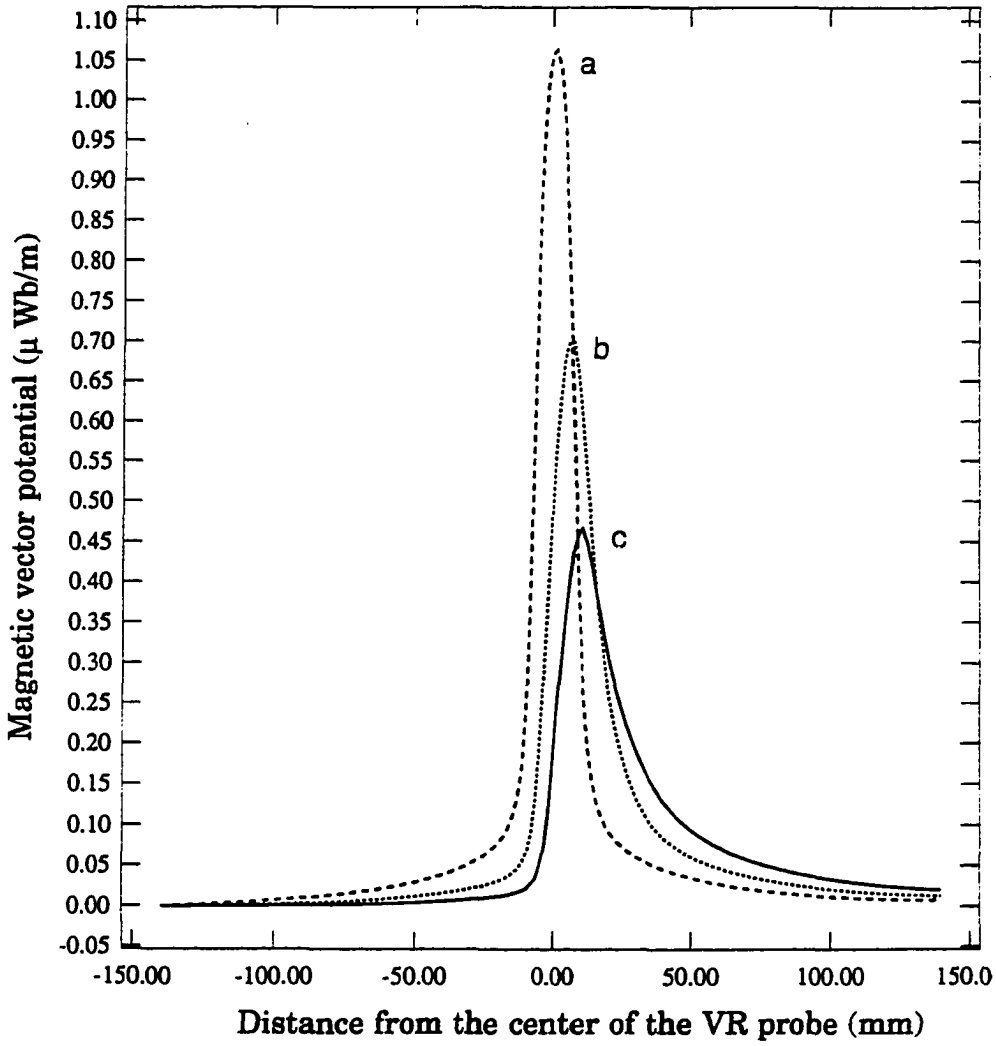

Figure 5.5. Upwinding results obtained by applying Neumann B.C.; a) V = 5 m/sec (R_m = 5.99), b) V = 50 m/sec (R_m = 59.94), c) V = 100 m/sec (R_m = 119.88)

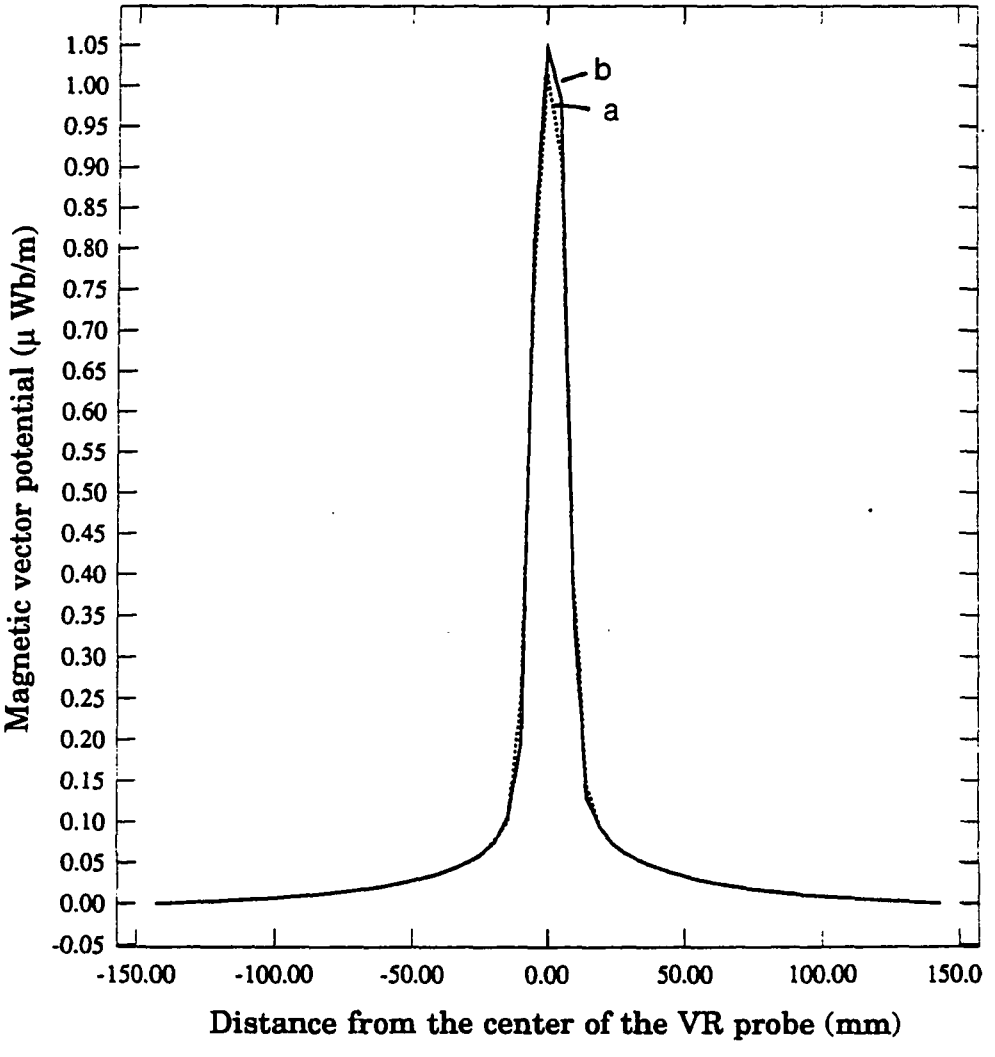

Figure 5.6. Comparison of results (R_m = 17.9);
a) upwinding result,
b) standard Galerkin result

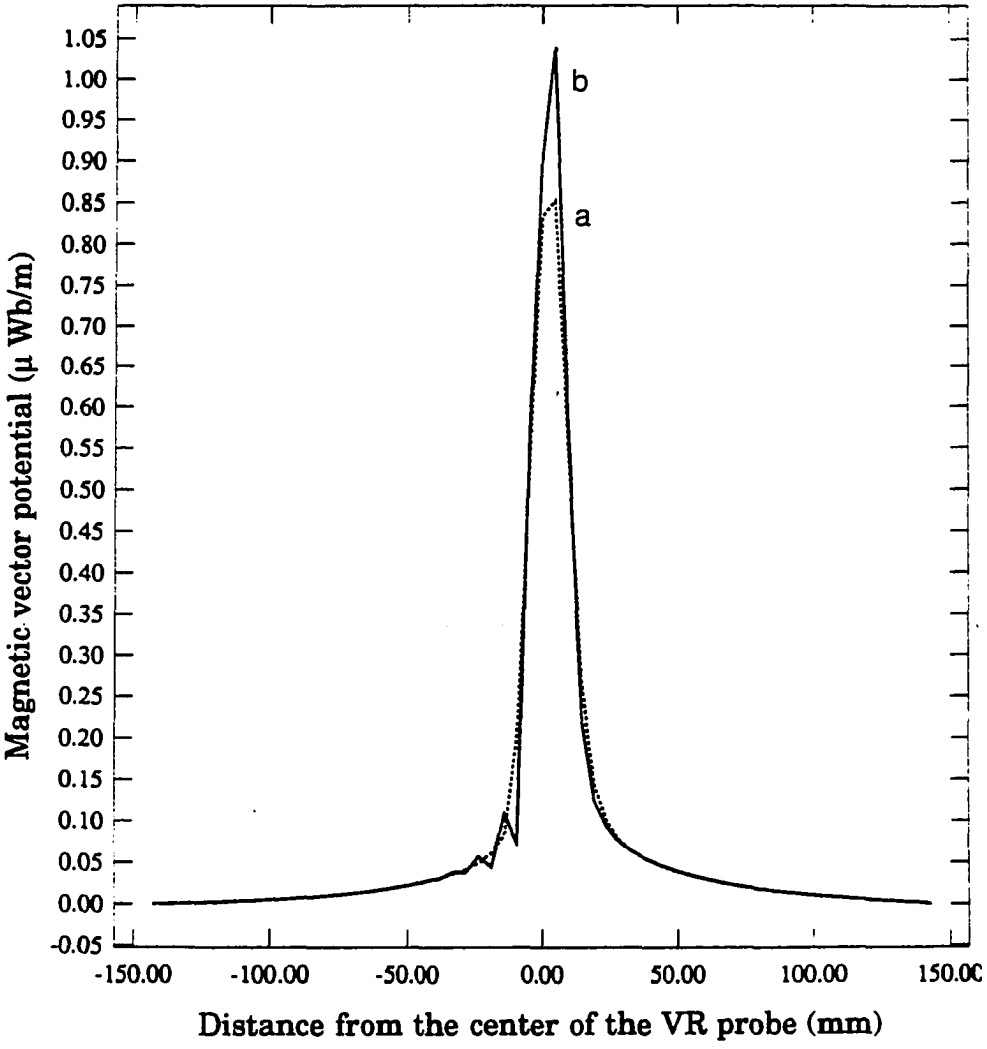

Figure 5.7. Comparison of results (R_m = 59.8);
a) upwinding result,
b) standard Galerkin result

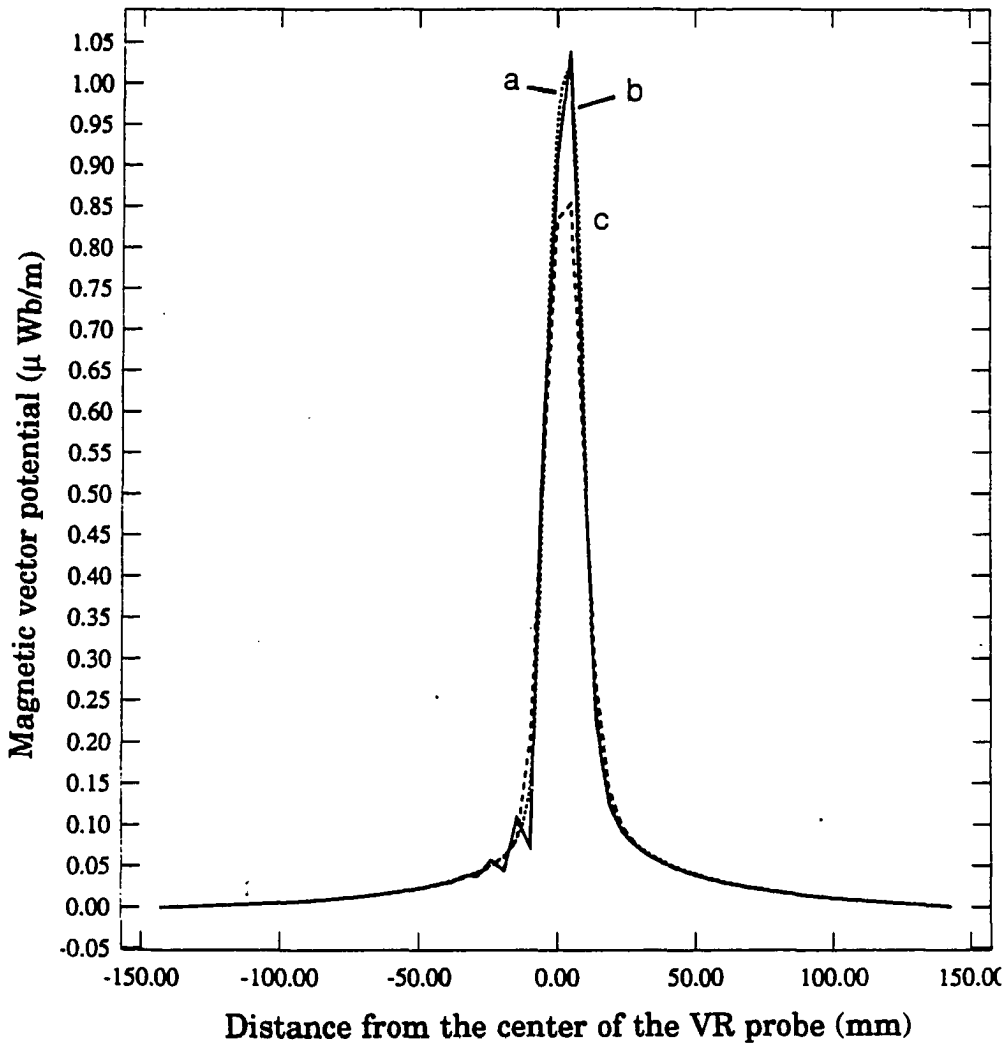

Figure 5.8. Comparison of results;
a) standard Galerkin result (small mesh, R_m=20)
b) standard Galerkin result (large mesh, R_m=59.8)
c) upwinding result (large mesh, R_m=59.8)

non-oscillatory result, Figure 5.8 shows that it is less accurate than the standard Galerkin result from smaller elements. Then, why is this technique used? The first reason is that there are situations where, especially in 3-D problems, heavy mesh discretization is practically impossible because of the limitations in today's computer resources. The second reason is that even if relatively heavy mesh discretization is used, when the material properties or probe velocities involved are too large, spurious oscillations cannot be avoided. We have already seen such oscillations due to a high material conductivity (Figure 4.6) and due to a high velocity (Figure 4.4) in Chapter IV.

Although this study of a uniform geometry cannot provide defect signals, it gives useful background information. One example is the optimal location of a sensing Hall plate for the variable reluctance probe. Figure 5.9 shows the normal component of flux along the line of possible Hall plate locations. Note that they are not output NDE signals. As the probe velocity increases, the normal component of flux is decreased. The possible locations of a Hall plate, which is mounted on the periphery of the bobbin (see Figure 2.3), are position numbers 13, 14, 15, 22, 23, and 24 in Figure 5.9. Among them, position 15 gives the maximum signal strength and is least affected by the probe velocity changes. Therefore, this position, i.e. the innermost side of the leading edge of the probe, would be the optimal position of the sensor.

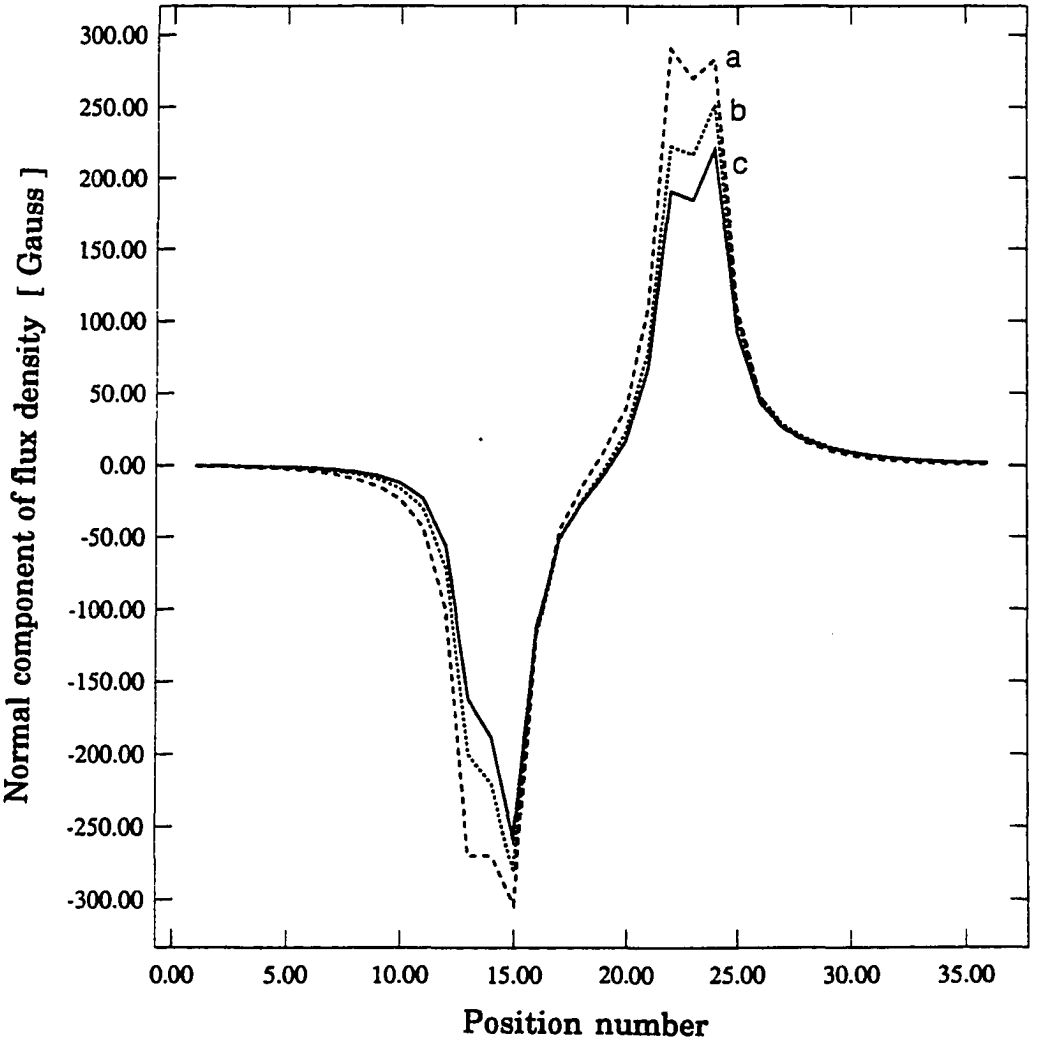

Figure 5.9. Normal component of flux along the line of possible Hall plate locations; a) V = 5 m/sec, b) V = 50 m/sec, c) V = 100 m/sec

C. Results of the Differential Eddy Current Probe Case

Figure 5.10 show the RMS equipotential plots around the differential eddy current probe at V = 0 m/sec and V = 5 m/sec. Again, the backward shift of the fields can be noticed. Figures 5.11 and 5.12 show the RMS magnetic vector potential values at the center line of the tube wall. As the probe velocity increases, the trailing RMS potential value and the imbalance between the two values increase. Figure 5.13 shows the individual impedance variations of the leading and trailing coils as the probe velocity increases. The resulting differential impedance variation due to the different probe velocities is shown in Figure 5.14.

At this point, we need to think about the benefit of using a differential eddy current probe. Because of the differential nature, this probe is relatively insensitive to environmental effects and highlights the variations due to defects by cancelling the quiescent values of each coil. However, if this probe is used in high speed moving inspection, the differential impedance changes together with the probe velocity, even in uniform geometries as can be seen in Figure 5.14. As a result, the output impedance contains this motional impedance variation. To extract only the defect signal, a similar normalization process as in the case of an absolute coil is required, but in this case, by using the base differential impedance value of the specified probe velocity. Then, the practical benefit of using a differential eddy current probe is lost. To utilize the beneficial aspects of this probe, it should not be used in high speed moving inspection.

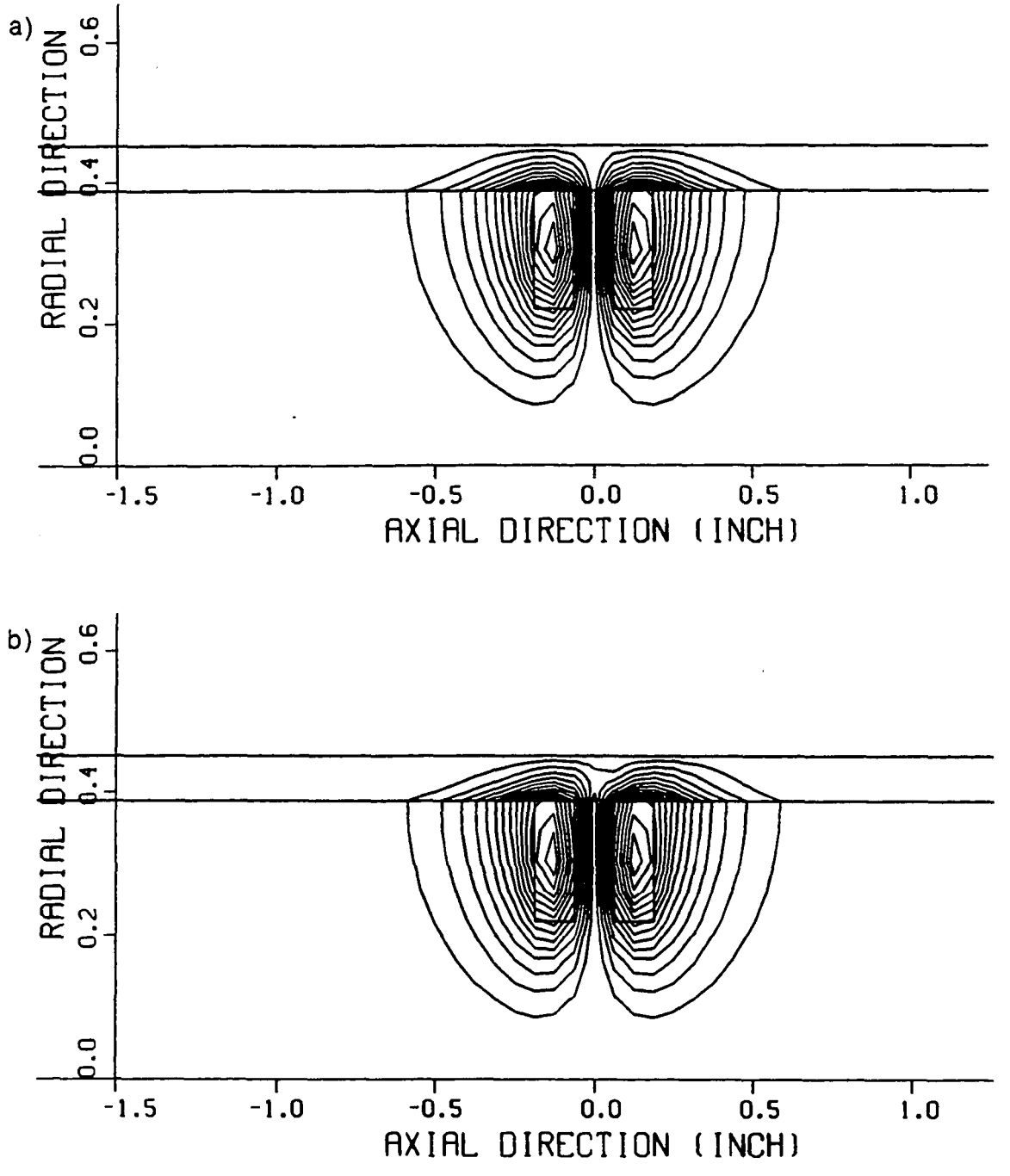

Figure 5.10. RMS equipotential plots around the differential eddy current probe; a) V = 0 m/sec, b) V = 5 m/sec

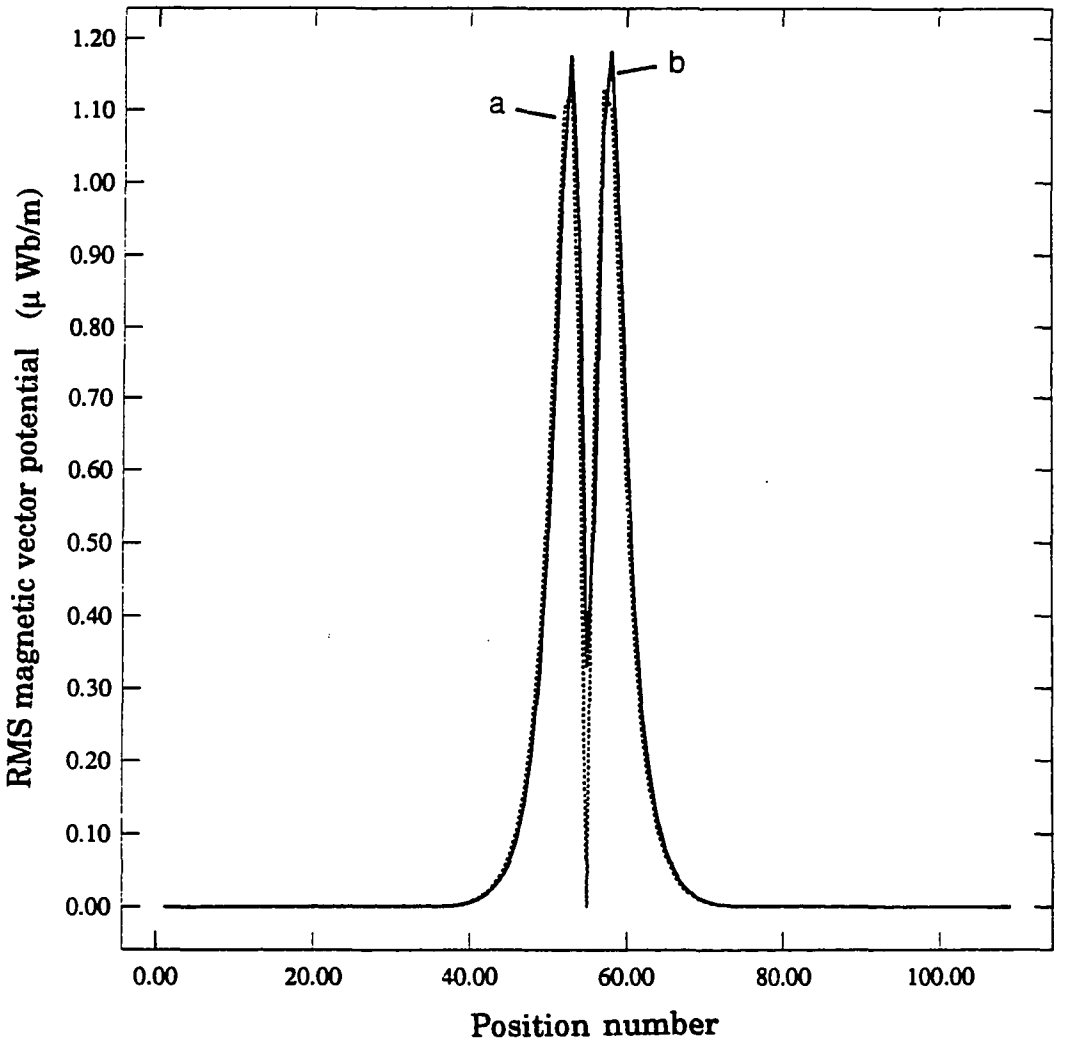

Figure 5.11. RMS magnetic vector potential values at the center line of the tube wall; a) V = 0 m/sec, b) V = 5 m/sec

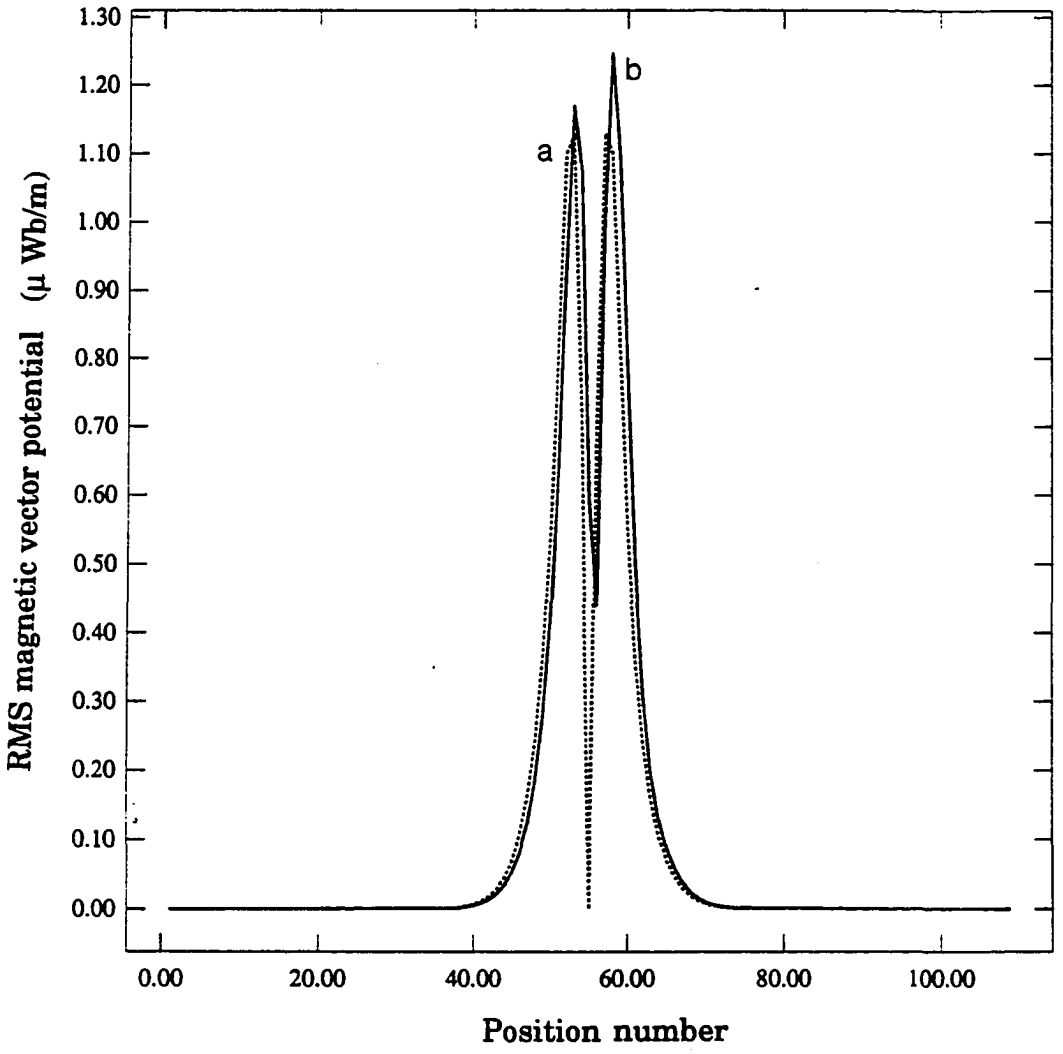

Figure 5.12. RMS magnetic vector potential values at the center line of the tube wall; a) V = 0 m/sec, b) V = 9 m/sec

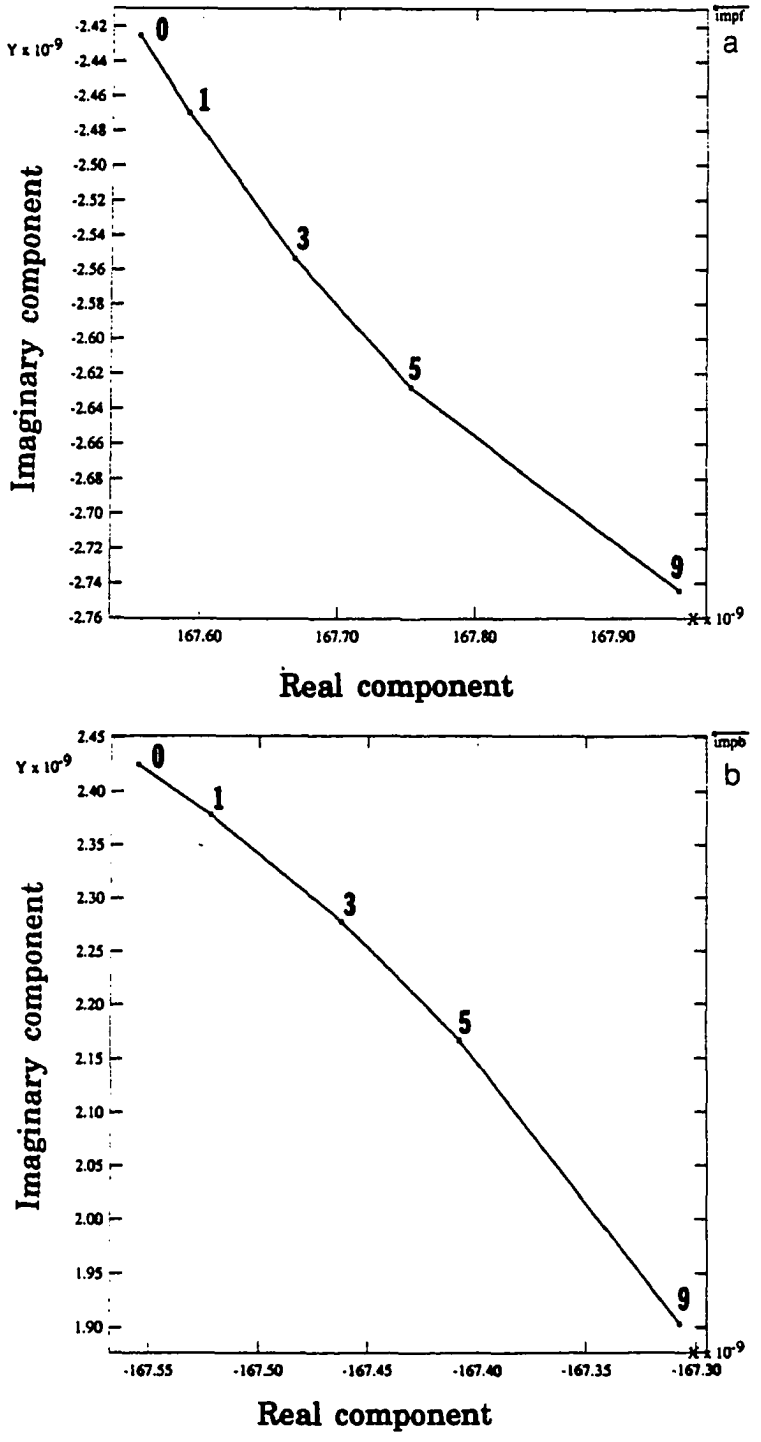

Figure 5.13. Impedance variations of each coil due to probe velocity;
a) leading coil impedance variation,
b) trailing coil impedance variation

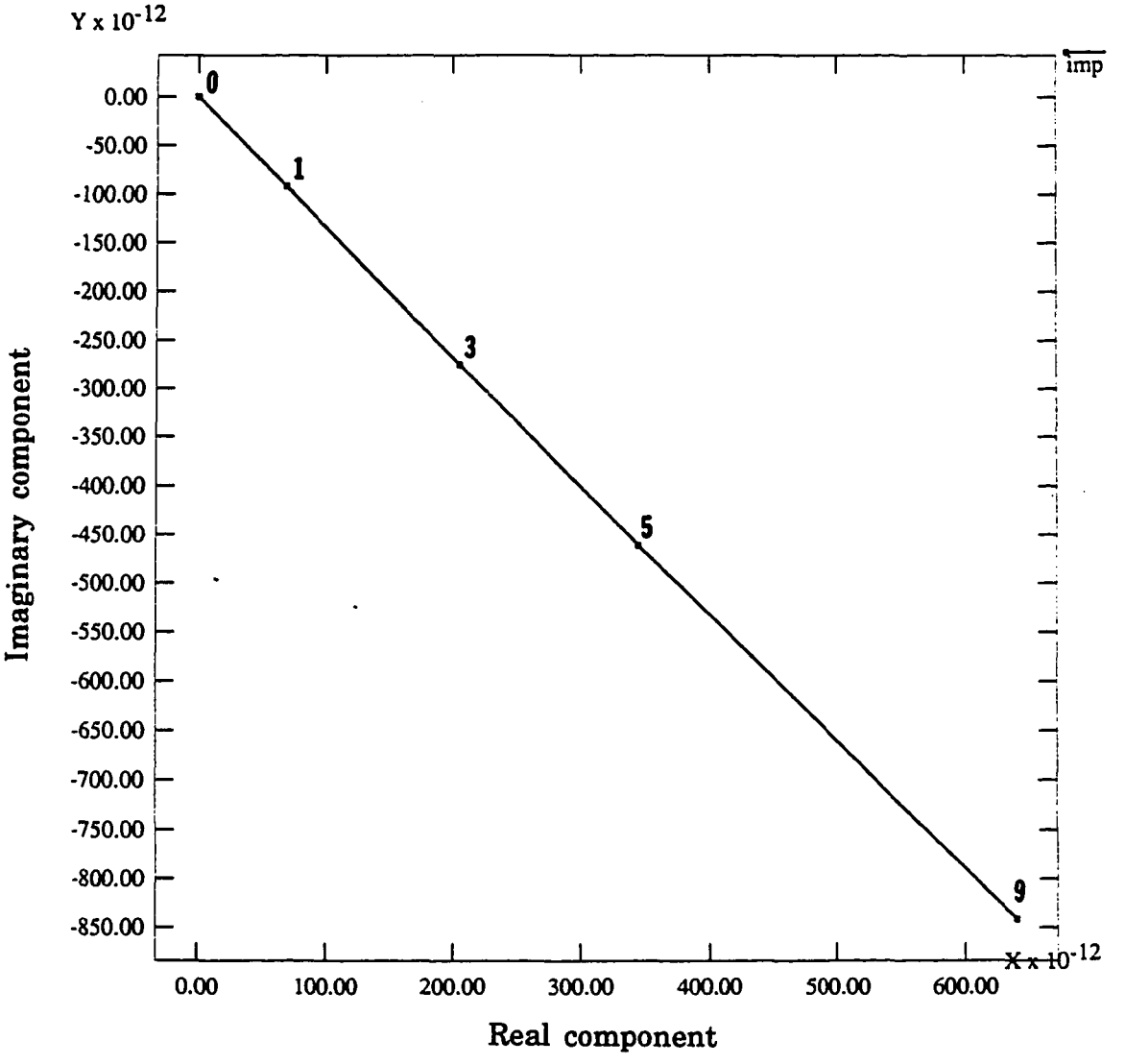

Figure 5.14. Differential impedance variation due to probe velocity

D. Results of the Remote Field Eddy Current Probe Case

In Figure 5.15, the RMS magnetic vector potential magnitude is plotted on a logarithmic scale at V = 0, 3, and 6 m/sec. Again, the backward shift of the fields can be noticed together with the shift of the potential valley. However, the potential valley in front of the exciter coil is not shifted much. The same phenomena are found in the phase knot locations as shown in Figure 5.16. Figure 5.17 and 5.18 show the RMS magnetic vector potential magnitude in a logarithmic scale and the phase of the magnetic vector potential at the center line of the tube wall. Again, the same phenomena are found in both figures. Figure 5.19 shows the phase knot location changes, found in Figure 5.18, with respect to the probe velocity.

Finally, the induced current density in the tube wall is investigated. In this case, the induced current density includes the motional induction current density so that it can be written as

$$J_i = j\omega\sigma A + \sigma V \frac{\partial A}{\partial z} \tag{5.23}$$

The investigation is performed at three locations. One is just above the exciter coil and the other two locations are ±3 tube diameters away from the exciter, that is, the front and trailing remote field regions. All the results of RMS induced current densities are shown in a logarithmic scale. Figure 5.20 shows the results obtained at just above the exciter coil. Since the induced currents at the inner diameter are larger than those at the outer diameter, we may confirm that the energy is directed from the inside to the outside of the tube. This pattern does not change even if the probe velocity is increased.

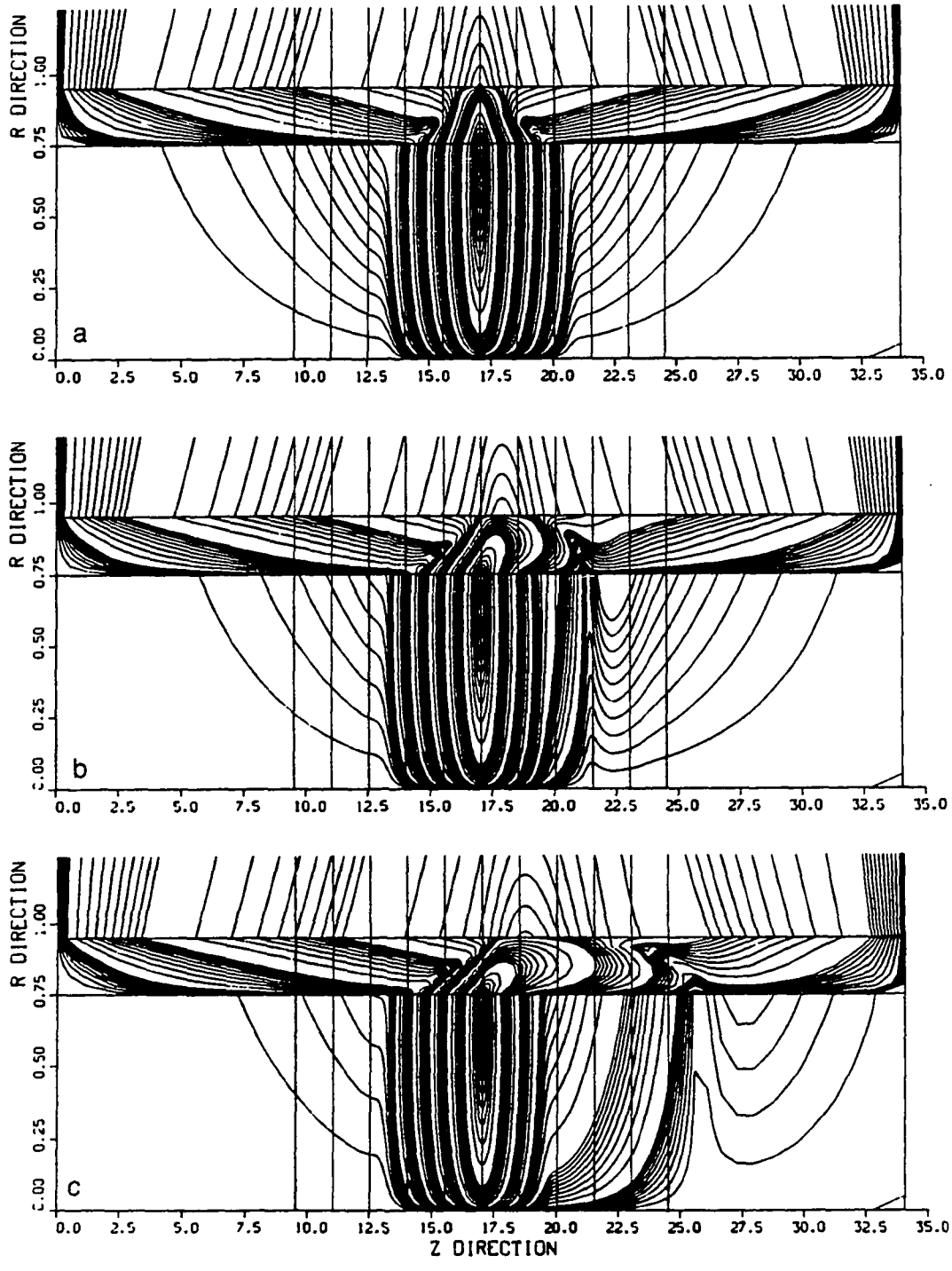

Figure 5.15. Logarithmic scale plots of RMS magnetic vector potential magnitude; a) V = 0 m/sec, b) V = 3 m/sec, c) V = 6 m/sec

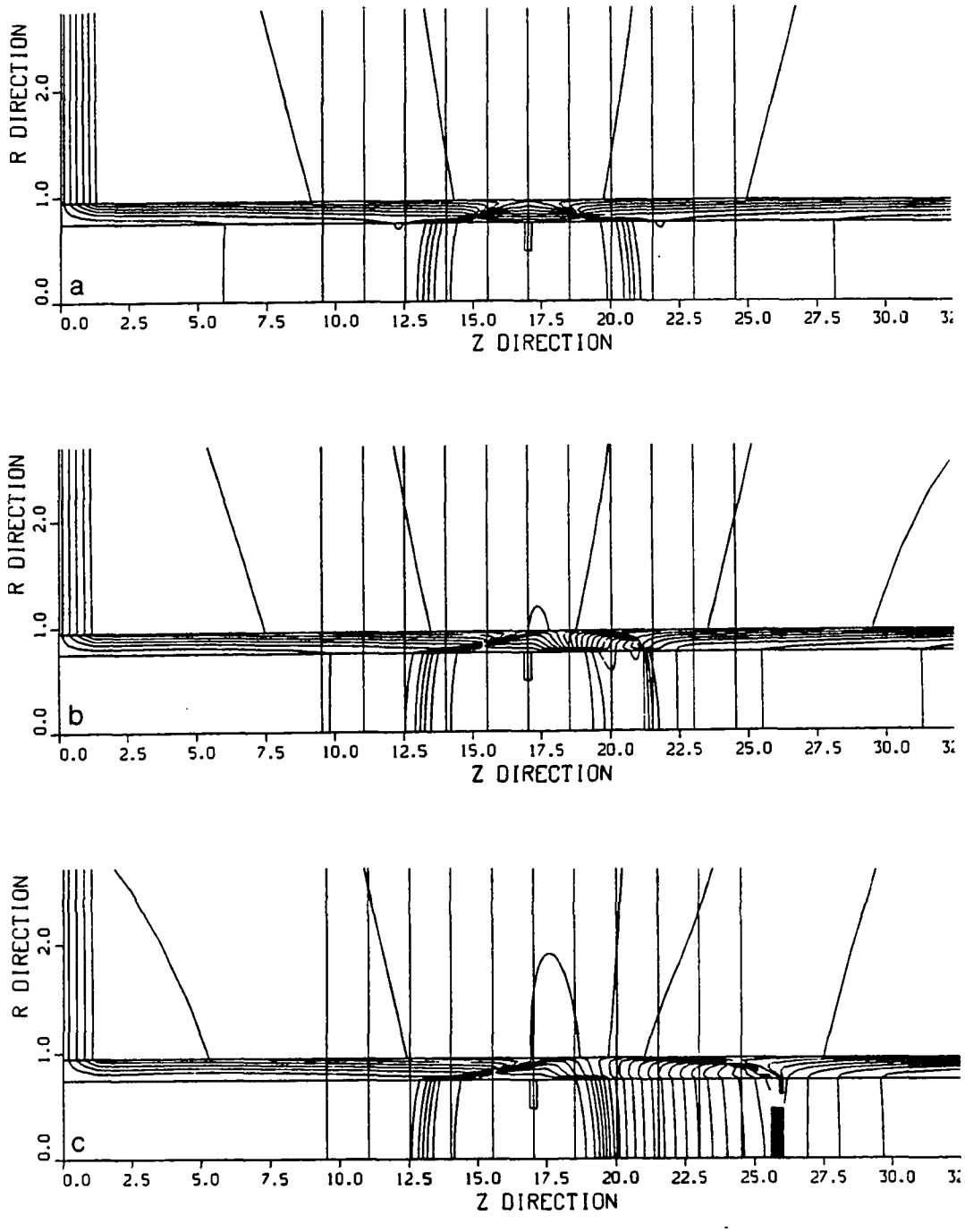

Figure 5.16. Equi-phase plots of magnetic vector potential;
a) V = 0 m/sec, b) V = 3 m/sec, c) V = 6 m/sec

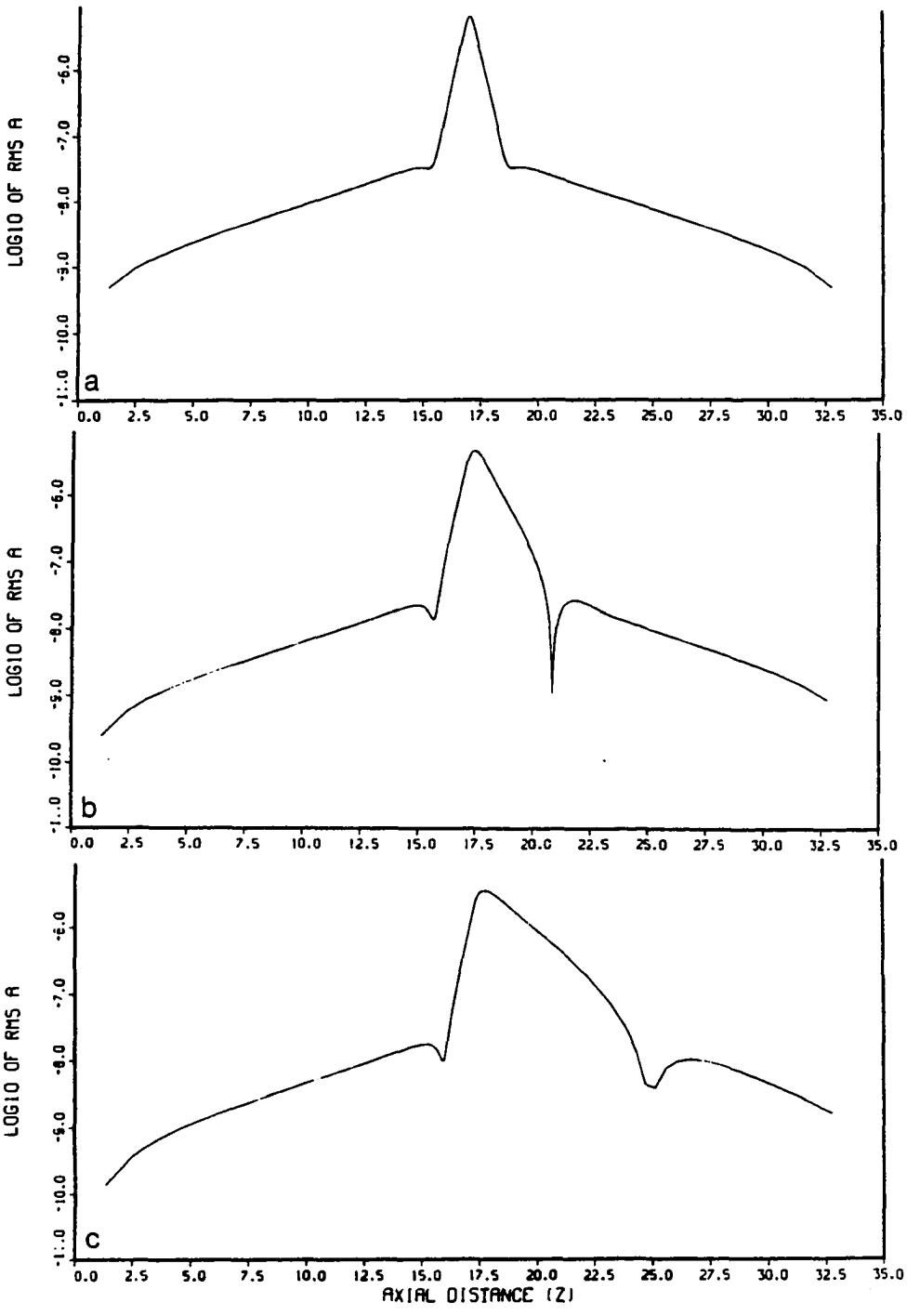

Figure 5.17. Log scaled RMS magnetic vector potential magnitude at the center line of the tube wall; a) V = 0 m/sec, b) V = 3 m/sec, c) V = 6 m/sec

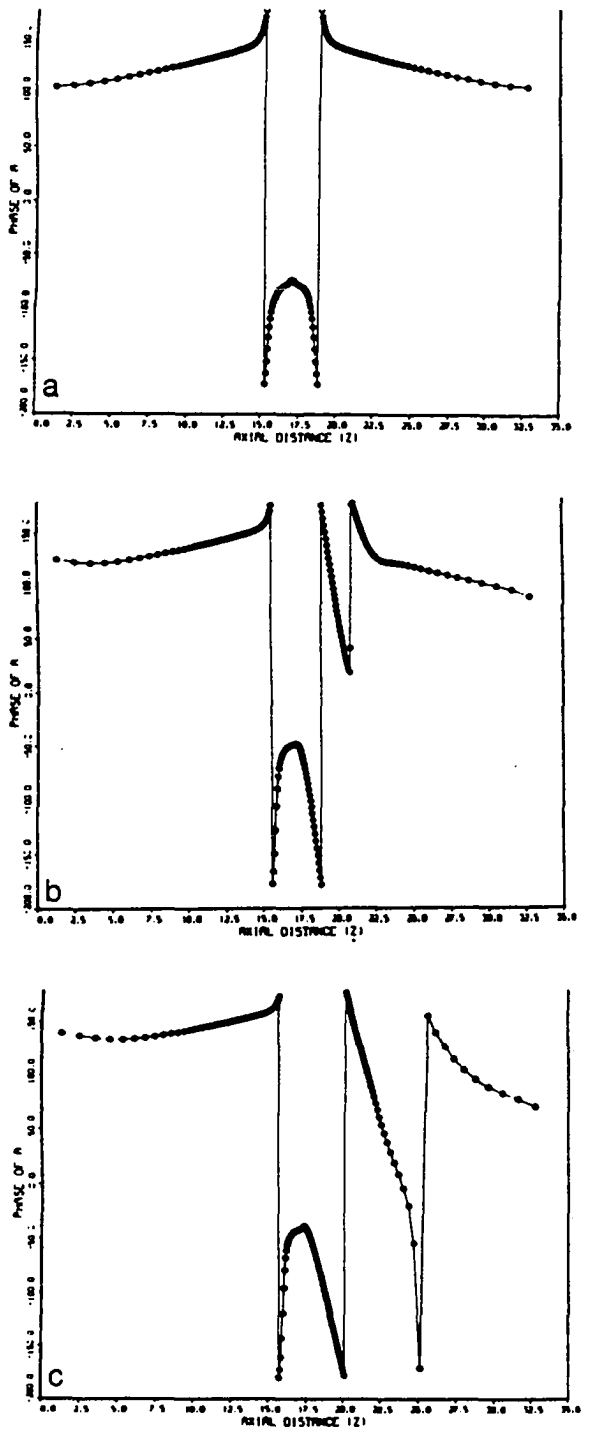

Figure 5.18. Phase of magnetic vector potential at the center line of the tube wall; a) V = 0 m/sec, b) V = 3 m/sec, c) V = 6 m/sec

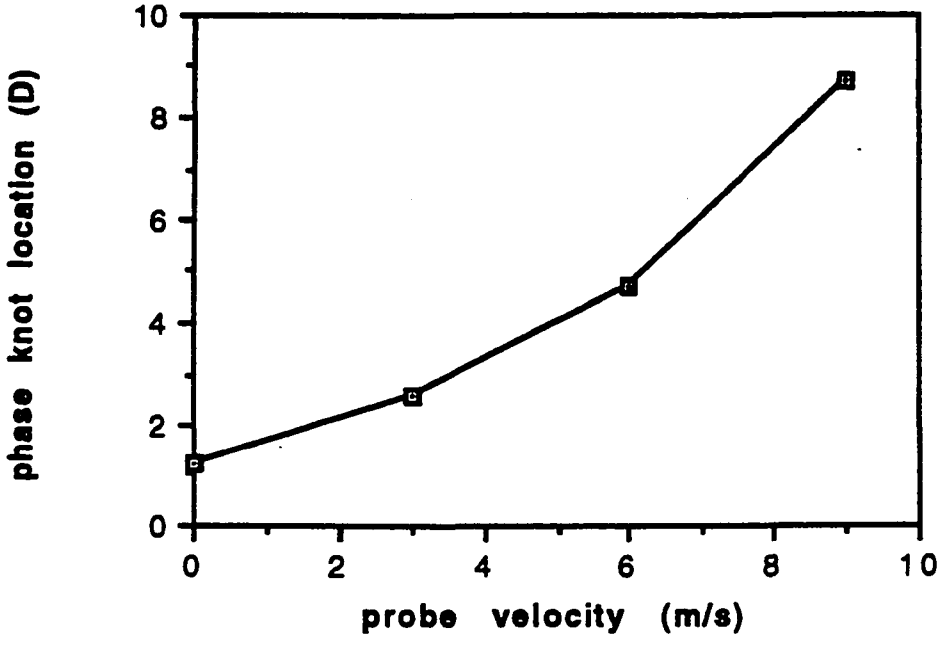

Figure 5.19. Changes in phase knot location due to probe velocity

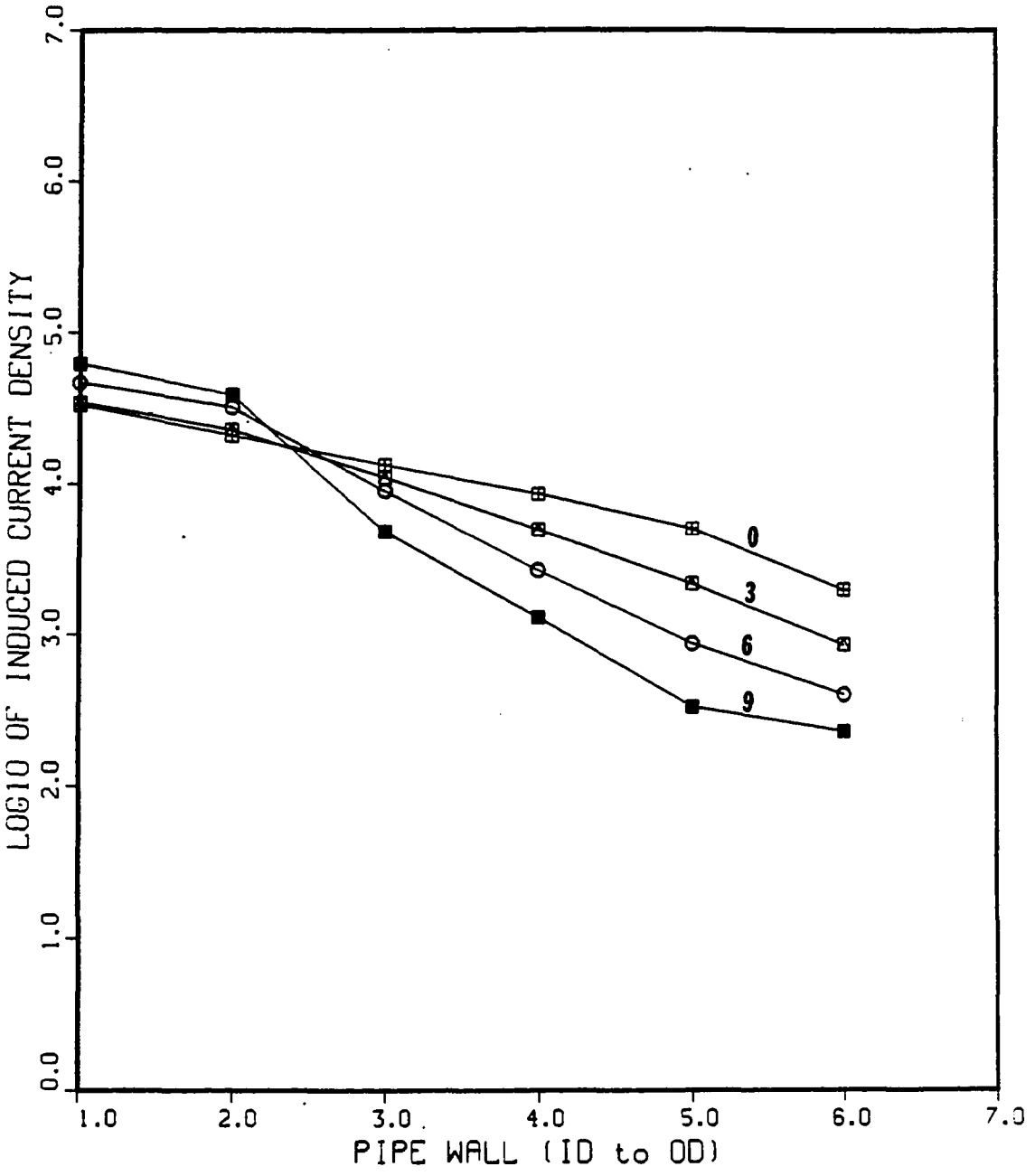

Figure 5.20. Log scaled RMS induced current densities near the exciter coil; (V = 0, 3, 6, and 9 m/sec)

Figure 5.21 shows the results at 3 diameters behind the exciter coil. When the probe velocity is low, the induced currents at the inner diameter are smaller than those at the outer diameter. Therefore, the energy is directed from the outside to the inside of the tube. However, this pattern changes as the probe velocity is increased. This indicates that if the sensor coil is located in this area, it is affected very much by the probe velocity effects. On the other hand, the results at 3 diameters ahead of the exciter show promise in finding the optimal sensor location. These results are shown in Figure 5.22. In this case, even if the probe velocity is increased, the characteristics of the remote field region do not change so that the probe velocity effects are at a minimum at this location. Therefore, the sensor coil needs to be located in front of the exciter coil when high speed moving inspection is performed.

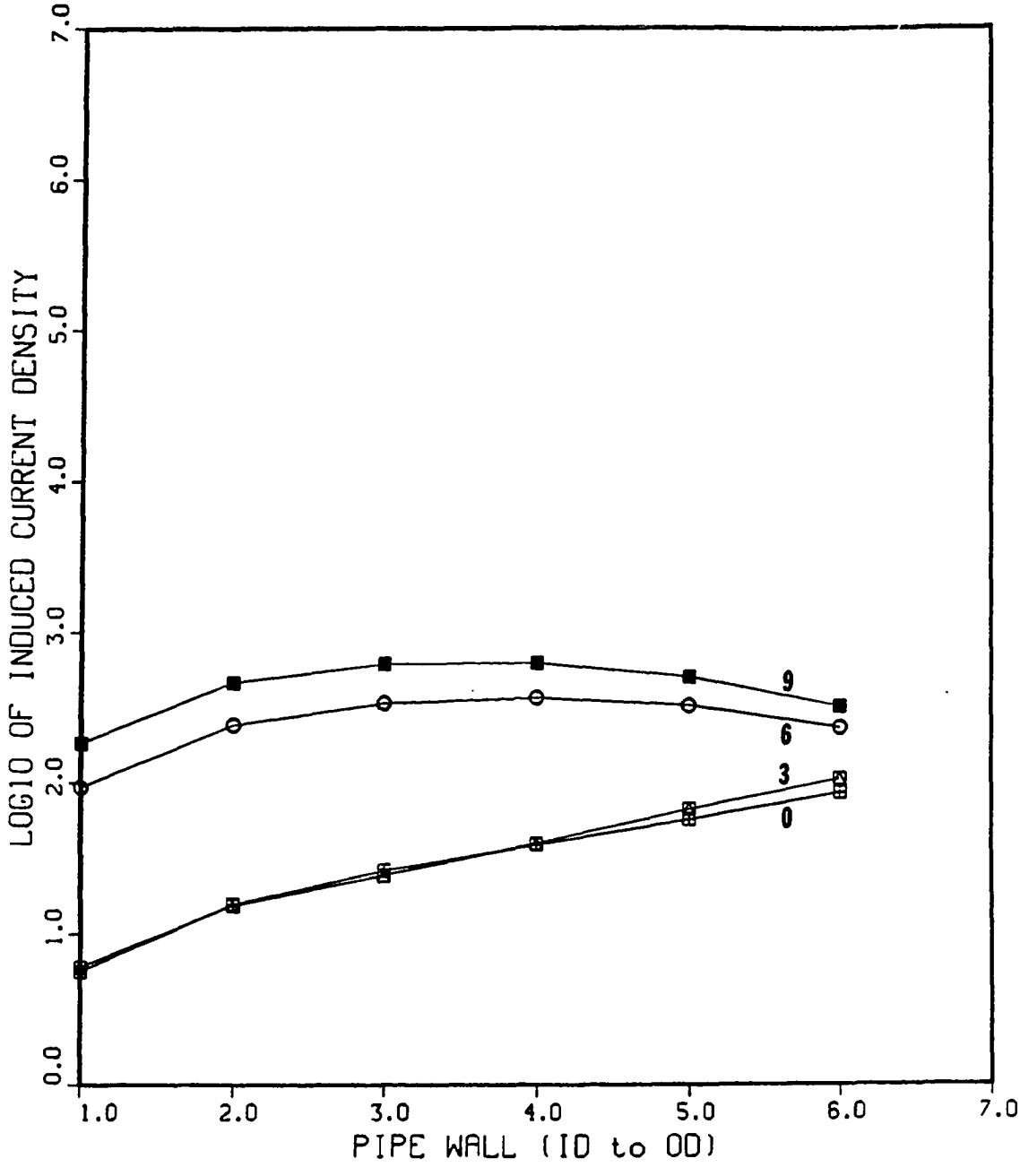

Figure 5.21. Log scaled RMS induced current densities at 3 diameters behind the exciter coil; (V = 0, 3, 6, and 9 m/sec)

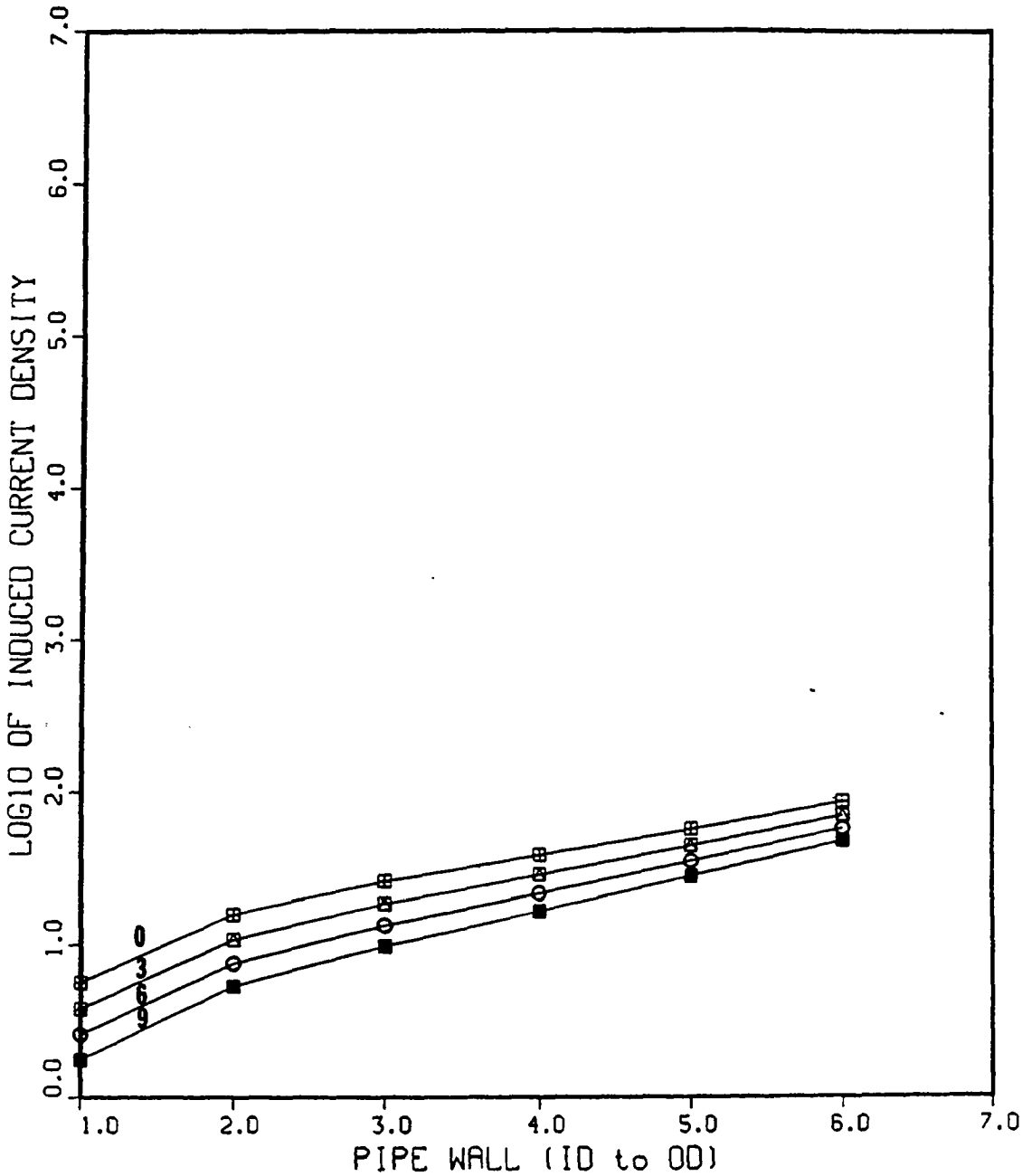

Figure 5.22. Log scaled RMS induced current densities at 3 diameters ahead of the exciter coil; (V = 0, 3, 6, and 9 m/sec)

CHAPTER VI
NON-UNIFORM NDE GEOMETRIES

When a moving electromagnetic probe passes a non-uniform geometry, the distribution of motionally induced currents is different at each probe position, thus at each time. This leads to a transient situation if DC or low frequency AC is used for excitation, as in the case of electromagnetic NDE. Unlike the turn-on/off transients, there is no steady state in this situation because the transient condition occurs only during the short traversal time of the probe passing the non-uniform geometry such as a defect or a support plate. Because of this truly transient nature of the moving inspection problem, sinusoidal AC steady state based eddy current methods of NDE are not suitable for high speed moving probe inspection and the probe velocity should be restricted to such a low speed as for motional induction currents to be ignored. Although eddy current testing equipment, such as the eddyscope, shows some signals even in fast moving probe inspection, they do not provide accurate information about the defect because impedance plane trajectories themselves cannot be defined in the transient situation. To model such testing equipment signals, an additional modeling for the equipment itself is thus required. Because of this reason, this dissertation restricts its attention to the magnetic flux leakage method of NDE and the variable reluctance probe.

The transient analyses in this situation are not often found in electromagnetics. Although the upwinding technique has been used with

time step methods [71,79], as we have seen in Chapter V, it shows some numerical dissipation even in steady state problems. Thus, if this technique is used with time step methods, it would produce too much error due to the accumulation of such numerical dissipation at each time step. Therefore, the analysis is concentrated on the transient problem itself, and successful time step algorithms are adapted from a study of the convective-diffusion equation in fluid mechanics. In this chapter, three such time step methods are studied to find out whether they can be used in our moving probe problem. They are Donea's method [142,143], Zienkiewicz's method [140,144,145], and Leismann and Frind's method [146]. For convenience, the 1-dimensional governing equation is used for the explanation of these methods. The results obtained by applying Donea's method and Leismann and Frind's method are shown and compared. The results show that Leismann and Frind's method is more suitable for our moving probe inspection problem.

In the transient analysis explained in Chapter III, spatial discretization is performed first and temporal discretization later. This is the traditional way of solving transient problems in the finite element method. However, the three methods described in this section consider temporal discretization first and then spatial discretization is performed by using the standard (Galerkin) finite element method. This is because the time dependent artificial term is found during the temporal discretization and this allows us to use the standard Galerkin method the same way as we have seen in the upwinding technique. Therefore, for simplicity, the explanation is restricted to temporal discretization.

A. Various Time Step Methods

1. Donea's Method

The 1-D version of the governing equation can be found from equation (4.58) by ignoring the r-component related term. Writing it in a different form,

$$\sigma\frac{\partial A}{\partial t}=\frac{1}{\mu}\frac{\partial^2 A}{\partial z^2}-\sigma V\frac{\partial A}{\partial z}+J_s \tag{6.1}$$

Now, consider the forward Taylor series expansion shown in equation (3.106), including up to the second order time derivative. Rewriting this equation by multiplying σ,

$$\sigma A^{n+1}=\sigma A^n+\Delta t\sigma\frac{\partial A^n}{\partial t}+\frac{\Delta t^2}{2}\sigma\frac{\partial^2 A^n}{\partial t^2} \tag{6.2}$$

Since the forward difference method is used, equation (6.1) needs to be evaluated at the old time level. Then, we can write

$$\sigma\frac{\partial A^n}{\partial t}=\frac{1}{\mu}\frac{\partial^2 A^n}{\partial z^2}-\sigma V\frac{\partial A^n}{\partial z}+J_s \tag{6.3}$$

and,

$$\sigma\frac{\partial^2 A^n}{\partial t^2}=\frac{\partial}{\partial t}\left(\sigma\frac{\partial A^n}{\partial t}\right)=\frac{\partial}{\partial t}\left(\frac{1}{\mu}\frac{\partial^2 A^n}{\partial z^2}-\sigma V\frac{\partial A^n}{\partial z}+J_s\right) \tag{6.4}$$

where J_s is the DC, constant, source current density so that $J_s^n = J_s^{n+1}$, thus it is written without time superscript. Since the order of the time derivative and the spatial derivative can be changed, equation (6.4) becomes

$$\sigma\frac{\partial^2 A^n}{\partial t^2} = \frac{1}{\mu}\frac{\partial^2}{\partial z^2}\frac{\partial A^n}{\partial t} - V\frac{\partial}{\partial z}\sigma\frac{\partial A^n}{\partial t} \tag{6.5}$$

Note here that the derivative of current density, which is constant, is zero. Now, approximating the time derivative term as

$$\frac{\partial A^n}{\partial t} = \frac{A^{n+1} - A^n}{\Delta t} \tag{6.6}$$

and leave equation (6.5) in its mixed spatial-temporal form, we have

$$\sigma\frac{\partial^2 A^n}{\partial t^2} = \frac{1}{\mu}\frac{\partial^2}{\partial z^2}\left(\frac{A^{n+1} - A^n}{\Delta t}\right) - \sigma V\frac{\partial}{\partial z}\left(\frac{A^{n+1} - A^n}{\Delta t}\right) \tag{6.7}$$

Substituting equations (6.3) and (6.7) into equation (6.2) gives

$$\left[\frac{\sigma}{\Delta t} - \frac{1}{2\mu}\frac{\partial^2}{\partial z^2} + \frac{\sigma V}{2}\frac{\partial}{\partial z}\right]A^{n+1} = J_s + \left[\frac{\sigma}{\Delta t} + \frac{1}{2\mu}\frac{\partial^2}{\partial z^2} - \frac{\sigma V}{2}\frac{\partial}{\partial z}\right]A^n \tag{6.8}$$

This is Donea's original work [143].

However, the interpretation of this work by Zienkiewicz [144,145] is slightly different. Replacing the first time derivative on the right hand side of equation (6.5) by using equation (6.2) and the second time derivative by using equation (6.3),

$$\sigma\frac{\partial^2 A^n}{\partial t^2} = \frac{1}{\mu}\frac{\partial^2}{\partial z^2}\left(\frac{A^{n+1} - A^n}{\Delta t}\right) + \sigma V^2\frac{\partial^2 A^n}{\partial z^2} - \frac{V}{\mu}\frac{\partial^3 A^n}{\partial z^3} - \frac{\Delta t}{2\mu}\frac{\partial^2}{\partial z^2}\frac{\partial^2 A^n}{\partial t^2} \tag{6.9}$$

Ignoring higher order terms, i.e., third and fourth terms on the right hand side, gives

$$\sigma\frac{\partial^2 A^n}{\partial t^2}=\frac{1}{\mu}\frac{\partial^2}{\partial z^2}\left(\frac{A^{n+1}-A^n}{\Delta t}\right)+\sigma V^2\frac{\partial^2 A^n}{\partial z^2} \tag{6.10}$$

Substituting equations (6.3) and (6.10) into equation (6.2) gives

$$\sigma\frac{A^{n+1}-A^n}{\Delta t}=\frac{1}{\mu}\frac{\partial^2 A^n}{\partial z^2}-\sigma V\frac{\partial A^n}{\partial z}+J_s+\frac{1}{2\mu}\frac{\partial^2}{\partial z^2}\left(A^{n+1}-A^n\right)+\frac{\Delta t}{2}\sigma V^2\frac{\partial^2 A^n}{\partial z^2} \tag{6.11}$$

Rearranging equation (6.11),

$$\left[\frac{\sigma}{\Delta t}-\frac{1}{2\mu}\frac{\partial^2}{\partial z^2}\right]A^{n+1}=J_s+\left[\frac{\sigma}{\Delta t}+\frac{1}{2\mu}\frac{\partial^2}{\partial z^2}+\frac{\Delta t}{2}\sigma V^2\frac{\partial^2}{\partial z^2}-\sigma V\frac{\partial}{\partial z}\right]A^n \tag{6.12}$$

This is Zienkiewicz's interpretation of Donea's work. This equation is compared with that of Zienkiewicz's method.

2. Zienkiewicz's Method

Consider equation (6.1). If this equation is written in the moving coordinate system, the convective derivative discussed in Chapter IV can be used and therefore, the velocity term disappears.

$$\sigma\left.\frac{DA}{Dt}\right|_{\xi}=\frac{1}{\mu}\frac{\partial^2 A}{\partial z^2}+J_s \tag{6.13}$$

where ξ , the moving coordinate, is constant for any moving body. This equation is self-adjoint in the spatial coordinate and thus the standard Galerkin finite element method can be used. We could use this equation directly, but this would necessitate the continuous use of updated meshes which has many practical inconveniences. As we wish to retain a fixed spatial mesh, the time domain is first discretized. Introducing the general θ method for the time domain approximation into equation (6.13), we can write

$$\sigma\left[A\left(\xi,t^{n+1}\right)-A\left(\xi,t^{n}\right)\right]=\theta\Delta t\left\{\frac{1}{\mu}\frac{\partial^2 A\left(\xi,t^{n+1}\right)}{\partial z^2}+J_s\right\}$$

$$+(1-\theta)\Delta t\left\{\frac{1}{\mu}\frac{\partial^2 A\left(\xi,t^{n}\right)}{\partial z^2}+J_s\right\} \qquad (6.14)$$

Since the current density is constant, it is written without time level indication. Now, consider the characteristic curve shown in Figure 6.1.

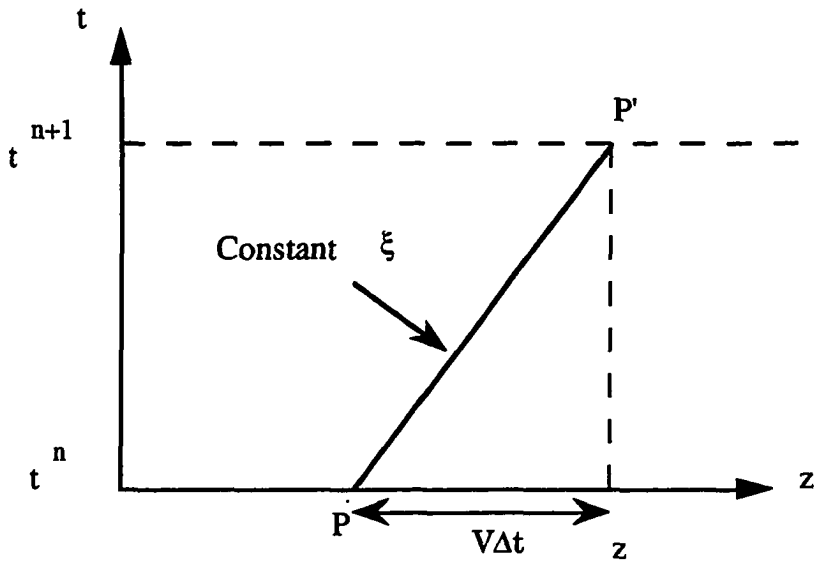

Figure 6.1. Relation between moving and fixed coordinate

Since the constant probe velocity is considered, the characteristic curve is a straight line. However, Zienkiewicz's method is based on the general variable velocity so that a local Taylor expansion is used to find $A(\xi, t^n)$ at point P from the value at point P'. The benefit of using a Taylor expansion is that mesh movement or updating can be avoided. This can be shown as follows. It is assumed that at time t^{n+1} the moving and fixed coordinates coincide at point P'. Now, define

$$A^{n+1} \equiv A\left(z, t^{n+1}\right) \tag{6.15}$$

and using a local Taylor expansion, evaluate A^n at point P in order to insert it into equation (6.14). That is,

$$\begin{aligned} A\left(\xi, t^n\right) &= A\left(z - V\Delta t, t^n\right) \\ &= A\left(z, t^n\right) - V\Delta t \frac{\partial A\left(z, t^n\right)}{\partial z} + \frac{V^2\Delta t^2}{2}\frac{\partial^2 A\left(z, t^n\right)}{\partial z^2} + \vartheta\left(V^3\Delta t^3\right) \\ &= A^n - V\Delta t \frac{\partial A^n}{\partial z} + \frac{V^2\Delta t^2}{2}\frac{\partial^2 A^n}{\partial z^2} + \vartheta\left(V^3\Delta t^3\right) \end{aligned} \tag{6.16}$$

Inserting this into equation (6.14) and ignoring the higher order terms, gives

$$\sigma\frac{A^{n+1} - A^n}{\Delta t} = J_s - \sigma V\frac{\partial A^n}{\partial z} + \frac{\sigma V^2\Delta t}{2}\frac{\partial^2 A^n}{\partial z^2} + \theta\left\{\frac{1}{\mu}\frac{\partial^2 A^{n+1}}{\partial z^2}\right\} + (1-\theta)\left\{\frac{1}{\mu}\frac{\partial^2 A^n}{\partial z^2}\right\} \tag{6.17}$$

Rearranging equation (6.17), we get

$$\left[\frac{\sigma}{\Delta t} - \theta\frac{1}{\mu}\frac{\partial^2}{\partial z^2}\right]A^{n+1} = J_s + \left[\frac{\sigma}{\Delta t} + (1-\theta)\frac{1}{\mu}\frac{\partial^2}{\partial z^2} + \frac{\sigma V^2\Delta t}{2}\frac{\partial^2}{\partial z^2} - \sigma V\frac{\partial}{\partial z}\right]A^n \tag{6.18}$$

The spatial discretization using the standard finite element method is then applied to this equation. Because of the general θ time step, this approach is more versatile than other methods.

3. Leismann and Frind's Method

In this method, an arbitrary artificial term is introduced *a priori* and separate, unknown time weighting factors are used for individual terms in the governing equation. The unknown artificial term and time weighting factors are decided during the process of minimizing the errors.

Consider equation (6.1). Introducing the artificial term (ν*) and using separate time weighting factors, we have

$$\sigma\frac{A^{n+1}-A^n}{\Delta t}=\theta_d\frac{1}{\mu}\frac{\partial^2 A^{n+1}}{\partial z^2}+(1-\theta_d)\frac{1}{\mu}\frac{\partial^2 A^n}{\partial z^2}-\theta_v\sigma V\frac{\partial A^{n+1}}{\partial z}-(1-\theta_v)\sigma V\frac{\partial A^n}{\partial z}$$

$$+\theta_a\nu^*\frac{\partial^2 A^{n+1}}{\partial z^2}+(1-\theta_a)\nu^*\frac{\partial^2 A^n}{\partial z^2}+J_s \qquad (6.19)$$

Now, apply a Taylor series expansion. For the second order accuracy, the origin of the Taylor expansion is chosen to be the midpoint $t_n+\Delta t/2$. Rewriting equations (3.107) and (3.108),

$$A^{n+1}=A\left[\left(t_n+\frac{\Delta t}{2}\right)+\frac{\Delta t}{2}\right]=A\left(t_n+\frac{\Delta t}{2}\right)+\frac{\Delta t}{2}\frac{\partial A\left(t_n+\frac{\Delta t}{2}\right)}{\partial t}+\frac{\Delta t^2}{8}\frac{\partial^2 A\left(t_n+\frac{\Delta t}{2}\right)}{\partial t^2}+\vartheta\left(\Delta t^3\right) \qquad (3.107)$$

$$A^{n}=A\left[\left(t_n+\frac{\Delta t}{2}\right)-\frac{\Delta t}{2}\right]=A\left(t_n+\frac{\Delta t}{2}\right)-\frac{\Delta t}{2}\frac{\partial A\left(t_n+\frac{\Delta t}{2}\right)}{\partial t}+\frac{\Delta t^2}{8}\frac{\partial^2 A\left(t_n+\frac{\Delta t}{2}\right)}{\partial t^2}+\vartheta\left(\Delta t^3\right) \qquad (3.108)$$

Now, substitute these two equations to equation (6.19). The term on the left hand side becomes

$$\sigma\frac{A^{n+1}-A^n}{\Delta t}=\sigma\frac{\partial A}{\partial t}+\vartheta\left(\Delta t^3\right) \tag{6.20}$$

where A = A(t_n + $\Delta t/2$). The two terms corresponding to the second order spatial derivative term become

$$\theta_d\frac{1}{\mu}\frac{\partial^2 A^{n+1}}{\partial z^2}+(1-\theta_d)\frac{1}{\mu}\frac{\partial^2 A^n}{\partial z^2}=\frac{1}{\mu}\frac{\partial^2 A}{\partial z^2}+(\theta_d-\frac{1}{2})\Delta t\frac{1}{\mu}\frac{\partial^2}{\partial z^2}\frac{\partial A}{\partial t}+\vartheta(\Delta t^2) \tag{6.21}$$

and those for the velocity term,

$$-\theta_v\sigma V\frac{\partial A^{n+1}}{\partial z}-(1-\theta_v)\sigma V\frac{\partial A^n}{\partial z}=(\frac{1}{2}-\theta_v)\sigma V\Delta t\frac{\partial}{\partial z}\frac{\partial A}{\partial t}-\sigma V\frac{\partial}{\partial z}A+\vartheta\left(\Delta t^2\right) \tag{6.22}$$

and those for the artificial term,

$$\theta_a\nu^*\frac{\partial^2 A^{n+1}}{\partial z^2}+(1-\theta_a)\nu^*\frac{\partial^2 A^n}{\partial z^2}=\nu^*\frac{\partial^2}{\partial z^2}A+(\theta_a-\frac{1}{2})\nu^*\Delta t\frac{\partial^2}{\partial z^2}\frac{\partial A}{\partial t}+\vartheta(\Delta t^2) \tag{6.23}$$

Substituting equations (6.20) ~ (6.23) into equation (6.19) gives

$$\begin{aligned}\sigma\frac{\partial A}{\partial t}=&\frac{1}{\mu}\frac{\partial^2 A}{\partial z^2}-\sigma V\frac{\partial}{\partial z}A+J_s\\&+(\theta_d-\frac{1}{2})\Delta t\frac{1}{\mu}\frac{\partial^2}{\partial z^2}\frac{\partial A}{\partial t}+(\frac{1}{2}-\theta_v)\sigma V\Delta t\frac{\partial}{\partial z}\frac{\partial A}{\partial t}\\&+\nu^*\frac{\partial^2}{\partial z^2}A+(\theta_a-\frac{1}{2})\nu^*\Delta t\frac{\partial^2}{\partial z^2}\frac{\partial A}{\partial t}+\vartheta\left(\Delta t^2\right)\end{aligned} \tag{6.24}$$

Note that the first row of equation (6.24) is exactly the same as the governing equation (6.1). Therefore, the rest of equation (6.24) is the error. In order to achieve second order accuracy, these terms have to be made zero.

The original purpose was to set up a symmetric coefficient matrix. This can be done by evaluating the velocity term at the old time level because only the velocity term produces a non-symmetric matrix and therefore, this term must not be in the coefficient of A^{n+1}. The next subsection discusses this further. As explained in Chapter IV, however, the reasoning of this dissertation for evaluating the motional induction term at the old time level, is different and is based on the observation of motional induction phenomena. Therefore, θ_v must be zero.

Rewriting error terms by using equation (6.1) and neglecting the fourth order derivative term, we get

$$(1-\theta_d-\theta_v)V\Delta t\frac{1}{\mu}\frac{\partial^3 A}{\partial z^3}+\left\{\nu^*-(\frac{1}{2}-\theta_v)\sigma V^2\Delta t\right\}\frac{\partial^2 A}{\partial z^2}+(\theta_a-\frac{1}{2})\nu^*\Delta t\frac{\partial^2}{\partial z^2}\frac{\partial A}{\partial t} \quad (6.25)$$

In this process, a division by σ has to be used so that for consistency, the conductivities should not be zero even in air. This is not a serious problem since a small value, such as 1, can be used and is negligible compared to the usual magnetic material conductivity of $10^6 \sim 10^7$. For equation (6.25) to disappear, each coefficient must be zero. But since θ_v needs to be zero from the earlier discussion, we can decide on θ_d and ν^*. That is

$$\theta_d = 1\,, \quad \nu^* = \frac{\sigma V^2\Delta t}{2} \quad (6.26)$$

Note that the artificial term just obtained can also be found in equations (6.12) and (6.18). The yet unknown value of θ_a is to be decided by stability analysis. For a Courant number of 1, the standard von Neumann stability analysis shows that stability can be achieved if $\theta_a \geq 1/3$ [53], and unlimited stability is guaranteed when $\theta_a \geq 1/2$ [146]. Finally, substituting these values into equation (6.19), we have

$$\left[\frac{\sigma}{\Delta t} - \frac{1}{\mu}\frac{\partial^2}{\partial z^2} - \theta_a \frac{\sigma V^2 \Delta t}{2}\frac{\partial^2}{\partial z^2}\right] A^{n+1} = J_s + \left[\frac{\sigma}{\Delta t} + (1-\theta_a)\frac{\sigma V^2 \Delta t}{2}\frac{\partial^2}{\partial z^2} - \sigma V \frac{\partial}{\partial z}\right] A^n \quad (6.27)$$

4. Comparison of Three Methods

If we compare the final equations of these three methods, we may be able to extract some valuable information. Table 6.1 compares these equations. First, consider equations (6.12) and (6.18). These are exactly the same if θ in equation (6.18) is 1/2. In the next subsection, various aspects of these equations are examined.

The symmetry of the coefficient matrix

As noted in Chapter IV and V, the second order spatial derivative term and time derivative term (in these cases, $1/\Delta t$, since it is separated into the left and right hand sides) always produce symmetric matrices, but the velocity term gives a non-symmetric matrix. Therefore, the coefficient in equations (6.12), (6.18), and (6.27) would produce a symmetric matrix, while that in equation (6.8) would produce a non-symmetric matrix. In steady state problems, we have noticed that the asymmetry of the stiffness matrix due to

Table 6.1. Comparison of final equations

Donea :

$$\left[\frac{\sigma}{\Delta t}-\frac{1}{2\mu}\frac{\partial^2}{\partial z^2}+\frac{\sigma V}{2}\frac{\partial}{\partial z}\right]A^{n+1}=J_s+\left[\frac{\sigma}{\Delta t}+\frac{1}{2\mu}\frac{\partial^2}{\partial z^2}-\frac{\sigma V}{2}\frac{\partial}{\partial z}\right]A^{n} \tag{6.8}$$

Donea-Zienkiewicz :

$$\left[\frac{\sigma}{\Delta t}-\frac{1}{2\mu}\frac{\partial^2}{\partial z^2}\right]A^{n+1}=J_s+\left[\frac{\sigma}{\Delta t}+\frac{1}{2\mu}\frac{\partial^2}{\partial z^2}+\frac{\Delta t}{2}\sigma V^2\frac{\partial^2}{\partial z^2}-\sigma V\frac{\partial}{\partial z}\right]A^{n} \tag{6.12}$$

Zienkiewicz :

$$\left[\frac{\sigma}{\Delta t}-\theta\frac{1}{\mu}\frac{\partial^2}{\partial z^2}\right]A^{n+1}=J_s+\left[\frac{\sigma}{\Delta t}+(1-\theta)\frac{1}{\mu}\frac{\partial^2}{\partial z^2}+\frac{\sigma V^2\Delta t}{2}\frac{\partial^2}{\partial z^2}-\sigma V\frac{\partial}{\partial z}\right]A^{n} \tag{6.18}$$

Leismann and Frind :

$$\left[\frac{\sigma}{\Delta t}-\frac{1}{\mu}\frac{\partial^2}{\partial z^2}-\theta_a\frac{\sigma V^2\Delta t}{2}\frac{\partial^2}{\partial z^2}\right]A^{n+1}=J_s+\left[\frac{\sigma}{\Delta t}+(1-\theta_a)\frac{\sigma V^2\Delta t}{2}\frac{\partial^2}{\partial z^2}-\sigma V\frac{\partial}{\partial z}\right]A^{n} \tag{6.27}$$

the velocity term causes spurious oscillations. Therefore, we may predict that Donea's original method, represented by equation (6.8), will produce such oscillations, too.

Artificial term

Note that the term $\frac{\sigma V^2\Delta t}{2}$ is present in equations (6.12), (6.18), and (6.27). However, equation (6.8) does not include this term. Also, if we investigate all the terms on the right and left hand sides ignoring the time levels, all

equations are well matched, but equation (6.8) is short of this term. In fact, this is the artificial term which corresponds to the artificial reluctivity found in the upwinding technique. However, it is now time dependent. Equating the two artificial terms gives

$$\frac{\sigma V^2 \Delta t}{2} = \frac{\alpha \sigma V h}{2} \Leftrightarrow \alpha = \frac{V \Delta t}{h} = C \tag{6.28}$$

where C is the grid Courant number as mentioned in Chapter IV. It should be noted that the grid Courant number should be 1 in the moving probe problem since the probe has to be relocated at each time step. Therefore, the probe should not move more than one element length during one time step. In relation to the upwinding technique, this means that we are using $\alpha = 1$, which corresponds to the finite element full upwinding, and the finite difference upwind scheme. In the upwinding technique, the artificial reluctivity term plays an important role of suppressing spurious oscillations. In a parallel sense, then, since equation (6.8) does not have the artificial term, spurious oscillatory results can be predicted. Also, since the artificial term is present, the standard finite element method can be used as we have seen in Chapter V.

Evaluation of motional induction term at the old time level

As was discussed in the time dependent interpretation of the motional induction term in Chapter IV, this velocity term (also equivalently, first order spatial derivative term) has to be evaluated at the old time level. In fact, this is related to the symmetry of the coefficient matrix. Since the velocity term always produces a non-symmetric matrix, it has to be evaluated at the old

time level to achieve a symmetric coefficient matrix. This idea of evaluating at the old time level is also supported by the concept of upwinding techniques and by a moving coordinate system analysis as mentioned in Chapter IV. Zienkiewicz's method also corresponds to the moving coordinate system analysis. Equations (6.12), (6.18), and (6.27) evaluate the motional induction term at the old time level. However, in equation (6.8), it is separated into the present and old time levels.

All of the comparisons predict that equation (6.8) would produce spurious oscillations. This has actually happened in the moving probe simulation. This result and that of Leismann and Frind's method are shown in the next section.

B. Results of Transient Analyses Applied to Non-Uniform Geometry

Numerical experiments are performed for two cases. First, to validate the time step algorithm, steady state results obtained by using a uniform geometry are compared with upwinding results. After validating the time step method, it is applied to a non-uniform geometry to obtain an output NDE signal.

In the first experiment, the steady state, magnetostatic solution is used for the initial condition to remove turn-on transient effects and the time step calculation is continued until steady state is reached. In the second experiment, a support plate is included as a non-uniform geometry. This situation is shown in Figure 1.6. Initial conditions are obtained from the

steady state result of a moving probe without a support plate, thus using the results of the former analysis. The sensing Hall plate is located at the innermost side of the leading edge of the variable reluctance probe since this location is found to be the optimal position of the sensor as we have seen in Figure 5.9.

Figure 6.2 shows the results obtained by applying Donea's time step method. Results from both Dirichlet boundary conditions and Neumann boundary conditions are shown. Compare these results with Figure 4.4 and Figure 4.5. Although there is an improvement in the front edge of the probe, these results show spurious oscillations. Figure 6.3 compares the result from Donea's method using Neumann boundary conditions with the standard Galerkin result and the upwinding result. The result is better than that of the standard Galerkin, but not as good as the upwinding result. In both figures, probe velocity is 100 m/sec and the element length used is 1.59 mm. The relative constant permeability and conductivity of the tube are 100 and 0.6×10^7 mho/meter, respectively. The resulting cell magnetic Reynolds number is 119.88.

Another oscillatory result from Donea's method is shown in Figure 6.4. In this case, $\mu_r = 100$, $\sigma = 2 \times 10^7$ mho/meter, V = 5 m/sec, and the element length is 4.76 mm ($R_m = 59.8$). The result exactly reproduces the standard Galerkin result. Since these two results are exactly superimposed, compare with Figure 5.7. From these results, the predictions on Donea's time step method are proven.

On the other hand, the results from Leismann and Frind's method exactly reproduce upwinding results. This is shown in Figure 6.5. If we

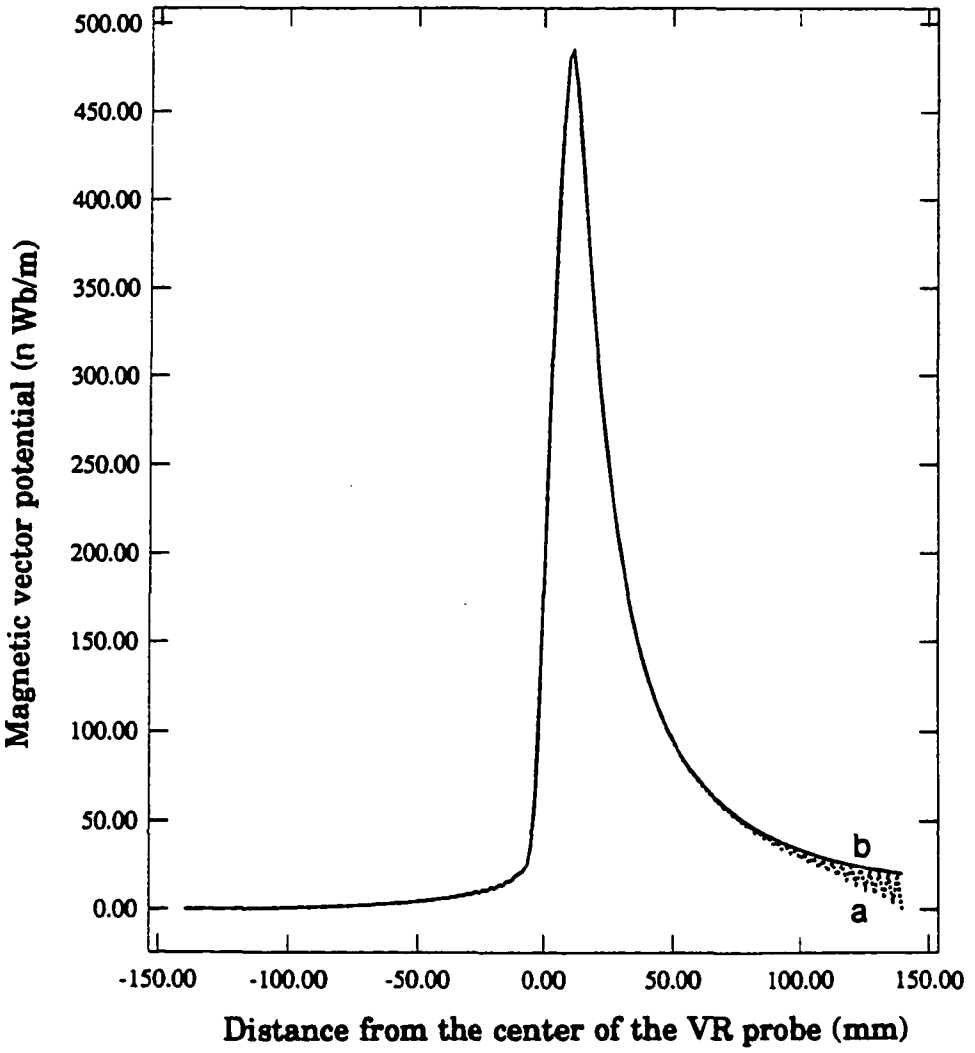

Figure 6.2. Results obtained from Donea's method;
a) Dirichlet B.C., b) Neumann B.C.

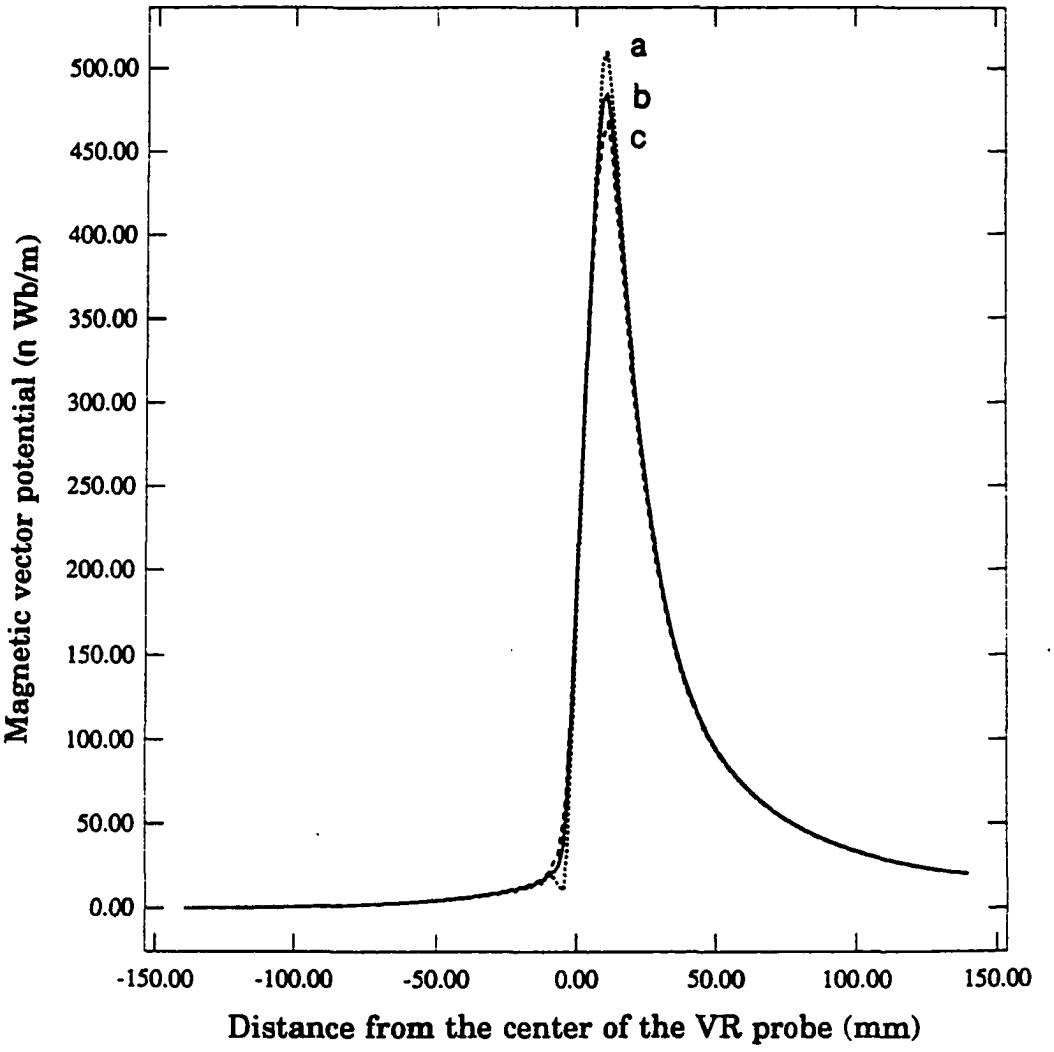

Figure 6.3. Comparison of results (R_m = 119.88);
a) standard Galerkin result,
b) result from Donea's method,
c) upwinding result

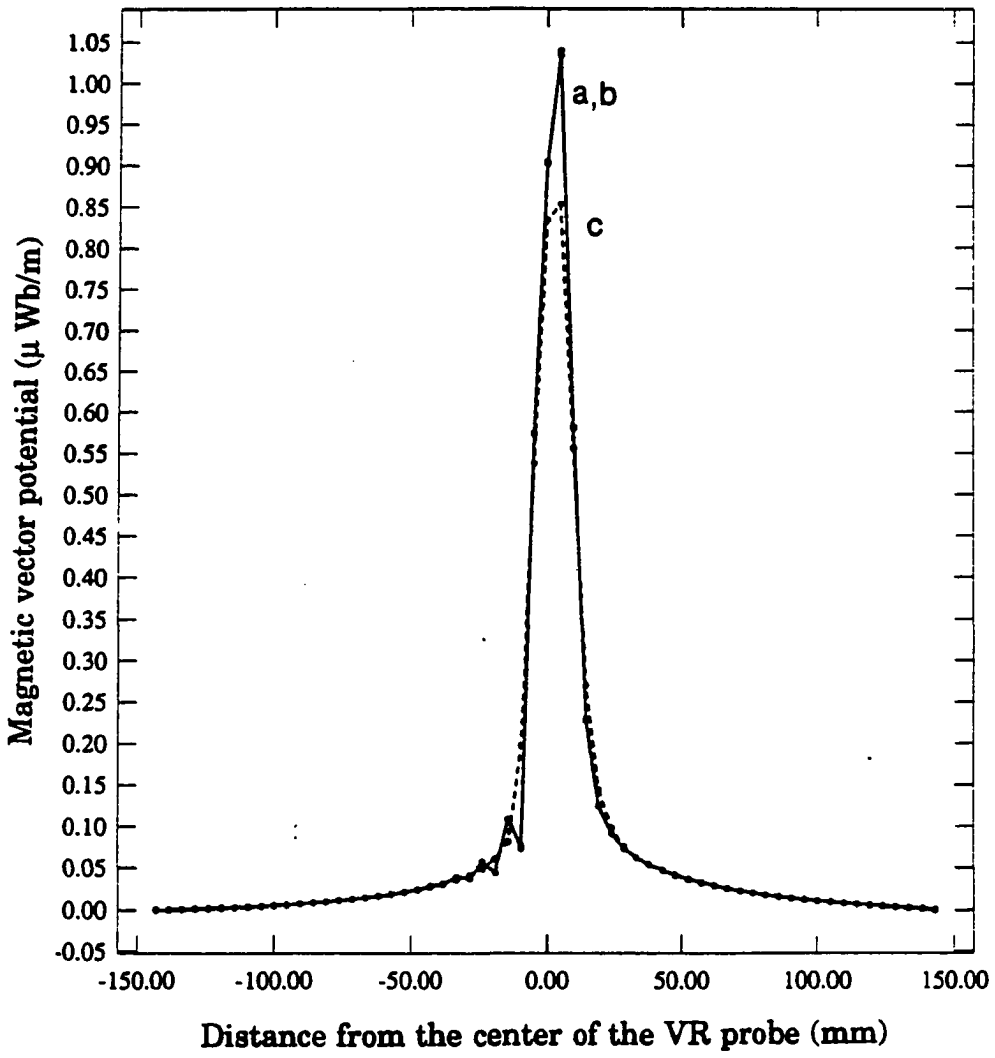

Figure 6.4. Comparison of results (R_m = 59.8);
a) standard Galerkin result,
b) result from Donea's method,
c) upwinding result

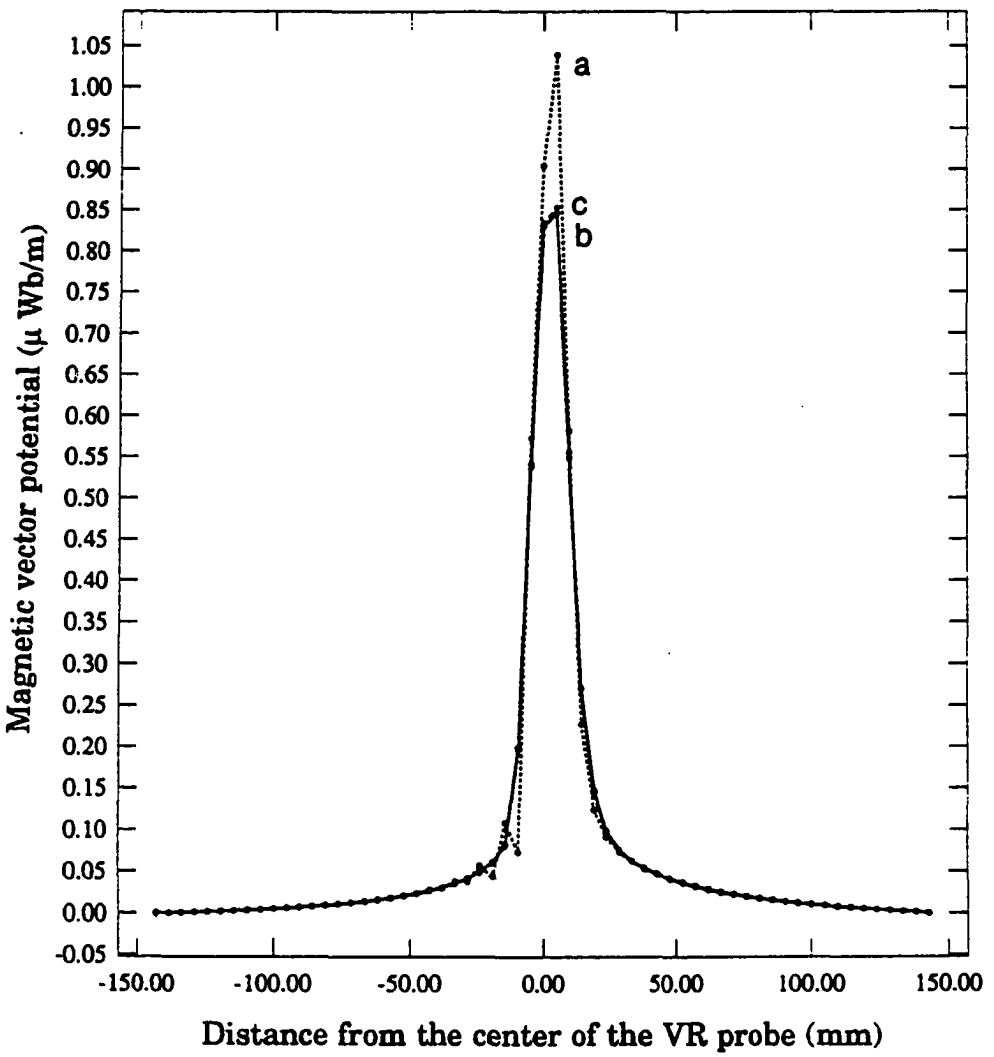

Figure 6.5. Comparison of results (R_m = 59.8);
a) standard Galerkin result,
b) result from Leismann and Frind's method,
c) upwinding result

compare Figure 6.5 with 6.4, the difference between the two time step methods can be clearly seen. The same tendency happens even in small R_m. This is shown in Figure 6.6 where R_m is 20. These results confirm the validity of Leismann and Frind's time step method.

Even though the results from Donea's method oscillate, this method is still applied to the non-uniform geometry case. In this case, the material properties of the tube used in the former steady state analysis are used as the support plate material properties. That is, $\mu_r = 100$, $\sigma = 2x10^7$ mho/meter, V = 5 m/sec, and the element length is 1.59 mm ($R_m = 20$). The results obtained from Donea's method and Leismann and Frind's method are compared in Figure 6.7. After the probe passes the support plate, the result from Donea's method starts oscillating. This can be seen more clearly in Figure 6.8 where the Hall plate signal is shown for an extended period. However, the results from Leismann and Frind's method do not show any oscillation. This result was unexpected because both methods reach steady state in the uniform geometry case. To find out the reason, the Hall plate signal is monitored to see how each method reaches steady state. For Donea's method, the outermost side of the leading edge of the probe (position number 13 in Figure 5.9) is chosen for monitoring the signal changes. For Leismann and Frind's method, the innermost side (position number 15 in Figure 5.9) is chosen. Figure 6.9 and 6.10 show the monitored results from Donea's method and Leismann and Find's method, respectively. These results show that Donea's method reaches steady state very slowly with dying out oscillations, while Leismann and Frind's method reaches steady state very quickly. These findings may explain the reason for the oscillation of Donea's method after

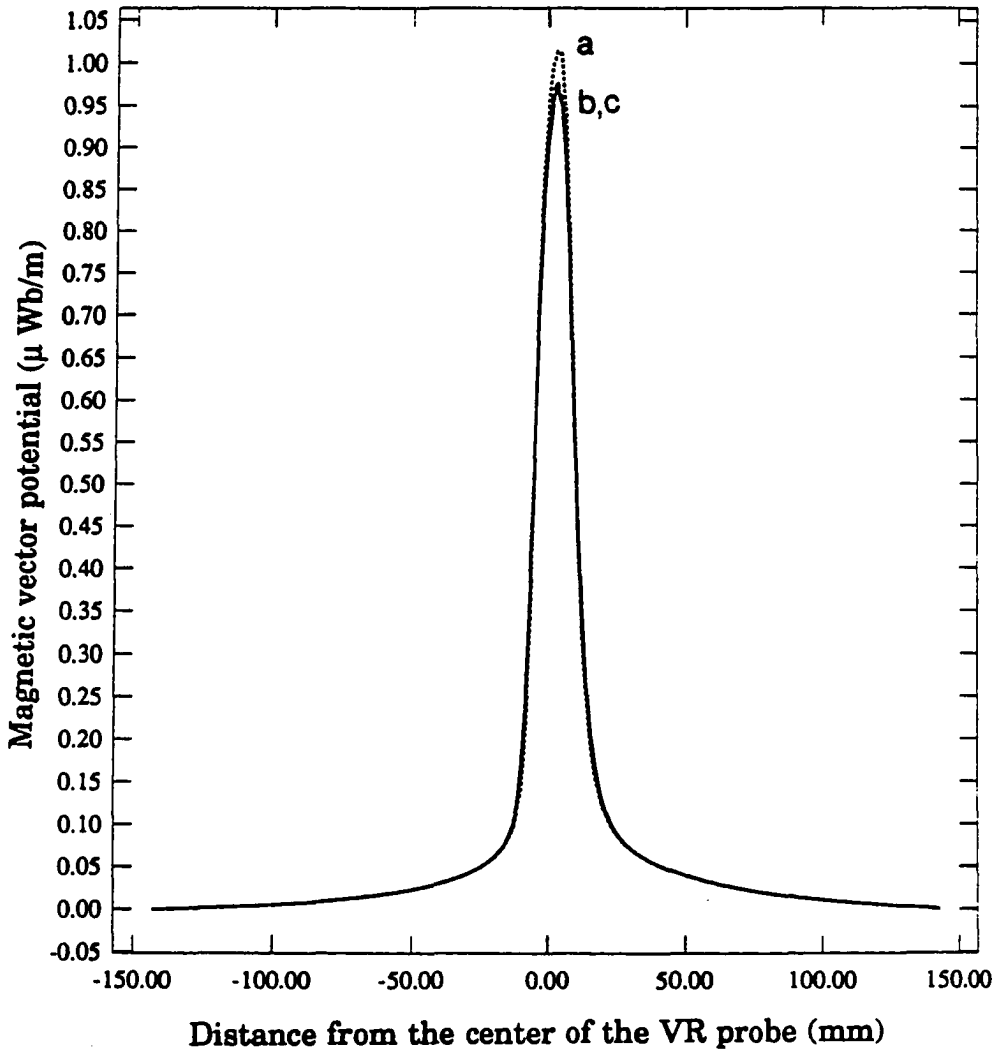

Figure 6.6. Comparison of results (R_m = 20);
a) standard Galerkin result,
b) result from Leismann and Frind's method,
c) upwinding result

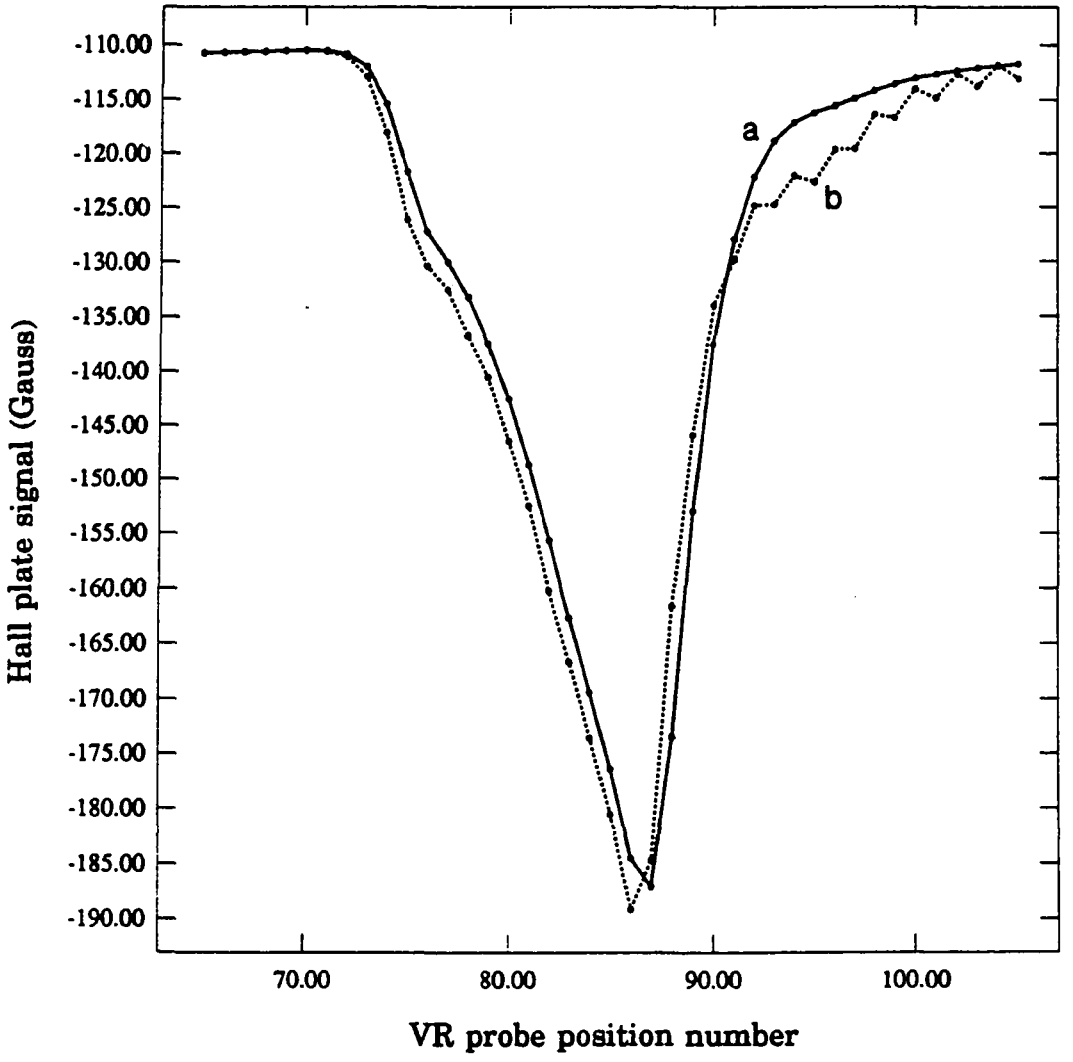

Figure 6.7. Comparison of Hall plate signals;
a) results from Leismann and Frind's method,
b) results from Donea's method

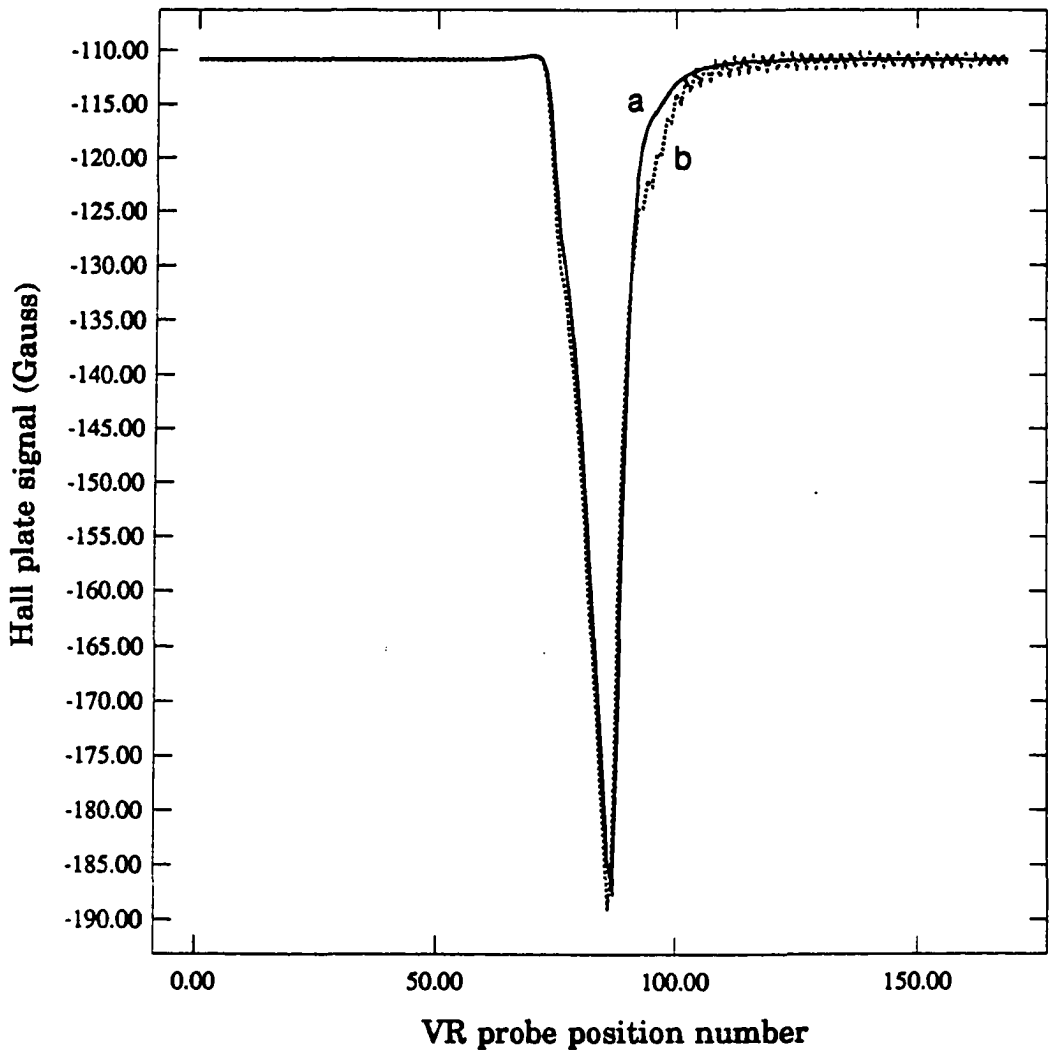

Figure 6.8. Comparison of Hall plate signals (extended period);
a) results from Leismann and Frind's method,
b) results from Donea's method

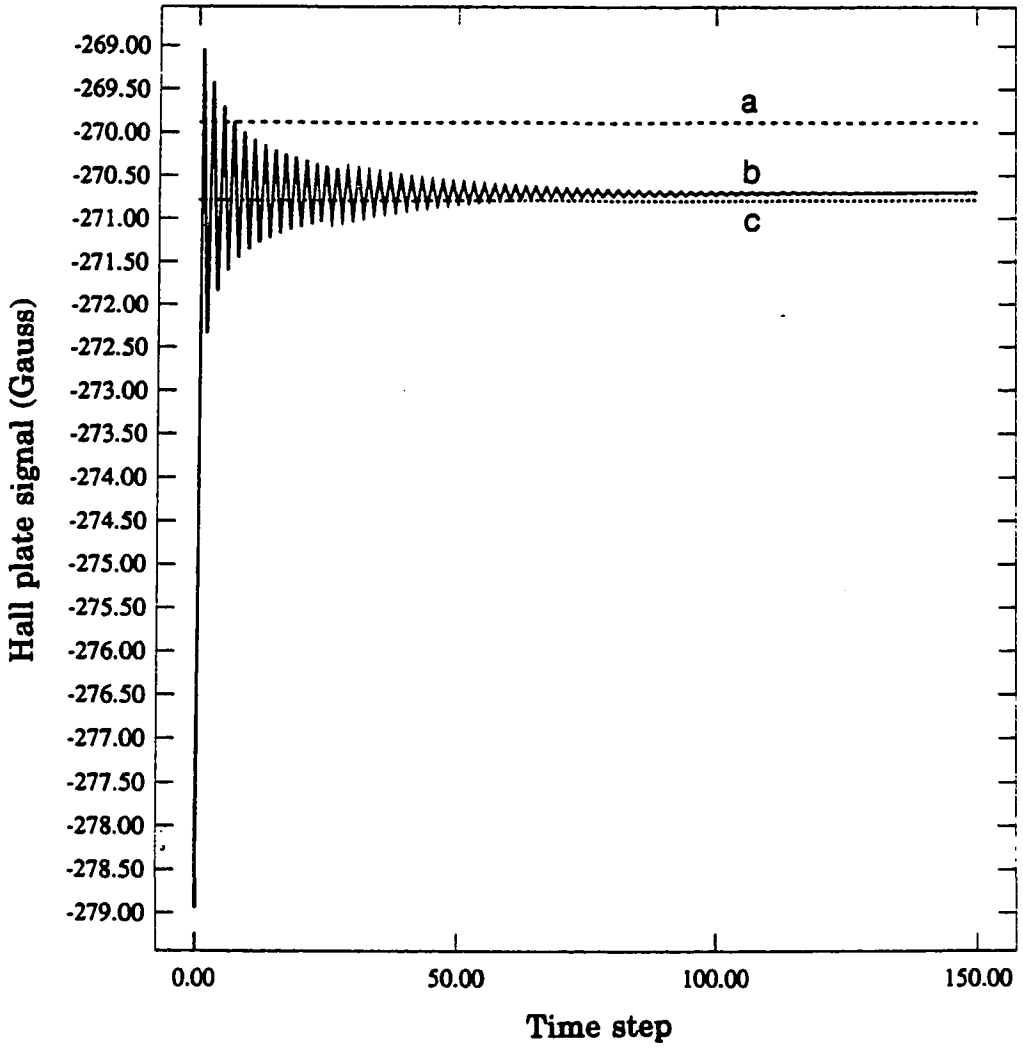

Figure 6.9. Convergence characteristic of Hall plate signal (Donea's method); a) upwinding result, b) results from Donea's method, c) standard Galerkin result

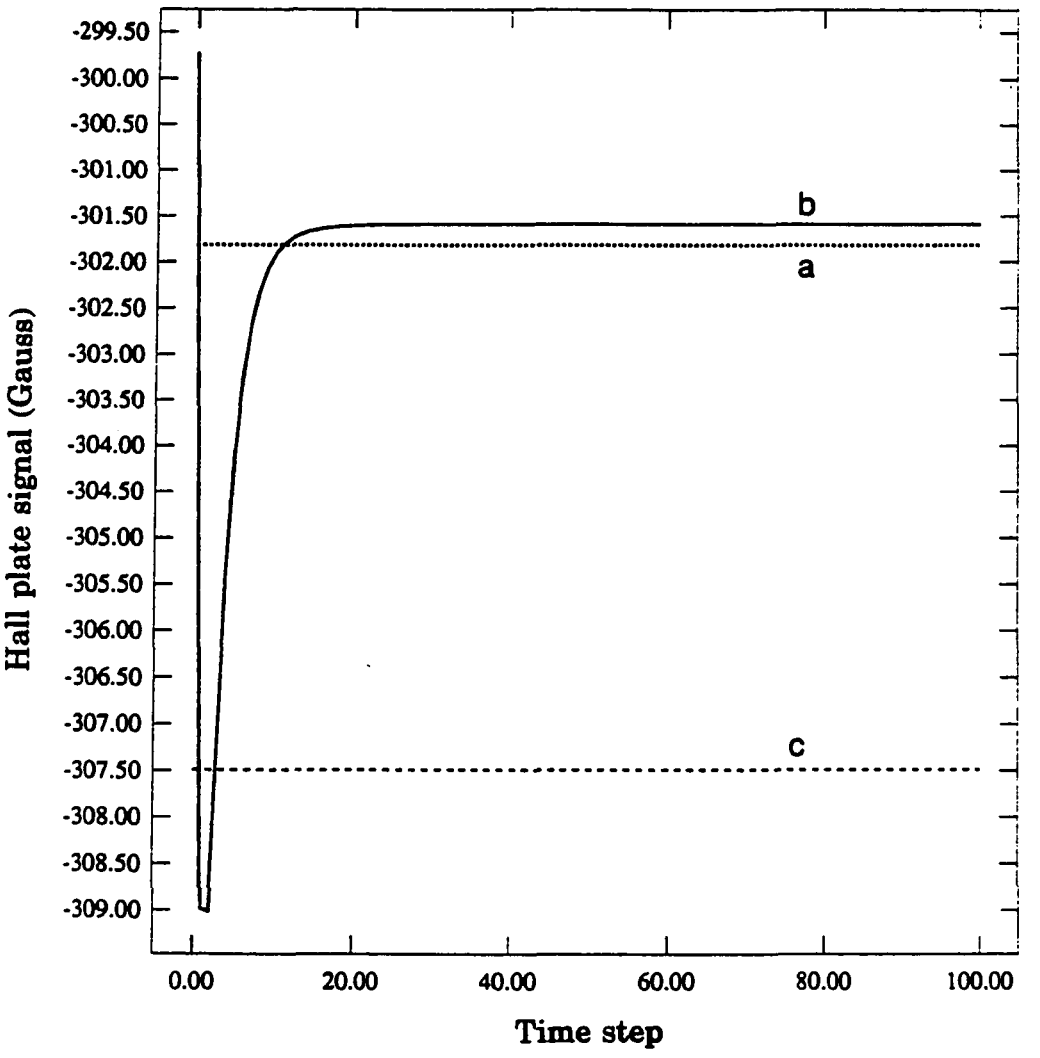

Figure 6.10. Convergence characteristic of Hall plate signal (Leismann and Frind's method);
a) upwinding result,
b) results from Leismann and Frind's method,
c) standard Galerkin result

passing the support plate. That is, in Donea's method, the transients caused by the support plate last long so that oscillations continue to exist, while in Leismann and Frind's method, the transients due to the support plate die out very quickly so that no oscillation occurs. These figures also show that the result from Donea's method converges to the standard Galerkin result and that from Leismann and Frind's method converges to the upwinding result.

Figure 6.11 compares the Hall plate signal obtained from Leismann and Frind's method with the magnetostatic result obtained at every probe position. In this specific problem, the probe speed of 5 m/sec is not critical in interpreting the output NDE signal, but it shows that the signal strength is weakened if the probe speed is increased.

Finally, the changes of flux patterns are shown as the probe passes the support plate. For comparison, Figure 6.12 is included which shows the magnetostatic result (V = 0) obtained at each probe position. Figure 6.13 shows the results when the probe velocity is 5 m/sec. In Figure 6.13, a skin effect on the surface of the ferromagnetic support plate is clearly seen. Since the excitation is DC, this skin effect has to be explained by motional induction currents, and therefore, it strongly supports the validity of the results and Leismann and Frind's time step algorithm.

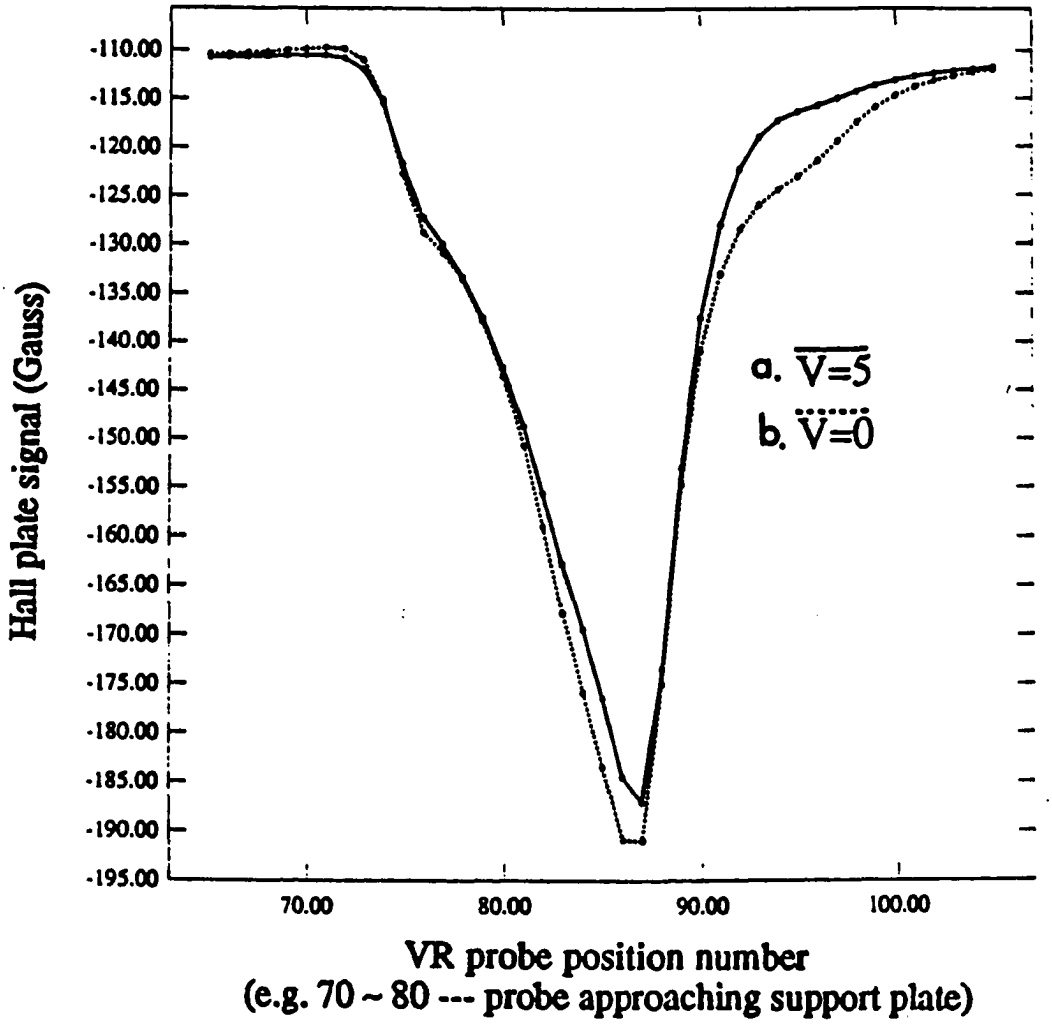

Figure 6.11. Comparison of Hall plate signals (Leismann and Frind's method); a) V = 5 m/sec, b) V = 0 m/sec

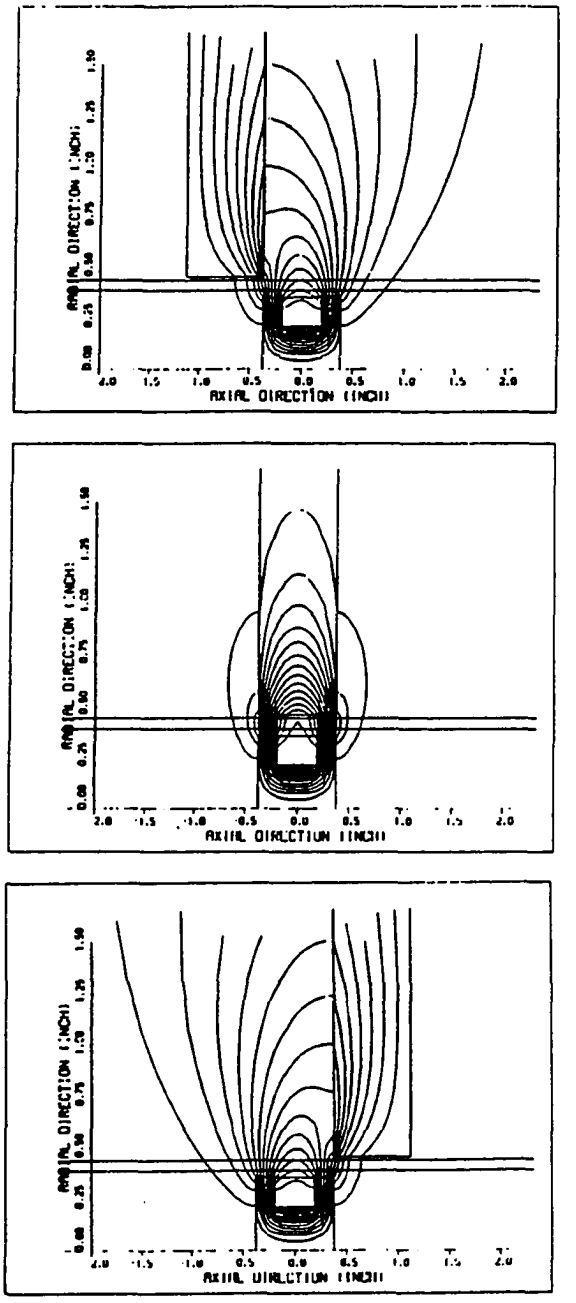

Figure 6.12. Flux plots at V = 0 m/sec (magnetostatic results)

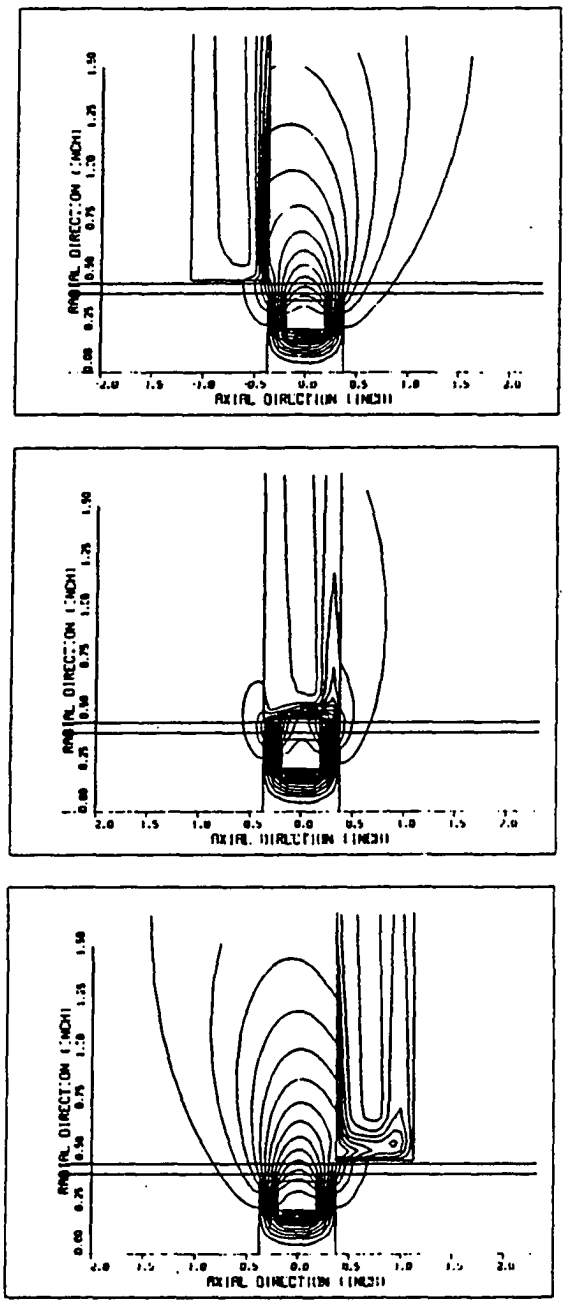

Figure 6.13. Flux plots at V = 5 m/sec (Leismann and Frind's method)

CHAPTER VII
CONCLUSION AND FUTURE WORK

The main objective of this dissertation is the finite element study of probe velocity effects for electromagnetic NDE. This chapter summarizes the work done in this dissertation and suggests areas of future work.

A. Summary and Conclusion

Magnetic flux leakage testing pigs used for the inspection of gas pipe lines are operated at a speed of 20 miles (33.3 Km) per an hour. At this speed, probe velocity effects are unavoidable and affect the output NDE signals. Numerical modeling of these effects has been very difficult because the governing equation is nonself-adjoint. Especially in NDE environments, the associated geometries are not uniform so that care should be taken in choosing the proper form of analysis. This dissertation has shown that probe velocity effects associated with non-uniform NDE geometries must be solved by a transient analysis.

Laboratory experiments for this high speed moving test situation are difficult to carry out. Under these circumstances, even if a theoretical solution is obtained, there is no way to prove the validity of the solution. For this reason, this dissertation starts with a uniform geometry and adopts a well established numerical technique, called upwinding, as a test bed. By

comparing the transient solutions at steady state with the upwinding results, the chosen transient analysis can be validated.

The upwinding technique was originally developed for steady state fluid flow problems and has been applied to electrical engineering problems such as electromagnetic levitation, electromagnetic launchers, and electromagnetic brakes. Although there exists a subtle difference between moving probe and fluid flow problems, the governing equations have the same form, known as the convective-diffusion equation in fluid mechanics. Unlike the most governing equations encountered in engineering problems, this equation includes a first order spatial derivative, which corresponds to the motional induction term in the case of moving electromagnetic probe problems. This term makes the governing equation nonself-adjoint and for this type of equation, standard numerical techniques based on the domain method suffer from spurious oscillations if the magnetic Reynolds number is larger than 2. This dissertation shows such oscillations caused by each component of the magnetic Reynolds number. Since the element size is the only component that can be freely chosen, heavy mesh discretization is required to avoid spurious oscillations. This causes practical difficulties in using computer resources and therefore, the upwinding technique is developed.

In this dissertation, this technique is applied to uniform geometries associated with the magnetic flux leakage, eddy current, and the remote field eddy current methods of NDE. For each method, representative probes are selected for axisymmetric numerical experiments. These are the variable reluctance, differential eddy current, and remote field eddy current probes

used in tube inspection. Although this technique cannot provide output NDE signals because of uniform geometries, it provides useful background knowledge when the relative motion is involved in the problem, such as the pattern of field distribution and the optimal position of the sensor. The results also show that the differential eddy current probe loses its benefits if it is used in high speed moving inspection.

Experiences with this technique also provide insights into motional induction phenomena. The technique's emphasis on the upwind condition supports the idea of evaluating the motional induction term at the old time level which is gained from the observation of motional induction phenomena. A nonlinear interpretation of motional induction phenomena in terms of velocity is also studied, but found that the solution converges to the upwinding result. The technique also provides information about the artificial reluctivity term whose existence is inevitable for oscillation free solutions. However, this artificial term causes numerical dissipation, so that the accuracy is lower than that of using extremely small elements. This inaccuracy is illustrated by using the magnetic potential values at the center line of the tube wall. Because of this numerical dissipation, if the upwinding technique were applied to time step recurrence calculations, large errors would build up.

To study probe velocity effects in a non-uniform geometry, therefore, the analysis has to be concentrated on the transient equation itself and a new time dependent artificial term needs to be found. For this purpose, three time step methods, originally developed in fluid dynamics, are studied and numerical experiments are performed to determine whether they can be applied to the moving probe problem. As a result, it is found that Leismann

and Frind's time step method that agrees with the findings from upwinding experiences, produces exactly the same results at steady state as those from the upwinding technique. These results prove the validity of Leismann and Frind's time step method. Therefore, the proper time step method should evaluate the motional induction term at the old time level and must include a time dependent artificial term.

After the verification, this time step method is applied to a study of support plate signals from the variable reluctance probe as an example of a non-uniform geometry problem. Also, from the resulting solution, flux patterns are plotted as the probe passes a ferromagnetic support plate. These flux plots show a skin effect on the surface of the support plate which occurs due to motional induction currents. Therefore, this skin effect also supports the validity of the solution and the time step algorithm used.

The fact that the probe movement in a non-uniform geometry causes a transient situation prevents the same analysis of AC steady state based eddy current methods. Therefore, the probe velocity in eddy current testing should be restricted to very low speeds. Also, new output variables for eddy current signals seem to be necessary for high speed moving inspection that are not defined under the sinusoidal steady state assumption.

B. Future Work

This dissertation considers only the axisymmetric model. However, this model suffers from a disadvantage in that only axisymmetric defects can be studied. Therefore, a 3-dimensional finite element model needs to be

developed. However, unlike 2-dimensional or axisymmetric problems, 3-dimensional problems have tremendous difficulties in the matrix solution as well as mesh discretization. Especially for motional induction problems, spurious oscillations in the solution prevent the use of large elements. Although the upwinding technique can be used, this technique is limited to steady state problems and large elements basically give less accurate results. Hence, there is a certain limit in using the upwinding technique. For the matrix solution of transient problems, however, there is a way to avoid expensive matrix inversion or Gaussian elimination. That is, if the forward difference method together with a lumping technique is used, matrix inversion can be avoided and the solution time can be greatly reduced. Since the restriction on the motional induction term is to evaluate it at the old time level, the forward difference method can naturally be employed.

One more suggestion in terms of the time step method is to investigate the proper time step size. Although stability analysis gives the general condition (i.e. grid Courant number less than or equal to 1), in the probe movement problem, the time step size is decided by the element length and the probe velocity. Therefore, if proper study of the time step size is made, optimal mesh discretization can be achieved. It seems that the time step size should be decided in relation to the diffusion time constant.

Although the upwinding technique could provide only indirect information in this dissertation, it is a powerful tool to study velocity effects in uniform geometries. The velocities of NDE probes are also somewhat restricted, but other applications require very high speed. For example, the goal of current research in magnetically levitated vehicles is to achieve a

speed more than 225 mph (= 104 m/sec, so-called 'super-speed') [77]. Therefore, the induction sensors measuring the rail to vehicle gap would be affected greatly by velocity effects. Also, drag forces and levitation forces need to be calculated in these areas. The upwinding technique would show its effectiveness in such high speed applications.

REFERENCES

[1] T. E. Bell. "When bust is best." *IEEE Spectrum* 28 (Mar. 1991): 56 - 59.

[2] H. L. Libby. *Introduction to Electromagnetic Nondestructive Test Methods*. New York: R.E. Krieger Publishing Co., 1979.

[3] R. Halmshaw. *Non-destructive testing*. Metallurgy and materials science series. London: Edward Arnold Publishers Ltd., 1987.

[4] J. Blitz. *Electrical and Magnetic Methods of Nondestructive Testing*. New York: Adam Hilger, 1991.

[5] W. Lord. "Forward and Inverse NDE Problems." In *Computer Applications in Design, Simulation and Analysis : Proceedings of the ISMM International Symposium Held in Hawaii 1 - 3 February 1988,* edited by N. F. Marsolan, 113 - 116. Hawaii: ACTA Press, 1988.

[6] W. Lord. "Applications of Numerical Field Modeling to Electromagnetic Methods of Nondestructive Testing." In *Electromagnetic Methods of Nondestructive Testing: Nondestructive Testing Monographs and Tracts (Vol. 3),* edited by W. Lord, 1 - 19. New York: Gordon and Breach Science Publishers, 1985.

[7] D. E. Bray and R. K. Stanley. *Nondestructive Evaluation: A Tool for Design, Manufacturing, and Service*. New York: McGraw-Hill Book Company, 1989.

[8] R. W. E. Shannon and L. Jackson. "Flux Leakage Testing Applied to Operational Pipelines." *Materials Evaluation* 46 (1988): 1516 - 1524.

[9] W. Lord and D. J. Oswald. "Leakage Field Methods of Defect Detection." *International J. NDT.* 4 (1972): 249 - 274.

[10] J. H. Hwang. "Defect Characterization by Magnetic Leakage Fields." Ph.D. dissertation, Colorado State University, 1975.

[11] W. Lord, J. M. Bridges, W. Yen, and R. Palanisamy. "Residual and Active Leakage Fields Around Defects in Ferromagnetic Materials." *Materials Evaluation* 36(1978): 47 - 54.

[12] J.F. Hinsley. *Non-destructive Testing*. London: MacDonald and Evans Ltd., 1959.

[13] W. Lord. "A Survey of Electromagnetic Methods of Nondestructive Testing." Chapter 3 in *Mechanics of Nondestructive Testing*, edited by W. W. Stinchcomb, 77 - 100. New York: Plenum Press, 1980.

[14] S. R. Satish. "Finite Element Modeling of Residual Magnetic Phenomena." M.S. Thesis, Colorado State University, 1980.

[15] S. E. Heath. "Residual and Active Magnetostatic Leakage Field Modeling." M.S. Thesis, Colorado State University, 1984.

[16] S. S. Udpa, W. Lord and Sun Yu-shi. "Numerical Modeling of Residual Magnetic Phenomena." *IEEE Trans. Mag.* 21 (1985): 2165 - 2168.

[17] S. S. Udpa, Y. S. Sun and W. Lord. "Alternative Demagnetization Curve Representations for the Finite Element Modeling of Residual Magnetism." *IEEE Trans. Mag.* 24 (1988): 226 - 229.

[18] R. C. McMaster. *Nondestructive Testing Handbook II*. New York: Ronald Press Co., 1959.

[19] M. Epstein. "The Hall Effect." *International J. NDT.* 2 (1970): 207 - 228.

[20] F. Förster. "The Automatic Detection of Flaws and Marking of Falws by the Magnetographic Method." *Förster Institute Reutlingen* 3, (1964).

[21] A. S. Fal'Kevich. "Magnetographic Testing of Welded Steel Joints in Long Distance and Other Pipelines." *Defektoskopiya* 1 (1965): 19 - 27.

[22] W. J. McGonnagle. *Nondestructive Testing*. New York: Gordon and Breach Science Publishers, 1961.

[23] N. S. Savorovskii. "Contactless System for Transverse Magnetization of Tubes." *Defektoskopiya* 2 (1970): 23.

[24] W. Lord and D. J. Oswald. "The Generated Reaction Field Method of Detecting Defects in Steel Bars." *Materials Evaluation* 29 (1971): 21 - 28.

[25] F. Förster. "Non-destructive Inspection of Tubing and Round Billets by means of Leakage Flux Probes." *British J. NDT* 19 (1977): 26.

[26] W. Lord. "Magnetic Flux Leakage for Measurement of Crevice Gap Clearance and Tube Support Plate Inspection." *EPRI NP-1427, Project S125-1, Final Report*, (June 1980).

[27] M. L. Burrows. "Theory of Eddy Current Flaw Detection." Ph.D. Dissertation, University of Michigan, 1964.

[28] R. Palanisamy. "Finite Element Modeling of Eddy Current Nondestructive Testing Phenomena." Ph.D. Dissertation, Colorado State University, 1980.

[29] S. R. Satish. "Parametric Signal Processing for Eddy Current NDT." Ph.D. Dissertation, Colorado State University, 1983.

[30] N. Ida. "Three Dimensional Finite Element Modeling of Electromagnetic Nondestructive Testing Phenomena." Ph.D. Dissertation, Colorado State University, 1983.

[31] L. Udpa. "Imaging of Electromagnetic NDT Phenomena." Ph.D. Dissertation, Colorado State University, 1986.

[32] D. J. Hagemaier. "Eddy Current Impedance Plane Analysis." *Materials Evaluation* 41 (1983): 211 - 218.

[33] C. V. Dodd. "Applications of a phase sensitive eddy current instrument." *Materials Evaluation* 22 (1964): 260 - 262.

[34] D. L. Waidelich. "Pulsed eddy-current testing of steel sheets." In *Eddy-Current Characterization of Materials and Structures*, edited by G. Birnbaum and G. Free, 367 - 373. Philadelphia: ASNT, 1979.

[35] G. Witting and H. M. Thomas. "Design of pulsed eddy-current test equipment with digital signal analysis." In *Eddy-Current Characterization of Materials and Structures*, edited by G. Birnbaum and G. Free, 387 - 400. Philadelphia: ASNT, 1979.

[36] S. D. Braun. "In service evaluation of multifrequency/multi-parameter eddy current technology for the inspection of PWR steam generator tubing." In *Eddy-Current Characterization of Materials and Structures*, edited by G. Birnbaum and G. Free, 189 - 203. Philadelphia: ASNT, 1979.

[37] R. Becker and K. Betzold. "Optimization of a multifrequency eddy-current test system concerning the defect detection sensitivity." In *Eddy-Current Characterization of Materials and Structures*, edited by G. Birnbaum and G. Free, 213 - 228. Philadelphia: ASNT, 1979.

[38] V. S. Cecco. "Design and Specifications of a High Saturation Absolute Eddy Current Probe with Internal Reference." *Materials Evaluation* 37 (1979): 51 - 58.

[39] "Pipeline Inspection Breaks New Ground." *Corrosion and Inspection,* (Oct. 1986): 67 - 68.

[40] D. L. Atherton and P. Laursen. "ATest Rig for Dynamic Measurements of Magnetic Flux Leakage Patterns." *British J. NDT* 33 (1991): 69 - 73.

[41] T. R. Schmidt. "History of the Remote-Field Eddy Current Inspection Technique." *Materials Evaluation* 47 (1989): 14 - 22.

[42] T. R. Schmidt. "The Remote Field Eddy Current Inspection Technique." *Materials Evaluation* 42 (1984): 225 - 230.

[43] W. Lord. "Finite Element Model for the Remote Field Eddy Current Effect." *AGA Project PR 179-520, Final Report*, (Sep. 1986).

[44] J. B. Nestleroth. "Remote Field Eddy Current Detection of Stress Corrosion Cracks in Gas Transmission Pipelines." *Review of Progress in Quantitative NDE.* 10A (1991): 935 - 942.

[45] "Request for Proposal- Characterization of Magnetic Flux Leakage (MFL) Indications Found During In-Line Inspection of Natural Gas Transmission Pipelines." GRI letter to W. Lord, (July 1992).

[46] N. Ida. "Modeling of Velocity Effects in Eddy Current Applications." *J. Appl. Phys.* 63 (1988): 3007 - 3009.

[47] D. L. Atherton, C. Jagadish, P. Laursen, V. Storm, F. Ham and B. Scharfenberger. "Pipeline Inspection - Tool Speed alters MFL Signals." *Oil & Gas J.* 88 (1990): 84 - 86,

[48] A. H. Kahn and M. L. Mester. "Through-Transmission Impedance Measurements on Moving Metallic Sheets." *Review of Progress in Quantitative NDE* 11A (1992): 249 - 255.

[49] A. H. Kahn and L. C. Phillips. "Development in the Theory and Analysis of Eddy Current Sensing of Velocity in Liquid Metals." paper dedicated on the occasion of the retirement of Professor B. A. Auld, to be published in *Research in Nondestructive Evaluation.* (1992).

[50] Y. K. Shin and W. Lord. "Numerical Modeling of Probe Velocity Effects for Eddy Current and Flux Leakage NDE." *Review of Progress in Quantitative NDE* 10A (1991): 921 - 925.

[51] Y. K. Shin, S. Nath, and W. Lord. "RFEC Probe Velocity Effects." presented in *the 2nd International Conference on Remote Field Technique Held in Queen's University, Kingston, Canada 27 - 28 Aug. 1991.*

[52] Y. K. Shin and W. Lord. "Numerical Modeling of Probe Velocity Effects for Electromagnetic NDE Methods." *Review of Progress in Quantitative NDE* 11A (1992): 257 - 264.

[53] Y. K. Shin and W. Lord. "Numerical Modeling of Moving Probe Effects for Electromagnetic NDE." to be published in *IEEE Trans. Mag.* ; issue of March 1993.

[54] H. Song and N. Ida. "Modeling of Velocity Terms in 3D Eddy Current Problems." *IEEE Trans. Mag.* 28 (1992): 1178 - 1181.

[55] J. B. Nestleroth and R. J. Davis. "The Effects of Magnetizer Velocity on Magnetic Flux Leakage Signals." presented in *Review of Progress in Quantitative NDE Held in University of California, San Diego, LaJolla, 19 -24 July 1992.*

[56] A. A. Abdel-Razek, J. L. Coulomb, M. Feliachi, and J. C. Sabonnadiere. "Conception of an Air-Gap Element for the Dynamic Analysis of the Electromagnetic Field in Electric Machines." *IEEE Trans. Mag.* 18 (1982): 655 - 659.

[57] F. Bouillault and A. Razek. "Dynamic Model for Eddy Current Calculation in Saturated Electric Machines." *IEEE Trans. Mag.* 19 (1983): 2639 - 2642.

[58] B. Davat, Z. Ren and M. Lajoie-Mazenc. "The Movement in Field Modeling." *IEEE Trans. Mag.* 21 (1985): 2296 - 2298.

[59] S. R. H. Hoole. "Rotor Motion in the Dynamic Finite Element Analysis of Rotating Electrical machinery." *IEEE Trans. Mag.* 21 (1985): 2292 - 2295.

[60] H. C. Lai, D. Rodger and P. J. Leonard. "Coupling Meshes in 3D Problems involving Movements." *IEEE Trans. Mag.* 28 (1992): 1732 - 1734.

[61] J. G. Van Bladel. "Motion of a conducting loop in a magnetic field." *IEE Proceedings* 135 (1988): 217 - 222.

[62] S. B. Pratap. "Transient Eddy Current Distribution in the Shield of the Passively Compensated, Compensated Pulsed Alternator: Iron-Core Machines." *IEEE Trans. Mag.* 26 (1990): 1256 - 1269.

[63] V. S. Rao. "Perturbation Technique for Fields and Forces due to Current Filaments Moving above a Conducting Plate of Finite Thickness." *IEE Proceedings* 133 (1986): 129 - 136.

[64] S. Panas and E. E. Kriezis. "Eddy Current Distribution due to a Rectangular Current Frame Moving above a Conducting Slab." *Archiv für Elektrotechnik* 69 (1986): 185 - 191.

[65] A. Foggia, J. C. Sabonnadiere and P. Silvester. "Finite Element Solution of Saturated Travelling Magnetic Field Problems." *IEEE Trans. PAS.* PAS-94 (1975): 866 - 871.

[66] T. Furukawa, K. Ogawa and S. Nonaka. "Finite Element Analysis of Eddy Currents Problem Subject to Convective Diffusion Equation." *IEEE Trans. Mag.* 23 (1987): 2660 - 2662.

[67] N. K. Deshmukh and K. C. Mukherji. "Finite-Element Analysis of Three-Dimensional Eddy Currents in Attractive Electromagnetic Levitation." *IEE Proceedings* 134 (1987): 651 - 662.

[68] S. Niikura and A. Kameri. "Analysis of Eddy Current and Force in Conductors with Motion." *IEEE Trans. Mag.* 28 (1992): 1450 - 1453.

[69] M. Tsuchimoto, K. Miya, A. Yamashita and M. Hashimoto. "An Analysis of Eddy Current and Lorentz Force of Thin Plates under Moving Magnets." *IEEE Trans. Mag.* 28 (1992): 1434 - 1437.

[70] K. Muramatsu, T. Nakata, N. Takahashi and K. Fujiwara. "Comparison of Coordinate Systems for Eddy Current Analysis in Moving Conductors." *IEEE Trans. Mag.* 28 (1992): 1186 - 1189.

[71] M. Odamura and M. Ito. "Up-wind Finite Element Solution of Saturated Travelling Magnetic Field Problems." In *Finite Element Flow Analysis: Proceedings of the Fourth International Symposium on Finite Element Methods in Flow Problems Held in Tokyo July 1982*, edited by T. Kawai, 819 - 826. Tokyo: North-Holland Publishing Company, 1982.

[72] S. Y. Hahn, J. Bigeon and J. C. Sabonnadiere. "An Upwind Finite Element Method for Electromagnetic Field Problems in Moving Media." *Int. J. Num. Meth. Engng.* 24 (1987): 2071 - 2086.

[73] D. Rodger, T. Karaguler and P. J. Leonard. "A Formulation for 3D Moving Conductor Eddy Current Problems." *IEEE Trans. Mag.* 25 (1989): 4147 - 4149.

[74] T. Furukawa, K. Komiya and I. Muta. "An Upwind Galerkin Finite Element Analysis of Linear Induction Motors." *IEEE Trans. Mag.* 26 (1990): 662 - 665.

[75] M. Ito, T. Takahashi and M. Odamura. "Upwind Finite Element Solution of Travelling Magnetic Field Problems." *IEEE Trans. Mag.* 28 (1992): 1605 - 1610.

[76] B. V. Jayawant. *Electromagnetic Levitation and Suspension Techniques*. London: Edward Arnold Publishers Ltd., 1981.

[77] D. R. Brown and E. P. Hamilton III. *Electromechanical Energy Conversion.* New York: Macmillan Publishing Company, 1984.

[78] F. C. Moon. *Magneto-Solid Mechanics.* New York: John Wiley & Sons, Inc., 1984.

[79] D. Rodger, P. J. Leonard and T. Karaguler. "An Optimal Formulation for 3D Moving Conductor Eddy Current Problems with Smooth Rotors." *IEEE Trans. Mag.* 26 (1990): 2359 - 2363.

[80] D. Rodger, P. J. Leonard and J.F. Eastham. "Modelling Electromagnetic Rail Launchers at Speed using 3D Finite Elements." *IEEE Trans. Mag.* 27 (1991): 314 - 317.

[81] L. E. Thurmond, B. K. Ahrens and J. P. Barber. "Measurement of the Velocity Skin Effect." *IEEE Trans. Mag.* 27 (1991): 326 - 328.

[82] J. Bigeon, J. C. Sabonnadiere and J. L. Coulomb. "Finite Element Analysis of an Electromagnetic Brake." *IEEE Trans. Mag.* 19 (1983): 2632 - 2634.

[83] Y. Marechal and G. Meunier. "Computation of 2D and 3D Eddy Currents in Moving Conductors of Electromagnetic Retarders." *IEEE Trans. Mag.* 26 (1990): 2382 - 2384.

[84] W. Lord. "Developments in the Numerical Modeling of NDT Phenomena." In *Applied Electromagnetics in Materials: Proceedings of the First International Symposium Held in Tokyo 3-5 October 1988*, edited by K. Miya, 117 - 125. Tokyo: Pergamon Press, 1988.

[85] W. Lord, S. Nath, Y. K. Shin and Z. You. "Electromagnetic Methods of Defect Detection." *IEEE Trans. Mag.* 26 (1990): 2070 - 2075.

[86] L. Lapidus and G. Pinder. *Numerical Solution of Partial Differential Equations in Science and Engineering.* New York: John Wiley & Sons, Inc., 1982.

[87] N. A. Demerdash and T. W. Nehl. "An Evaluation of the Methods of Finite Elements and Finite Differences in the Solution of Nonlinear Electromagnetic Fields in Electrical Machines." *IEEE Trans. PAS.* PAS-98 (1979): 74 - 87.

[88] L. Udpa, Y. S. Sun, W. Lord and Y. K. Shin. "Mesh and Boundary Considerations in the Numerical Modeling of Large 3-D Electromagnetic NDT Geometries." *Review of Progress in Quantitative NDE* 8A (1989): 793 - 800.

[89] Y. Sun, H. Lin, Y. K. Shin, Z. You, S. Nath and W. Lord. "3-D Finite Element Modeling of the Remote Field Eddy Current Effect." *Review of Progress in Quantitative NDE* 9A (1990): 319 - 326.

[90] J. F. Imhoff, G. Meunier and J. C. Sabonnadiere. "Finite Element Modeling of Open Boundary Problems." *IEEE Trans. Mag.* 26 (1990): 588 - 591.

[91] P. Bettess. "Infinite Elements." *Int. J. Num. Meth. Engng.* 11 (1977): 53 - 64.

[92] G. Beer and J. L. Meek. "Infinite Domain Elements." *Int. J. Num. Meth. Engng.* 17 (1981): 43 - 52.

[93] S. Pissanetzky. "An Infinite Element and a Formula for Numerical Quadrature over an Infinite Interval." *Int. J. Num. Meth. Engng.* 19 (1983): 913 - 927.

[94] O. C. Zienkiewicz, K. Bando, P. Bettess, C. Emson and T. C. Chiam. "Mapped Infinite Elements for Exterior Wave Problems." *Int. J. Num. Meth. Engng.* 21 (1985): 1229 - 1251.

[95] P. P. Silvester, D. A. Lowther, C. J. Carpenter and E. A. Wyatt. "Exterior Finite Elements for 2-Dimensional Field Problems with Open Boundaries." *IEE Proceedings* 124 (1977): 1267 - 1270.

[96] C. J. Carpenter. "3-Dimensional Magnetic-Field and Eddy Current Problems at Power Frequencies." *IEE Proceedings* 124 (1977): 1026 - 1034.

[97] J. Simkin and C. W. Trowbridge. "On the Use of the Total Scalar Potential in the Numerical Solution of Field Problems in Electromagnetics." *Int. J. Num. Meth. Engng.* 14 (1979): 423 - 440.

[98] C. S. Biddlecombe, E. A. Heighway, J. Simkin and C. W. Trowbridge. "Methods for Eddy Current Computation in Three Dimensions." *IEEE Trans. Mag.* 18 (1982): 492 - 497.

[99] J. Penman and J. R. Fraser. "Unified Approach to Problems in Electromagnetism." *IEE Proceedings* 131 (1984): 55 - 61.

[100] S. E. Harris. "Symmetry of Electromagnetism." *IEE Proceedings* 135 (1988): 363 - 368.

[101] S. Hasebe and Y. Kano. "Analysis of Three-Dimensional Magnetic Field Inducing Eddy Currents-on the Nature of Scalar Potential." *Electrical Engineering in Japan* 103 (1983): 17. - 25.

[102] T. Yoshimoto, S. Yoshida and K. Bessho. "A Finite-Element Analysis of a Three-Dimensional Eddy Current Diffusion Problem and its Application to a Flux Concentration Apparatus." *Electrical Engineering in Japan* 107 (1987): 127. - 134.

[103] C. A. Brebbia. *The Boundary Element Method for Engineers.* London: Pentech Press, 1978.

[104] S. R. H. Hoole. *Computer-Aided Analysis and Design of Electromagnetic Devices.* New York: Elsevier Science Publishing Co., Inc. , 1989.

[105] T. J. Rudolphi. *EM 526: Boundary Element Method. Class Notes,* Iowa State University, Spring 1990.

[106] S. Nath, Y. K. Shin, W. Lord and T. J. Rudolphi. "Boundary Integral and Finite Element Simulation of Electromagnetic NDE Phenomena." *Review of Progress in Quantitative NDE* 9A (1990): 303 - 310.

[107] S. Nath. "Boundary Integral and Finite Element Simulation of Potential Drop NDE Measurement." *Electrosoft* 2 (1991): 92 - 104.

[108] S. Nath, T. J. Rudolpi and W. Lord. "Comparative Study of Finite-Element and Boundary-Element Analyses of the DC Potential Drop Method." *Materials Evaluation* 51 (1992): 51 - 55.

[109] S. J. Salon. "The Hybrid Finite Element-Boundary Element Method in Electromagnetics." *IEEE Trans. Mag.* 21 (1985): 1829 - 1834.

[110] A. Bossavit and J. C. Verite. "A Mixed FEM-BEM Method to solve 3-D Eddy-Current Problems." *IEEE Trans. Mag.* 18 (1982): 431 - 435.

[111] Z. Ren, F. Bouillault, A. Razek, A. Bossavit and J. C. Verite. "A New Hybrid Model Using Electric Field Formulation for 3-D Eddy Current Problems." *IEEE Trans. Mag.* 26 (1990): 470 - 473.

[112] M. Enokizono and S. Nagata. "Convection-Diffusion Analysis at High Peclet Number by the Boundary Element Method." *IEEE Trans. Mag.* 28 (1992): 1651 - 1654.

[113] G. F. Carey and J. T. Oden. *Finite Elements-Computational Aspects.* Vol. III, Englewood Cliffs, New Jersey: Prentice-Hall, 1984.

[114] E. Thompson, *CE665;Finite Element Method. Class Notes,* Colorado State University, Fall 1988.

[115] O. C. Zienkiewicz. "Finite Elements - The Basic Concepts and an Application to 3-D Magnetostatic Problems." Chapter 1 in *Finite Elements in Electrical and Magnetic Field Problems,* edited by M. V. K. Chari and P. P. Silvester, 11 - 31. New York: John Wiley & Sons, Inc., 1980.

[116] N. Ida. "Modeling of Velocity Effects for Low Frequency Eddy Current Testing." In *Non-destructive Evaluation of Ferromagnetic Materials: Proceedings of the Second National Seminar Held in Houston 1986.*

[117] T. J. R. Hughes. "A Simple Scheme for Developing Upwind Finite elements." *Int. J. Num. Meth. Engng.* 12 (1978): 1359 - 1365.

[118] O. C. Zienkiewicz and R. L. Taylor. *The Finite Element Method* Vol. 1. New York: McGraw-Hill Book Company, 1989.

[119] K. Hulbert of Innovative Sciences Inc. Written communication to Satish Udpa, 1987.

[120] G. L. Guymon. "A Finite Element Solution of the One-Dimensional Diffusion-Convection Equation." *Water Resources Research* 6 (1970): 204 - 210.

[121] G. L. Guymon, V. H. Scott and L. R. Herrman. " A General Numerical Solution of the Two-Dimensional Diffusion-Convection Equation by the Finite Element Method." *Water Resources Research* 6 (1970): 1611 - 1617.

[122] J. W. Barrett and K. W. Morton. "Optimal Finite Element Solutions to Diffusion-Convection Problems in One Dimension." *Int. J. Num. Meth. Engng.* 15 (1980): 1457 - 1474.

[123] A. Prakash. "Finite Element solutions of the Non-Self-Adjoint Convective-Dispersion Equation." *Int. J. Num. Meth. Engng.* 11 (1977): 269 - 287.

[124] A. K. Runchal. "Convergence and Accuracy of Three Finite Difference Schemes for a Two-Dimensional Conduction and Convection Problem." *Int. J. Num. Meth. Engng.* 4 (1972): 541 - 550.

[125] D. B. Spalding. "A Novel Finite Difference Formulation for Differential Expressions involving Both Fist and Second Derivatives." *Int. J. Num. Meth. Engng.* 4 (1972): 551 - 559.

[126] I. Christie, D. F. Griffiths, A. R. Mitchell and O. C. Zienkiewicz. "Finite Element Methods for Second Order Differential Equations with Significant First Derivatives." *Int. J. Num. Meth. Engng.* 10 (1976): 1389 - 1396.

[127] J. C. Heinrich, P. S. Huyakorn, O. C. Zienkiewicz and A. R. Mitchell. "An Upwind Finite Element Scheme for Two Dimensional Convective Transport Equation." *Int. J. Num. Meth. Engng.* 11 (1977): 131 - 143.

[128] G. Payre, M. D. Broissia and J. Bazinet. "An Upwind Finite Element Method via Numerical Integration." *Int. J. Num. Meth. Engng.* 18 (1982): 381 - 396.

[129] D. W. Kelly, S. Nakazawa, O. C. Zienkiewicz and J. C. Heinrich. "A Note on Upwinding and Anisotropic Balancing Dissipation in Finite Element Approximations to Convective Diffusion Problems." *Int. J. Num. Meth. Engng.* 15 (1980): 1705 - 1711.

[130] K. H. Huebner and E. A. Thornton. The Finite Element Method for Engineers. New York: John Wiley & Sons, Inc., 1982.

[131] J. C. Heinrich. "On Quadratic Elements in Finite Element Solutions of Steady State Convection-Diffusion Equation." *Int. J. Num. Meth. Engng.* 15 (1980): 1041 - 1052.

[132] E. K. C. Chan and S. Williamson. "Factors Influencing the Need for Upwinding in Two-Dimensional Field Calculation." *IEEE Trans. Mag.* 28 (1992): 1611 - 1614.

[133] G. DeMey. "Field Calculation in a Moving Conductor by an Integral Equation." *Archiv für Elektrotechnik* 64 (1981): 101 - 103.

[134] M. Ikeuch. "A Transformed Boundary Element Method for Steady-State Convective Diffusion Problem." *Trans. IECE Japan* E68 (1985): 602 - 608.

[135] M. Ikeuch, M. Sakakihara and K. Onishi. "Constant Boundary Element Solution for Steady-State Convective Diffusion Equation in Three Dimensions." *Trans. IECE Japan* E66 (1983): 373 - 376.

[136] T. Honma, Y. Tanaka and I. Kaji. "Regular Boundary Element Solutions to Steady-State Convective Diffusion Equations." *Engineering Analysis* 2 (1985): 95 - 99.

[137] M. Ikeuch. "Boundary Element Steady-State Solutions of the Traveling Magnetic Field Problem." *IEEE Trans. Mag.* 21 (1985): 2629 - 2634.

[138] N. Burais, A. Foggia, A. Nicolas, J. P. Pascal and J. C. Sabonnadiere. "Numerical Solution of Eddy Current Problems including Moving Conducting Parts." *IEEE Trans. Mag.* 20 (1984): 1995 - 1997.

[139] Y. Marechal, G. Meunier, J. L. Coulomb and H. Magnin. "A General Purpose Tool for Restoring Inter-Element Continuity." *IEEE Trans. Mag.* 28 (1992): 1728 - 1731.

[140] O. C. Zienkiewicz, R. Löehner, K. Morgan and S. Nakazawa. "Finite Elements in Fluid Mechanics - A Decade of Progress." *Finite Elements in Fluids* 5 (1984): 1 - 26.

[141] B. Aldefeld. "A Numerical Solution of Transient Nonlinear Eddy-Current Problems Including Moving Iron Parts." *IEEE Trans. Mag.* 14 (1978): 371 - 373.

[142] J. Donea. "A Taylor-Galerkin Method for Convective Transport Problems." *Int. J. Num. Meth. Engng.* 20 (1984): 101 - 119.

[143] J. Donea, S. Giuliani, H. Laval and L. Quartapelle. "Time-Accurate Solution of Advection-Diffusion Problems by Finite Elements." *Comp. Meth. Appl. Mech. Eng.* 45 (1984): 123 - 145.

[144] R. Löehner, K. Morgan and O. C. Zienkiewicz. "The Solution of Non-Linear Hyperbolic Equation Systems by the Finite Element Method." *Int. J. Num. Meth. Fluids* 4 (1984): 1043 - 1063.

[145] O. C. Zienkiewicz, R. Löehner, K. Morgan and J. Peraire. "High-Speed Compressible Flow and Other Advection-dominated Problems of Fluid Dynamics." *Finite Elements in Fluids* 6 (1985): 41 - 88.

[146] H. M. Leismann and E. O. Frind. "A Symmetric-Matrix Time Integration Scheme for the Efficient Solution of Advection-Dispersion Problems." *Water Resources Research* 25 (1989): 1133 - 1139.

[147] W. Lord. "Development of a Finite Element Model for Eddy-Current NDT Phenomena." *EPRI NP-2026, Project 1395-2, Interim Report,* (Sep. 1981).

[148] N. Ida, H. Hoshikawa and W. Lord. "Finite Element Prediction of Differential Eddy Current Probe Signals from Fe_3O_4 Deposits in PWR Steam Generators." NDT International 18 (1985): 331 - 338.

[149] W. Lord and R. Palanisamy. "Detection and Modeling of Magnetite Buildup in Steam Generators." *IEEE Trans. Mag.* 16 (1980): 695 - 697.

[150] W. Lord and R. Palanisamy. "Magnetic Probe Inspection of Steam Generator Tubing." *Materials Evaluation* 38(1980): 38 - 40.

[151] R. Palanisamy and W. Lord. "Sensitivity Analysis of Variable Reluctance Probe for Steam Generator Tubing Inspection." *IEEE Trans. Mag.* 19 (1983): 2213 - 2215.

[152] S. R. Satish and W. Lord. "Hall-Plate Measurements of Magnetite Buildup in Pressurized-Water Reactor Steam Generators." *IEEE Trans. IM.* IM-32 (1983): 414 - 418.

[153] R. Palanisamy and W. Lord. "Finite Element Modeling of Electromagnetic NDT Phenomena." *IEEE Trans. Mag.* 15 (1979): 1479 - 1481.

[154] N. Ida, R. Palanisamy and W. Lord. "Eddy Current Probe Design using Finite Element Analysis." Materials Evaluation 41 (1983): 1389 - 1394.

[155] W. Lord. "Eddy Current Methods of Flaw Detection and Their Modeling." In *Electromagnetomechanical Interactions in Deformable Solids and Structures: Proceedings of the IUTAM Symposium Held in Tokyo 12-17 October 1986*, edited by Y. Yamamoto and K. Miya, 203-213. Amsterdam: North-Holland Publishing Company, 1987.

[156] W. R. MacLean. "Apparatus for Magnetically Measuring Thickness of Ferrous Pipe." US Patent No. 2 573 799, 1951.

[157] W. Lord, Y. S. Sun, S. S. Udpa and S. Nath. "Physics of the Remote Field Eddy Current Effect." *Review of Progress in Quantitative NDE* 7 (1988): 165 - 172.

[158] W. Lord, Y. S. Sun, S. S. Udpa and S. Nath. "A Finite element Study of the Remote Field Eddy Current Phenomenon." *IEEE Trans. Mag.* 24 (1988): 435 - 438.

[159] S. Nath. "Remote Field Eddy Current Phenomena." M.S. Thesis, Colorado State University, 1988.

[160] K. Krzywosz and G. Dau. "Comparison of Electromagnetic Techniques for Nondestructive Inspection of Ferromagnetic Tubing." Materials Evaluation 48 (1990): 42 - 45.

[161] S. S. Udpa, T. H. Ou-Yang and W. Lord. "Signal Processing for Remote Field Eddy Current Inspection Technique." *Review of Progress in Quantitative NDE* 7 (1988): 331 - 338.

[162] R. Courant. "Variational Methods for the Solution of Problems of Equilibrium and Vibrations." *Bull. Am. Math. Soc.* 49 (1943): 1 - 23.

[163] W. Prager and J. L. Synge. "Approximations in Elasticity Based on the Concept of Function Space." *Quart. Appl. Math.* 5 (1947): 241 - 269.

[164] A. Hrenikoff. "Solution of Problems in Elasticity by the Framework Method." *J. Appl. Mech.* 8 (1941): 169 - 175.

[165] D. McHenry. "A Lattice Analogy for the Solution of Plane Stress Problems." *J. Inst. Civil Eng.* 21 (1943): 59 - 82.

[166] N. M. Newmark. "Numerical Methods of Analysis of Bars, Plates and Elastic Bodies." In *Numerical Methods of Analysis in Engineering*, edited by L. E. Grinter. New York: Macmillan, 1949.

[167] M. J. Turner, R. W. Clough, H. C. Martin and L. J. Topp. "Stiffness and Deflection Analysis of Complex Structures." *J. Aeronautical Sciences* 23 (1956): 805 - 823, 854.

[168] R. W. Clough. "The Finite Element Method in Plane Stress Analysis." In *Electronic Computation: Proceedings of the 2nd ASCE Conference Held in Pittsburgh, PA. September 1960*, 345 - 378.

[169] O. C. Zienkiewicz and Y. K. Cheung. "Finite Elements in the Solution of Field Problems." *The Engineer* 220 (1965): 507 - 510.

[170] D. S. Burnett. *Finite Element Analysis from Concepts to Applications*. Reading, Massachusetts: Addison-Wesley Publishing Company, 1988.

[171] A. M. Winslow. "Numerical Solution of the Quasilinear Poisson Equation in a Nonuniform Triangle Mesh." *J. Comp. Phys.* 2 (1967): 149 - 172.

[172] P. P. Silvester. "Finite Element Solution of Homogeneous Waveguide Problems." *Alta Frequenza* 38 (1969): 313 - 317.

[173] S. Ahmed and P. Daly. "Waveguide Solutions by the Finite Element Method." *Radio and Electronic Engineer* 38 (1969): 217 - 223.

[174] P. P. Silvester and M. V. K. Chari. "Finite Element Solution of Saturable Magnetic Field Problems." *IEEE Trans. PAS* PAS-89 (1970): 1642 - 1651.

[175] O. W. Anderson. "Transformers Leakage Flux Program Based on the Finite Element Method." *IEEE Trans. PAS* PAS-92 (1973): 682 - 689.

[176] M. V. K. Chari. "Finite Element Solution of the Eddy Current Problem in Magnetic Structures." *IEEE Trans. PAS* PAS-93 (1974): 62 - 72.

[177] J. R. Brauer. "Finite Element Analysis of Electromagnetic Induction in Transformers." Presented at the *IEEE Winter Power Meeting*, New York, 1977.

[178] M. V. K. Chari. "Finite Element Applications in Electrical Engineering." *Guest Lecture at the 5th IEEE Conference on Electromagnetic Field Computation Held in Claremont, CA. 3-5 August 1992*, to be published in *IEEE Trans. Mag.* ; issue of March 1993.

[179] W. Lord and J. H. Hwang. "Convergence and Mesh Subdivision for Finite Element Analysis of Nonlinear Magnetic Fields." *Computer & Elec. Engng.* 1 (1974): 513 - 520.

[180] J. H. Hwang and W. Lord. "Finite Element Modeling of the Magnetic Field/Defect Interactions." *ASTM J. Testing and Evaluation* 3 (1975): 21 - 25.

[181] G. Arfken. *Mathematical Methods for Physicists*. New York: Academic Press, Inc., 1970.

[182] E. N. Moor. *Theoretical Mechanics*. New York: John Wiley & Sons, Inc., 1983.

[183] Y. K. Shin. "Solution of cyclic nonlinear magnetic fields in three dimensions." M.S. Thesis, Drexel University, 1987.

[184] R. Wait and A. R. Mitchell. *Finite Element Analysis and Applications*. New York: John Wiley & Sons, Inc., 1985.

[185] A. C. Hindmarsh, P. M. Gresho and D. F. Griffiths. "The Stability of Explicit Euler Time-Integration for Certain Finite Difference Approximations of the Multi-Dimensional Advection-Diffusion Equation." *Int. J. Num. Meth. Fluids* 4 (1984): 853 - 897.

[186] R. Haberman. *Elementary Applied Partial Differential Equations*. New Jersey: Prentice-Hall, Inc., 1987.

[187] D. Schieber. *Electromagnetic Induction Phenomena*. Berlin: Springer-Verlag, 1986.

[188] D. A. Dunn. *Models of Particales and Moving Media*. New York: Academic Press, Inc., 1971.

[189] J. D. Jackson. *Classical Electrodynamics*. New York: John Wiley & Sons, Inc., 1975.

[190] C. T. Tai. "On the Presentation of Maxwell's Theory." *Proceedings of the IEEE*, 60 (1972): 936 - 945.

[191] H. H. Woodson and J. R. Melcher. *Electromechanical Dynamics, Part II. Fields, Forces, and Motion*. New York: John Wiley & Sons, Inc., 1968.

[192] H. von Helmholtz. "On Integrals of the Hydrodynamical Equations Which Express Vortex-Motion." *Phil. Mag.* 33 (1867): 485 - 512.

[193] A. Sommerfeld. *Electrodynamics*. New York: Academic Press Inc., 1952.

[194] W. K. H. Panofsky and M. Phillips. *Classical Electricity and Magnetism*. Reading: Addison-Wesley Publishing Company, Inc., 1962.

[195] Zhongqing You. "Finite Element Study of Ultrasonic Imaging." Ph.D. Dissertation, Iowa State University, 1991.

[196] W. F. Hughes and F. J. Young. *The Electromagnetodynamics of Fluids*. New York: John Wiley & Sons, Inc., 1966.

[197] J. H. Hwang and W. Lord. "Finite Element Analysis of the Magnetic Field Distribution Inside a Rotating Ferromagnetic Bar." *IEEE Trans. Mag.* 10 (1974): 1113 - 1118.